A functionalizable nerve graft design based on an organized electrospun silk fibroin nanofiber biomaterial for peripheral nerve regeneration

Kayla Ann Belanger

Par **Kayla Ann BELANGER**

A functionalizable nerve graft design based on an organized electrospun silk fibroin nanofiber biomaterial for peripheral nerve regeneration

Thèse présentée
pour l'obtention du grade
de Docteur de l'UTC

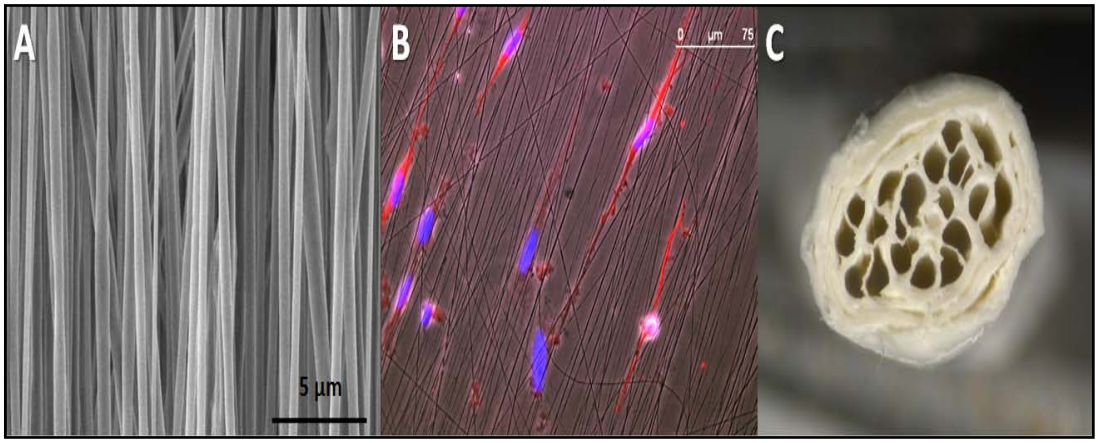

Soutenue le 6 novembre 2017
Spécialité : Biomécanique et Bio-ingénierie : Unité de Recherche Biomécanique et Bio-ingénierie (UMR-7338)
D2410

Université de Technologie de Compiègne

BioMécanique et BioIngénierie (BMBI)
Laboratoire CNRS UMR 7338 : Cellules Biomatériaux Bioréacteurs

Thèse

Pour obtenir le grade de
Docteur de l'Université de Technologie de Compiègne

A FUNCTIONALIZABLE NERVE GRAFT DESIGN BASED ON AN ORGANIZED ELECTROSPUN SILK FIBROIN NANOFIBER BIOMATERIAL FOR PERIPHERAL NERVE REGENERATION

Présentée et Soutenue par

Kayla Ann Belanger

le 6 Novembre, 2017

Jury :

Directeur de Thèse :	
Pr. Christophe EGLES	Université de Compiègne
Rapporteurs :	
Pr. Emmanuel PAUTHE	Université de Cergy Pontoise
Pr. Thomas CLAUDEPIERRE	Université de Lorraine
Professeur UTC :	
Pr. Marion RISBET	Université de Compiègne
Examinateurs :	
Pr. Catherine PICART	Grenoble INP
Pr. Bernard DEVAUCHELLE	CHU d'Amiens
Pr. Guy SCHLATTER	Université de Strasbourg

Acknowledgements

I would like to thank, first and foremost, my PhD advisor, Professor Christophe Egles, for having accepted me for this PhD opportunity in the Biomechanics and Bioengineering laboratory at the Université de Technologie de Compiègne. I would like to thank you for your support and mentorship from the beginning until the end of my PhD not only pertaining to the research subject of this thesis, but also for your advice and guidance in respect to orienting myself in order to reach future career goals both in academia and in industry. I would like to thank you for your availability throughout my thesis, providing counseling on the progress of the research project whenever needed. I would especially like to thank your open-mindedness during our conversations always evoking progressive discussions for the advancement of the research project and your optimistic perspective encouraging the freedom to explore many different interesting research paths. I appreciate greatly the role you have played during my time as a PhD student at UTC.

I would like to thank Professor Bernard Devauchelle for his collaboration and his availability despite his very busy schedule. It was an honor to work with such a renowned and talented surgeon and this project would not have been able to advance as quickly or as successfully without your experience and advice.

I would like to thank Professor Frédéric Marin and Khalil Ben-Mansour for their enriching collaboration and assistance with everything pertaining to motion capture analysis. You both have helped advance this project much further than it could have gone without your expertise. In addition, I want to thank you for your help in interpreting results obtained from the mechanical tests done during my thesis.

I would like to thank Professor Guy Schlatter and Professor Anne Hébraud for their collaboration and availability during a very short but compact week spent as a guest in their lab. You both took a lot of time to collaborate on the creation of a new material that became the basis of the implants used in this work. I am very grateful for the time spent and experience gained during this week in your university under your guidance.

I would like to thank Professor David Kaplan and Dr. James White for the warm welcome into your lab during the first year of my thesis. This month was a great learning experience where I was able to acquire experience needed for the rest of my PhD. I was able to collaborate with a few of the PhD students and post docs which made this a very enriching experience. I want to especially thank Jimmy for his time and his guidance during the whole month I was at Tufts.

I would like to thank Professor Didier Gamet for his collaboration on electrophysiological analyses in this study. You gave much of your time in order to share your knowledge and expertise

on this subject which allowed me to present a more comprehensive evaluation on the results of my in vivo study.

I would like to thank Dr. Kamelia Ghazi-Naiji for all of her guidance during the time she was in BMBI C2B. You helped me immensely with all the DRG extractions we had to do together and always were there to give me advice when I needed it. I appreciate so much the time we were able to work together.

I would like to thank Pascale Vigneron for all the help you have given me throughout my time in Compiègne. Not only did you give me infinite advice and help with things involving my project and the lab (including staying with me during August vacation last year to help me take care of the animals), but you also were always there to guide me through confusion with French administration and any other issues I ran into during my time here!

I would like to thank everyone in the C2B team for their kindness and assistance throughout my PhD. From the engineer assistants to professors, you all helped me at different moments throughout my stay in Compiègne and I appreciate that a lot. I want to thank especially the other doctorate students in C2B including several from other BMBI teams who created a great ambiance in lab and who became a support system in and out of the lab!

I want to thank specifically Risa for being one of the first people I met at UTC and who has been a consistent support throughout our respective PhD's. I would also like to thank Delphine for being exactly what I needed in an office mate and in consequence became a very good friend.

I would like to thank all the jury members who have accepted to be a part of my PhD defense. I am extremely grateful for the time you all have dedicated in order to assist in my defense in addition to the travel most of you will make to be present for my presentation.

Most importantly, I would like to thank my family, specifically my parents for always supporting me and believing in me. When I told you both I may want to move to France for 3 years to do my PhD, you were always supportive even knowing how seldom you would be able to see me during this period. And I want to especially thank you for buying my plane tickets home for Christmas every year so I could spend the holiday with the whole family.

Finally, I would like to thank the Université de Technologie de Compiègne, La Région Hauts-de-France, FEDER, and CNRS for the financial support throughout this PhD.

Summary (English)

Injury to a peripheral nerve can cause loss of sensory and motor function, and if the injury is very severe where the nerve undergoes neurotmesis, unassisted nerve regeneration may not occur. In this case, where the gap between nerve segments is too large to carry out a direct end to end suture, a graft is sutured to bridge the gap between sectioned nerve segments. The autologous nerve graft, where a portion of a less important nerve from the same patient is removed and grafted between nerve segments, continues to be the gold standard procedure for nerve repair. However, there are several drawbacks of this technique including a second surgical procedure, loss of function at the donor site, possibility of developing a painful neuroma at the donor site, and the 50% success rate of autografts used in large gaps. There is therefore a need for a tissue engineered nerve graft that can replace the autograft, and this study aims to advance toward an effective autograft alternative.

This PhD is presented as a three part study consisting first of the development of a novel nerve guidance conduit based on a tri-layered silk fibroin nanofiber material comprised of a complex organization including two aligned fiber surfaces and a randomly deposited fiber interior to improve the mechanical properties of the material while not compromising the guidance capabilities of aligned nanofibers for nerve regeneration. The material is then used to fabricate a multi-channeled tube with an additional “jacket layer” in order to facilitate surgical implantation. This NGC has been submitted to be patented on July 12, 2017 and is the subject of the second article submitted for review for publication.

The second part of this study explores the different possibilities of the functionalization of the material in order to improve the effectiveness for nerve regeneration. This study explores functionalizing the silk fibroin with a second protein, several growth factors, and nanoparticles that all have potential to add favorable properties to the natural biocompatible silk fibroin material.

The final part of this study tests the effectiveness of growth factor-embedded silk fibroin NGCs for peripheral nerve regeneration in comparison with non-functionalized silk fibroin devices and a direct suture to simulate results obtained with an autograft. Three different techniques for

the evaluation of nerve regeneration were used in order to produce a more comprehensive analysis. As there are many mechanisms involved in nerve regeneration, only one or two analysis techniques cannot paint a complete picture of the success of nerve regeneration. Therefore, histological analyses, electromyography analyses, and motion capture analyses were carried out and considered together in order to make a conclusion on the level of nerve regeneration success during this study. The conclusions from this study were that a NGC functionalized with a combination of growth factors appeared to exhibit the most successful nerve regeneration and functional recovery.

Résumé (Français)

Une lésion au niveau d'un nerf périphérique peut provoquer la perte de fonction sensorielle et motrice, et dans le cas de neurotmésis, la régénération spontanée ne se produira pas. De plus, si l'espace entre les deux segments de nerf est trop important, une suture directe n'est pas possible et l'implantation d'une greffe est nécessaire afin de créer une liaison entre les deux segments de nerf. L'autogreffe de nerf est le « gold standard » pour des procédés de réparation nerveuse : une portion d'un nerf sein (qui est considéré comme un nerf moins important) est prise du même patient et implantée au site de la lésion. Cependant, il existe plusieurs désavantages avec ce procédé comme une deuxième chirurgie, la perte de fonction au site du don, la possibilité de développer un neurome sur ce même site, ainsi qu'un taux de réussite de 50% dans les cas où l'espace entre les deux segments de nerf est très important. Il reste donc, un besoin de trouver un procédé alternatif afin d'augmenter le taux de réussite et d'éliminer les désavantages de l'autogreffe. L'objectif de cette étude est d'avancer vers une solution alternative de l'autogreffon en utilisant des biomatériaux.

Cette thèse se divise en trois parties. La première se focalise sur le développement d'un modèle de guide nerveux basé sur des nanofibres de fibroïne de soie. Ce matériau est composé d'une organisation complexe qui inclut deux surfaces de nanofibres alignées avec une couche de nanofibres aléatoires à l'intérieur afin d'améliorer des propriétés mécaniques du matériau sans la perte d'orientation des fibres pour la régénération nerveuse. Le matériau est ensuite manipulé pour fabriquer un tube, multi-canaux avec une « enveloppe » supplémentaire afin de faciliter le procédé d'implantation chirurgicale. Ce guide nerveux a été soumis pour l'obtention d'un brevet européen le 12 juillet 2017 et cela est le sujet d'un deuxième article qui a été soumis pour publication.

La deuxième partie de cette étude explore des possibilités d'une fonctionnalisation du matériau afin d'améliorer son efficacité pour la régénération nerveuse. Cette étude explore la fonctionnalisation de la fibroïne de soie avec une deuxième protéine, plusieurs facteurs de croissance, et des nanoparticules. Chacune de ces fonctionnalisations donne une possibilité d'ajouter des propriétés favorable à la fibroïne de soie, un matériau naturel et biocompatible.

La troisième partie de cette étude examine l'efficacité d'un guide nerveux composé de la fibroïne de soie fonctionnalisée avec des facteurs de croissance pour la régénération nerveuse périphérique en comparaison avec un guide nerveux composé de la fibroïne de soie sans aucune fonctionnalisation et une suture direct (qui simule une autogreffe). Trois techniques d'évaluation différentes de la régénération nerveuse ont été réalisées afin d'obtenir une analyse plus complète. Il y a de nombreux mécanismes impliqués dans la régénération nerveuse, il est donc nécessaire d'étudier différents paramètres pour analyser l'efficacité de régénération. Les résultats d'analyses histologiques, d'électromyographie, et de capture de mouvement, ont été considérées ensemble afin d'arriver à une conclusion sur la réussite d'une régénération nerveuse pendant cette étude. Pour conclure cette étude, les guides nerveux fonctionnalisés avec une combinaison de facteurs de croissance démontrent une meilleure régénération nerveuse et une récupération de fonction supérieure.

Table of Contents

List of Figures

Chapter 1

Chapter 2

Chapter 3

Part 1

Part 2

Part 3

List of Tables

Chapter 1

Chapter 3

Part 3

List of Abbreviations

BPheptyne	1-hydroxy-1-phosphonohept-6-ynyl)phosphonic acid
CA	Carbonic anhydrase
CE	Cholinesterase
CNS	Central nervous system
CNPase	Cyclic nucleotide protease
CNTF	Ciliary neurotrophic factor
DMSO	Dimethyl sulfoxide
DRG	Dorsal root ganglion
FN	Fibronectin
FTIR	Fourier-transform infrared spectroscopy
GF	Growth factor
GNP	Gold nanoparticle
HBSS	Hank's balanced salt solution
HE	Hematoxylin and eosin
IONP	Iron oxide nanoparticle
L929	Mouse fibroblast cell line
LiBr	Lithium bromide
MAG	Myelin associated glycoprotein
MBP	Myelin basic protein
Na_2CO_3	Sodium carbonate
NCAM	Neural cell adhesion molecule
NGC	Nerve guidance conduit
NGF	Nerve growth factor
NT-3	Neurotrophin-3
P0	Protein zero
PCL	Poly(ε-caprolactone)
PBS	Phosphate buffer saline
PEO	Poly(ethylene oxide)
PLP	Myelin proteolipid protein
PMP22	Myelin protein 22
PNS	Peripheral nervous system
SEM	Scanning electronic microscope
SF	Silk fibroin
TENG	Tissue engineered nerve graft

Chapter 1

Introduction

1. Context

Injuries to the peripheral nervous system affect a large population globally each year. Vehicular crashes are the most frequent cause of peripheral nerve injuries, with other common physical injuries including construction accidents, sports injuries, and combat-related trauma (Gu et al., 2011; Koppes & Thompson, 2015). Motorcycle accidents often result in an injury to the brachial plexus due to shoulder dislocations from falls at high speeds, while injuries from combat often affect the radial and ulnar nerves (Koppes & Thompson, 2015). However, approximately 75% of extremity trauma patients needing surgery sustain injuries at the median or digital nerves (in the wrist or the arm) (Koppes & Thompson, 2015). Lower extremity trauma are much less common, but most often affects the peroneal nerve (Kaiser, 2016). Millions of people are affected by nerve trauma and over 200,000 surgical procedures are performed annually in the United States for peripheral nerve injuries (Kehoe et al., 2012; Gaudin et al., 2016) as nerve gaps measuring at least 5 mm are unlikely to result in successful repair without a support (Kehoe et al., 2012; Cunha et al., 2011).

Since the 17th century, when the first end-to-end nerve suture technique was reported (Little et al., 2004; Gu et al., 2011), attempts to improve the efficacy of clinical nerve repair have continued. Throughout World War I and World War II, allografts and tubulation techniques were being extensively studied for nerve repair with disappointing results (Little et al., 2004). The autograft was first reported in the late 19th century by Ferrara (Dellon & Dellon, 1993), but it wasn't until 1947 that Seddon published results of satisfactory results of approximately 39-52% of patients who underwent autograft procedures (Little et al., 2004). Nerve autograft procedures gained popularity in the 1960s and became the generally preferred method in the 1970s (Grinsell & Keating, 2014). The nerve autograft is known to yield satisfactory results in only about 50% of patients (Safa & Buncke, 2016) and, despite continuous research effort, is still considered the gold standard technique for nerve repair today (Grinsell & Keating, 2014; Liu et al., 2015).

The need for a superior alternative to the nerve autograft is evident due to the drawbacks of this procedure such as the need for an additional surgical procedure, the loss of function at the donor site, and the risk of developing a painful neuroma at the donor site. In response, tissue engineered nerve grafts have recently been extensively studied with the goal to provide a

replacement to the nerve autograft yielding greater success in nerve regeneration and fewer disadvantages concerning the clinical technique. Therefore, the goal of this work was to develop an effective alternative to the nerve autograft using a natural biomaterial-based tissue engineered nerve graft.

2. The Nervous System

The mammalian nervous system is made up of the central nervous system (CNS) and the peripheral nervous system (PNS) that work together directly through chemical and electrical communication networks. The CNS comprises the brain and the spinal cord while the PNS consists of all cranial and spinal nerves that branch out from the CNS to the periphery. The CNS and PNS each contain several types of neurons and glial cells specific to each system that are able to communicate with each other and support the proper functioning of the nervous system as a whole.

2.1. The central nervous system

Six components of the brain exist as well as several components of the spinal cord, which together make up the human CNS. The subdivisions of the brain include the cerebrum, the diencephalon, the cerebellum, the midbrain, the pons, and the medulla oblongata. Among the components of the spinal cord, the ventral and dorsal roots contain portions of motor and sensory neurons respectively. Neurons found in the CNS are almost exclusively interneurons which communicate with each other as well as between afferent and efferent neurons located mainly in the PNS. In addition to neurons, the CNS contains several different types of neuroglia including astrocytes, oligodendrocytes, microglia, and ependymal cells which serve to support and nourish the neurons aiding in proper function.

2.2. The peripheral nervous system

The PNS includes all cranial and spinal nerves allowing communication between the CNS and the receptors, muscles, and glands throughout the body. Similar to the CNS, the PNS contains certain types of glial cells, including Schwann cells and satellite cells, and neurons, including

efferent and afferent neurons. The PNS is divided into two subdivisions: the autonomic nervous system and the somatic nervous system.

2.2.1. The autonomic nervous system

The autonomic nervous system is responsible for regulating involuntary bodily processes. Stimuli from sensory receptors are communicated to the CNS by sensory nerves were the information is processed and the response is sent to target organs by autonomic motor nerve cells. Examples of target organs in the autonomic nervous system include smooth muscle, cardiac muscles, blood vessels, and glands (Farley et al., 2014). A few functions of the autonomic nervous system include digestion, regulation of body temperature, urination, regulation of heart rate, and production of bodily fluids. The autonomic system is comprised of two subdivisions: the sympathetic nervous system and the parasympathetic nervous system (Figure 1).

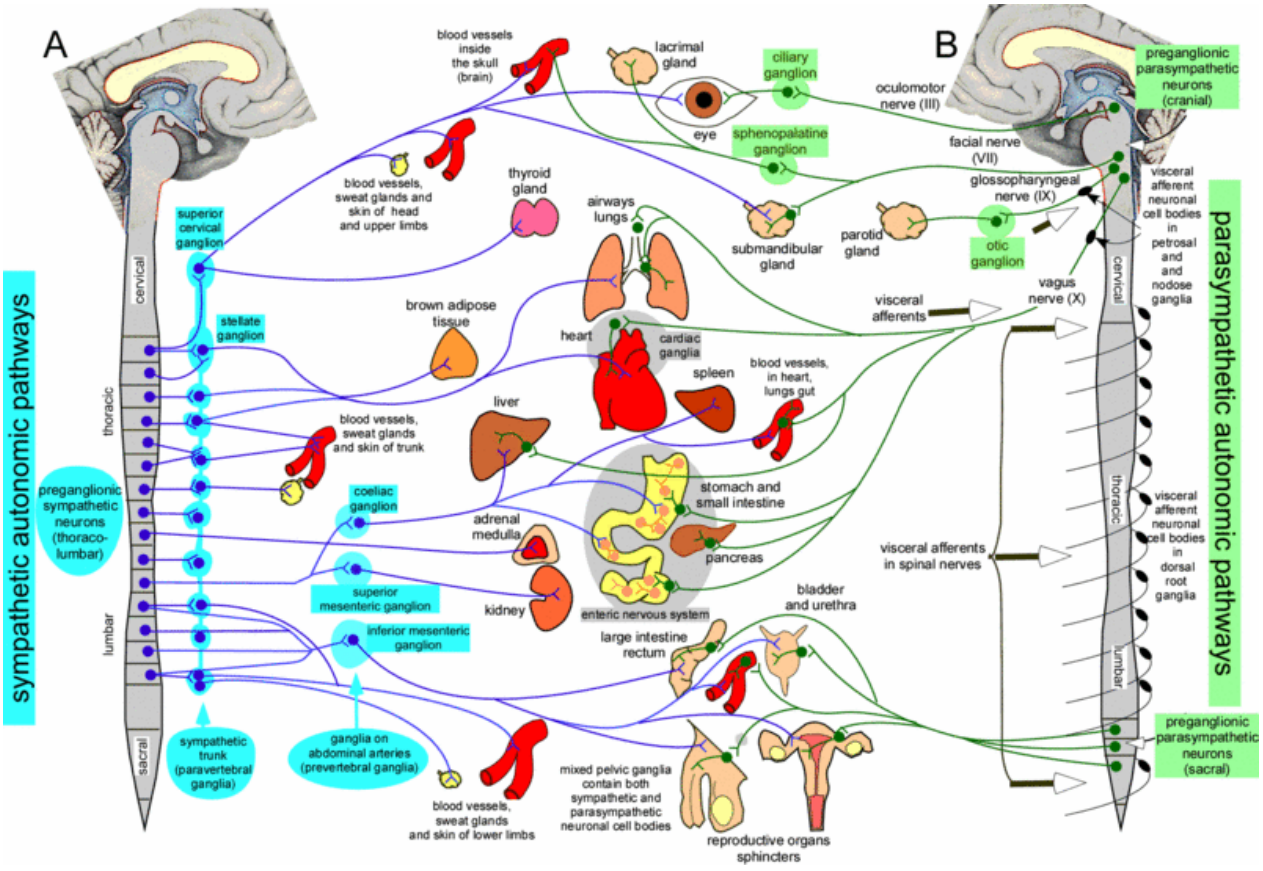

Figure 1. The sympathetic and the parasympathetic pathways in the autonomic system of the peripheral nervous system (Blessing & Gibbins, 2008).

Sympathetic system pathways are triggered in situations of stress which result in what is commonly referred to as the fight or flight response. Sympathetic nervous responses may include bronchodilation (allowing increased airflow to and from the lungs), increased sweat gland activation, pupil dilation, and elevation of heart rate and blood pressure (Farley et al., 2014; Blessing & Gibbins, 2008). The sympathetic division is most attributed to be responsible for stressful situational responses, but there are also many pathways that are continuously being activated in order for the body to function properly day to day. Examples of common sympathetic activity includes control over central blood pressure, excessive water loss prevention in the gastrointestinal tract, and sweating to control body temperature (Blessing & Gibbins, 2008).

The parasympathetic nervous system, in contrast to, yet working in harmony with the sympathetic nervous system, is predominantly activated during rest. Examples of parasympathetic activation include control over secretory glands in order to regulate saliva, tears, and mucus, pupil diameter regulation, bronchoconstriction, decreasing heart rate, and stimulated secretion of digestive enzymes (Farley et al., 2014; Blessing & Gibbins, 2008).

2.2.2. The somatic nervous system

The somatic nervous system therefore is responsible for voluntary movements through the efferent neurons innervating skeletal muscles as well as afferent nerve cells that communicate interpreting external stimuli. There are four modalities of the sensory somatic system that together (1) permit the sensation of external objects in contact with the body and (2) provide bodily self-awareness. The first is discriminative touch, allowing a person to recognize pressure, vibration, shape, and the texture of an object. The second modality is nociception which is the ability to feel itching and pains such as sharp pains, dull burning pains, and deep aching pains. The third modality is proprioception which allows a person to recognize position and movement of the body such as muscle tension, joint pressure, and joint angle. The fourth modality is temperature allowing a person to distinguish between cold, cool, warm, and hot temperatures.

2.3. Cells of the nervous system

There are two principal cell types that are critical for the proper development and function of the nervous system: neurons, also known as nerve cells, and neuroglia, or glial cells. There are an estimated 100 billion neurons in the human body and about ten times as many glial cells (Azevedo et al., 2009). Neurons are the only cells in the nervous system responsible for the processing of information through electrical connections, while glial cells hold important roles not only assisting in in the support of neurons, but also maintaining efficiency in normal neural function (Birch, 2013; Jessen, 2004).

2.3.1. Glial cells

Once thought only to provide support, protection, and nutrition for the neurons within the nervous system (Ndubaku & de Bellard, 2008), glial cells are now understood to be responsible for performing important functions during neural development, assisting in healthy, developed function, and reacting to trauma or disease (Jessen, 2004). Glial cells are most commonly known for their formation of myelin that surrounds a nerve fiber allowing for more efficient conduction and faster transport of information. In more recent years, it has been discovered that glial cells are also essential elements to the formation and maintenance of synapses, the key functional unit in the nervous system allowing neurons to communicate with each other and to other cells (Verkhratsky & Butt, 2007). During development, glial cells are the support units creating a cellular framework for the formation of a functional nervous system (Jessen, 2004). Given the specific needs of the CNS and PNS, different types of glial cells are found in each system. Glia occupying the CNS include macroglia (astrocytes, oligodendrocytes, and ependymal cells) and microglia, and glia found in the PNS include Schwann cells, satellite cells, and enteric glial cells (Verkhrasty & Butt, 2007; Jessen, 2004).

2.3.1.1. Glia of the central nervous system

Astrocytes are the most abundant glial cells found in the CNS (~80%), accounting for around half of the volume of the CNS (Jessen, 2004). They received their name in 1893 by Michael von Lenhossek because of their star-like shape formed by the many cytoplasmic extensions from

the cell body that intertwine between nerve fibers and neuron cell bodies (Figure 2) (Ndubaku & de Bellard, 2008). The two main types of astrocytes are the protoplasmic astrocytes which are found in CNS grey matter and have many processes measuring about 50 µm on average and the fibrous astrocytes found in white matter with longer extensions measuring up to 300 µm (Verkhrasty & Butt, 2007). Astrocytes are known to connect blood vessels and neurons at synapse, but more recently have also been found to control the activity of surrounding non-neuronal cells (Volterra & Meldolesi, 2005). They also proliferate in proximity to sites of trauma for healing in the CNS (Silver & Miller, 2004).

Oligodendrocytes are highly specialized cells, accounting for about 5% of all glia in the CNS, that produce myelin, a lipid-rich insulation layer surrounding nerve fibers which are responsible for speeding up electrical impulse conduction. The myelin isolates the ionic channels of the enveloped axons and is therefore able to accelerate action potential propagation by saltatory conduction (Verkhrasty & Butt, 2007). Oligodendrocytes have fewer and shorter processes than astrocytes (often between ten and twenty) which are each capable of myelinating a separate nerve fiber (Ndubaku & de Bellard, 2008).

Ependymal cells constitute about 5% of glia in the CNS. This macroglia subtype forms a barrier between cells and cerebrospinal fluid acting as the intermediary for nutrient exchange. Ependymal cells are multiciliated and are responsible for the production and circulation of the cerebrospinal fluid through the brain and the spinal cord (Spassky et al., 2005; Verkhrasty & Butt, 2007).

Microglia (10-15% of CNS glia) originate from macrophages during early brain development and make up the brain immune system. These cells have many thin, branched, motile processes and are present throughout the brain each with their own domain. The processes are continually extending and contracting constantly scanning their territory for abnormalities. In fact, the entire brain can be fully surveyed by its microglia in several hours (Verkhrasty & Butt, 2007). When introduced to trauma or disease, microglia become activated as the brain's defense system and gain the capability to migrate to the damaged area, proliferate, and phagocytose (Kettenmann et al., 2011).

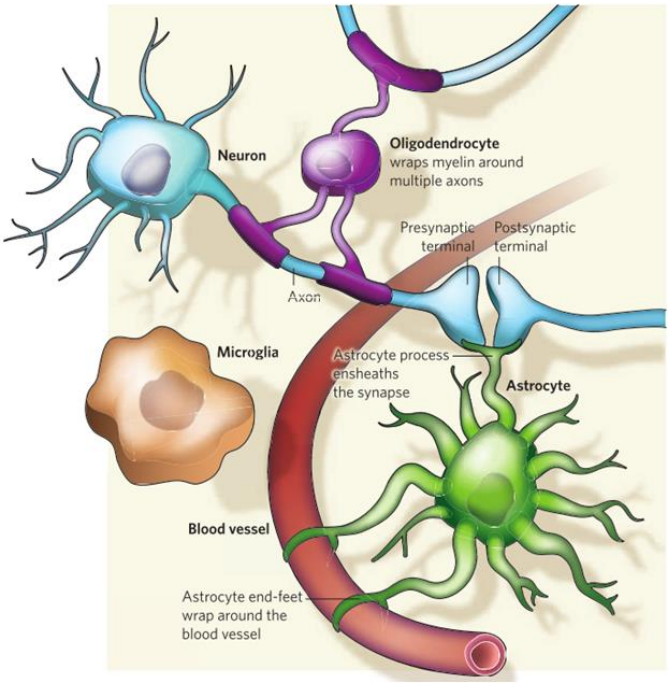

Figure 2. Interactions of glial cells, tissue, and neurons in the central nervous system (Allen & Barres, 2009).

2.3.1.2. Glia of the peripheral nervous system

Glial cells similar to the oligodendrocytes of the CNS due to their capability of myelinating neurons were discovered in the PNS by Theodore Schwann in 1839 (Bhatheja & Field, 2006) and the term Schwann cell was coined by Louis Ranvier in 1871 (Ndubaki & de Bellard, 2008). Schwann cells are the most abundant glial cells found in the PNS accounting for about 80% of all cell nuclei within the endoneurium, the smallest structural pathways of peripheral nerves and nerve roots (Birch, 2013). Like the neuroglia found in the CNS, Schwann cells are not only responsible for support and trophic properties, but also directing developing and regenerating neurons, regulating the microenvironment, signaling, and eliminating cellular debris (Verkhratsky & Butt, 2007; Bhatheja & Field, 2006).

Schwann cells develop from the neural crest, a group of cells originating in the dorsal section of the neural tube (Birch, 2013). In the beginning of development, neural crest cells form precursor Schwann cells. Precursor Schwann cells have not yet ensured their survival and depend entirely on signals from axons in order to avoid apoptosis (Jessen & Mirsky, 2005). Precursor Schwann cells then form immature Schwann cells around the time of birth that hold the potential

to further differentiate into four different types of Schwann cells: myelinating Schwann cells, non-myelinating Schwann cells, perisynaptic Schwann cells of neuromuscular junctions, and terminal Schwann cells of sensory neurites (Verkhratsky & Butt, 2007).

Immature Schwann cells start to ensheath the nerve fibers of the PNS before differentiation into mature Schwann cells; the Schwann cell lineage is highly dependent on the size of the axons with which it is in contact (Verkhratsky & Butt, 2007). Immature Schwann cells in contact with large axons (axons with a diameter larger than the critical diameter of about 0.7 µm) will differentiate into myelinating Schwann cells (Figure 3).

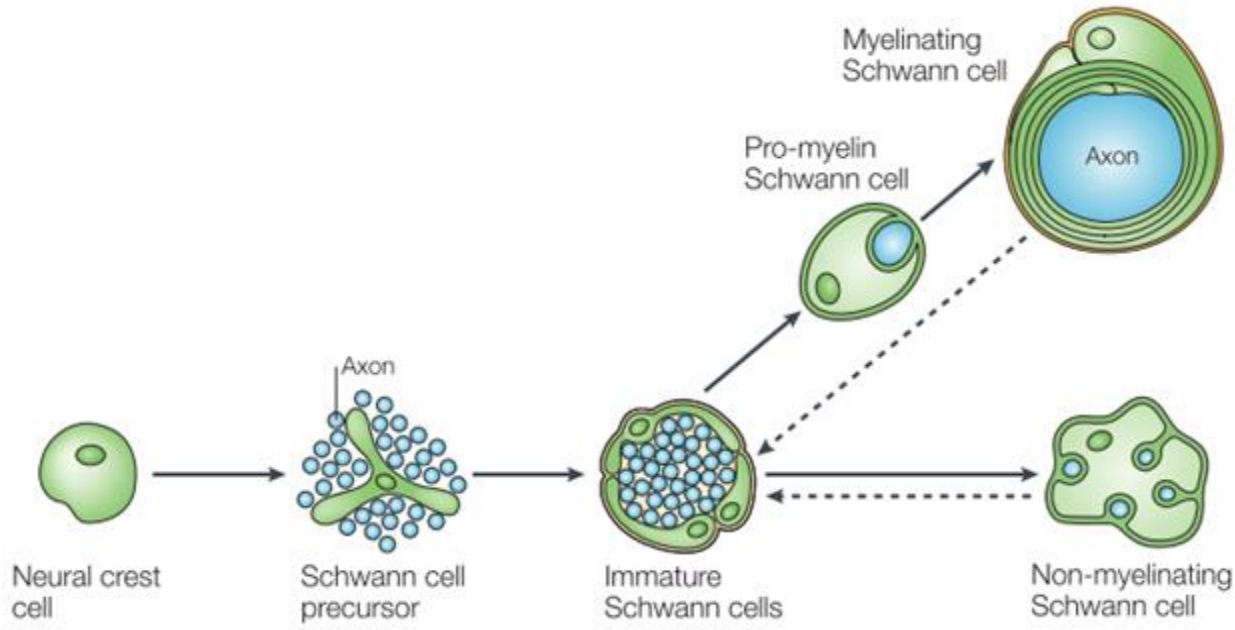

Figure 3. The development and differentiation of myelinating and non-myelinating Schwann cells from a neural crest cell. (Jessen & Mirsky, 2005)

Immature Schwann cells initially envelop several nerve fibers, but then migrate to myelinate a single axon as the cells differentiate into mature myelinating Schwann cells (Ndubaku & de Bellard, 2008). Mature myelinating Schwann cells eventually line the length of an axon and, similar to oligodendrocytes in the CNS, form a myelin sheath around the axon increasing the conduction velocity of electrical impulses as seen in Figure 4. Conduction velocity of an unmyelinated axon is directly related to the diameter, therefore the transport speed of

information in large diameter axon would be inefficiently slow without the insulation of the myelin sheath (Allen & Barres, 2009).

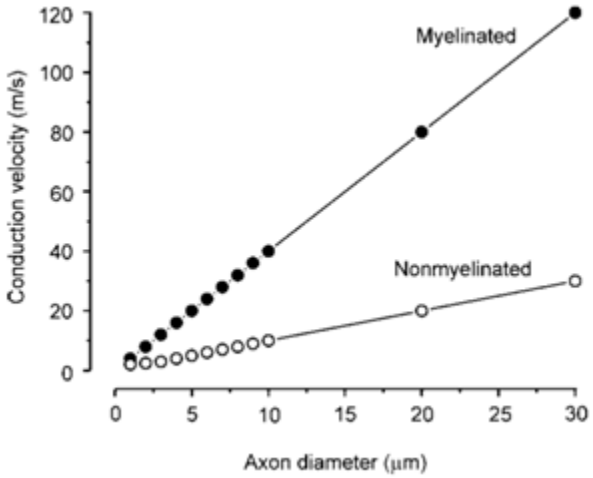

Figure 4. Relationship between axon diameter and conduction velocity of myelinated and non-myelinated axons (Verkhratsky & Butt, 2008).

In order to produce the myelin sheath, Schwann cells wrap its membrane around the axon in a spiraling movement (as depicted in Figure 5), extruding nearly all cytoplasm while compacting the stacked membrane bilayers, and increasing the membrane area several thousand fold (Jessen, 2004). The layers of compacted membrane of myelin is referred to as lamellae, and the quantity of lamellae along with the length of myelin along the axon, or internode, are determined by the diameter of the axon and determine conduction properties including the speed of conduction. There can be between 10 and 100 lamellae and internode lengths between 100 and 1000 µm (Verkhratsky & Butt, 2007).

The myelin sheath is made up of layers of Schwann cell membrane and is therefore composed mostly of lipids (around 70%) in addition to several different membrane proteins. The primary membrane protein of myelin produced by Schwann cells, accounting for between 50 and 60% of membrane proteins in PNS myelin, is protein zero (P0) which has essential adhesive properties that facilitate myelin formation. Other membrane proteins found in PNS myelin include myelin basic protein (MBP) (5-15% of myelin proteins), myelin protein 22 (PMP22) (2-5% of myelin proteins), myelin associated glycoprotein (MAG) (~0.1% of myelin proteins), myelin

proteolipid protein (PLP), and cyclic nucleotide protease (CNPase) and are also essential for the compaction of the cell membrane forming lamellae (Birch, 2013; Verkhratsky & Butt, 2007).

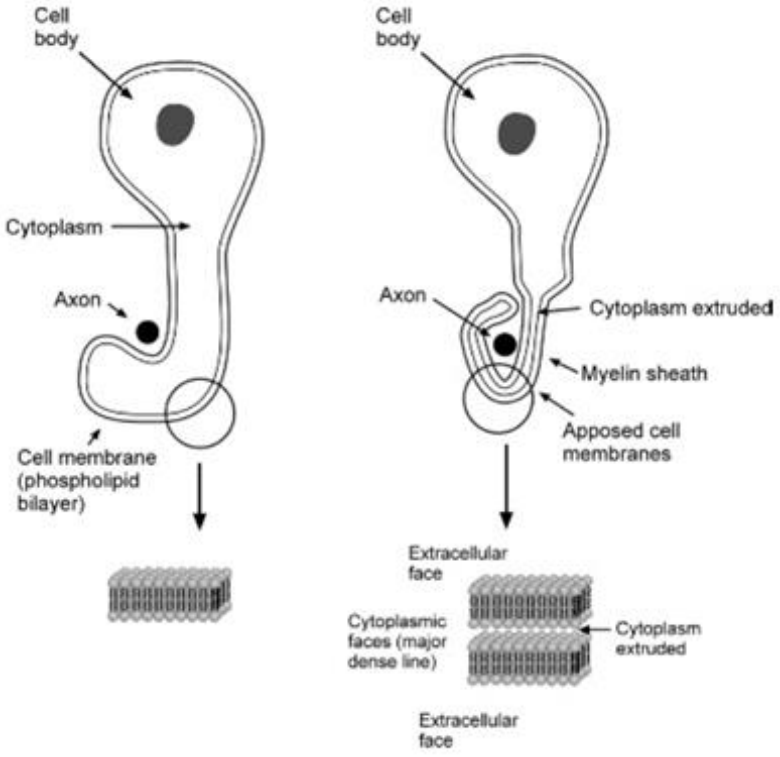

Figure 5. Myelination of an axon in the peripheral nervous system by a Schwann cell (Verkhratsky & Butt, 2008).

Immature Schwann cells connected with axons smaller than the critical diameter (~0.7 µm) will not produce myelin and undergo ensheathment of several nerve fibers in the PNS creating a structure called a Remak bundle (Bhatheja & Field, 2006). This type of non-myelinating Schwann exhibits several surface characteristics identical to immature Schwann cells such as the neural cell adhesion molecule (NCAM) which provides support to unmyelinated axons while also providing a physical boundary preventing ephaptic transmission between the unmyelinated axons (Verkhratsky & Butt, 2007).

The final two types of mature Schwann cells are terminal Schwann cells found at motor and sensory terminals. The processes of terminal Schwann cells are integrated closely at nerve terminals and are essential regulators of synapses as seen in Figure 7. (Verkhratsky & Butt, 2007).

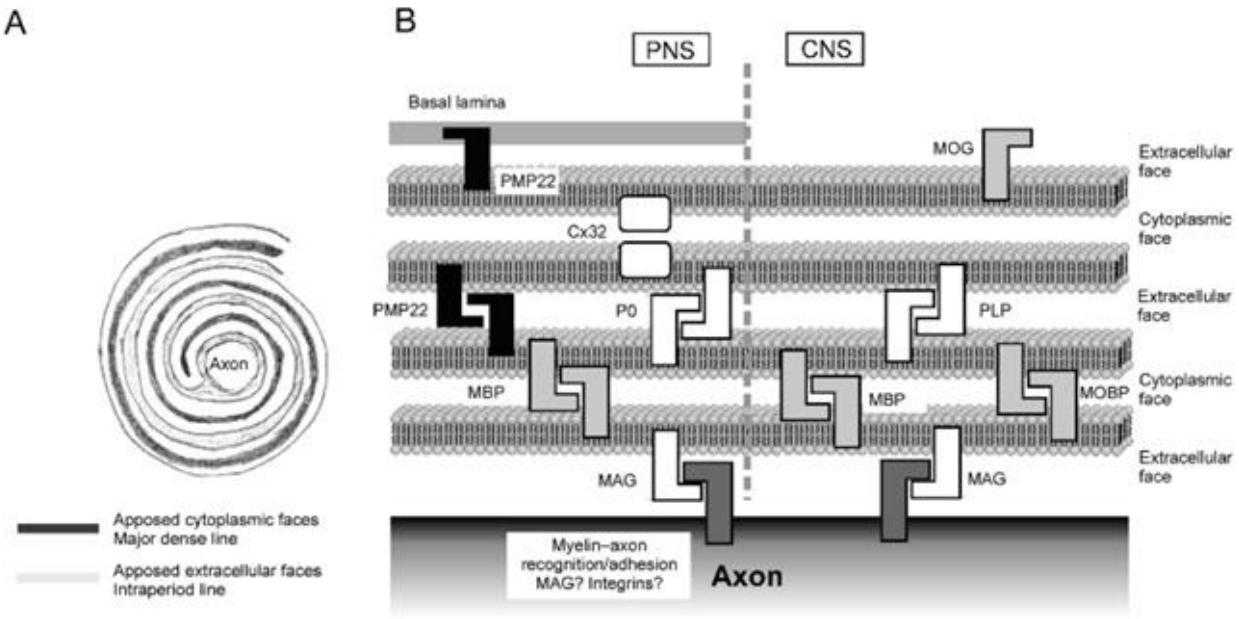

Figure 6. Composition of the myelin sheath of a Schwann cell in the peripheral nervous system and an oligodendrocyte in the central nervous system (Verkhratsky & Butt, 2008).

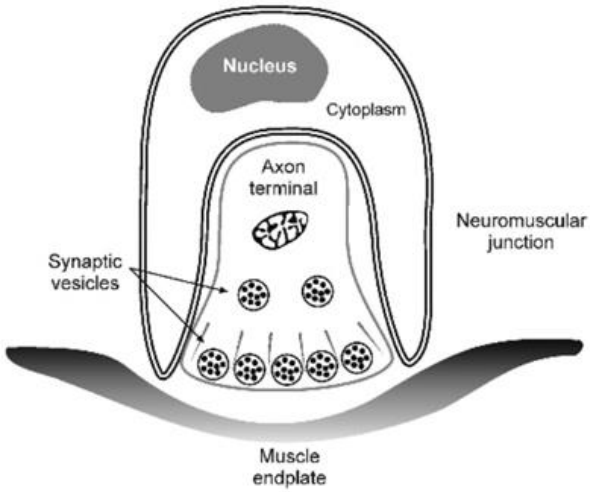

Figure 7. A perisynaptic Schwann cell in the peripheral nervous system (Verkhratsky & Butt, 2008).

Dissimilar to glial cells in the CNS, Schwann cells have an exceptional response to the injury of the nerve. Once Schwann cells lose contact with the axon after trauma, they will de-differentiate back to immature Schwann cells in order to prepare for nerve regeneration. Unlike precursor Schwann cells, immature and mature Schwann cells have the capacity to survive without the contact of a nerve fiber. Schwann cells begin to clear cellular debris and proliferate guiding the regenerating axons by signaling and providing a physical support (Jessen & Mirsky, 2005).

Satellite cells and enteric glial cells are secondary types of glial cells found in the PNS and are much less abundant that Schwann cells. Satellite cells are glial cell that surround the neuron cell bodies in dorsal root ganglia and autonomic ganglia providing support and nourishment (Birch, 2013; Jessen & Mirsky, 2005). Enteric glial cells are found in the autonomic ganglia in the gastrointestinal tract and have a form and biochemistry similar to astrocytes of the CNS (Jessen, 2004).

2.3.2. Neurons

Neurons are the most highly specialized cells in the human body pertaining to intercellular communication and are the functional foundation of the nervous system. These cells are capable of receiving, processing, and communicating information through electrical and chemical signals between themselves and innervated tissue throughout the body. Neurons are non-dividing cells, and therefore possess extreme longevity. Depending on the type and position in the nervous system, the size of a neuron can be between around 20 µm in diameter to up to 2 meters long (Bear et al., 2007).

The three main structural segments of the neuron are the soma, the dendrites, and the axon (Figure 8.). The soma, or the cell body, of neurons are either located in the CNS (including all CNS neurons and PNS somatic efferent neurons), or within ganglia located in the PNS. Found in the cytoplasm of the soma are all organelles commonly found in animal cells with the exception of centrioles which are organelles specific for assisting in cell division. Rough endoplasmic reticulum and mitochondria are particularly important in proper neuronal function and are in

abundance in the neuron cell body compared glial cells and other non-neuronal cells (Bear et al., 2007).

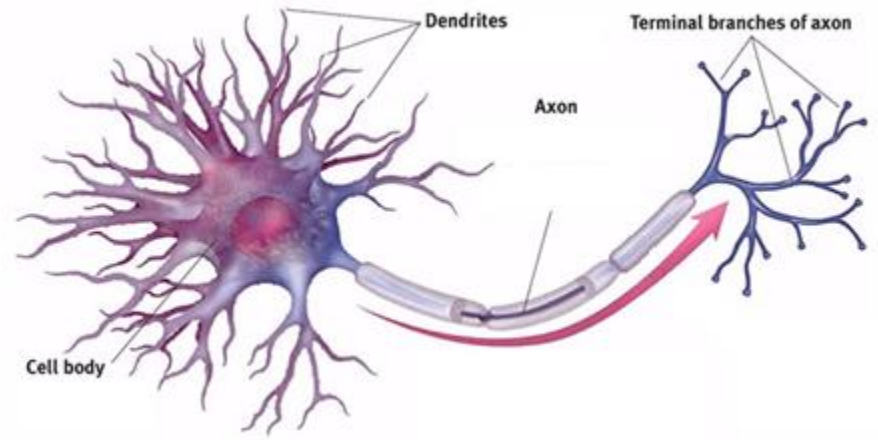

Figure 8. Diagram of a multipolar neuron and its structural components.

One of the types of processes of a neuron is the dendrite. Neurons often have several or many of these extensions with branches called dendritic branches covered in thousands of synapses facilitating the retrieval of information. The second type of neuronal process is the axon. There is only one axon for each nerve cell and it is a highly specialized structure of the neuron that allows the transportation of electrical impulses throughout the body in order for the nervous system to communicate. Axons no not contain any rough endoplasmic reticulum and virtually no free ribosomes which means that there is no protein synthesis in the axon. Information is therefore relayed over the distance of the axon by membrane proteins (Bear et al., 2007). The point at which the axon joins the cell body is called the axon hillock and is where action potential usually occurs.

Neurons can be classified in a few different groups depending on the number of neurites they have. For example, a neuron contained a single neurite is classified as a unipolar neuron, a neuron containing two neurites is classified as bipolar, and a neuron containing 3 or more neurites is classified at multipolar (Figure 9) (Bear et al., 2007).

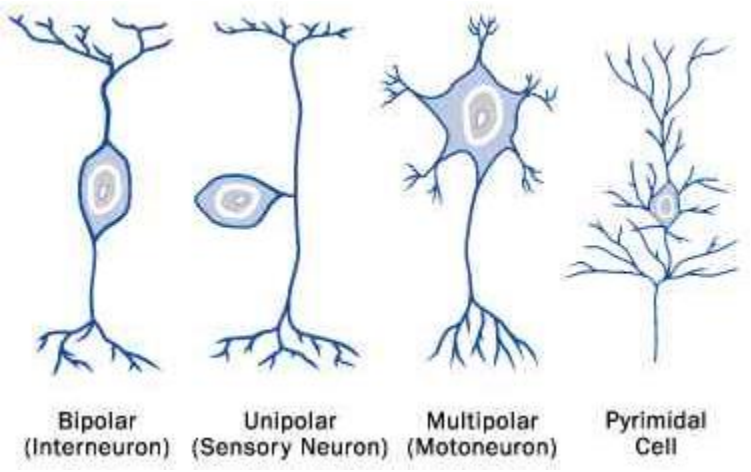

Figure 9. Diagram of the classification of neurons by morphology and number of neurites.

Neurons can also be classified by their function. In the peripheral nervous system, there are sensory neurons and motor neurons. Sensory neurons are unipolar neurons that form the afferent signaling route which propagates from the peripheral nerve terminals toward the CNS. The cell bodies of sensory neurons are located in the dorsal root ganglia as seen in Figure 10. Motor neurons are multipolar neurons make up the efferent pathways driving information from the brain toward muscles and signaling glands (Kendel and Schwartz, 2013). Motor neuron cell bodies are located in the ventral horn of the spinal cord (Figure 10). Other neurons can interneurons serve as liaisons between peripheral neurons and central neurons.

When either motor or sensory neurons are regenerating, growth cones can be found at the tip of the axonal extensions and they are finger-like extensions searching for the most favorable environment towards which to grow (Figure 11). The phenomenon of this guidance factor is called chemotropism and has been proven true for the orientation of nerve extensions (Fuh et al., 2013). At the end of these growth cones are filopodia that extend and retract under the influence of the environment. There are made up of mainly cytoskeleton molecules but also membrane proteins specialized in adhesion and environmental exploration. These structures contain specific receptors that induce significant growth while interacting with guidance molecules (Claudepierre et al., 2008). When a growth cone meets an unfavorable environment it has the tendency to retract to find a more favorable environment toward which to orient itself.

The four mechanisms that guide a growth cone are attraction mediated by contact, repulsion mediated by contact, chemoattraction, and chemorepulsion (Goodman, 1996).

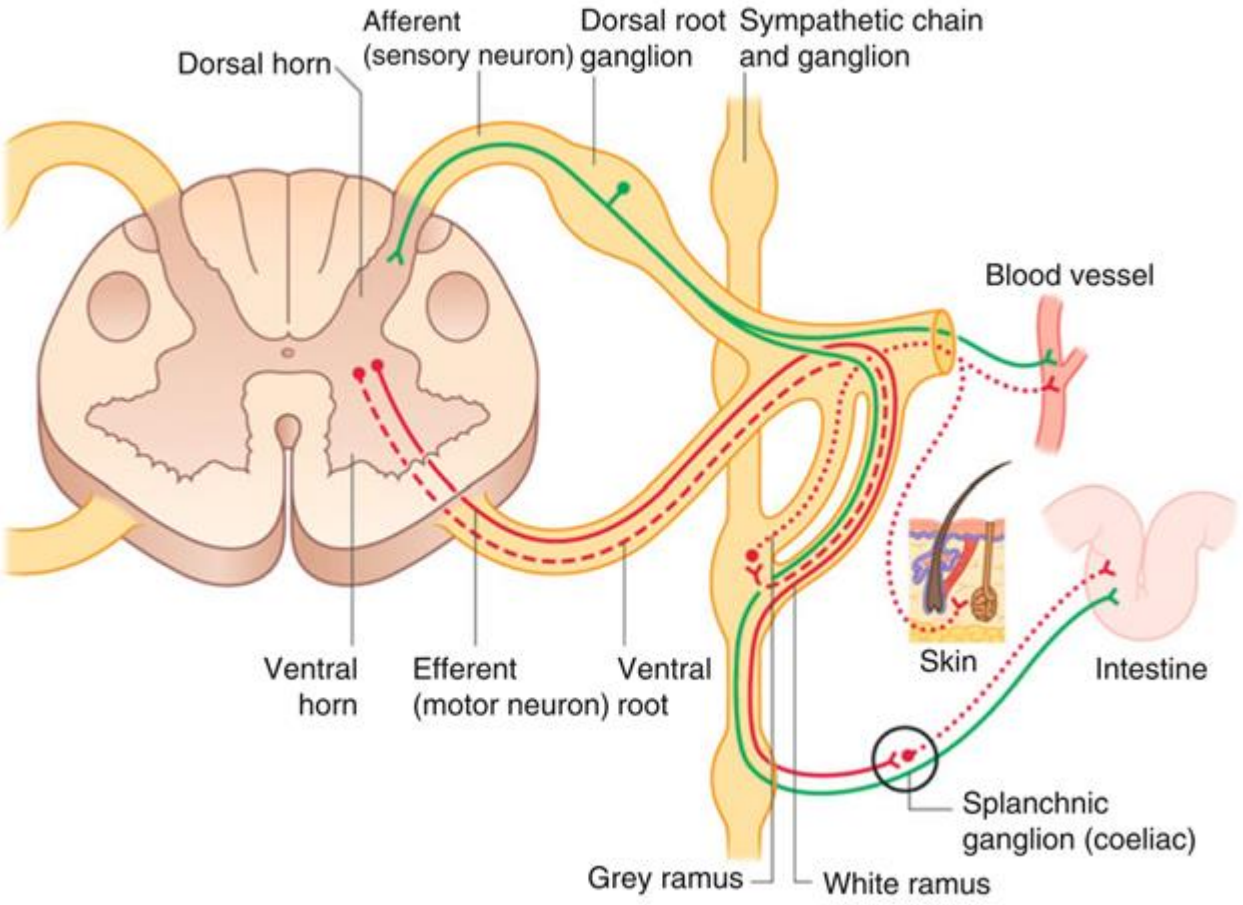

Figure 10. Diagram of the cross section of the spinal cord depicting the location and paths of motor and sensory neurons in the peripheral nerve regeneration (Birch, 2013).

Finally, neurons contain axon terminals that intervene in cellular communication. These terminals are composed of terminal buttons containing synaptic vesicles. These structures enclose neurotransmitters that influence the activity of other cells by their release.

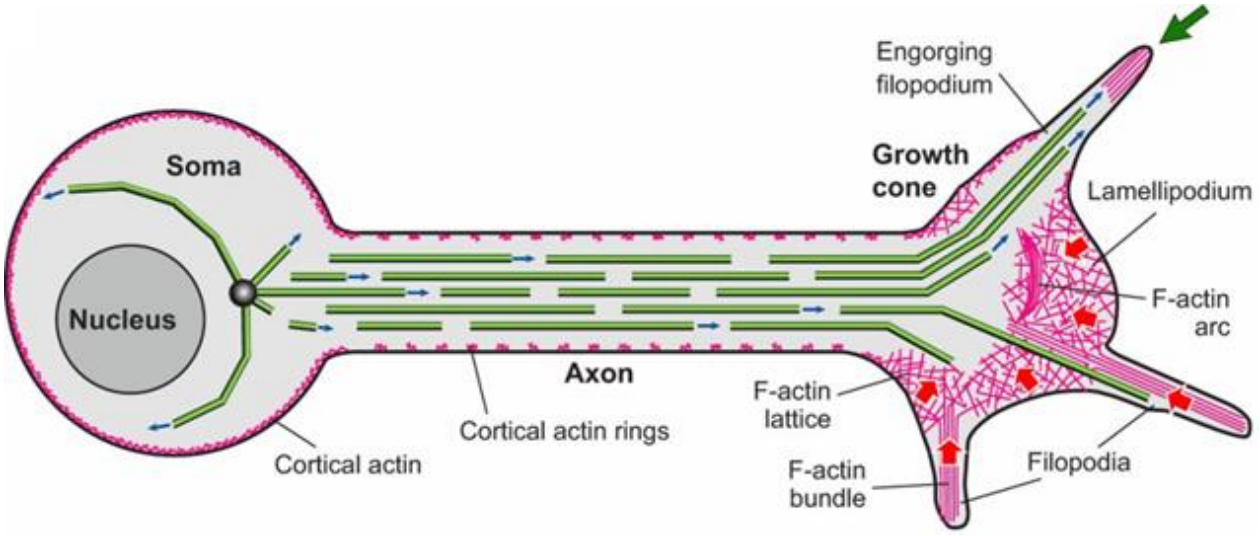

Figure 11. Depiction of a growth cone in the peripheral nerve regeneration.

2.4. Action Potential and Synapse

2.4.1. Action potential

Neural communication is carried out through electrical impulses which is a consequence of external stimuli. The plasma membrane of a neuron has a resting electrical potential of about -70 mV which represents the difference in charge between interior and the exterior of the cell (the exterior of the cell is positively charged and the interior of the cell is negatively charged) (Marieb, 2006). This difference in charge is maintained by membrane pumps and a selective permeability of specific ions at the plasma membrane. After an external stimulus, a large influx of sodium and potassium ions occurs as voltage-gated sodium and potassium channels open. A change in ionic concentration depolarizes the neuron and may allow the membrane potential to reach about +30 mV which will produce an action potential (Purves, 2005).

The moment an action potential is produced, a chain reaction throughout the axon occurs. The action potential causes a changes in the structures of voltage-gated ion channels which travels down the length of the axon. The propagation speed of this reaction depends on the myelination of an axons since one the channels found at the Nodes of Ranvier (located between myelinating Schwann cells along the length of the nerve fiber as depicted in Figure 12) (Marieb, 2006). The increased rate of action potential transmission is due to salutatory conduction which

refers to the action potentials jumping between Nodes of Ranvier. The result of an action potential is the release of neurotransmitters at a synapse.

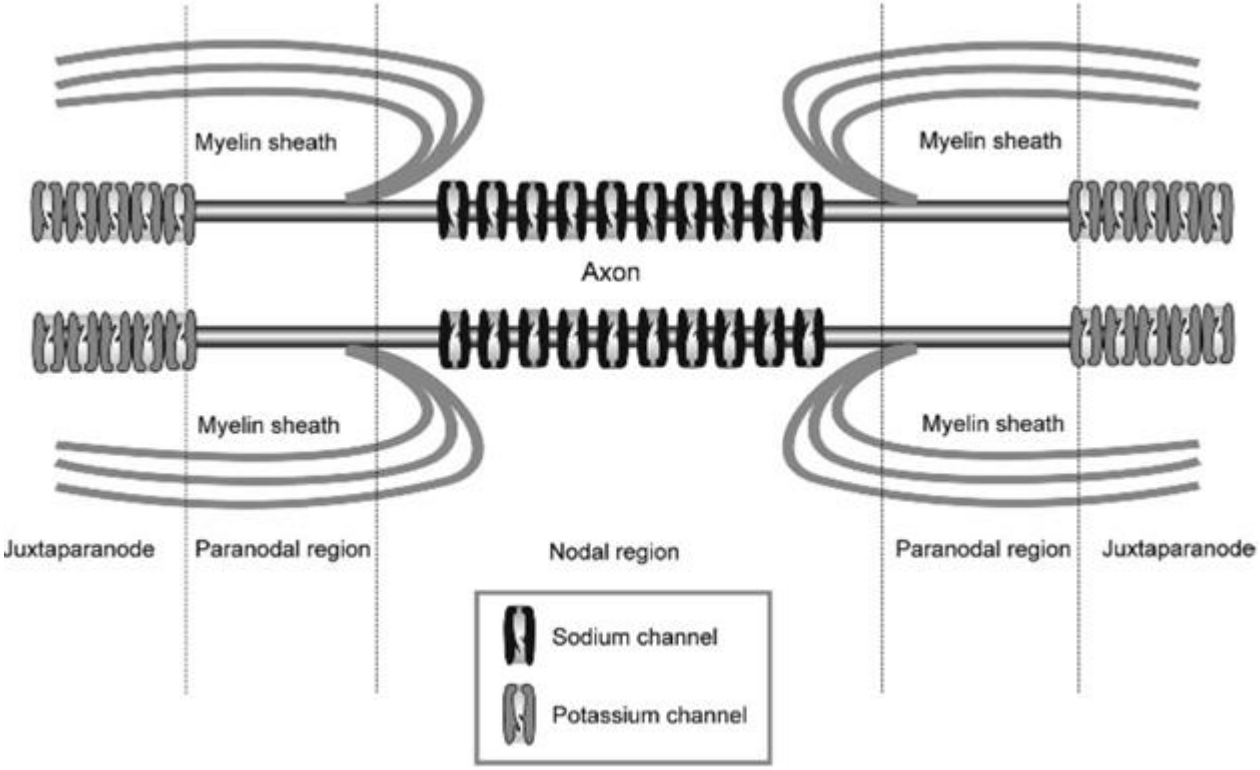

Figure 12. Representation of ion channels at the Node of Ranvier (Verkhratsky & Butt, 2008).

2.4.2. Synapse

Synapses are the junctions with other neurons or innervated tissue that permit a transfer of information from one cell to another. This junction was discovered by Charles Scott Sherrington in 1897 who named this site a synapse (Sherrington, 1906). A synapse involves a unidirectional current of neurotransmitters which are intermediaries of cell-to-cell communication consisting of presynaptic and postsynaptic elements (Bear, et al., 2007). The space between these two elements is called the synaptic cleft.

The presynaptic side at synapse is usually the axon terminal of a neuron which contains mitochondria and cytoskeletal filaments for sufficient energy and the transport of necessary synaptic elements for the transmission of information (Tansey, 2006). The postsynaptic element contains numerous receptors and channels on the surface of the cell membrane which assist in

the transfer of information. The synaptic cleft is about 30 nm wide and consists of an interstitial liquid where the physicochemical exchanges take place (Pereda, 2014).

Both chemical and electrical synapse occur within the nervous system (Figure 13). The most common synaptic transmission of information is assisted by chemical synapse, an indirect process that uses chemical messengers called neurotransmitters transported by synaptic vesicles. The production of an action potential eventually arrives at the axon terminal and causes calcium channels to open allowing calcium ions to enter the cell. The rapid increase of the concentration of calcium activates the production of synaptic vesicles containing neurotransmitters. The neurotransmitters then diffuse across the synaptic cleft and attach to receptor channels on the postsynaptic element. The neurotransmitters signal the opening or closing of membrane channels on the postsynaptic cell membrane. This communication may excite or inhibit the postsynaptic cell depending on the receptors involved during synapse (Pereda, 2014; Bear et al., 2007).

Electrical synapse are much less common than chemical synapse in the nervous system and contain a direct transmission to the postsynaptic element. Information is passed from cell to cell with the assistance of direct and passive ionic transport from gap junction channels (Figure 14) (Purves, 2001). The gap junctions are highly specialized and align with paired channels on the presynaptic and postsynaptic cell membranes forming a pore that is larger than the pores of voltage-gated ion channels. There, there is a simple and direct diffusion of substances to the interior of the postsynaptic cell from the interior of the presynaptic neuron. The main purpose of electrical synapses is to allow synchronization of electrical activity between connected neurons (Purves, 2001).

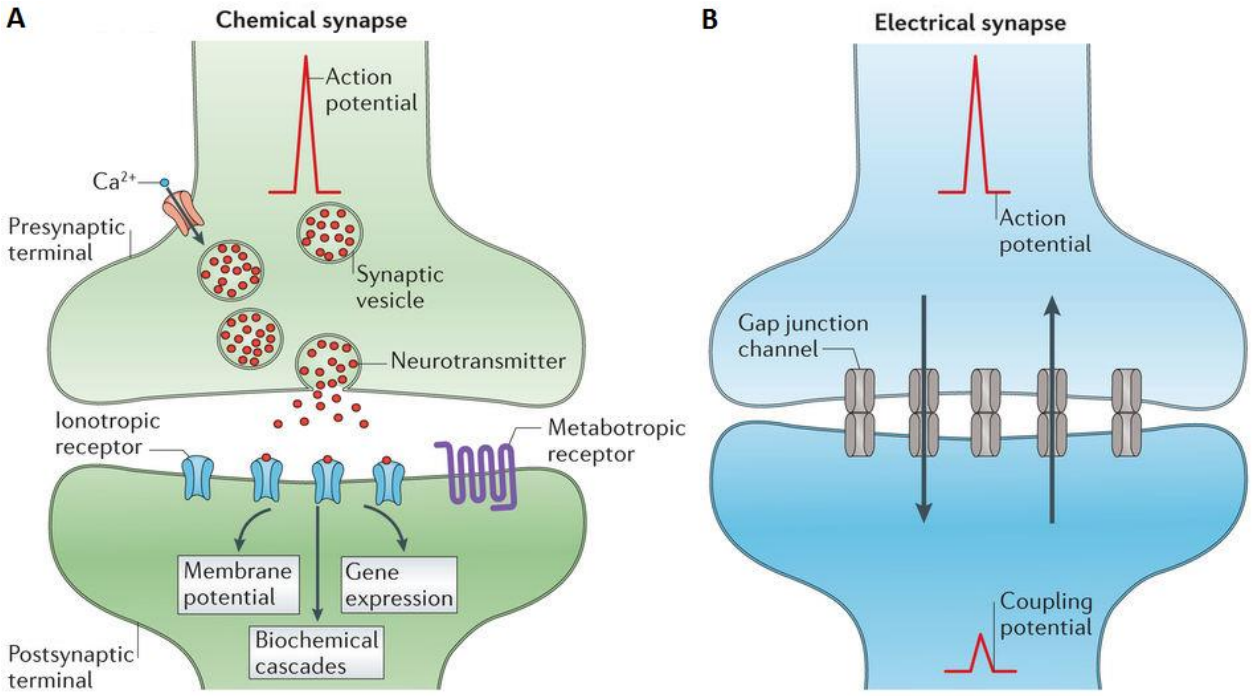

Figure 13. Depictions of chemical and electrical synapse of the nervous system (Pereda, 2014).

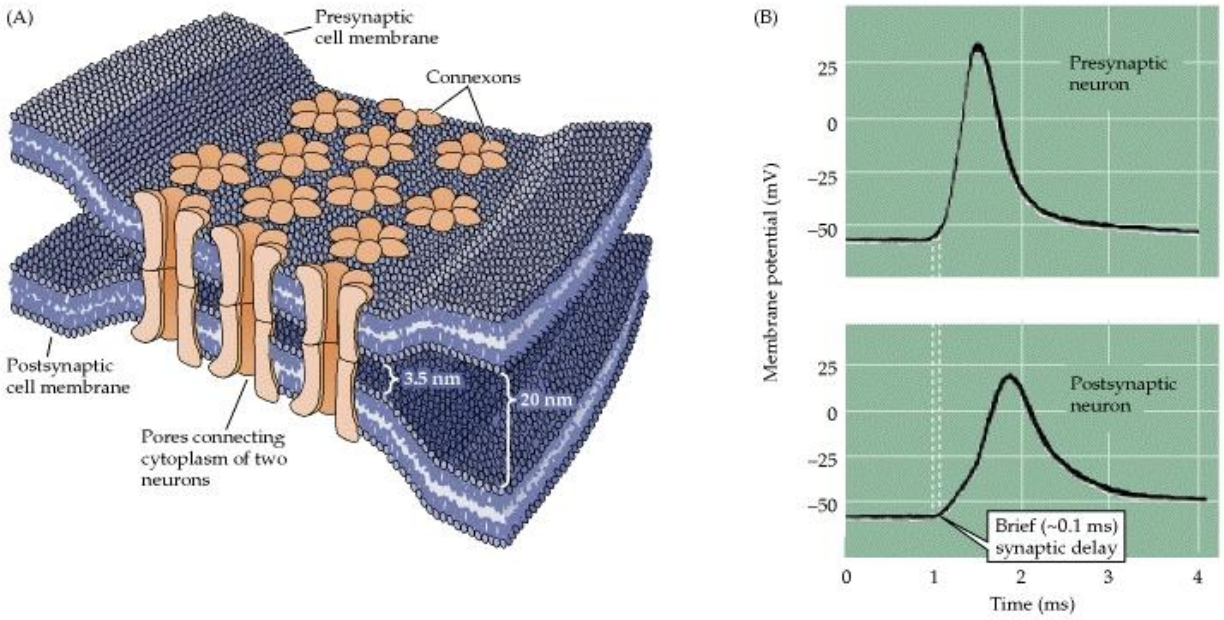

Figure 14. Illustration of gap junctions at an electrical synapse with membrane potential behavior graphics (Purves et al., 2001).

3. Nerve Injury and Repair Strategies

Nerve injury and recent repair strategies have been outlined in a review entitled “Recent strategies in tissue engineering for guided peripheral nerve regeneration” published in Macromolecular Bioscience in April, 2016 (doi: 10.1002/mabi.201500367).

Recent strategies in tissue engineering for guided peripheral nerve regeneration

Kayla Belanger, Tony M. Dinis, Sami Taourirt, Guillaume Vidal, David L. Kaplan, and Christophe Egles*

K. Belanger, Dr. T. M. Dinis, S. Taourirt, Dr. G. Vidal, Prof. C. Egles
Sorbonne University, Université de Technologie de Compiègne, CNRS, UMR 7338 Biomechanics and Bioengineering, Centre de Recherches Royallieur – CS 60 3019, 60203 Compiègne cedex, France
E-mail: kayla.belanger@utc.fr

Prof. D. L. Kaplan
Department of Biomedical Engineering, Tufts University, 4 Colby Street, Medford, MA, 02155, United States of America

Prof. C. Egles
Department of Oral and Maxillofacial Pathology, Tufts University, School of Dental Medicine, 55 Kneeland Street, Boston, MA, 02111, United States of America

Abstract

The repair of large crushed or sectioned segments of peripheral nerves remains a challenge in regenerative medicine due to the complexity of the biological environment and the lack of proper biomaterials and architecture to foster reconstruction. Traditionally such reconstruction was only achieved by using fresh human tissue as a surrogate for the absence of the nerve. However, recent focus in the field has been on new polymer structures and specific biofunctionalization to achieve the goal of peripheral nerve regeneration by developing artificial nerve prostheses. This review presents various tested approaches as well their effectiveness for nerve regrowth and functional recovery.

Keywords: bioengineering, biomaterials, peripheral nervous system, polymers, regenerative medicine

1. Nerve Injury and Nerve Degeneration

Injury to a peripheral nerve, known as peripheral neuropathy, often leads to an impairment of motor and sensory functions within the PNS due to an interference in nerve conduction. Motor vehicle accidents are the primary cause of traumatic peripheral neuropathy and more than half of nerve injuries affect the lower limbs (such as deriving from the peroneal nerve). Peripheral neuropathies are mainly caused by elongation, laceration, or compression. Elongation is the most frequent form of traumatic neuropathy. The connective tissue making up the nerve presents a certain elasticity, however when tension is greater than its capacity of resistance, the result is a neuropathy. In the case of nerve laceration, which accounts for about 30% of severe peripheral nerve injuries, a complete tear may occur, but generally nerve continuity is maintained by at least several fragments of the nerve.[1,2] Conversely, nerve compression does not involve severing of the nerve and continuity is maintained. However, the mechanical stress acting on the conductive membrane can still cause loss of motor and sensory function as a result of several mechanisms including mechanical compression, ischemia, and mechanical deformation. Prolonged mechanical compression, whether singular or repetitive events, can damage endoneurial channels resulting in increased permeability and result in endoneurial oedema. An oedema consequently alters the ionic balance of the endoneurium and alters fascicular microcirculation thus causing an ischemia due to the increase in endoneurial fluid pressure.[3]

There are two widely used grading systems to classify the severity of peripheral nerve injuries. The simpler of the two, the Seddon classification, was developed in 1943 by Sir Herbert Seddon and includes three grades of nerve injury: neuropraxia, axonotmesis, and neurotmesis.[4] However, the Sunderland classification, proposed in 1951 by Sir Sydney Sunderland, is a more comprehensive grading system which provides more detailed information related to surgical intervention needs after nerve injury.[5] The Sunderland grading system includes five degrees of nerve injury. The first degree is equivalent to neuropraxia in the Seddon system and involves a temporary disruption of conduction resulting in local demyelination and short-term sensory impairment. The second degree is equivalent to axonotmesis in the Seddon system, which refers to axonal rupture while neural connective tissue remains undamaged. The third, fourth, and fifth degrees further delineate axonal rupture by damage of the endoneurium, perineurium, and

epineurium, respectively.[4,5] Injuries qualifying as second, third, fourth, or fifth degree will lead to Wallerian degeneration, and injuries of the fifth degree, completely sectioned nerves, may require a nerve graft.[5]

1.1. Wallerian Degeneration

A severe injury to a nerve fiber leads to its degeneration, and in the case of axotomy, the distal segment will progressively degenerate whereas the proximal axon and perikaryon undergo physiological and metabolic modifications to prepare for regeneration. This process was first studied by Augustus Volney Waller in 1850[6] who gave it the named Wallerian degeneration (Figure 1). When the axon is damaged, the myelin sheath, which provides necessary contact with the axon in order to maintain its integrity, forces the Schwann cells to split and retract their sheaths. The loss of contact with the axon stimulates and activates macrophages that phagocytose the myelin debris and axon fibers over three to six weeks. The lack of contact also acts as a stimulant for the proliferation of Schwann cells to migrate toward the damaged site. Schwann cells and fibroblasts orient themselves in columns known as Bands of Bünger, or tubes of regeneration. These bands function to attract neurites by producing neurotrophic factors. During the degeneration process, Schwann cells overexpress the class II receptors which link the free nerve growth factors to the extracellular matrix in order to offer a substrate with neurotrophic support and a chemotactic guide for axonal regrowth.

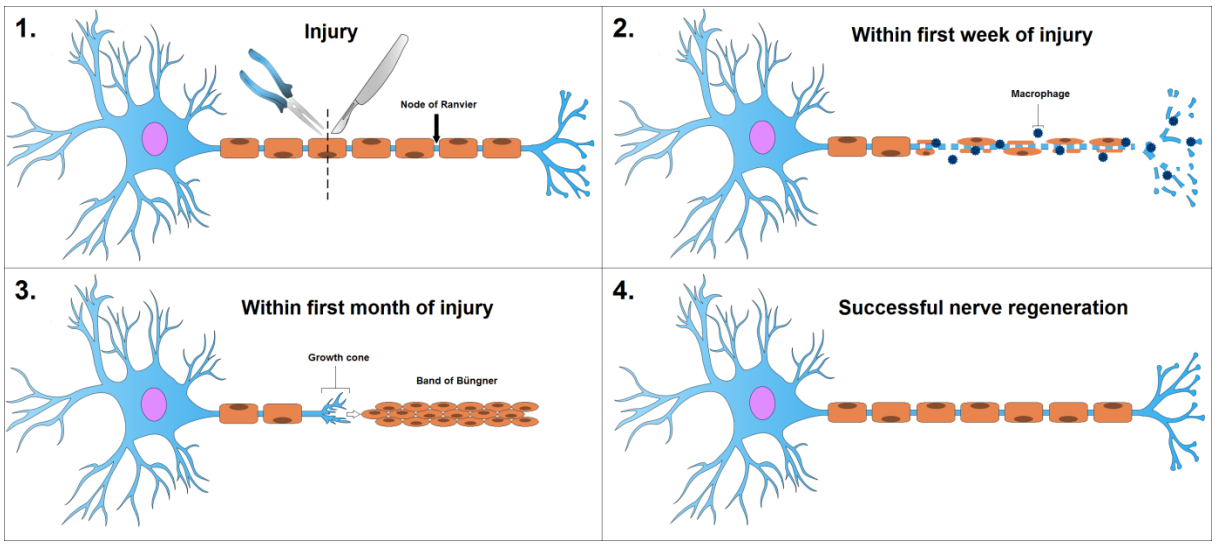

Figure 1*. Schematic representation of Wallerian Degeneration

*Representative of Figure 15 of chapter 1.

1.2. Natural Nerve Regeneration

In the hour following a nerve lesion, metabolic disruption within the nerve cells takes place. The focus turns to the manufacture of structural elements necessary for nerve regeneration in contrast to the usual priority to transmit nervous influx. This is a biological process that puts in place a permissive environment in order to restore the architecture, metabolism, and functions of the damaged tissue.[7] Genomic regulations are also modified, particularly those involved in synthesizing proteins found at the surface of Schwann cells and the axolemma.[8]

Regeneration begins with a phase of neural reorganization intended to reestablish cellular integrity. The process then promotes and guides the elongation of axons in the direction of the target at a rate of about 2-5mm per day.[9] Finally, new synaptogenesis is established. Upstream from the axotomy, the plasma membrane fuses shut in order to close off the axon. This terminal then begins to structure itself in a budding manner forming a growth cone[10] which contain filopodia that extend and retract under the influence of the environment. When the growth cone meets an unfavorable environment, it has the tendency to retract to search for a more favorable one towards which it then orients itself. The four mechanisms guiding a growth cone are attraction mediated by contact, repulsion mediated by contact, chemoattraction, and chemorepulsion.

2. Autograft and Allograft

The autograft is currently considered the gold standard for the treatment of nerve lesions, consisting of harvesting a peripheral nerve directly from the patient. The first clinical trials for autografts date back to the 1870's when Phillipeaux and Vulpian grafted optic nerve segments within the same dog.[11] The greatest disadvantage of using an autograft is inevitably the necessity of creating an additional nerve injury that can result in loss of function near the donor site. In addition, the supplementary deficiency can potentially induce the formation of a painful neuroma at the site of the secondary injured nerve.[12]

Due to advances in medical research, an alternative to the autograft, the allograft, has been developed which consists of using a nerve sample from a different patient. Immunology research has led to the development of methods to limit the risks of rejection of these allografts by

irradiation, successive freezing and defrosting.[13] The immunosuppressive treatments administered to the recipient are more efficient; however they compromise the immune system rendering it more vulnerable to other complications.

3. Autologous Tissue Graft

In the past several years, regenerative medicine has oriented itself toward decellularized autologous tissue grafts in order to overcome the disadvantages of autologous nerves. The biological tissues that have received the most attention include blood vessels, skeletal muscles, and tendons.

3.1. Blood Vessels

The concept of using vascular tissue has been studied since the end of the 19th century. Arterial conduits were first used by Bünger in 1891.[14] The exploration of nerve regrowth via arterial conduit grafts between two separated peripheral nerve segments after lesion has long been considered less promising compared to venous conduit grafts. Yet recently, a rodent study comparing three biological material conduits (nerve, artery, dermis) demonstrated encouraging use with the artery as a biological conduit.[15] The regeneration of myelinated axons and the rescue from muscular atrophy following an arterial conduit graft led to nerve repair to the same extent as that from nerve autografts.

Throughout the years, venous conduits have been the object of many experimental and clinical studies. Using a venous conduit graft for the reparation of damaged human nerves was reported for the first time in 1909 by Wrede.[14] In 1990, Chie and Strauch described a case in which 15 patients received autologous venous conduit grafts for the treatment of painful neuromas or nerve segment injuries of 3 cm in length.[16] This study demonstrates that venous conduits can be used for lesions inferior to 3 cm and is comparable to nerve regeneration obtained from autografts. Later, a clinical study on the repair of the digital nerve with a venous conduit embedded with one or more nerve slices was performed.[17] The study demonstrated that more than 65% of patients presented good results following surgical intervention. Two years later, another study using the same method for 16 patients was reported and the results

suggested that the venous conduit graft with the interposition of nervous tissue in the lumen of the conduit is a reliable alternative for lesion distances between 2 and 4.5 cm.[18] In addition, it was recently demonstrated that replacing the venous conduit lumen with type I collagen amplifies axonal regeneration.[19] However, for segments greater than 4 cm, vein constriction preventing regrowth as a result of scarring was observed.

3.2. Muscles

Skeletal muscles are composed of a tubular basal lamina similar to that of nerve conduits. The basal lamina is also oriented longitudinally and contains constituents in its extracellular matrix, like collagen type IV and laminin, that direct and advance the regeneration of nerve fibers.[20-22] In the human body, muscle tissue is present in significant quantities which prompts its use for autologous tissue grafts. The first muscle tissue grafts for nerve repair date back to the 1940's.[14] Graft conduits from decellularized muscle tissue are described in two clinical studies by Pereira et al. in 1991. The first concerned peripheral nerve guides in 10 patients suffering from leprosy,[23] and following surgery, 70% of the patients presented better perception and improved sensation from the affected limb. In addition, the same team reported 24 cases of digital nerve repair from decellularized muscle grafts.[24] Monitoring 6 to 40 months after the procedures indicated better outcomes compared to patients who underwent nerve autografts. Nevertheless, the use of decellularized muscles presents some disadvantages such as the possibility of the nerve fibers growing outside of the graft and creating a neuroma.[25]

3.3. Tendons

Tendons can be used as nerve conduits to fill gaps with maximum distances of 1 cm. The architecture of the tendon, a longitudinal arrangement of the collagen bundles, provides favorable grafts for nerve regeneration in the rat sciatic nerve.[26] The axons align themselves on the collagen fibers of the tendon for nerve regrowth. In order to verify the validity of this model, tendon tissue grafts have been compared to muscle tissue with functional and morphological similarities.[27] Tendons can therefore support nerve regeneration in a similar manner to decellularized muscle.

Other tendon grafts supplementing Schwann cells have been generated in order to improve the results of nerve regeneration.[28] These tests showed an acceleration in axonal regeneration, however, after 12 weeks, no differences were observed between tendon grafts and those supplementing Schwann cells. The authors concluded that the principal advantage of this technique would be that the tendon represents an abundant biologic material with limited loss of function near the donor site.

4. Biomaterials

In addition to conduits of biological origin, researchers have turned to biomaterials for support in nerve regeneration. This approach avoids compatibility issues of donors and also avoids the complications associated with creating a second injury site for the patient. However, the selected biomaterial for the fabrication of a tissue engineered nerve graft (TENG) must address certain criteria; biocompatibility, porosity, and mechanical properties. Nerve conduits can be prepared from synthetic or natural materials. Several biomaterial conduits have already been approved and commercialized for clinical use, yet none of these conduits offer complete functional recovery.

4.1. Material Properties

Today, nerve guides derived from tissue engineering represent promising alternatives to autografts, but choosing the right biomaterial is essential for good conduit design. Biocompatibility is largely based on how the material interacts in the biological environment in which it is used. The implant must mimic the unusual reactions within tissues, which means that tissue-material interactions should not show significant signs of irritation or provoke significant inflammatory, allergic, or immunological responses.

In addition to being biocompatible, the material should provide mechanical and structural properties similar to those of a peripheral nerve in order to optimize outcomes. The biomaterial needs to be flexible, especially when the conduit is destined for the treatment of extensive lesions, but the degree of flexibility must not be excessive so that it is subject to twists and tears.[29] Sufficient permeability allows the diffusion of nutrients to the interior of the conduit and

influences the production of the fibrin matrix in the beginning stages of nerve regeneration.[29] Ideally, conductivity is an element to consider in stimulation for nerve regeneration for axon regrowth and orientation due to the charged surface. However, to date most of these types of biomaterials are nondegradable.[30]

In the field of tissue engineering, a biomaterial must resist and support changes in physico-chemistry during cell proliferation. Mechanical properties such as traction force, elongation at rupture, and tenacity (resistance to crack propagation) need to be tested in order to verify the utility of the biomaterial.

4.2. Synthetic Materials

The synthetic materials used in tissue engineering for nerve grafts typically possess adequate mechanical integrity, but can vary in their level of degradability, some are classified as biodegradable and others as non-biodegradable. Synthetic TENGs classified as non-biodegradable are capable of provoking a foreign body response which can lead to scarring, infections, and inflammatory responses. In this case, a second surgical procedure for removing the TENG is necessary. In addition, if the synthetic material is not fully absorbable, it presents the risks of chronic inflammation and nerve compression.[31] Silicone was one of the first synthetic materials used as an implantable material, but is non degradable. Silicone is considered a biologically inert material, and extraction from the implant site may be necessary after nerve repair. Furthermore, while implantation of silicone-based TENGs in the median nerve of the cubital fossa to repair a short lesion (up to 1 cm) produces similar results to microsurgery, the results were not as encouraging for larger nerve lesions.[32,33] Some other synthetic materials may include polylactic acid (PLA), poly(lactic acid-co-glycolic acid) (PLGA), poly(ε-caprolactone) (PCL), polyamidoamines (PAAs), and polyethylene glycol (PEG) (Table 1).

4.3. Natural Materials

Previous work suggests that natural materials offer improved performance in regeneration of nerves than synthetic materials,[42] yet natural materials tend to have weak mechanical

properties. Some natural materials include chitosan, collagen, gelatin, fibronectin, hyaluronic acid, keratin, and silk fibroin.

The use of biomaterial composites (blends of natural and synthetic materials) to form TENGs can provide suitable properties. Some examples include collagen and crosslinked laminin scaffolds,[43] collagen-PCL electrospun scaffolds,[44] and chitosan and PLA scaffolds.[45] The interface between the internal and external environments also very influences regeneration and the integration of a material. Therefore, grafts using a synthetic outer shell filled with a supple natural material as the inner layer may allow better migration of the nerve through the conduit.[46] Among recently studied natural materials, silk fibroin protein has demonstrated promising material features for use in nerve regeneration. Silk is a naturally biodegradable, biocompatible material containing primarily the hydrophobic protein fibroin and the hydrophilic sericins (which are removed during extraction). Silk proteins are naturally extracted from silkworm cocoons which have been cultivated and used for thousands of years in textile manufacturing and now recently in biomedical applications. Silk presents robust mechanical properties, an absence of toxicity, and can easily be functionalized by chemical modifications permitting the acquisition of new physico-chemical properties. While the sericin proteins are immunogenic,[47,48] the fibroin protein generates a weaker inflammatory response than that of collagen and PLA.[49] In addition, silk materials are permeable to oxygen and water and the range of properties have encouraged research into the formation of silk fibroin-based nerve conduits (Table 2).

4.4. Commercialized Nerve Conduits

The first approved nerve conduit for medical use in the human body was in 1999. Table 3 presents the seven principal devices in clinical applications that have been approved by the Food and Drug Administration. Neuragen®, Neurotube®, and Neurolac® have been tested within the human body whereas NeuroMatrix™, NeuroFlex™, Salubridge™, and SaluTunnel™ have not undergone clinical studies.

It remains difficult to compare the different conduits currently found on the market in terms of performance. For example, a review by Meek and Coert recommends using PGA-based TENGs or Neurotube®.[65] However, an animal study using rats compared Neurotube®, Neurolac® and

Neuragen® to autografts for the treatment of 1 cm lesions in the sciatic nerve, and after histological and functional analyses, Neurlac® produced similar results to the autografts while Neurotube® was crushed and demonstrated less functional recovery.[66]

The most significant advantage to using commercial nerve conduits is to avoid sacrificing the patient's functional nerve for an autograft. In addition, the results from clinical studies, particularly with Neuragen® and Neurotube®, are often comparable to autografts in the treatment of lesions with a maximum length of 3 cm and a small diameter. Unfortunately, these models do not assure nerve regeneration in more extensive lesions or in larger nerves.[67]

Table 1.* Synthetic materials used for the fabrication of nerve conduits

Material	Material Properties	Result(s)	Reference(s)
PAA polyamidoamines	Biocompatible Biodegradable Elastic	Improved axon size and density Thick myelin sheaths	Magnaghi et al., 2011[34]
PCL poly(ε-caprolactone)	Structurally resistant Permeable	Improved nerve fibers and myelination	Maturana et al., 2013;[35] Nikolaev et al., 2014[36]
PEG polyethylene glycol	Biocompatible Adjustable mechanical properties	Production of LDH +++ Inflammatory	Koob et al., 2008;[37] Stukel et al., 2014[38]
PLGA poly(lactic acid-co-glycolic acid)	Rigid Inflammatory	Large axon diameters Thick myelin sheaths	de Boer et al., 2011;[39] Kehoe et al., 2012[40]
PVC Polyvinyl chloride	High structural integrity	Improved myelination	Penna et al., 2012[41]
Silicone	Biologically inert Non-degradable	Accumulation of growth factors Weak growth and myelination	Braga-Silva, 1999;[32] Lundborg et al., 2004[33]

*Representative of Table 1 of chapter 1.

Table 2.* Natural materials used for the fabrication of nerve conduits

Material	Material Properties	Result(s)	Reference(s)
Chitosan	Weak degradability Low structural integrity Inflammatory	Myelinated axons Muscular potential	Ao et al., 2006;[50] Wang et al., 2006;[51] Zeng et al., 2014[52]
Collagen	Biocompatible Degradable Fragile	Partially recovered nerve functionality	Ding et al., 2011;[53] Phillips et al., 2005[54]
Fibrin	Easily manipulated Angiogenic	Glial cell invasion Axonal growth	Kalbermatten et al., 2009;[55] Scott et al., 2011[56]
Fibronectin	Low structural integrity	Growth of fibroblasts and Schwann cells	Ahmed et al., 2003[57]
Gelatin	Low structural integrity Economic	Unmyelinated axons Excrescence Proliferation of Schwann cells	Liu, 2008;[58] Tonda-Turo et al., 2014[59]
Keratin	Biocompatible	Improved density and size of axons Improved conduction	Apel et al., 2008;[60] Hill et al., 2011[61]
Silk Fibroin	Biodegradable Biocompatible High structural integrity	Mildly inflammatory Nervous tissue colonization	Hopkins et al., 2013;[62] S. Madduri et al., 2010;[63] Wittmer et al., 2011[64]

*Representative of Table 2 of chapter 1.

Table 3.* FDA approved and commercialized TENGs

Material	Product Name	Degradation	FDA Approval Year
PGA	Neurotube®	3 months	1999
Type 1 collagen	Neuragen®	3-4 years	2001
Type 1 collagen	NeuroMatrix™	4-8 months	2001
Type 1 collagen	NeuroFlex™	4-8 months	2001
PLCL	Neurolac®	16 months	2005
PVA	Salubridge™	Non-absorbable	2000
PVA	SaluTunnel™	Non-absorbable	2010

5. Biofunctionalization by Neurotrophic Factors

Neurotrophic factors are released endogenously by peripheral nerve tissues following lesions. Therefore, a large number of neurotrophic factors are utilized in tissue engineering to improve peripheral nerve regeneration (Table 4). The most common factors are nerve growth factor (NGF), glial cell-line derived neurotrophic factor (GDNF), brain-derived neurotrophic factor (BDNF), neurotrophin-3 (NT-3), and neurotrophin-4/5 (NT-4/5).

5.1. Nerve Growth Factor

Nerve growth factor (NGF) is the most studied neurotrophic factor for the treatment of peripheral nerve damage.[68] NGFs are found in low concentrations in healthy nerves, but after injury NGF concentrations increase at the lesion site.[69,70] Schwann cells synthesize increasing amounts of specific membrane NGF receptors in order to present the growth factor to axonal extensions. NGF plays an important role in the survival of sensory neurons and in the extension of axons. One of the goals of tissue engineering is to develop different functionalized biomaterials with NGFs. NGFs have been incorporated into many different types of supports such as fibrous conduits or gel conduits.[38,71-73] In incorporating NGFs to these different supports, the number of mature nerve fibers increases resulting in better functional recovery, including the speed of nerve conduction, compared to control groups where NGF is absent. In the presence of NGFs, the diameters of the axons found in the functionalized conduits were larger than the nerve conduits

*Representative of Table 3 of chapter 1.

not containing NGFs.[74] The addition of this growth factor influences the proliferation and migration of Schwann cells, which in turn facilitates axonal regeneration.[75] These conduits were able to fill a distance of 13 mm in the rat sciatic nerve producing the same amount of nerve fibers found in the group having undergone autografting. However, NGFs have little influence over motor neurons and the growth of their neurites.[76]

5.2. Neurotrophin-3

Following a nerve lesion, a continuous infusion of NT-3 is effective in the restoration of the conduction speed of motor and sensory neurons in a dose-dependent manner.[59] The exogenous administration of NT-3 offers a trophic effect on the sensory nerve fibers even in the absence of the target organ.[77] Administration of NT-3 also restores muscle mass and improves the reinnervation of muscle fibers.[78,79] In a study of rat sciatic nerve regeneration, the addition of NT-3 to biomaterial matrices composed of grafted fibronectin increased axonal regrowth after the 15th day. Furthermore, 8 months after surgery, rats presenting the functionalized grafts contained more myelinated axons than the control groups.[80]

5.3. Multi-functionalization

In order to stimulate multiple sub-populations involved in nerve regeneration, materials functionalized with more than one growth factor have been pursued.[75] Glial cell line-derived neurotrophic factor (GDNF) is a neurotrophic factor secreted by Schwann cells and improves the survival of motor and sensory neurons, the growth of neurites, and the migration of Schwann cells.[81] GDNFs also improve the speed of conduction of motor neurons along with small diameter sensory neurons following regeneration.[82,83] Collagen-based conduits have been functionalized by NGFs and GDNFs, and the results have revealed a significant increase of Schwann cell migration in the proximal end of the conduits within the first two weeks of regeneration. Furthermore, the amount of myelinated axons was higher in the functionalized conduits for both NGF and GDNF. The limit of this approach lies in the difficulty of finding the appropriate dose for each growth factor integrated into the nerve conduit.

5.4. Other Neurotrophic Factors

Many other neurotrophic factors, although less commonly found in peripheral nerves, have shown equally efficient improvement in peripheral nerve regeneration including ciliary neurotrophic factor (CNTF),[84] vascular endothelial growth factor (VEGF),[85] leukemia inhibitory factor (LIF),[86] and insulin-like growth factor 1 (IGF-1).[87] In general, these proteins are either injected directly into the lumen of the nerve conduits or embedded within a hydrogel-based conduit that guides the nerve through its lumen. It is clear that a more detailed understanding of the dose response of neurotrophic factors and their combinations for nerve regeneration is necessary for designing the optimal scaffold.

Most studies intended for peripheral nerve repair use the typical neurotrophic factors mentioned earlier, however, other growth factors not yet identified specific for the differentiation and regeneration of nerve tissue may also be pertinent. For example, in one rat study, the injection of bone morphogenetic protein 2 (BMP-2) supported an increase in the number and the diameter of axons compared to the control group after 4 weeks.[88] The addition of fibroblast growth factors (FBFs) allowed a faster return of motor function and an increase of muscular action potential after a lesion in the rat sciatic nerve.[89] The mechanisms by which growth factors that are not specific to nerve tissue regeneration, such as BMP and FGF, induce these neurological outcomes are not clear.

Although neurotrophic factors have been successfully incorporated in different systems proposed by tissue engineering for protecting neurons from induced death and favoring regeneration, drawbacks remain. For example, the half-life of these proteins is usually very short,[39] and the growth factors released into the environment may not be as bioactive.[90] The release kinetics varies depending on the system and factor used, and therefore the dose needs to be optimized.

Table 4.* Growth factors used for nerve repair

FC(s)	Methods	Nerve	Advantage(s)	Reference(s)
NGF	Nanofibers Microspheres Microgels	Rat sciatic nerve	Mature nerve fibers Better nerve conduction Functional recuperation	Wang et al., 2012;[91] Uebersax et al., 2007;[73] Stukel et al., 2014[38]
NGF GDNF	Collagen tubes	Rat sciatic nerve	Regeneration of tissues is faster	Madduri et al., 2010[75]
NT-3	Fibronectin scaffold	Rat sciatic nerve	Act on sensory and motor neurons Improved reinnervation of the target	Hopkins et al., 2013;[59] Sterne et al., 1997[80]
GDNF	Microspheres	Rat sciatic nerve	Increased muscle strength Better colonization of tissues	Kokai et al., 2011[92]
CNTF	Silicone conduits	Rat sciatic nerve	Increased diameter and number of axons Better nerve conduction Increased muscular potential	Zhang et al., 2004[84]
BMP-2	Injection	Rabbit facial nerve	Greater density and thickness of axons	Wu et al., 2010[88]
IGF-1	Muscle basal lamina conduits	Rat sciatic nerve	Increased muscle mass More efficient regeneration in the case of supplemented grafts in IGF-1	Fansa et al., 2002[87]

*Representative of Table 4 of chapter 1.

6. Conclusion

The autograft has long been considered the gold standard for peripheral nerve repair, but the drawbacks of this method continue to encourage the development of novel techniques that yields similar or enhanced success in nerve regeneration. Various tested approaches and their effectiveness as alternatives to the autograft were reviewed. While many of these alternative techniques have found some success, no biomaterial system has been shown to offer complete functional recovery for all peripheral nerve regeneration needs. Nevertheless, given the wide variety of synthetic and natural biomaterial based TENGs being developed and their encouraging results compared with the autografts for short lesions, tissue engineering remains a promising approach for the future of nerve repair. Indeed, choosing the proper biomaterials that incorporate the characteristics necessary to mimic the natural biological system paired with an optimal combination and dose of neurotrophic factors should continue to lead to advancements and eventually to nerve grafts that fully address the needs for peripheral nerve regeneration.

Acknowledgements

The authors thank the Picardie Region for its financial support, the Tissue Engineering Resource Center (TERC) from Tufts University (NIH Center – P41 EB002520). Tony M. Dinis received a fellowship from the French Ministry of Science and Technology. Kayla Belanger received a doctoral fellowship from the Picardie Region and FEDER.

References

[1] P. Ciaramitaro, M. Mondelli, F. Logullo, S. Grimaldi, B. Battiston, A. Sard, C. Scarinzi, G. Migliaretti, G. Faccani, D. Cocito, *J. Peripher. Nerv. Syst.* **20010**, *15*, 2.

[2] W. W. Campbell, *Clin. Neurophysiol.* **2008**, *119*, 9.

[3] J. Mitsingou, P. Goma, *Médecine Afr. Noire* **1993**, *40*, 12

[4] R. Birch, *Surgical Disorders of the Peripheral Nerves*, 2nd ed., Springer, London, UK **2011**

[5] A. Chhabra, S. Ahlawat, A. Belzberg, G. Andreseik, *Indian J. Radiol. Imaging* **2014**, *24*, 3.

[6] Waller, A. *Philos. Trans. R. Soc. Lond.* **1850**, *140*.

[7] G. Stoll, H. W. Müller, *Brain Pathol.* **1999**, *9*, 2.

[8] R. Martini, *J. Neurocytol.* **1994**, *23*, 1.

[9] C. E. Schmidt, J. B. Leach, *Annu. Rev. Biomed. Eng.* **2003**, *5*.

[10] T. Fuhs, L. Reuter, I. Vonderhaid, T. Claudepierre, J. A. Käs, *Cytoskeleton* **2013**, *70*, 1.

[11] E. S. Dellon, A. L. Dellon, *J. Hand Surg.* **1993**, *18*, 2.

[12] J. Wu, D. T. Chiu, *Ann. Plast. Surg.* **1999**, *43*, 6.

[13] L. Marmor, *Clin. Orthop.* **1964**, *34*.

[14] P. Konofaos, J. Ver Halen, *J. Reconstr. Microsurg.* **2013**, *29*, 3.

[15] I.-C. Liao, H. Wan, S. Qi, C. Cui, P. Patel, W. Sun, H. Xu, *J. Tissue Eng.* **2013**, *4*.

[16] D. T. Chiu, B. Strauch, *Plast. Reconstr. Surg.* **1990**, *86*, 5.

[17] J. B. Tang, Y. Q. Gu, Y. S. Song, *J. Hand Surg. Br.* **1993**, *18*, 4.

[18] J. B. Tang, D. Shi, H. Zhou, *Microsurgery* **1995**, *16*, 3.

[19] B.-H. Choi, S.-J. Zhu, S.-H. Kim, B.-Y. Kim, J.-H Huh, S.-H. Lee, J.-H. Jung, *J. Reconstr. Microsurg.* **2005**, *21*, 4.

[20] D. Edgar, R. Timpl, H. Thoenen, *EMBO J.* **1984**, *3*, 7.

[21] P. J. Lein, G. A. Banker, D. Higgins, *Dev. Brain Res.* **1992**, *69*, 2.

[22] G. Lundborg, L. Dahlin, N. Danielsen, Q. Zhao, *J. Reconstr. Microsurg.* **1994**, *10*, 5.

[23] J. H. Pereira, D. D. Palande, A. Subramanian, T. S. Narayanakumar, J. Curtis, J. L. Turk, *Lancet* **1991**, *338*, 8777.

[24] J. H. Pereira, R. E. Bowden, J. M. Gattuso, R. W. Norris, *J. Hand Surg. Br.* **1991**, *16*, 5.

[25] M. F. Meek, A. S. P. Varejão, S. Geuna, *Tissue Eng.* **2004**, *10*, 7-8.

[26] J. Brandt, L. B. Dahlin, G. Lundborg, *J. Hand Surg. Br.* **1999**, *24*, 3.

[27] J. Brandt, L. B. Dahlin, M. Kanje, G. Lundborg, *Exp. Neurol.* **1999**, *160*, 2.

[28] Y. Nishiura, J. Brandt, A. Nilsson, M. Kanje, L. B. Dahlin, *Tissue Eng.* **2004**, *10*, 1-2.

[29] G. C. W. De Ruiter, M. J. A. Malessy, M. J. Yaszemski, A. J. Windebank, R. J. Spinner, *Neurosurg. Focus* **2009**, *26*, 2.

[30] A. R. Nectow, K. G. Marra, D. L. Kaplan, *Tissue Eng. Part B Rev.* **2012**, *18*, 1.

[31] K. Kakinoki, N. Nishijima, Y. Ueba, M. Oka, T. Yamamuro, *Neuroscience Research* **1995**, *23*, 1.

[32] J. Braga-Silva, *J. Hand Surg. Br.* **1999**, *24*, 6.

[33] G. Lundborg, B. Rosén, L. Dahlin, J. Holmberg, I. Rosén, *J. Hand Surg. Br.* **2004**, *29*, 2.

[34] V. Magnaghi, V. Conte, P. Procacci, G. Pivato, P. Cortese, E. Cavalli, G. Pajardi, E. Ranucci, F. Fenili, A. Manfredi, P. Ferruti, *J. Biomed. Mater. Res. A* **2011**, *98*, 1.

[35] L. G. Maturana, A. Pierucci, G. F. Simões, M. Vidigal, E. A. R. Duek, B. C. Vidal, A. L. R. Oliveira, *Brain Behav.* **2013**, *3*, 4.

[36] S. I. Nikolaev, A. R. Gallyamov, G. V. Mamin, Y. A. Chelyshev, *Bull. Exp. Biol. Med.* **2014**, *157*, 1.

[37] A. O. Koob, J. M. Colby, R. B. Borgens, *J. Biol. Eng.* **2008**. *2*, 9.

[38] J. Stukel, S. Thompson, L. Simon, R. Willits, *J. Biomed. Mater. Res. A.* **2014**, *103*, 2.

[39] R. De Boer, A. M. Knight, A. Borntraeger, M.-N. Hébert-Blouin, R. J. Spinner, M. J. A. Malessy, M. J. Yaszemski, A. J. Windebank, *Microsurgery* **2011**. *31*, 4.

[40] S. Kehoe, X. F. Zhang, L. Lewis, H. O'Shea, D. Boyd, *Mech. Behav. Biomed. Mater.* **2012**, *14*.

[41] V. Penna, K. Wewetzer, B. Munder, G. B. Stark, E. M. Lang, *Microsurgery* **2012**, *32*, 5.

[42] Z. Li, J. Peng, G. Wang, Q. Yang, H. Yu, Q. Guo, A. Wang, B. Zhao, S. Lu, *Exp. Neurol.* **2008**, *214*, 1.

[43] J. Cao, C. Sun, H. Zhao, B. Chen, J. Gao, T. Zheng, W. Wu, S. Wu, J. Wang, J. Dai, *Biomaterials* **2011**, *32*, 16.

[44] W. Yu, W. Zhao, C. Zhu, X. Zhang, D. Ye, W. Zhang, Y. Zhou, X. Jiang, Z. Zhang, *BMC Neurosci.* **2011**, *12*, 68. DOI: 10.1186/1471-2202-12-68.

[45] J. Xie, X. Li, J. Lipner, C. N. Manning, A. G. Schwartz, S. Thomopoulos, Y. Xia, *Nanoscale* **2010**, *2*, 6.

[46] E. Goto, M. Mukozawa, H. Mori, M. Hara, *J. Bioschi. Bioeng.* **2010**, *109*, 5.

[47] G. H. Altman, F. Diaz, C. Jakuba, T. Calabro, R. L. Horan, J. Chen, H. Lu, J. Richmond, D. L. Kaplan, *Biomaterials* **2003**, *24*, 3.

[48] B. Panilaitis, G. H. Altman, J. Chen, H.-J. Jin, V. Karageorgiou, D. L. Kaplan, *Biomaterials* **2003**, *24*, 18. DOI:10.1016/S0142-9612(03)00158-3.

[49] Y. Wang, D. D. Rudym, A. Walsh, L. Abrahamsen, H.-J. Kim, H. S. Kim, C. Kirker-Head, D. L. Kaplan, *Biomaterials* **2008**, *29*, 24-25. DOI: 10.1016/j.biomaterials.2008.05.002.

[50] Q. Ao, A. Wang, W. Cao, L. Zhang, L. Kong, Q. He, Y. Gong, X. Zhang, *J. Biomed. Mater. Res. A.* **2006**, *77A*, 1.

[51] A. Wang, Q. Ao, W. Cao, M. Yu, Q. He, L. Kong, L. Zhang, Y. Gong, X. Zhang, *J. Biomed. Mater. Res. A* **2006**, *79*, 1.

[52] W. Zeng, M. Rong, X. Hu, W. Xiao, F. Qi, J. Huang, Z. Luo, *PloS One* **2014**, *9*, 7.

[53] T. Ding, W. W. Lu, Y. Zheng, Z. Y. Li, H. B. Pan, Z. Luo, *Regen. Med.* **2011**, *6*, 4.

[54] J. B. Phillips, S. C. J. Bunting, S. M. Hall, R. A. Brown, *Tissue Eng.* **2005**, *11*, 9-10.

[55] D. F. Kalbermatten, J. Pettersson, P. J. Kingham, G. Pierer, M. Wiberg, G. Terenghi, *J. Reconstr. Microsurg.* **2009**, *25*, 1.

[56] J. B. Scott, M. Afshari, R. Kotek, J. M. Saul, *Biomaterials* **2011**, *32*, 21.

[57] Z. Ahmed, S. Underwood, R. A. Brown, *Tissue Eng.* **2003**, *9*, 2.

[58] B. S. Liu, *J. Biomed. Mater. Res. A* **2008**, *87*, 4.

[59] C. Tonda-Turo, S. Gnavi, F. Ruini, G. Gambarotta, E. Gioffredi, V. Chiono, I. Perroteau, G. Ciardelli, *J. Tissue Eng. Regen. Med.* **2014**.

[60] P. J. Apel, J. P. Garrett, P. Sierpinski, J. Ma, A. Atala, T. L. Smith, L. A. Koman, M. E. Van Dyke, *J. Hand Surg.* **2008**, *33*, 9.

[61] P. S. Hill, P. J. Apel, J. Barnwell, T. Smith, L. A. Koman, A. Atala, M. Van Dyke, *Tissue Eng. Part A* **2011**, *17*, 11-12.

[62] A. M. Hopkins, L. De Laporte, F. Tortelli, E. Spedden, C. Staii, T. J. Atherton, J. A. Hubbell, D. L. Kaplan, *Adv. Funct. Mater.* **2013**, *23*, 41.

[63] S. Madduri, M. Papaloïzos, B. Gander, *Biomaterials* **2010**, *31*, 8.

[64] C. R. Wittmer, T. Claudepierre, M. Reber, P. Wiedemann, J. A. Garlick, D. Kaplan, C. Egles, *Adv. Funct. Mater.* **2011**, *21*, 22.

[65] M. F. Meek, J. H. Coert, *J. Plast. Reconstr. Aes.* **2013**, *66*, 10.

[66] R. H. Shin, P. F. Friedrich, B. A. Crum, A. T. Bishop, A. Y. Shin, *J. Bone Joint Surg. Am.* **2009**, *91*, 9.

[67] A. M. Moore, R. Kasukurthi, C. K. Magill, H. F. Farhadi, G. H. Borschel, S. E. Mackinnon, *HAND* **2009**, *4*, 2.

[68] L. Aloe, *Arch. Ital. Biol.* **2011**, *149*, 2.

[69] T. Saika, E. Senba, K. Noguchi, M. Sato, S. Yoshida, T. Kubo, T. Matsunaga, M. Tohyama, *Arch. Ital. Biol.***1991**, *9*, 1-2.

[70] M. V. Sofroniew, C. L. Howe, W. C. Mobley, *Annu. Rev. Neurosci.* **2001**, *24*, 1.

[71] M. Savignat, C. Vodouhe, A. Ackermann, Y. Haikel, P. Lavalle, P. Libersa, *J. Oral Maxil. Surg.* **2008**, *66*, 4.

[72] M. Savignat, L. De-Doncker, C. Vodouhe, J. M. Garza, P. Lavalle, P. Libersa, *J. Dent. Res.* **2007**, *86*, 11.

[73] L. Uebersax, M. Mattotti, M. Papaloïzos, H. P. Merkle, B. Gander, L. Meinel, *Biomaterials* **2007**, *28*, 30.

[74] H. Xu, Y. Yan, S. Li, *Biomaterials* **2011**, *32*, 20.

[75] S. Madduri, P. di Summa, M. Papaloïzos, D. Kalbermatten, B. Gander, *Biomaterials* **2010**, *31*, 32.

[76] S. Braun, B. Croizat, M. C. Lagrange, J. M. Warter, P. Poindron, *J. Neurol. Sci.* **1996**, *136*, 1-2.

[77] M. E. Helgren, K. D. Cliffer, K. Torrento, C. Cavnor, R. Curtis, P. S. DiStefano, S. J. Wiegand, R. M. Lindsay, *J. Neurosci.* **1997**, *17*, 1.

[78] R. A. Oakley, F. B. Lefcort, D. O. Clary, L. F. Reichardt, D. Prevette, R. W. Oppenheim, E. Frank, *J. Neurosci.* **1997**, *17*, 11.

[79] G. D. Sterne, G. R. Coulton, R. A. Brown, C. J. Green, G. Terenghi, *J. Cell Biol.* **1997**, *139*, 3.

[80] G. D. Sterne, R. A. Brown, C. J. Green, G. Terenghi, *Eur. J. Neurosci.* **1997**, *9*, 7.

[81] M. S. Airaksinen, M. Saarma, *Nat. Rev. Neurosci.* **2002**, *3*, 5.

[82] J. B. Munson, S. B. McMahon, *Eur. J. Neurosci.* **1997**, *9*, 6.

[83] D. L. Bennett, G. J. Michael, N. Ramachandran, J. B. Munson, S. Averill, Q. Yan, S. B. McMahon, J. V. Priestley, *J. Neurosci.* **1998**, *18*, 8.

[84] J. Zhang, W. C. Lineaweaver, T. Oswald, Z. Chen, Z. Chen, F. Zhang, *J. Reconstr. Microsurg.* **2004**, *20*, 4.

[85] M. I. Hobson, C. J. Green, G. Terenghi, *J. Anat.* **2000**, *197 Pt 4*.

[86] A. McKay Hart, M. Wiberg, G. Terenghi, *Br. J. Plast. Surg.* **2003**, *56*, 5.

[87] H. Fansa, W. Schneider, G. Wolf, G. Keilhoff, *Muscle Nerve* **2002**, *26*, 1.

[88] G. Wu, L. Ju, T. Jin, L. Chen, L. Shao, Y. Wang, B. Liu, *J. Int. Med. Res.* **2010**, *38*, 5.

[89] M. A. Walter, R. Kurouglu, J. B. Caulfield, L. O. Vasconez, J. A. Thompson, *Lymphokine Cytokine Res.* **1993**, *12*, 3.

[90] S. Esaki, J. Kitoh, S. Katsumi, F. Goshima, H. Kimura, M. Safwat, K. Yamano, N. Watanabe, N. Nonoguchi, T. Nakamura, R. S. Coffin, S.-I. Miyatake, Y. Nishiyama, S. Murakami, *Gene Ther.* **2011**, *18*, 11.

[91] C.-Y. Wang, J.-J. Liu, C.-Y. Fan, X.-M. Mo, H.-J. Ruan, F.-F. Li, *J. Biomat. Sci.-Pol. E.* **2012**, *23*, 1-4.

L. E. Kokai, D. Bourbeau, D. Weber, J. McAtee, K. G. Marra, *Tissue Eng. Part A* **2011**, *17*, 9-10.

4. Silk Fibroin

Silk fibroin is a natural protein found in the cocoons produced by the *Bombyx mori* silk worm. Silk worm cocoons have been cultivated and used for hundreds of years in textile manufacturing; the global production of silk worm cocoons is around 400,000 tons per year. Fibroin makes up about 75% of the cocoon which consists of one singular fibroin thread that can reach up to one kilometer in length. The other 25% of the cocoon consists of sericin proteins that act as the glue keeping the fibroin fibers in place (Figure 16) (Rockwood et al., 2011). Sericin proteins are soluble glycoproteins that have found to produce unwanted immune responses and therefore must be extracted from the silk before use as a biomaterial (Yang et al., 2007).

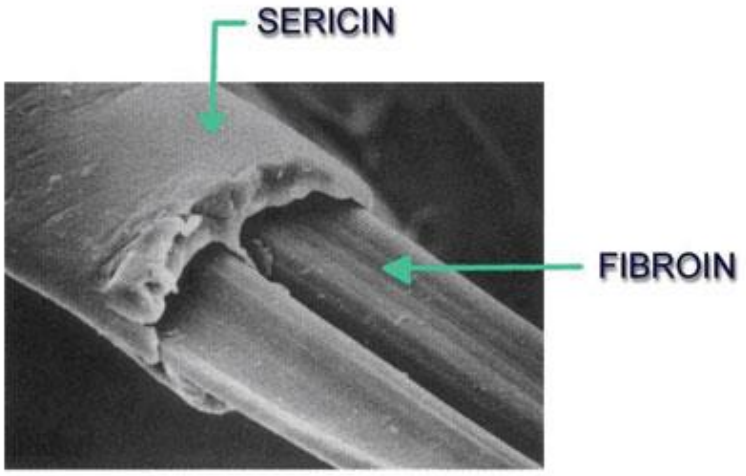

Figure 16. Image of sericin glue-like proteins holding together two silk fibroin fibers.

In order for a material to be considered biocompatible, certain criteria must be met; the interaction between tissue and the material lust not present signs of irritation or provoke a significant inflammatory, allergic, or immunological response, and the material must be strictly non-carcinogenic (Cao and Wang, 2009). Silk fibroin meet all of these criteria and is therefore defined as a biomaterial (Yang et al., 2007). In addition, silk fibroin is a natural and biodegradable polymer (Table 5) which means that the degradation of the polymer is at least partly mediated by a biological system (Cao and Wang, 2009). Silk fibroin degrades principally by proteolytic enzymes including chymotrypsin, actinase, and carboxylase in a two-step process: the- enzyme is first adsorbed to the surface followed by hydrolysis of the ester bond (Cao and Wang, 2009; Arei et al., 2004; Nair and Laurencin, 2007).

Table 5. Properties of silk from *Bombyx mori* cocoons (Cao and Wang, 2009).

***Bombyx mori* silk worm**				
Silk fiber	Silk fibroin (72-81%)			Silk sericin (19-58%)
	H chain	L chain	P 25 glycoprotein	a glue-like protein
Molecular Weight	325 kDa	25 kDa	25 kDa	~300 kDa
Polarity	Hydrophobic			Hydrophilic
Structure	silk I(random-coil or unordered structure) silk II(crystalline structure) silk III (unstable structure)			non-crystalline structure
Function	the structure protein of fibers filament core protein			binds two fibroins together coating protein

Silk fibroin is a system of organized polypeptide chains with a secondary structure of antiparallel β-sheets. The primary structure of fibroin is defined by a repeating sequence of glycine-serine -glycine-alanine-glycine-alanine $(GSGAGA)_n$ (Figure 17). The stacked sheets interact by van der Waal forces (Mita et al., 1994). Each amino acid within the chain interacts with its counterpart located antiparallel on another chain (Figure 18); for example, the alanine or serine residues line up with the same residues of an antiparallel chain with an interchain distance of 5.7 Å (the distance between glycine residues in 3.5 Å (Sashuba et al., 2006). As a result of this chemical configuration, fibroin is one of the most robust natural polymers and possesses remarkable mechanical properties.

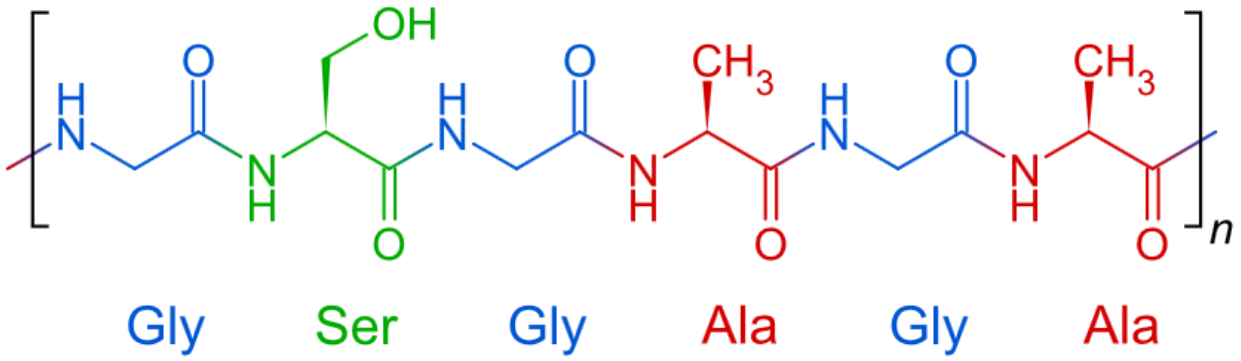

Figure 17. Primary structure of silk fibroin.

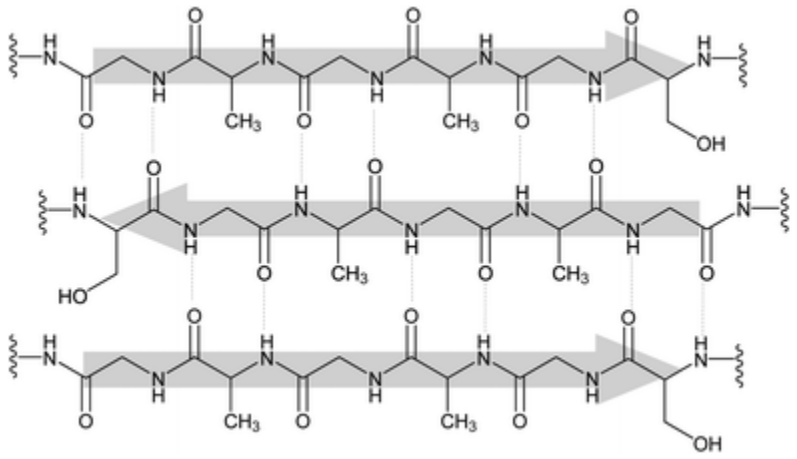

Figure 18. Secondary structure of silk fibroin representing antiparallel β-sheets.

Table 6. Degradation properties of silk fibroin (Cao and Wang, 2009).

Type of silk	*In vivo/vitro*	Mechanism	Degree and measure of degradation
Extracted fibroin film	*In vitro*	Proteolytic degradation	~10% weight loss 5 days following enzymatic digestion
Unknown/ assumed black raided	Rat/ subcutaneous	Unknown/ assumed foreign body response	55% loss in tensile strength 6 weeks *in vivo*
Black braided	Rat/ subcutaneous	Unknown/ assumed foreign body response	83% loss in tensile strength 10 weeks *in vivo*
Unknown/ assumed black raided	Rat/ abdominal wall muscle	Foreign body response (proteolytic degradation)	Fragmentation at 6 weeks; not detected at 24 weeks
Black braided	Rabbit/ cornea, sclera and ocular muscle	Foreign body response (proteolytic degradation)	Reduced number of filaments and diameter at 42 days; absorption at 90 days *in vivo*
Unknown/ assumed virgin silk	Rabbit/ abdominal wall muscle	Foreign body response (proteolytic degradation)	80% decrease in tensile strength at 12 weeks; 0% strength at 2 years; decrease in the number of fibers observed histologically; fragmentation following 4 weeks *in vivo*

Silk fibroin can be readily transformed into several chemical forms which makes this natural polymer a very versatile biomaterial. To fabricate different silk fibroin-based materials, the fibroin fibers extracted from cocoons must first be solubilized. The solubilization damages the crystalline secondary structure of the polymer but conserved the integrity of the primary structure. Solubilization of silk fibroin can be achieved by immersion in lithium bromide solution or lithium thiocyanate solution and the process is done at temperatures between 60 and 80°C (Bhat and Ahirrao, 1983). Materials such as films, hydrogels, sponges, and nanofibers can be achieved from soluble silk fibroin for many potential biomedical applications (Table 7).

Table 7. Various biomedical applications for silk fibroin (Rockwood et al., 2011).

Application	Tissue type	Material format
Tissue engineering		
	Bone	HFIP sponges[41,43,44]
		Aqueous sponges[43,45,46]
		Electrospun fibers[36]
	Cartilage	HFIP sponges[47]
		Aqueous sponges[48–50]
		Electrospun fibers[51]
	Soft tissue	HFIP sponges[52]
		Aqueous sponges[52]
		Hydrogels[15]
	Corneal	Patterned silk films[31,53]
	Vascular tissues	Tubes[22]
		Electrospun fibers[54–56]
	Cervical tissue	Aqueous sponges[57]
	Skin	Electrospun fibers[58,59]
Disease models		
	Breast cancer	HFIP sponges[60]
		Aqueous sponges[61,62]
	Autosomal dominant polycystic kidney disease	Aqueous sponges[63]
Implant devices		
	Anterior cruciate ligament	Fibers[64,65]
	Femur defects	HFIP sponges[17]
	Mandibular defects	Aqueous sponges[66,67]
Drug delivery		
	Drug delivery	Spheres[34,68–70]
	Growth factor delivery	Spheres[71]
	Small molecule	Spheres[33]

Note: The sources for the reagents and equipment described in these protocols are given only as examples. Equivalent materials can be used unless otherwise noted.

Fibroin films, for example, are generally prepared simply by the slow evaporation of water. The solution is dispensed on a mold to create the desired shape and water is evaporated naturally creating a solid fibroin film. Films can be immersed in methanol in order to induce β-sheet formation and creating an insoluble film (Rockwood et al., 2011).

Fibroin hydrogels are formed from a network of compact fibroin protein positioned in three dimensions in a solution. Hydrogels can be fabricated through a thermal process where the temperature is raised, through a chemical process where the pH is lowered, or a physical process where the solution undergoes agitation all accelerating the gelation of the fibroin solution.

Fibroin sponges have recently been studied in tissue engineering and there are numerous fabrication techniques available. A few of the most commonly used techniques are freeze-drying (Li et al., 2001), using saline agents (Kim et al., 2005), or using gas (Nazarov et al., 2004). Depending on the technique and the parameters of the chosen technique, properties such as pore size and material density can be controlled.

Fibroin nanofibers are fabricated by electrospinning. A material based on organized or unorganized nanofibers can be created using this technique. The organization of electrospun silk fibroin-based materials can become very complex depending on the equipment used during the material fabrication (Rockwood et al., 2011). The produced material must then be immersed in methanol or undergo water vapor annealing in order to insolubilize the material inducing β-sheets in the secondary structure.

5. Electrospinning

Electrospinning was discovered in the 1930's and the technique has been improved over the past decades (Kakade et al., 2007). Electrospinning is a technique used to produce nanofibers between 50 nm to 1μm in diameter (Vepari and Kaplan, 2007) from a multitude of both natural and synthetic materials. Materials produced by the electrospinning process exhibit a considerably high surface to volume ratio and tend to possess improved mechanical properties, such as tensile strength, compared to their mico- or macro-sized counterparts (Huang et al., 2003). Electrospinning has been exploited in the field of tissue

engineering due to several advantages including the biomimicking characteristics of easily generated, non-woven nanofiber mats. These porous nanofiber mats resemble the structure of extracellular matrices and therefore have excellent prospect for numerous applications in regenerative medicine (Agarwal et al., 2008).

There are three main components of an electrospinning setup: a high voltage generator, a capillary needle, and a grounded collector (Figure 19). In order to perform the electrospinning process, a polymer solution contained within a syringe is continuously pushed through a spinneret which is subjected to a high voltage (often between 1 and 30kV) at the output of the capillary (Li and Xia, 2004). The charged polymer leaving the capillary is subject to attractive forces between the solution and the grounded collector. As the strength of the attractive forces on the droplet leaving the capillary output increases, the solution is pulled toward the collector transforming the naturally hemispherical shape of the extruding solution into a conical shape commonly known as the Taylor cone as portrayed in Figure 19 (Doshi and Reneker, 1995). Once these attractive forces overcome the surface tension of the solution, a thin jet stream is produced from the tip of the Taylor cone that travels toward the collector. The path of the jet is not straight, however; the jet undergoes violent whipping and stretching within the open space which allows the solvent to evaporate, and a charged nanofiber is deposited in a randomized manner onto the collector (Aznar-Cervantes et al., 2012; Li and Xia, 2004).

There are many parameters of the electrospinning process that influence the resulting material morphology obtained including solution properties and controllable operational variables. Solution properties include viscosity, conductivity, elasticity, and surface tension while working parameters include the applied electric potential, the hydrostatic pressure at the capillary tip, the distance between the spinneret and the collector, temperature, humidity, and air velocity (Huang et al., 2003; Doshi and Reneker, 1995); all parameters can be adjusted in order to fabricate materials with varying fiber diameters, fiber organization, or material porosity (Rockwood et al., 2011).

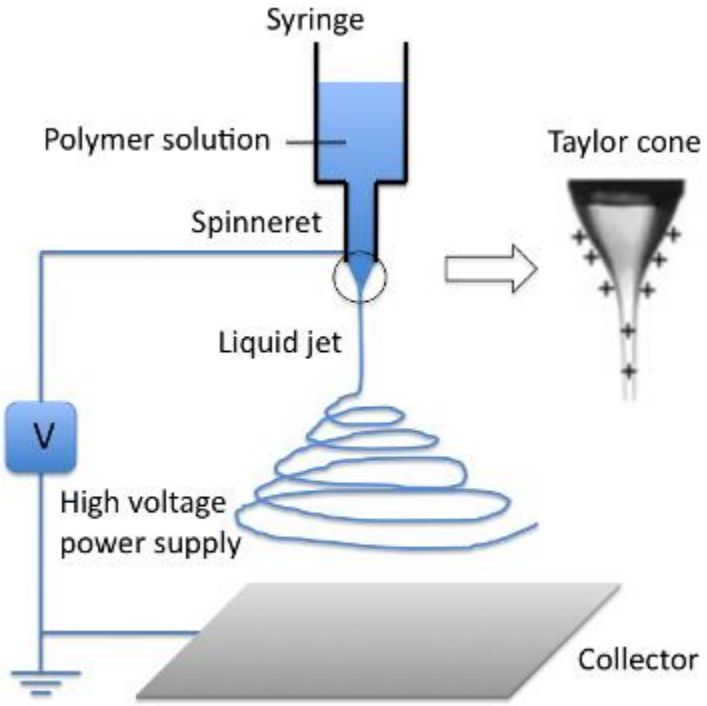

Figure 19. Setup for electrospinning simple, randomly deposited polymer nanofibers.

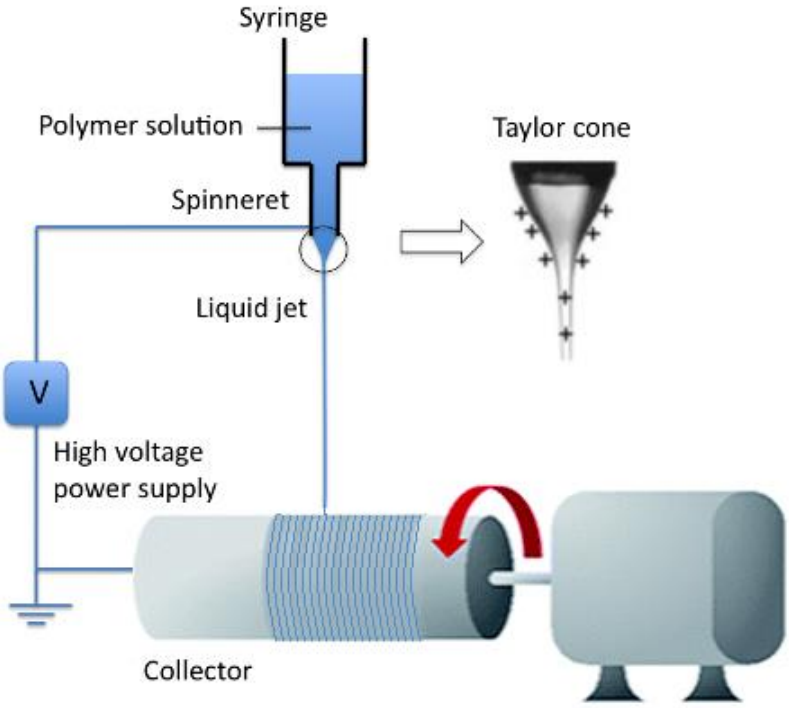

Figure 20. Electrospinning set up for the production of aligned nanofibers using a rotating drum collector.

The standard electrospinning technique to create non-woven nanofiber mats is interesting for various applications in biomedical engineering and many other fields, however, by changing the type of collector or deposition unit(s) used during the process, more elaborate and organized materials can be created meeting the needs of even more research problems leading to ever-growing application prospects. For example, aligned fiber-based materials are possible by the use of a high-velocity (up to thousands of revolutions per minute) rotating drum collector (Figure 20) (Huang et al., 2003). Optimization of this alignment method requires choosing a rotation velocity high enough for the desired degree of fiber alignment but not one as high as to cause the fiber jet to break (Huang et al., 2003). More complex nanofiber-based structures may be acquired by the use of patterned collectors such as the design developed by Nedjari et al. in order to mimic hemi-osteon structures. In this study, honeycomb micro-patterned collectors were fabricated resulting in a fibrous biomimicking scaffold of Poly(ε-caprolactone) (PCL) (Figure 21) able to support the adhesion and proliferation of osteoblast-like cells (Nedjari et al., 2014).

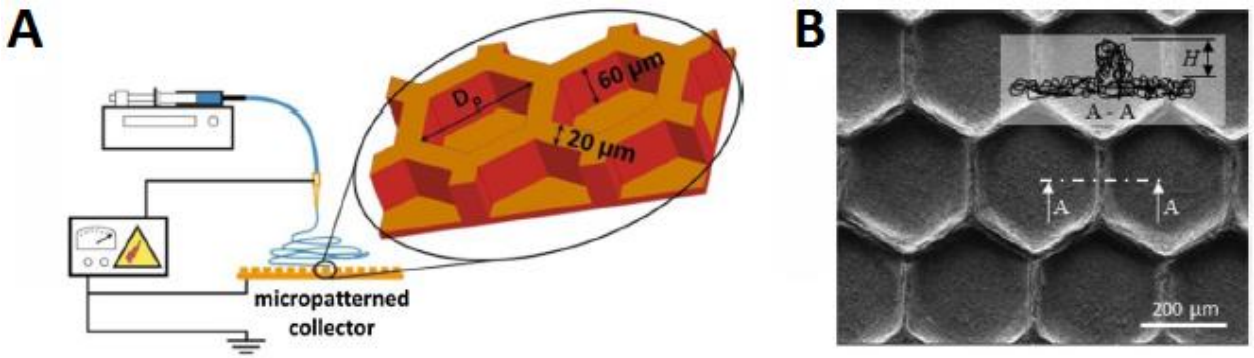

Figure 21. (A) Principle of electrospinning on micro-patterned honeycomb collectors with Dp=40, 80, 160, and 360µm. (B) SEM image of a PCL honeycomb scaffold obtained with Dp=360µm (Nedjari et al., 2014).

Other examples of electrospinning modification include the use of a coaxial spinneret (Figure 22) or a dual-spinneret system. In the case of a coaxial spinneret, fibers with a core and sheath made of different materials in order to obtain desired characteristics of both materials may be produced. Fibers with hollow interiors may also be produced using a coaxial spinneret

with the aim to improve the mechanical properties of the material (Li and Xia, 2004). A dual-spinneret system is a simpler method to create a composite material, but may also be used to carry out reactive electrospinning between polymers using a cross-linking agent during the electrospinning process (Figure 23) (Agarwal et al., 2008).

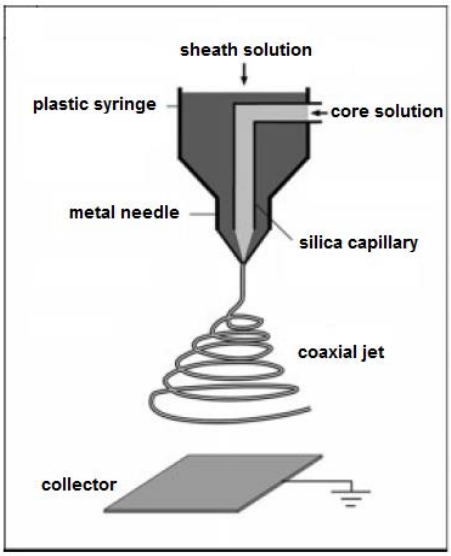

Figure 22. Schematic illustration of a coaxial spinneret for production of fibers with different core and sheath materials (Li and Xia, 2004).

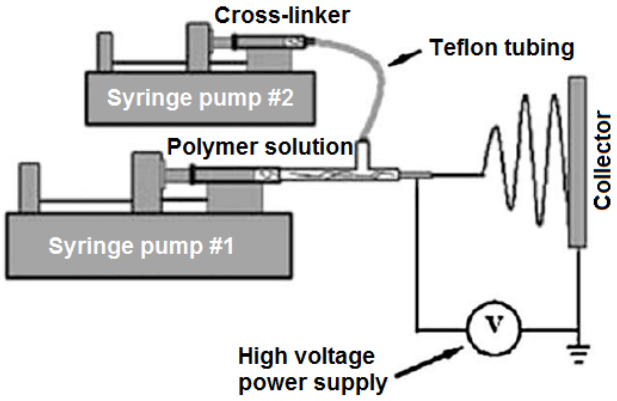

Figure 23. Schematic illustration of dual-spinneret reactive electrospinning using a polymer solution and a cross-linking agent (Agarwal et al., 2008).

Chapter 2

Materials and Methods

1. Silk fibroin-based material fabrication

1.1. Silk fibroin extraction and solution preparation

Cocoons from the *Bombyx mori* silk worm (Tajima Shoji Co., Yojohama, Japan) were cut into dime-sized pieces. 2 L of a 0.02 M sodium carbonate (Na_2CO_3) solution was brought to boil, and 5 g of cocoon pieces were added to the boiling solution. The silk cocoon pieces were immersed in the boiling solution under continuous stirring for exactly 30 minutes in order to dissolve the immunogenic sericin proteins. The degummed silk fibroin (SF) fibers were then rinsed in 1 L of deionized water at room temperature for 20 minutes 3 times. The rinsed fibroin fibers were squeezed to remove excess water and left to dry overnight. Dried SF fibers were dissolved in a 9.3 M lithium bromide (LiBr) solution at 60°C for 4 hours. The resulting solution was dialyzed for 3 days using dialysis cassettes (3,500 MWCO, Thermo Fisher Scientific) against 2 L of deionized water to remove salts. The resulting solution was then centrifuged twice to remove solid contaminants. The weight concentration of the SF solution is calculated by measuring the mass of 1 mL of the silk solution, allowing the water to evaporate overnight at 60°C, and measuring the mass of the solid SF film left over. SF solution concentrations vary between 5 and 7 wt% with a neutral pH. The SF stock solution is stored at 4°C for up to 2 months before spontaneous gelation occurs.

1.2. Silk fibroin electrospinning solutions preparation

The aqueous SF solution is concentrated to 10 wt% by adding the solution to a dialysis cassette and allowing sufficient water to evaporate. At 10 wt%, the aqueous SF solution does not have sufficient surface tension and viscosity to undergo electrospinning. Therefore, a 5% poly(ethylene oxide) (PEO) (MM=900 kDa, M_v ~900,000, Sigma-Aldrich) solution is added at a 1:4 ratio to the 10 wt% SF solution. The final solution contains 8 wt% SF and 1 wt% PEO.

1.2.1. Functionalization

To functionalize the SF/PEO solutions, amounts of substances found in Table 1 were incorporated.

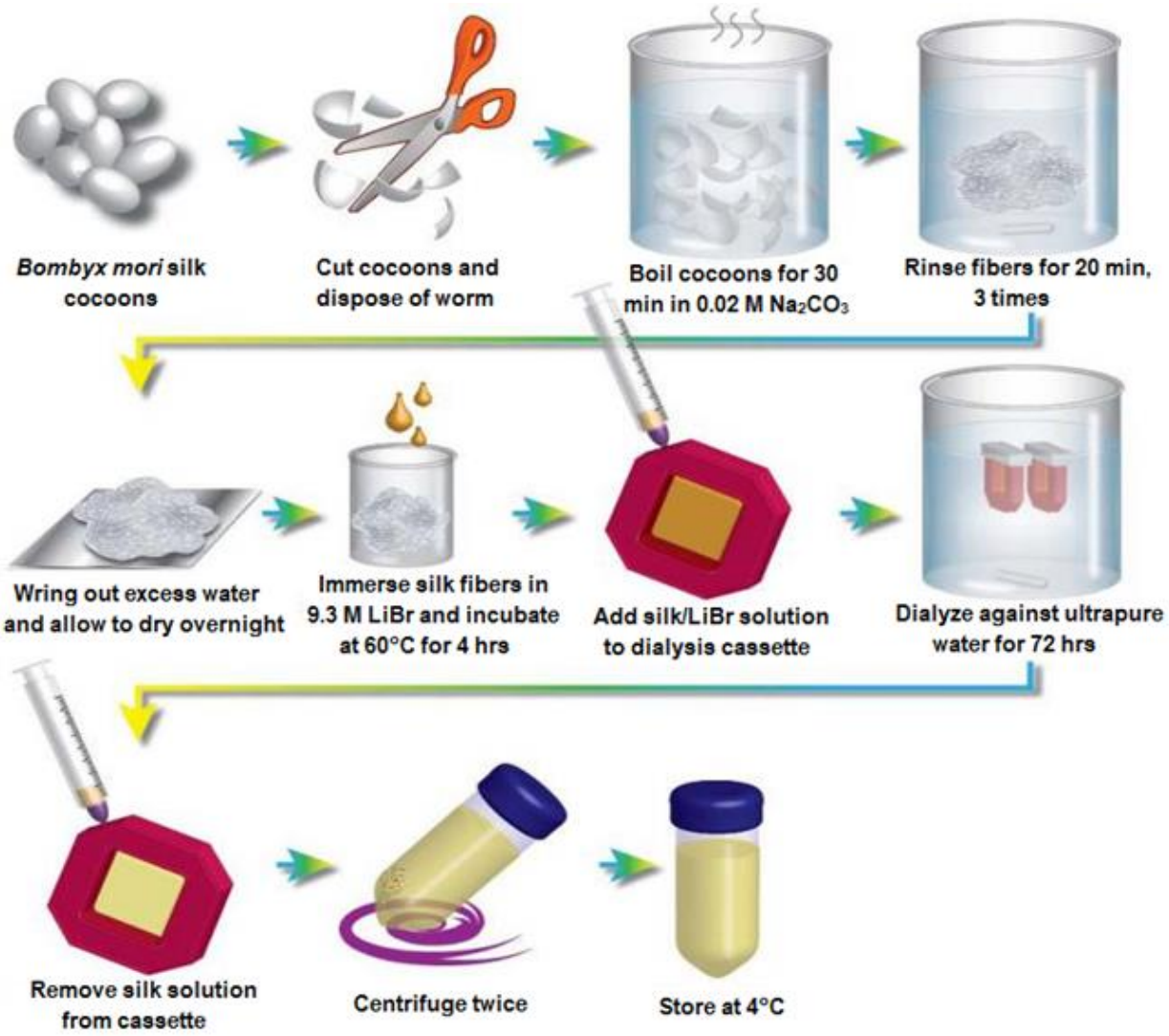

Figure 1. Degumming and solubilization of silk fibroin from *Bymbyx mori* cocoons.

Table 1. Functionalization of SF/PEO spinning solution

Substance	**NGF**	**NT-3**	**CNTF**	**Fn**	**GNP**	**IONP**
Amount in spinning solution	100 (ng/mL)	50 (ng/mL)	10 (ng/mL)	0.01 (% w/v)	0.05 / 0.11 (mM)	22 / 45 (mM)

1.3. Electrospinning: fabrication of nanofiber-based materials

1.3.1. Fabrication of randomly deposited fiber-coated coverslips for in vitro testing

The SF/PEO electrospinning solution (functionalized or non-functionalized) was added to a syringe with a 19 G stainless steel spinneret (Ramé-Hart Instrument Co) and placed on a syringe pump. The electrospinning solution was dispensed with a pump (Thermo Scientific, Waltham, MA) at a flow rate of 1 $mL \cdot hr^{-1}$ while a voltage between 10-15 kV was administered from high voltage generator (Gamma High Voltage Research ES-30P, Ormond Beach, FL, USA) to the spinneret. A rotating drum collector with a diameter of 7.75 cm and a width of 5 cm was positioned on the same axis as the spinneret at a distance of 12.5 cm from the spinneret tip. The humidity ranged between 30-50%. A layer of aluminum foil was secured on the surface of the drum before each procedure and 6 22x22 mm glass coverslips were secured to the aluminum foil with a small piece of electrical tape leaving a small space between each coverslip. the spinning solution was dispensed continuously for 10-20 minutes while the drum collector rotated at 250 RPM resulting in a surface velocity of 1 $m \cdot s^{-1}$. The coverslips were then removed and stored in a dust-free, moisture-free environment until used.

1.3.2. Fabrication of aligned fiber-coated coverslips for in vitro testing

The SF/PEO electrospinning solution (functionalized or non-functionalized) was added to a syringe with a 19 G stainless steel spinneret and placed on a syringe pump. The electrospinning solution was dispensed at a flow rate of 1 $mL \cdot hr^{-1}$ while a voltage between 10-15 kV was administered to the spinneret. The humidity ranged between 30-50%. A Styrofoam block was positioned at 12.5 cm from the spinneret tip. A strip of aluminum foil was placed horizontally around the Styrofoam block with a width slightly smaller than the width of the coverslips. 2-4 22x22 mm glass coverslips were secured across the aluminum strip using electrical tape with a small gap in between each coverslip and on each end. The spinning solution was dispensed continuously for 5-15 minutes. The coverslips were then removed and stored in a dust-free, moisture-free environment until used.

1.3.3. Fabrication of randomly-deposited, aligned, and tri-layered fiber materials for in vivo testing

The SF/PEO electrospinning solution (functionalized or non-functionalized) was added to a syringe with a 19 G stainless steel spinneret and placed on a syringe pump. The electrospinning solution was dispensed at a flow rate of 1 $mL \cdot hr^{-1}$ while a voltage between 10-15 kV was administered to the spinneret. A rotating drum collector with a diameter of 12.8 cm and a width of 3 cm was positioned on the same axis as the spinneret at a distance of 12.5 cm from the spinneret tip. A layer of aluminum foil was secured on the surface of the drum before each procedure for easy material collection. The entire system was enclosed in a Plexiglas containment area with a controlled humidity range of 30-40%. To obtain an aligned fiber material, the spinning solution was dispensed continuously for 90 minutes while the drum collector rotated at 4,000 RPM resulting in a surface velocity of 26.8 $m \cdot s^{-1}$. To obtain an unaligned material composed of randomly deposited fibers, the spinning solution was dispensed continuously for 90 minutes while the drum collector rotated at 400 RPM resulting in a surface velocity of 2.68 $m \cdot s^{-1}$. To obtain a tri-layered material consisting of a first layer of aligned fibers, then a layer of randomly deposited fibers, followed by a final layer of aligned fibers, the spinning solution was dispensed for a total of 90 minutes: 30 minutes with a collector rotation speed of 4,000 RPM, followed immediately by 30 minutes at a rotation speed of 400 RPM, then followed immediately by 30 minutes at 4,000 RPM. After each procedure is complete, the strip of aluminum foil is carefully detached from the drum collector and the fiber material is carefully peeled from the foil strip. Each final electrospun materials had a length of 40 cm, a width of 3 cm, and a thickness of 80 μm (± 10 μm) and was stored in a dust-free, moisture-free environment until used.

1.4. Primary to secondary structure transition for SF-based material

In order to preserve the nanofiber architecture and insolubilize the SF-based material, the material was water vapor annealed for 4 hours or immersed in methanol for 5 minutes. Water vapor annealing is carried out by enclosing the material in a humid desiccator under vacuum. Once the water vapor annealing process or the methanol immersion process has been completed, the material will hold its shape and is no longer soluble in water do to the formation of β-sheets

as the SF transitions to its secondary structure. The resulting stable material was rinsed in deionized water at 37°C overnight in order to remove PEO which remains soluble in water. The material was rinsed once more, allowed to dry and stored in a dust-free environment until used.

1.5. Sample preparation for in vitro studies

1.5.1. Fiber-coated coverslips from 1.3.1 and 1.3.2.

Each fiber-coated glass coverslip was rinsed to remove PEO and sterilized in 70% ethanol overnight. Samples were stored in a dry, sterile environment until used for culture.

For DRG, PC12, and rat Schwann cell culture preparation, the following procedure was respected. One day preceding cell culture, samples were coated with poly-D-lysine (Sigma Aldrich) and laminin (Sigma Aldrich) for improved cell adhesion in order to protect cells from shear stress during media changes. 200 µL of filtered Poly-D-lysine (100 µg/mL) in 9% NaCl solution was added on each sample to cover the entire coverslip surface and left for 20 minutes at room temperature. Samples were rinsed with sterile Milli-Q water. 200 µL of filtered laminin (5 µg/mL) in PBS was added on each sample to cover the entire coverslip surface. Samples were left overnight at 4 °C. Samples were rinsed with sterile Milli-Q water and left to dry. Individual dry samples were placed in wells of a 6-well plate ready for culture.

For L929 cell culture preparation, the following procedure was respected. 200 µL FBS (Thermo Fisher Scientific) was added on each sample to cover the entire coverslip surface and left for 3 hours at 37 °C. Samples were rinsed with sterile Milli-Q water and left to dry. Individual dry samples were placed in wells of a 6-well plate ready for culture.

1.5.2. Material samples from 1.3.3.

Before the water annealing treatment of the electrospun materials, a material sample 25 mm long (in the direction of the aligned fibers) and 15 mm wide (in the direction perpendicular to the aligned fibers) was cut from the electrospun material using a clean scalpel blade. The 25x15 mm sample was secured to a 22x22 mm glass coverslip with a drop of water to the material edges which were folded underneath the coverslip. The coverslips were water vapor annealed for 4

hours which resulted in the material samples to be securely attached to the coverslips with a flat fiber material surface for cell culture. The samples were rinsed to remove PEO and sterilized in 70% ethanol overnight. Samples were stored in a dry, sterile environment until used for culture.

One day preceding cell culture, samples were coated with poly-D-lysine and laminin for improved cell adhesion in order to protect cells from shear stress during media changes. 200 µL of filtered Poly-D-lysine (100 µg/mL) in 9% NaCl solution is added to each well of a 6-well plat. Each sample was placed upside-down on the drop of poly-D-lysine solution (20 min at room temperature) in order to stay in contact with the material surface as the thick fiber material tends to absorb and transport the solution under the sample very quickly preventing an effective coating. Samples were rinsed with sterile Milli-Q water. 200 µL of filtered laminin (5 µg/mL) in PBS is added to each well of a 6-well plat. Samples were placed similarly to the previous step and were left overnight at 4 °C. Samples are rinsed with sterile Milli-Q water and left to dry. Individual dry samples were places in wells of a 6-well plate (material surface up) ready for culture.

1.6. Sample preparation for in vivo studies

1.6.1. Multi-channeled tube

Before the water annealing treatment of the electrospun materials (aligned, tri-layered, functionalized, and non-functionalized materials), material samples 5 mm long (in the direction of the aligned fibers) and 30 mm wide (in the direction perpendicular to the aligned fibers) were cut from the electrospun materials using a clean scalpel blade. The materials were then rolled while adding a Teflon-coated stick (0.2 mm diameter) after every full rotation. Once completely rolled, the free edge of each material was tightly pressed to the outside of the rolled tube and the tubes were immediately immersed in methanol for 5 minutes to induce β-sheet formation. The tubes were allowed to air-dry for 1 hour and the Teflon-coated sticks were then removed resulting in 5 mm long multi-channeled tubes. The tri-layered samples were rinsed to remove PEO and stored in a dry, dust-free environment until use. The aligned samples were rinsed to remove PEO, sterilized in 70% ethanol overnight, and stored in a dry, sterile environment until use.

1.6.2. Tri-layered jacket layer

Before the water annealing treatment of the tri-layered electrospun material, material samples 7 mm long and 30 mm wide were cut from the electrospun materials using a clean scalpel blade. Each multi-channeled tube was placed at the bottom-center of a 7x30 mm tri-layered material sample (aligned fibers in the same direction). The larger material was then rolled around the tube for 3 rotations to create a "jacket". The edge was tightly pressed to the tube and the resulting devices were water vapor annealed at room temperature for 4 hours to induce β-sheet formation. The jacketed implants were rinsed in order to remove PEO then sterilized in 70% ethanol overnight. The implants were stored in a dry, sterile environment until use.

2. Nanoparticle solution preparation

2.1. Gold nanoparticles

Protocol taken from Aufaure et al. Two precursor solutions were prepared: solution A-38.8 mg of chloroauric acid ($HAuCl_4 \cdot 3H_2O$, ≥99.9%, Sigma-Aldrich, St Louis, MO) were dissolved in 5 mL of DI water. Solutions B-59.1 mg of trisodium citrate ($Na_3C_6H_5O_7$, ≥99%, Acros Organics) were dissolved in 5 mL of DI water. 125 mL of solution A and 250 mL of solution B were added to 9.5 mL of DI water in a 30 mL MW tube. The mixture was heat at 100 C during 10 min. A red wine coloured solution of 14.1 ± 1.1 nm diameter GNPs was obtained. 25 mL of solution B were added to this Au@Ct NPs solution in order to adjust the citrate concentration on previously described HMBPene–$HAuCl_4$ ratio. (Aufaure et al., 2014)

2.2. Iron oxide nanoparticles

Protocol taken from Demay-Drouhard et al. Maghemite (γ-Fe_2O_3) nanocrystals were synthesized by soft chemistry according to a procedure originally described by Lalatonne et al. Coating with BPheptyne was achieved by adding a solution of the bisphosphonate (5 mL, 60 mg, 0.2 mmol) in water at pH 2 to an aqueous solution of γ- Fe_2O_3 nanocrystals (20 mL, [Fe]=0.1–0.15 M). The solution was stirred at room temperature for 2 h. The γ-Fe2O3@BPheptyne particles were collected under a magnetic field and washed ten times with acidic water (pH 2). The as-synthesized nanoparticles were then dispersed in distilled water and the pH was adjusted to 7.

The average number of molecules of BPheptyne per nanocrystal was measured by 31P NMR spectroscopy, ATG, and EDX measurements. (Demay-Drouhard et al., 2013)

3. Fabrication of Alexa Fluor-tagged fibronectin

A 5 µL solution of Alexa Fluor 488 or Alexa Fluor 568 at a concentration of 10 mg/mL in DMSO was added to a 1 mL solution of fibronectin at a concentration of 1.78 mg/mL in a 0.1 M carbonate/bicarbonate buffer solution at pH 8.3 and left for 1 hr at room temperature in the dark. The tagged fibronectin is then separated using a Sephadex G25 column with PBS. The concentration of tagged fibronectin was obtained by the measured absorbance in a spectrometer using the following equations:

$$(1)\ A_{prot} = A_{280} - (A_{578} \cdot CF_{AF578})\ ,\ where\ CF_{AF578} = 0.46$$

$$(2)\ A_{prot} = A_{280} - (A_{494} \cdot CF_{AF488})\ ,\ where\ CF_{AF488} = 0.11$$

4. Mechanical strength testing

4.1. Tensile strength testing

For tensile strength tests, purely aligned, randomly deposited, and tri-layered electrospun material samples were rolled 4 rotations to produce a hollow tube. The tubes were water vapor annealed for 4 hours at room temperature then immersed in Milli-Q water overnight at 37°C to extract the PEO from the fibers. The tubes were subsequently rinsed then immersed in PBS prior to testing. Hydrated material samples were consecutively secured lengthwise between the upper and lower holding grips of the universal testing machine (BOSE Electroforce 3230) with a gauge length of 3 mm. Each trial was carried out at a cross-head speed of 0.06 mm·s-1 while recording load measurements every 100 ms until rupture. Assays for each material were done in triplicate. All values are represented by mean ± standard deviation.

4.2. Tear resistance testing

In order to test the tear strength of the materials, aligned and tri-layered material samples wear punctured with a 9-0 round bodied suture needle with a polyamide 6/6 thread 1 mm from

the materials' edge. The suture thread was trimmed on both sides of the puncture, but not knotted. The threaded material was secured in the lower holding grips of the universal testing machine (BOSE Electroforce 3230) at the opposite edge of the puncture while the two free suture threads were secured in the upper holding grips. The sutured material was adjusted automatically in order to assure equal tension between both sides of the suture thread. The tensile force of the system was then measured with a cross-head speed of 0.06 mm·s-1 up to a maximum displacement of 4 mm. Essays were done in triplicate. All values are represented by mean ± standard deviation.

5. In vitro studies

All cells were incubated in an incubator set to 37 °C in providing a humid environment with a CO_2 content of 5%.

5.1. Fetal rat dorsal root ganglia extraction and culture

Dorsal root ganglia (DRG) are ganglia located along the length of the spinal cord and contain several cell types including sensory neuron (the cell body of peripheral sensory neurons are located in the DRG) and glial cells. Motor neurons are not present in a DRG culture since the cell body of motor neurons is located in the spinal cord. DRG are taken from rat fetuses shortly after the nervous system has been developed and therefore the neurons are young and more resilient than adult rat sensory neurons. All procedures have been carried out in compliance with the 2010/63/UE European guidelines and the ethics committee of the Université de Technologie de Compiègne.

Ham's F-12 nutrient media (Thermo Fisher Scientific) was supplemented with horse serum, glutamine, and antibiotics penicillin and streptomycin in order to produce the culture media used in sections 4.1.1 and 4.1.2.

5.1.1. Fetal rat dorsal root ganglia culture

A timed pregnant (d 15-17) Sprague-Dawley rat is euthanized by an injection of pentobarbital (1 mL per 100g of animal mass). The fur on the ventral surface of the animal is

disinfected by application of 70% ethanol. The abdomen of the animal is then cut open, the uterus is dissected out and transferred to a 10 cm Petri dish containing sterile, ice-cold HBSS (Gibco). The embryos are then dissected from the uterus using small pointed surgical scissors and transferred to a second sterile, ice-cold HBSS-filled Petri dish and placed on ice. Individual embryos are transferred to a third Petri dish with sterile ice-cold HBSS placed on ice under a stereo microscope. The DRG appear as two rows of white ball-like structures lining each side of the spinal cord. Therefore, the spinal cord is isolated from the body and the DRG are cut one-by-one from the spinal cord with small pointed surgical scissors. DRG are then immersed in a small Petri dish filled with Ham's F-12 culture media at 37 °C.

DRG are selected with a pipette and placed on the surface of the sample with minimum media. 3-5 DRG are positioned on each sample with sufficient space between DRG. Culture plates were left in the incubator overnight to allow initial cell adhesion. 2 mL of culture media with 100 ng/mL of NGF was added to each well making sure that the samples stay completely immersed in the media. The media containing NGF was changed every 2-3 days and cells were fixed after a period of between 2 and 9 days.

5.1.2. Dissociated fetal rat dorsal root ganglia culture

DRG are extracted as described in section 4.1.1 and collected in a 15 mL conical tube containing sterile, ice-cold HBSS. The tube is centrifuged at 500xg for 2 min and the supernatant is discarded. The DRG are resuspended in 3 mL of 0.25% trypsin in HBSS at 37 °C for 15 min. DRG are then centrifuged at 500xg for 2 min and the supernatant is discarded. The DRG are resuspended in 3 mL of culture media at 37 °C. Using three fire-polished glass Pasteur pipettes at decreasing tip diameters, mechanical agitation was carried out by pipette trituration (10-20 times) in order to break up clusters of cells attached to DRG tissue. The solution containing the extracted cells in mixed and 100 µL of the cell suspension is mixed with 100 µL of trypan blue and counted immediately. The cell suspension is diluted or concentrated as needed and between 30,000 and 35,000 in 100 µL of media is added to the surface of each sample. Culture plates are incubated overnight and 2 mL of culture media containing 100 ng/mL of NGF is added to each

well the following day. The media containing NGF was changed every 2-3 days and cells were fixed after a period of between 2 and 9 days.

5.2. Rat Schwann cell culture on functionalized silk fibroin fiber-coated samples

Rat Schwann cells were provided by Innoprot; cells were isolated from rat sciatic nerve and were cryopreserved at passage one. Schwann cell culture media supplied by Innoprot for rat Schwann cell cultures was supplemented with FBS, Schwann cell growth supplement, and antibiotics penicillin and streptomycin. Cells were added to the surface of the fiber-coated coverslips at a density of 10,000 cells/cm^2 in 150 µL of the cell suspension. Once cells had adhered to the surface, 2 mL of culture media was added to each well and culture plates were incubated. Schwann cells were fixed after 48 hours in culture.

5.3. L929 cell culture on functionalized silk fibroin fiber-coated samples

L929 cells were cultured on material samples with Dulbecco's Modified Eagle's Medium (DMEM) with 1% glutamine, 1% penicillin/streptomycin, and 10% fetal bovine serum (FBS). Cells were fixed after 3 days in culture.

5.4. PC12 cell culture on functionalized silk fibroin fiber-coated samples

Cells at passage 3 were regularly cultivated in a media consisting of Roswell Park Memorial Institute Medium (RPMI) with 10% horse serum, 5% FBS, 1% penicillin/streptomycin, and 1% L-glutamine. A concentration of 100 ng/mL of NGF was added to the media in order to promote cell differentiation into neuron-like cells. Media was changed every 2-3 days and cells were fixed after between 5 and 7 days in culture.

5.5 MTS cytotoxicity assay

To test the cytotoxicity of the functionalized materials, an MTS assay was performed using the ISO 109933-515 standard. In this study, the mouse fibroblast cell line L929 was used which satisfied the ISO standard which states that a mammalian cell line should be used for the assay. L929 cells were used at passage 20. The MTS assay (Promega CellTiter 96® Aqueous One Solution

Proliferation Assay kit) is a colorimetric method for the sensitive quantification of viable cells in the proliferation and cytotoxicity assay in order to measure the metabolic activity of these cells. The reaction is based on the reduction of the compound [3-(4,5-dimethylthiazol-2-yl)-5-(3-carboxymethoxyphenyl)-2-(4-sulfophenyl)-2H-tetrazolium, inner salt; MTS] (Figure 2) by viable cells in order to generate a colored formazan product in the cell culture media.

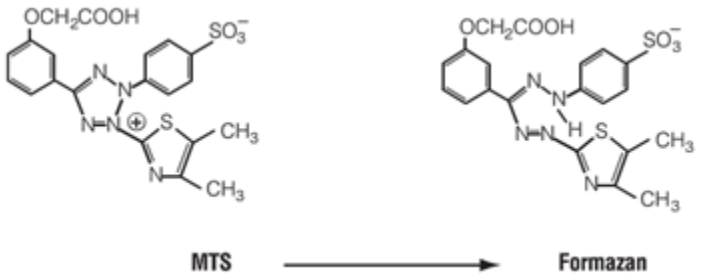

Figure 2. Enzymatic reaction of MTS to form formazan

The cytotoxicity study was carried out indirectly with the extract of the biomaterial: the extract was obtained by incubating the sample materials with the L929 culture medium for 24 hours. The materials were synthesized in the form of a flat surface of 170 cm^2 in accordance with the standard. The cells were incubated in the extract of the functionalized SF films with two different nanoparticle concentrations for GNPs (0.11 mM and 0.05 mM) and a single concentration for IONPs (45 mM). For each biomaterial sample, three dilutions were performed (30%, 60%, and 100%). A medium extract from incubation with latex was used as a positive control and media from cell culture not containing extract media was used as a negative control. 200 µL of MTS reagent was added to each culture well, then transferred to a 96-well plate and incubated for 3 hours at 37°C. The absorbance was measured at 490 nm in the spectrometer.

5.6. Immunostaining (in vitro)

Samples were immunostained with DAPI, anti-β-tubulin III antibody (Sigma Aldrich), and Alexa Fluor™ 488 phalloidin (Thermo Fisher Scientific) in order to visualize cell nuclei, microtubules found in the axons of neurons, and actin from non-neuronal cells. Samples were permeabilized in 0.5% Triton X-100 in PBS for 5 minutes at room temperature. Samples were

rinsed twice with PBS. Samples were then soaked in 1% BSA/PBS for 1 hour at room temperature. A solution of 0.66% anti-β-tubulin III in 0.1% BSA/PBS was added to samples and left for one hour. Samples were rinsed twice with 0.1% BSA/PBS. A solution of 0.8% Cy3-conjugated secondary antibody (Jackson Immunoresearch), 1% phalloidin, and 0.2% DAPI in 0.1% BSA/PBS was added to samples and left for one hour protected from light. Samples were rinsed 3 times. Samples were mounted on a microscope slide with Mowiol and left to dry, protected from light. Samples were stored at 4°C.

6. In vivo studies

6.1. Surgery

Surgery was performed at the animal center located at the research center of the Université de Technologie de Compiègne: Etablissement utilisateur d'animaux 0435 numéro d'agrément (D6015901).

12 six week old, male Sprague Dawley rats (Janvier Labs, France) were each anesthetized with Vetflurane (Virbac) throughout the entirety of the operation. The rats' right hind limbs were each shaved and sterilized. For each rat, an incision parallel to the femur was made and the sciatic nerve was exposed, isolated, and fixed with two micro clips 10 mm apart. The nerve was severed at the distal end of the fixed section and the implant's outer layer was sutured (Ethicon Ethilon Polyamide 6/6 suture, 9-0 round bodied) twice to the distal segment's epineurium (at 0° and 180°) enveloping the epineurium and nerves fascicles. From the proximal nerve segment, a 3-4 mm portion of nerve was extracted and discarded. The exposed epineurium and fascicles of the proximal nerve segment were inserted into the small cavity of the implant, and the implant's outer layer was sutured twice to the epineurium (at 0° and 180°). The operated area was then cleaned and the wound was closed and sutured.

6.2. Surgery follow up

After suture, wound was sanitized with Betadine. In order to limit the post-operative pain, we administered 10 mg/kg of xylazine once per day for 3 days following surgery. Then, 1.3 mg/mL of acetaminophen was added to the water given to the animals for three more days. A cast

consisting of a plastic tubes cut from plastic pipette droppers and bandage was secured on the right limb of each animal and replaced daily or as needed for the first few weeks after surgery in order to prevent the animals from chewing on the desensitized limb. Animals were housed alone for 2 weeks following surgery then put in cages of two or three animals. Food and water was administered to animals ad libitum. Animals were weighed once per week.

6.3. Swimming sessions

2 months after surgery, animals were subjected twice per week to swimming sessions lasting one month. A 120 cm long, 80 cm wide, and 85 cm high recipient (Manutan, France) was filled with water at about 30°C reaching a depth of 30 cm. rats were allowed to swim freely for a session lasting between 5 and 10 minutes. After the session, animals were dried with a towel and allowed to completely dry under a heated lamp.

6.4. Motion capture analyses (Figure 3)

Experiments were carried out in the BMBI UMR CNRS 7338 Sport Health Technology platform. 18 cameras were used (Vicon Motion System Ltd. UK). In order to study the displacement of the animal, the rat walked across a board 10 cm in width and 150 cm in length located at 60 cm from the ground. A displacement is considered successful when the rat performs at least five steps without interruption. The capture of locomotion of the rat is ensured by the placement of retroreflective markers (Biometrics, France) on anatomical points portrayed in Figure 2. Following a shaving procedure ten markers are glued to the skin and to the anatomical points using hypoallergenic double-faced scotch. This makes it possible to study the kinematics of the underlying bone structures (sacrum, femur, tibia and metatarsus) during the locomotion of the rat.

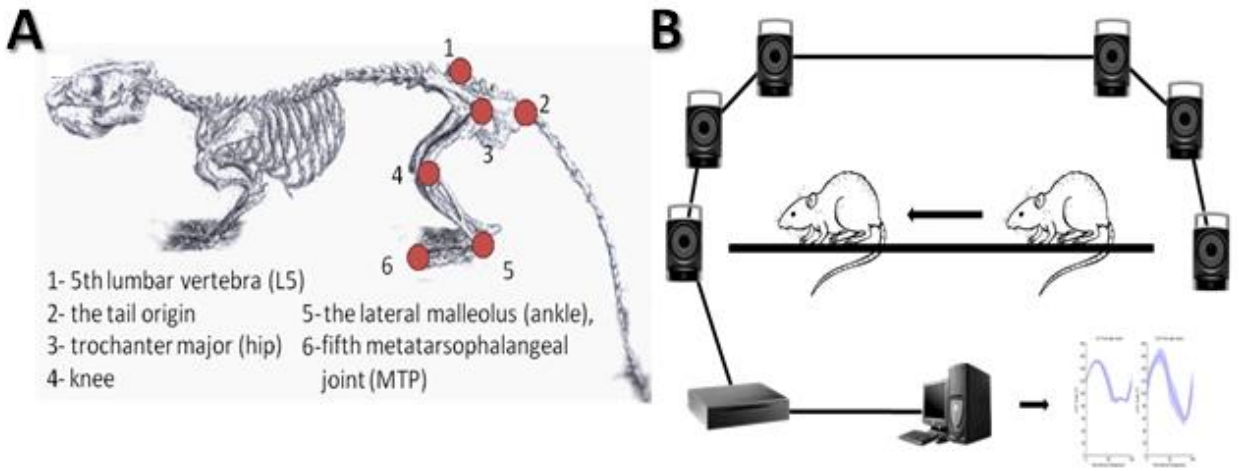

Figure 3. (A) placement of retroreflective markers for motion capture analysis and (B) general dipiction of the setup for motion capture assays; 18 cameras are positioned around a plank on which the animal walks in a a straight line.

6.5. EMG tests

The sciatic nerve was located and isolated, excess tissue was removed. A needle was pierced into a proximal portion of the injured nerve. An electrode was inserted into the gastrocnemius of the right limb. A reference needle was inserted under the skin of the rat at an area nearby the open wound. Increasing voltage intensities were administered through the proximal needle and the muscle response was recorded with a specialized software. Results were treated with a software made in house to measure peak amplitudes of muscle response.

6.6. Nerve sample retrieval and block preparation

At 4 and 8 months, a segment of nerve leaving space proximal and distal to the NGC was extracted from the animal and the animal was euthanized with an overdose of pentobarbital. Nerve segments were immersed in 4% formaldehyde for at least 3 days.

6.6.1. Nerve segment for cryostat sectioning

Fixed nerve segments were immersed in 15% sucrose solution until tissues sank. Nerve segments were then immersed in 30% sucrose solution until tissues sank. Samples were blotted dry and immersed in OCT compound overnight. Samples were then frozen using dry ice. Solid

blocks were stored at -20°C. Sections 8 µm thick were collected on SuperFrost® Plus microscope slides (Thermo Scientific) using a cryomicrotome (Leica CM 3050 S). Samples were stored until use at -20°C.

6.6.2. Nerve segment for paraffin embedded sectioning

Nerve segments were rinsed in PBS. Samples were then dehydrated with consecutive baths of 70% ethanol, 96% ethanol, 98% ethanol, and Xylene for one hour each. Dehydrated samples were immersed in paraffin at 60°C overnight. Samples were then positioned in a metal mold and put on ice to solidify. Samples were stored at room temperature. Sections 5-8 µm thick were collected on SuperFrost® Plus microscope slides (Thermo Scientific) using a microtome (Leica RM 2245). Slides were placed in an oven at 60°C in order to melt excess paraffin.

6.7. Immunostaining (in vivo)

6.7.1. Immunostaining with DAPI, anti-β-tubulin III antibody and Alexa Fluor™ 488 phalloidin

Cryostat sections were immunostained with DAPI, anti-β-tubulin III antibody (Sigma Aldrich), and Alexa Fluor™ 488 phalloidin (Thermo Fisher Scientific) in order to visualize cell nuclei, microtubules found in the axons of neurons, and actin from non-neuronal cells. Samples were permeabilized in 0.5% Triton X-100 in PBS for 5 minutes at room temperature. Samples were rinsed twice with PBS. Samples were then soaked in 1% BSA/PBS for 1 hour at room temperature. A solution of 0.66% anti-β-tubulin III in 0.1% BSA/PBS was added to samples and left for one hour. Samples were rinsed twice with 0.1% BSA/PBS. A solution of 0.8% Cy3-conjugated secondary antibody (Jackson Immunoresearch), 1% phalloidin, and 0.2% DAPI in 0.1% BSA/PBS was added to samples and left for one hour protected from light. Samples were rinsed 3 times. Samples were mounted with Mowiol and left to dry, protected from light. Samples were stored at 4°C.

6.7.2. Immunostaining with DAPI and anti-myelin protein zero antibody

Cryostat sections were immunostained with DAPI and anti-myelin protein zero antibody (Abcam) in order to visualize cell nuclei and protein zero found in the myelin sheaths formed by Schwann cells. Samples are permeabilized in 0.5% Triton X-100 in PBS for 5 minutes at room

temperature. Samples are rinsed twice with PBS. Samples are then soaked in 1% BSA/PBS for 1 hour at room temperature. A solution of 0.3% anti-myelin protein zero antibody in 0.1% BSA/PBS was added to samples and left for one hour. Samples were rinsed twice with 0.1% BSA/PBS. A solution of 0.5% Alexa Fluor 488 (Abcam) and 0.2% DAPI in 0.1% BSA/PBS was added to samples and left for one hour protected from light. Samples were rinsed 3 times. Samples were mounted with Mowiol and left to dry, protect from light. Samples were stored at 4°C.

6.8. HE staining

Paraffin-embedded sections immersed in two consecutive baths of xylene for 5 minutes each. Samples were then immersed in 98% ethanol, followed by 96% ethanol, followed by 70% ethanol each for 2 minutes. Samples were then immersed in DI water for 10 minutes followed by 5 minutes in hematoxylin bath. Samples were rinsed with running water for 5 minutes then immersed in eosin for 2 minutes. Finally, samples were redehydrated by imersion in consequtive baths of 70% ethanol, 96% ethanol, and 98% ethanol each for 2 minutes. Finally, samples were immersed in two consequtive baths of xylene for 5 minutes each before being mounted with EUKITT®. Samples are left to dry and stored protected from light at 4°C.

6.9. CE activity stain

Cryostat sections were stained for cholinesterase activity demonstrating motor axons in a nerve section. Combination of protocols developed by Szabolcs et al., Kawwasaki et al., and Karnovsky & Roots was followed. Samples were incubated in an incubation medium containing 4 mmM $CuSO_4$, 0.5 mM $K_3[Fe(CN)_6]$, 10 mM sodium citrate, and 2 mM acetylthiocholine in 0.1 M NaOH-maleate buffer (pH 6.5) for 19 hours at 4°C. Slides are rinsed in distilled water and mounted with Mowiol. Samples were allowed to dry and stored at room temperature.

7. Sample imaging

7.1. SEM

The diameter calculation of electrospun fibers along with the qualitative analyses of non-functionalized fibers or fibers functionalized with nanoparticle were done using a scanning

electron microscope (SEM) (FEI Quanta 250 FEG). Non-functionalized fibers were first gold sputter coated for enhanced visualization. Nanoparticle functionalized fibers were not gold sputter coated in order to visualize the embedded nanoparticles in and on the fibers.

7.2. TEM/STEM

The characterization of the size of the GNPs and IONPs was evaluated using a transmission electron microscope (TEM) (JEOL 2100F HT: 200kV); a small sample of each nanoparticle solution was left to evaporate on a TEM copper grid support. The TEM was used on both mode TEM and mode STEM for the visualization of GNP- and IONP-embedded fibers. In order to visualize the fibers, a TEM copper grid support was secured onto the electrospinning collector for direct fiber collection. The grids were treated by water vapor annealing and were rinsed as described in section 1.4.

7.3. Light microscopy

HE stained samples and CE activity stained samples were visualized under a light microscope (Leica DM 1000 LED).

7.4. Epifluorescence microscopy

Immunostained samples were visualized under an epifluorescence microscope (Leica DMI 6000B, 20x/0.40).

7.5. Confocal microscopy

Immunostained samples were visualized under a confocal microscope (Zeiss LSM 710, 63x/1.40 Oil DIC) and imaging was done using z-stacking in order to obtain a more comprehensive image since 8 µm samples were difficult to visualize at a single z value. DAPI and Alexa Fluor 488 filters were used.

7.6. ImageJ software

Measurement functions from the image analysis program ImageJ were used for the calculation of average particle diameters, neuron extension lengths, fiber angles and diameters, axon diameters, and myelin thickness. From the obtained measurements, values are reported as mean ± standard deviation unless otherwise specified.

Chapter 3

Results: Part 1

Nerve Guidance Conduit Design

Introduction

The material and implant design is presented by the following manuscript entitled “A Multi-layered Nerve Guidance Conduit Design Adapted to Facilitate Surgical Implantation.” This manuscript outlines the fabrication of the fibroin-based, aligned nanofiber material and the nerve guidance conduit design to be tested in Parts 2 and 3. The electrospun material possesses a complex, tri-layered architecture containing two aligned nanofiber surface layers and a randomly deposited nanofiber center layer. To create the nerve guidance conduit, the material was first rolled into a multi-, micro-channeled tube. This tube was then enclosed around a “jacket layer” of the tri-layered material which measured approximately 1 mm longer than the tube on each end.

This design was developed in order to first improve upon the weak structural support provided by the hollow nerve guides currently available on the market by the addition of micro-channels. In addition to structural support, the micro-channels in the presented device also improve the guidance capability of the NGC by increasing the surface area to volume ratio and providing an aligned fiber surface readily available for both nerve fibers and Schwann cells to adhere and follow. The jacket layer was added to the design in order to simplify the surgical process. The jacket layer creates two small pockets at either end of the device which facilitates correct positioning of the severed nerve segments and the epineurial micro-suture process. Finally, the tri-layered design yields an improvement on certain mechanical properties of the foundation material while not sacrificing the guidance properties of the surface fiber alignment. In particular, the tear strength was drastically improved which aids the surgeon during microsurgery.

The manuscript presents this device as a base design NGC possessing essential foundational elements of an effective NGC but focuses primarily on the surgical application which is regularly overlooked in peripheral nerve repair research. The material may therefore be further modified, as silk fibroin is a versatile biomaterial, to develop a system that may serve as a favorable alternative to the autograft.

*This device has been submitted for patenting on July 12, 2017 (Application N°: EP17305917)

A Multi-layered Nerve Guidance Conduit Design Adapted to Facilitate Surgical Implantation

Kayla Belanger, Guy Schlatter, Anne Hébraud, Frédéric Marin, Sylvie Testelin, Stéphanie Dakpé, Bernard Devauchelle, and Christophe Egles*

K. Belanger, Prof. F. Marin, Prof. C. Egles
Sorbonne universités, Université de Technologie de Compiègne, CNRS, UMR 7338, Biomécanique et Bioingénierie, Centre de recherches de Royallieu, CS 60319, 60203, Compiègne cedex, France
E-mail: Christophe.egles@utc.fr

Prof. G. Schlatter, Dr. A. Hébraud
ICPEES Institut de Chimie et Procédés pour l'Energie, l'Environnement et la Santé, UMR 7515, CNRS, Université de Strasbourg, 25 Rue Becquerel, 67089, Strasbourg cedex, France

Prof. S. Testelin, Dr. S. Dakpe, Prof B. Devauchelle
Facing Faces Institute, Amiens University Hospital Center 80054, Amiens Cedex 1, France

Prof. C. Egles
Tufts University, School of Dental Medicine, 1 Kneeland Street, Boston MA 02111, USA

Submitted to *Health Science Reports*

Abstract

The gold standard procedure after a severe nerve injury is the nerve autograft yet this technique has drawbacks. In recent years, progress has been made on the development of artificial nerve guides to replace the autograft, but no device has been able to demonstrate superiority. The present study introduces an adaptable foundation design for peripheral nerve repair. Silk fibroin was electrospun creating a tri-layered material with aligned fiber surfaces and a randomly deposited fiber interior. This material was rolled into a micro-channeled conduit which was then enveloped by a jacket layer of the same tri-layered material. The proposed implant design succeeds in incorporating various desirable aspects of synthetic nerve guides while facilitating the surgical implantation process for medical application. The aligned fiber surfaces of the conduit support axon guidance while the tri-layered architecture improves its structural integrity compared to a fully aligned fiber material. Moreover, the multi-channeled design increases contact with the material surface compared to hollow nerve guides which aids in axon guidance. In addition, the jacket layer creates a small niche on each end which facilitates surgical implantation. Taken together, our results advance the development of artificial nerves by creating a surgically implantable device made of silk fibroin.

Keywords: nerve regeneration, nerve guidance conduit, implant, silk fibroin, electrospinning

1. Introduction

The nervous system is made up of the central nervous system (CNS) and the peripheral nervous system (PNS). The CNS includes the brain and spinal cord while the PNS includes all nerves that branch out from the CNS. Nerves in the PNS contain sensory, or afferent, neurons that carry information to the CNS and motor, or efferent, neurons that transmit information from the CNS to the periphery. The cell bodies of motor and sensory neurons are located in the spinal cord and in dorsal root ganglia respectively, and each have long extensions called axons that innervate the various organs throughout the body. Due to environmental constraints in the CNS, spontaneous neuronal repair after injury does not occur.[1,2] The PNS differs in this characteristic supporting axon regeneration after a minor injury to the nerve, but if the injury is severe, spontaneous regeneration will not be successful.

After a severe injury to a peripheral nerve, the axon segments distal to the trauma site begin to degrade and the result is a loss of function locally as organs are denervated during a process called Wallerian degeneration.[3,4] Once the distal axon segments degrade, the proximal axon stubs begin to regrow toward their respective innervation targets assisted by biochemical cues and structural guidance from proliferating Schwann cells[3,5] In many minor nerve injury cases, nerves will regenerate naturally resulting in functional recovery without the need of surgical intervention. However, for more serious injuries where the gap between uninjured nerve segments cannot achieve a tension-free coaptation, a nerve graft must be implanted in order to bridge the gap between the proximal and distal segments of the nerve.[6]

In North America, between roughly 50,000 and 200,000 surgeries for nerve repair are performed each year.[7] The current gold standard for nerve repair is the nerve autograft which consists of grafting the damaged nerve with a nerve sample taken directly from the patient; samples are most often taken from the sural nerve located in the leg and the medial antebrachial cutaneous nerve located in the arm.[8] Other sensory nerve harvesting locations may be considered by surgeons such as the superficial cervical plexus. Not only is this method's

effectiveness in nerve regeneration less than optimal resulting in full functional recovery in only half of cases, it has several other drawbacks such as the need for multiple operations, limited donor tissue availability, loss of function at the donor site, and the risk of developing a painful neuroma at the donor site.[5,9] Before following through with a nerve autograft procedure, it is important that the surgeon inform the patient of the consequential postoperative sensory loss in either the lateral portion of the foot or the medial portion of the mid-forearm (a common side effect of an autograft from the sural nerve and medial antebrachial cutaneous nerve respectively) as the loss of sensory function in one area may be more or less significant for each patient.

In order to overcome the drawbacks presented by the autograft, researchers have turned to tissue engineering in order to develop a more effective alternative using biomaterials. In particular, the natural polymer silk fibroin is a promising material for the fabrication of a nerve guidance conduit since it is biocompatible, biodegradable, easily functionalized, easily chemically modified, and has robust mechanical properties compared to other natural materials.[10] In addition to the choice of biomaterials, an effective nerve guidance conduit must provide an environment that encourages healthy, guided axon regrowth.[5] The conduit must therefore succeed in preventing the regrowing axons from straying far from their original paths towards their innervation targets. If regenerated neurons were misdirected during regrowth, not only will functional recovery be significantly reduced in intensity, but the patient may also require sensory and motor re-education therapy in order for the brain to recognize entirely new input as neurons that once innervated one area of the body may have reinnervated a different area.[8] In cases of minor injuries to the nerve, axons are directed by the naturally realigning Schwann cells that release biological cues thus attracting growth cones and successfully leading the axons along their original paths toward their innervation targets. The autograft has an advantage regarding guidance capabilities due to the numerous micro-channels in the predeveloped fascicles which increase the surface area to volume ratio and lower the possibility of axons to stray from a predetermined

route.[11,12] Most artificial nerve guidance conduits on the market however are hollow tubes that do not provide as much mechanical support.[11]

The epineurium is the outermost layer of the nerve made up of dense connective tissue which houses the nerve fascicles that have their own layer of protective connective tissue called the perineurium. In most cases, autografts or nerve guidance conduits are sutured at the epineurium of the nerve at the proximal and distal nerve stumps in order to connect a severed nerve.[13] In some cases, several nerve grafts are sutured directly at perineurium of each fascicle, but a puncture to the epineurium will cause the least physical disturbance to regenerating neurons.[6,12] However, after a nerve is severed, surgeons observe that the epineurium will naturally retract a small percentage further than the nerve fascicles due to a release in tension. This consequence poses a challenge for surgeons to correctly position implants with blunt edges such as an autologous nerve graft. This is because as the epineurium is stretched to connect with the outer layer of a blunt-edged implant, the fascicles may become deformed weakening the prospect of successful neuron guidance. Hollow nerve guidance conduits such as Neuroflex or NeuraGen overcome this obstacle since the protruding nerve fascicles are simply inserted into the hollow cavity of the implant.[14] However, hollow conduits provide minimal directionality due to lower physical support.

Finally, the mechanical strength of the device is an important parameter that must be considered.[15] The implant must be resistant to all forces acting upon the implant during and after implantation. For example, a weak resistance to tensile forces after surgery can lead to poor regeneration, and surgeons request that regenerating neurons travel a longer distance through a longer implant as opposed to a shorter implant that is put under excessive stress.[8,12] Therefore, the implant must uphold a certain stability while under tensile stress in order to achieve a conduit with a relatively small length and an environment that will promote healthy neuron growth. The material must also withstand the trauma of suture during the surgery and therefore must possess strong tear strength in order to facilitate successful implantation.

The goal of this study was to develop an adaptable implant foundation design capable of providing enhanced guidance to regenerating neurons that also caters to the needs of the surgeon during implantation.

2. Results

2.1. Nerve Guidance Conduit Design

After a total of 3×30 minutes of electrospinning, a tri-layered fibrous silk fibroin material 3 cm wide and 80 µm (±10 µm) thick was obtained. The tri-layered material consisted of an internal layer of randomly deposited fibers which was sandwiched between two layers of aligned fibers. Fibers diameters were found to be 417 ± 134 nm with 94% of diameters within the range of 200 nm and 600 nm. 86% of fiber angles were found to be within ± 5° of the primary alignment. The tri-layered material presented three distinct layers visible through SEM analyses (Figure 1). The aligned-fiber surfaces of the tri-layered material were also shown to completely cover the random fiber center layer (figure 1B) assuring that the guidance factor of this material was not compromised.

A multi-channeled conduit capable of maintaining its structure after water vapor annealing (necessary to induce the formation of silk fibroin β-sheets) was obtained and is shown in Figure 2.

2.2. Mechanical Tests

Ultimate tensile strength and Young's modulus characterizations of aligned, random, and tri-layered material samples are represented in Figures 3, 4, and 5 respectively. For the samples with aligned fibers, the tensile strength tests were carried out according to the direction of the fibers. The considered apparent tensile stress σ is calculated from the cross sectional area (A=0.08mm×30mm) of the sample.

The aligned and tri-layered material samples were shown to possess similar average ultimate strength measurements of 2.89 MPa and 2.63 MPa respectively which were slightly

higher than that of the rat sciatic nerve (2.55 MPa) and significantly higher than that of the randomly deposited material demonstrating an average ultimate strength of 0.49 MPa. The aligned material was found to be significantly more resistant to elongation than both the randomly deposited and tri-layered material samples exhibiting an average elongation of 85% at the ultimate strength. This behavior is comparable to the rat sciatic nerve which had an elongation of 80% at ultimate strength. Randomly deposited and tri-layered material samples had similar elongation values at ultimate strength (250% and 263% respectively) which were thus significantly higher than that of aligned fibers. This behavior can be explained by the rearrangement and the alignment of the random fibers with respect to the tensile direction.[16] Randomly deposited and tri-layered material samples also showed some elasticity, i.e. a linear relationship between the stress and elongation, before permanent deformation whereas the aligned material did not present any apparent elastic characteristics. Young's modulus values of the aligned, tri-layered, and randomly deposited materials were found to be 14.9 MPa, 13.0 MPa, and 1.2 MPa respectively compared to the Young's modulus of the rat sciatic nerve at 3.6 MPa. Finally, in comparison to randomly deposited and tri-layered material samples, aligned material samples were found to be more brittle demonstrated by complete rupture very shortly after reaching the maximum stress (Figure 3). The tri-layered material samples preserved continuity long after initial rupture (Figure 3).

Tear strength characterizations of both aligned and tri-layered materials are shown in Figure 6. The sutured tri-layered material was able to resist an average maximum force of 50.7 mN ± 2.0 mN which was reached at a displacement of 2.2 mm ± 0.2 mm. The aligned material was able to withstand a maximum force of 13.7 mN ± 0.6 mN which was reached at a displacement of 0.3 mm ± 0.2 mm.

2.3. Surgery

Surgery was carried out on the right sciatic nerve of 12 male Sprague Dawley rats by following a 4-step process depicted in Figure 7. The implant was sutured to the distal nerve segment while

avoiding any disturbance to the nerve fascicles due to the small pocket provided by the jacket layer enveloping the multi-channeled conduit. The implant was then readily positioned to be sutured to the proximal nerve segment as the hollow pocket secured the nerve in the correct position for the final sutures as demonstrated in Figure 7c.

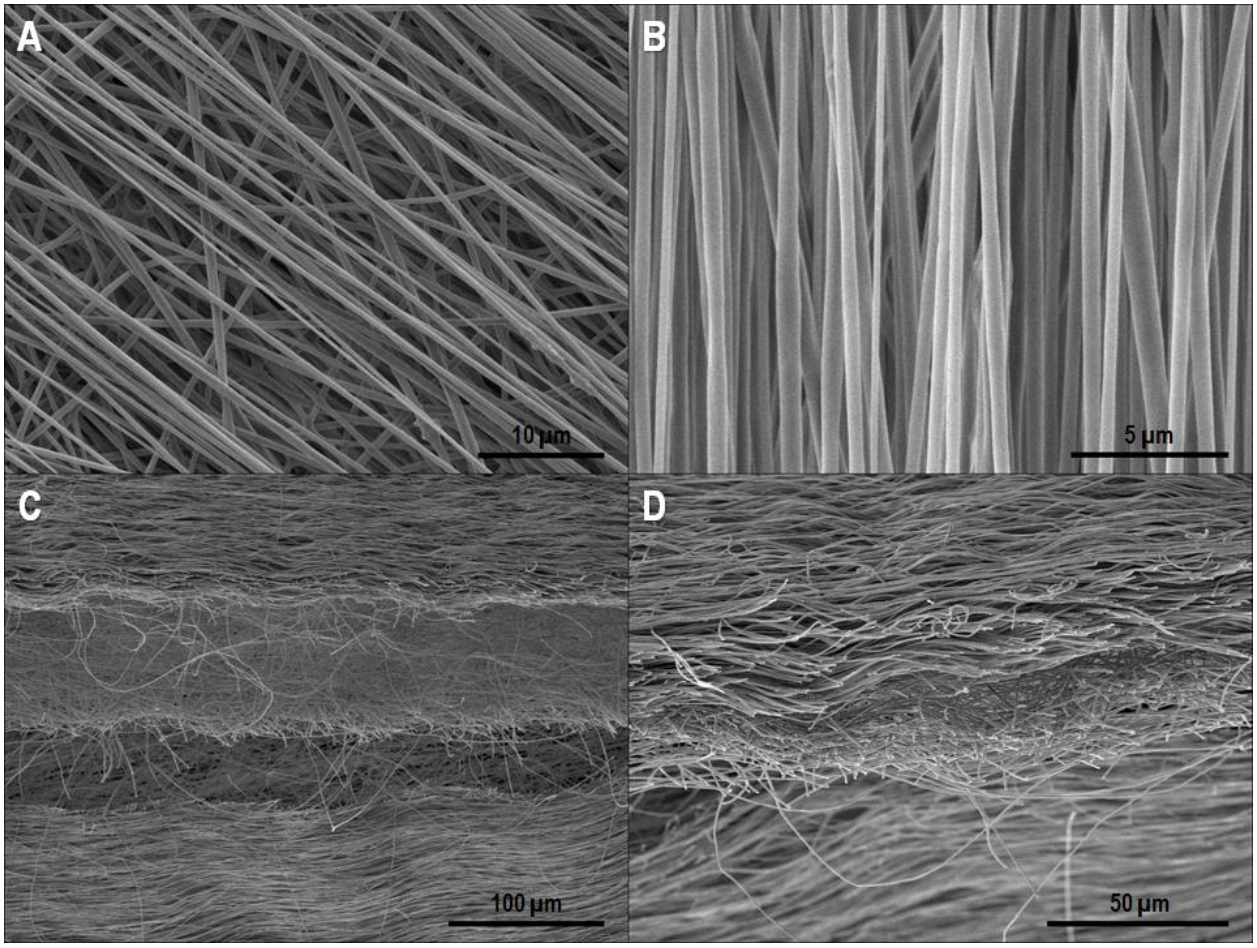

Figure 1*. SEM images of (A) beginning of the final aligned layer deposited on center unaligned layer; (B) material's aligned surface layer; (C) & (D) cross sections of the tri-layered material after snap frozen in liquid nitrogen and sectioned longitudinally

*Representative of Figure 1.1 of chapter 3.

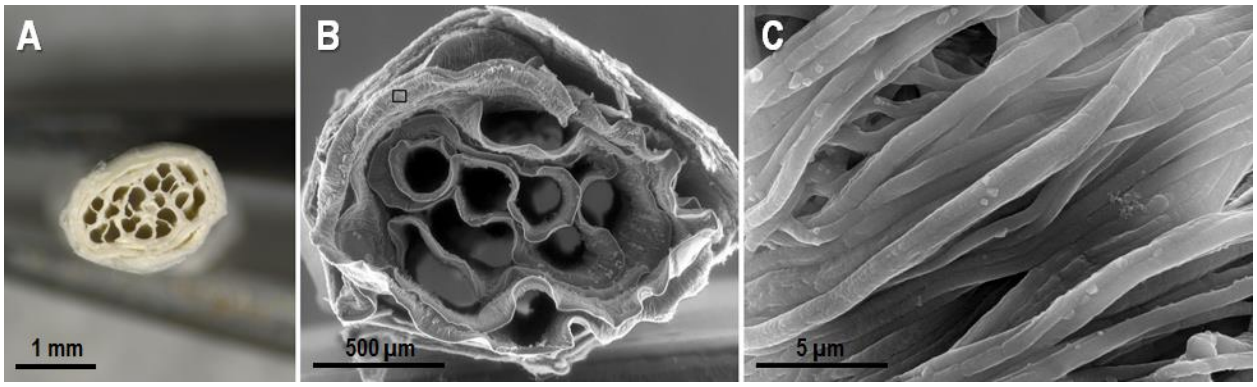

Figure 2*. (A) Cross section of implant, (B) SEM cross section of implant, and (C) close up of material surface from square frame in image B

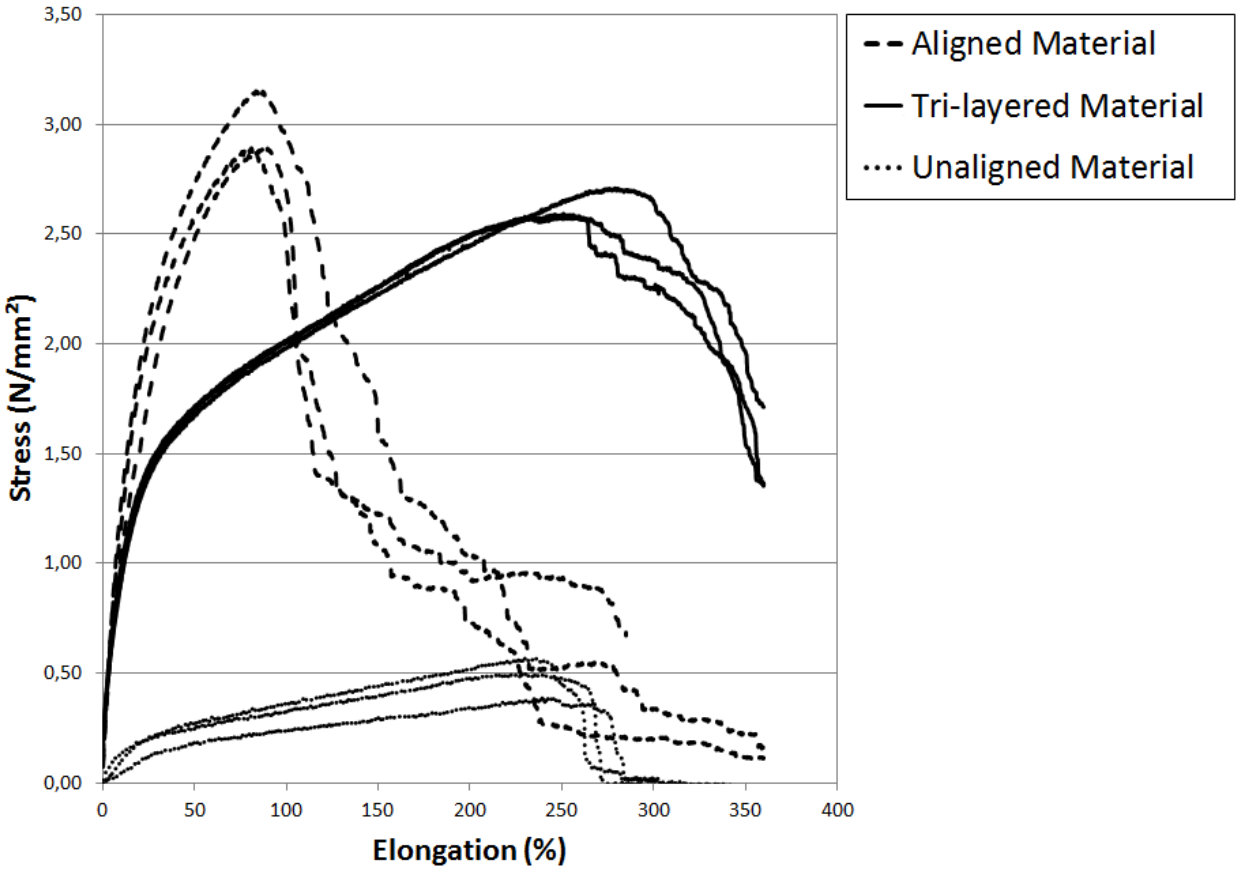

Figure 3.** Stress-Elongation curves of aligned, tri-layered, and unaligned material samples

*Representative of Figure 1.2 of chapter 3.

** Representative of Figure 1.3 of chapter 3.

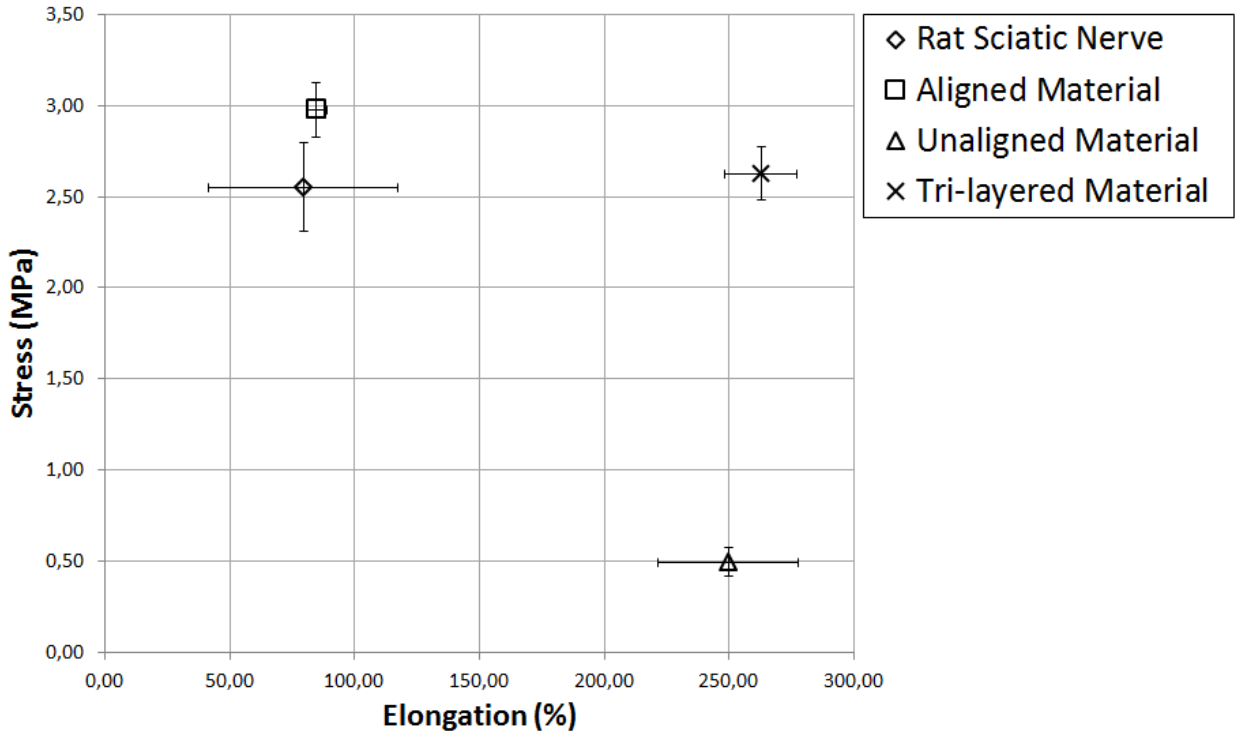

Figure 4*. Average Stress-Elongation measurements at maximum stress values of silk materials and rat sciatic nerve

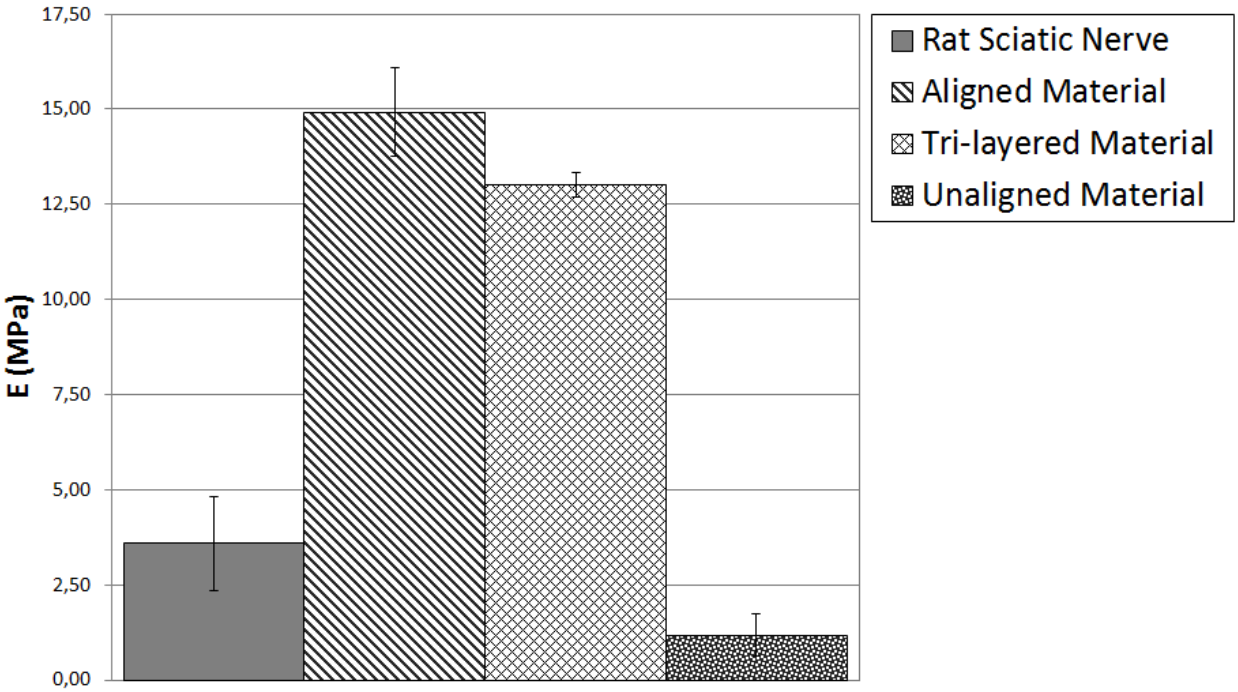

Figure 5.** Average Young's modulus measurements of silk materials and rat sciatic nerve

*Representative of Figure 1.4 of chapter 3.

** Representative of Figure 1.5 of chapter 3.

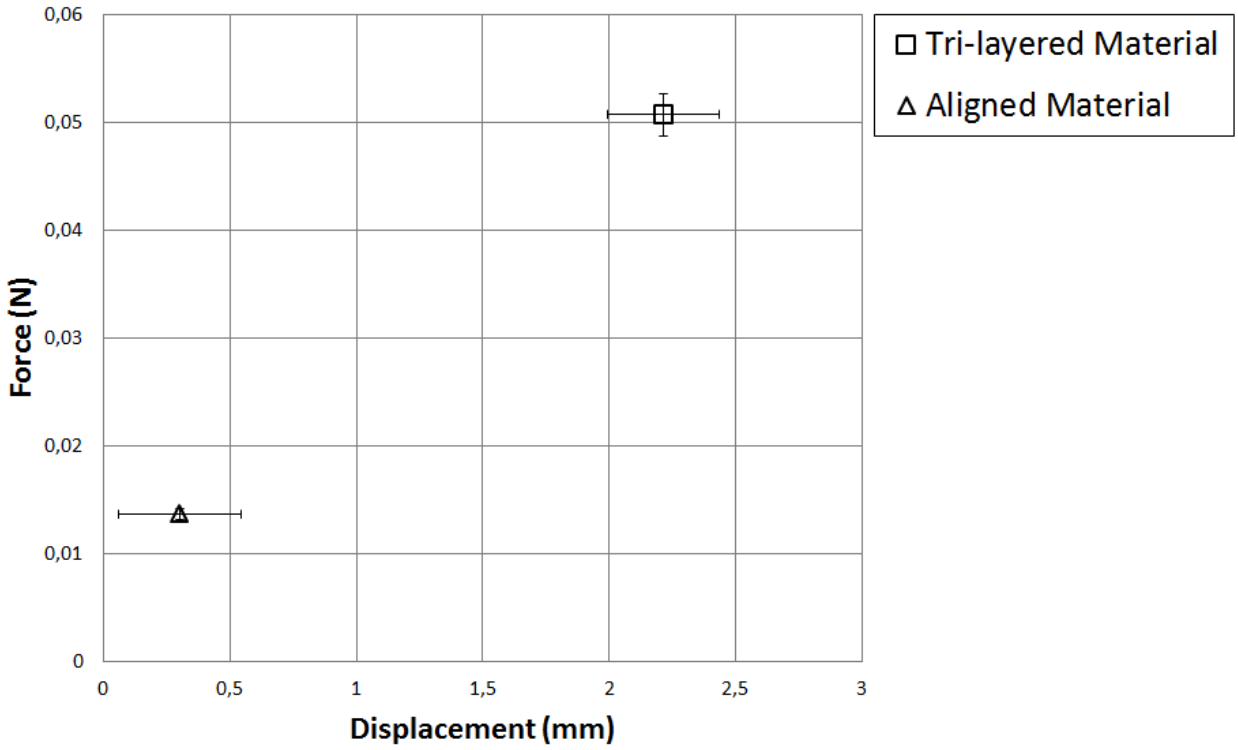

Figure 6*. Average displacement and tensile force measurements at the average maximum force withstood by the sutured aligned and tri-layered silk materials

*Representative of Figure 1.6 of chapter 3.

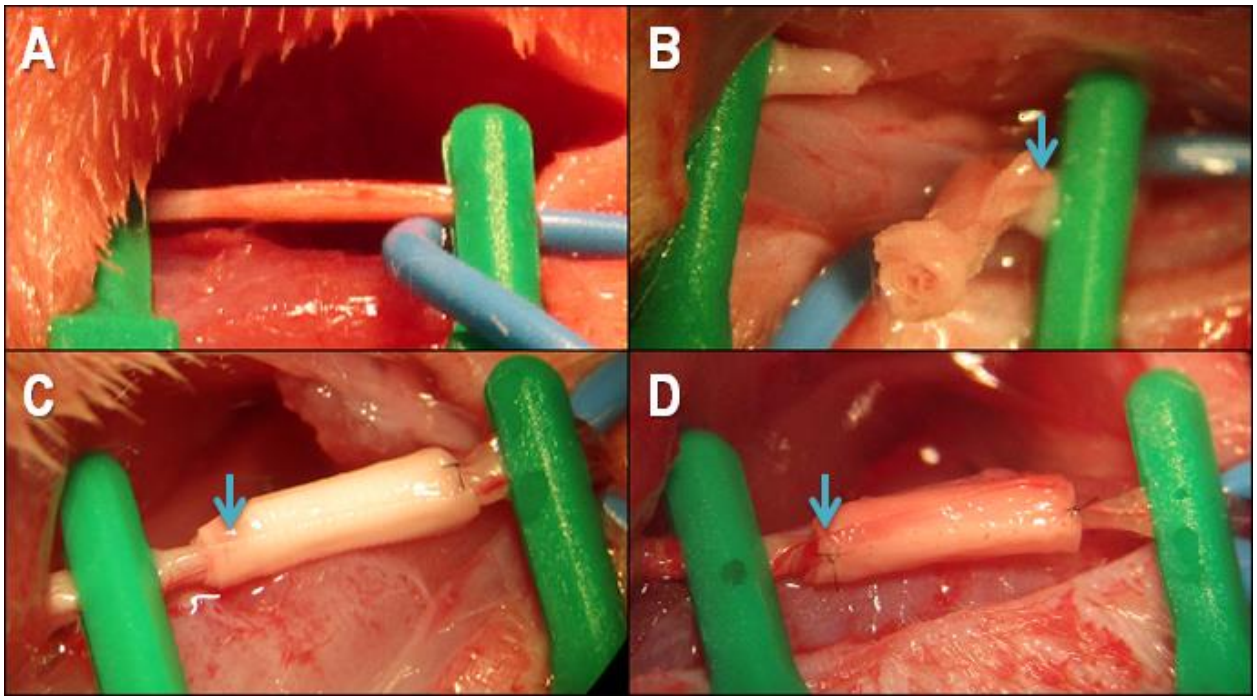

Figure 7*. Implantation procedure: (A) the rat sciatic nerve was exposed and secured; (B) the implant was sutured twice at 0° and 180° at the distal nerve segment; (C) the proximal nerve segment was placed inside implant cavity; (D) the implant was sutured twice at 0° and 180° at the proximal nerve segment

3. Discussion

For over 30 years the nerve autograft has been considered the gold standard for nerve repair yet it has been reported to only result in successful functional recovery in 50% of patients.[9] A significant structural advantage of the autograft, however, is the presence of pre-established pathways through which axons are guided until they reach the distal section of the severed nerve.[13] The hollow nerve guides currently found on the market, such as Neuroflex or NeuraGen, lack this important factor to ensure that axons do not lose their way in pursuit of their innervation targets. This guidance component is not lacking however with the presented implant design due to the micro-channels lined with an aligned silk nanofiber surface. By creating a multi-channeled

*Representative of Figure 1.7 of chapter 3.

tube, the interior surface area of the material is significantly increased thus improving the guidance capabilities of the conduit.

An immediate concern of a multi-channeled conduit that is constantly overlooked in the literature (e.g. Yao et al., Bender et al., Dinis et al.) however is the result of surgical complications not present during the implantation of hollow nerve guides.[15,17,18] A hollow nerve guide is easily sutured to the epineurium of each nerve segment without disturbing the positions of the fascicles both at the proximal and distal nerve segments, but a multi-channeled conduit has blunt edges and risks the deformation of nerve fascicles as the outer layer of the conduit is sutured directly to the edge of the nerve segments' epineurium. In consequence to the increased retraction of the epineurium in respect to the nerve fascicles after the nerve is sectioned, fascicle deformation is virtually impossible to avoid. Responding to this concern, the presented implant design features a "jacket" layer enveloping the guidance conduit. The jacket, which is 1 mm longer than the multi-channeled conduit on each end, presents a hollow cavity for the placement of each nerve segment before it is sutured to the epineurium. This allows the proximal and distal nerve fascicles to be placed in contact with the multi-channeled conduit without deforming the natural paths of the regenerating axons.

The presented tri-layer material used to manufacture the nerve guidance conduit optimizes both surface architecture and mechanical properties in order to incorporate all necessary characteristics of an effective nerve prosthetic while also taking into consideration the complications of the surgical procedure. First of all, the tri-layer material exhibits two surface layers of aligned silk fibroin fibers with an average diameter of 417nm ± 134nm. The aligned fiber surface of the material is a crucial property allowing maximal guidance of the regenerating neurons which is supported both by Dinis et al. who have shown the capability of neurites to attach and grow along silk nanofibers and Qu et al. who have demonstrated that smaller fiber diameters (e.g. 400nm) result in more efficient neurite attachment and extension compared to larger fiber diameters (e.g. 1.2µm).[11,19]

Structure and functionalization are most frequently the primary focus of a tissue engineered nerve prosthetic, but analysis of the implantability of the nerve conduit is a fundamental exercise regularly overlooked in the literature. Yet, if the surgical procedure of a nerve prosthetic is not straightforward, mistakes could result in reduced effectiveness or the surgeon may simply prefer to use a more reliable prosthetic. The randomly deposited center fiber layer therefore proves to be an important component that improves the mechanical properties of the material in order to enhance the ease of implantation.

Two clear mechanical benefits of the tri-layered material in respect to the purely aligned material revealed by the tensile strength test results were the increases in the elasticity and the ductility of the material. A higher elasticity represented by a lower Young's modulus in the tri-layer material results in an implant more resistant to permanent deformation when enduring the various loads involved with a person's everyday movements. The significant increase in ductility of the tri-layer material is represented by the necking observed from the tensile strength tests and the continuity of the tri-layer material that was kept long after reaching ultimate strength. In contrast, the aligned fiber material met complete or quasi-complete rupture immediately after ultimate strength was reached. The increased ductility in parallel with a satisfactory elasticity is a benefit for a material used to create a nerve prosthetic in order to ensure that the implant will not fail if the implant experiences an exceptionally large load. Despite the slight decrease in tensile strength with the addition of the center random fiber layer, the tri-layer material has a greater capability than the aligned fiber material to keep continuity after experiencing a similar load that reaches or exceeds slightly the maximum tensile stress of either material.

An additional mechanical property that needs to be addressed for a nerve prosthetic is the material's resistance to tearing. Nerve prosthetics are often sutured to the epineurium during the surgical procedure which requires a puncture to the material very close to the material's edge.[12] If the material has a poor resistance to tearing, a small load from the suture thread after puncturing the material will cause the implant to detach from either nerve segment and the implant will fail.

The tri-layer material was shown to possess a much higher resistance to tearing than the aligned material. With the addition of the center random fiber layer, the maximum force withstood from the sutured tri-layer material increased by 371.6%. In addition, the elongation of the sutured tri-layer material at its maximum force was 734.5% higher than that for the aligned material. There are two principle benefits of this significant increase of the maximum force and elongation withstood by the tri-layer material. The first is an increased resistance to tearing which will more successfully prevent the implant from detaching from the nerve segments in the weeks following the surgery. The second benefit is the increased ease for surgeons to successfully suture the device while devoting less attention to the force being applied to the device during suture.

This novel implant's design application efficacy was tested compared to a blunt-edged multi-channel design using purely aligned silk fiber material. The surgeon who carried out all implantation procedures highly preferred using the presented system for three main reasons. The first benefit that the surgeon observed was the ease of placement of the implant for suture. Unlike with the blunt-edged implants, the jacketed design allows a hollow cavity for each severed nerve edge and does not distort the protruding nerve fascicles. The second advantage of the jacketed implant identified by the surgeon was the ability of the same cavity to gently secure the nerve in place before applying the sutures. This allowed the surgeon to carefully adjust the position of the nerve to more easily ensure that the nerve segments were not twisted as twisted nerve segments can significantly hinder successful functional recovery. Finally, the surgeon confirmed that the tri-layered material was much better adapted for micro-suture than the purely aligned material as it successfully resisted tearing.

While attempting to suture the aligned material to the nerve segments' epineurium, the surgeon encountered a recurring complication that did not exist with the tri-layered material. While attempting suture, the material often teared in consequence of the trauma from the puncture. This was due (1) to the poor tear strength of the material and (2) to the necessary placement of the suture. Since the multi-channeled conduit made from the aligned material contained blunt ends,

the surgeon was forced to pierce the material for suture very close to the edge of the material itself in attempt to avoid deforming the nerve fascicles as much as possible. The consequences of this inconvenience were first, that the surgeon was obligated to use a smaller needle (10-0 round bodied) than was used for the tri-layered material (9-0 round bodied). The need for a smaller needle consequently obliges a higher level of skill and concentration from the surgeon. Second, the surgeon was sometimes required to attempt multiple times in order to achieve a clean suture of the material. This resulted in a loss of time and the need for greater precision and more delicate gestures. Third, the surgeon was only satisfied with the stability and positioning of the connection after administering 4 micro-sutures for each nerve segment (at 0°, 90°, 180°, 270°). In contrast, the surgeon reported a superior connection using the jacketed device for which the nerve fascicles were gently brought in contact with the edge of the micro-channeled conduit only requiring two sutures (at 0° and 180°).

Due to the adapted implant design of the jacketed guidance conduit, the surgeon also suggested that it may be possible to use fibrin glue instead of traditional sutures which has demonstrated advantages in some cases compared to traditional sutures such as reducing operative time and suture-associated inflammation.[20] This could therefore serve as an alternative coaptation method for all surgeons performing the implantation, and would provide surgeons with the convenience to choose their personally preferred method for each unique case.

4. Conclusion

The jacketed, micro-channeled conduit based on a nanofibrous material organized in a tri-layered architecture presented in this work is a base design for a nerve guidance conduit that addresses the surgical application concerns that are regularly overlooked in the literature. As a result of the micro-channels, the device presents a high surface area to volume ratio providing an aligned nanofiber surface in order to increase axon guidance during regeneration. Furthermore, the conduit contains a tri-layered jacket which significantly increases the ease of surgical implantation.

The device may be adapted further to ameliorate nerve regrowth efficacy by modifications of the material or bio-functionalization. Silk fibroin was used for this model because of the advantageous properties for biological devices. Silk fibroin is a natural, biocompatible polymer with robust mechanical properties that is biodegradable, easily chemically modifiable, and easily functionalized. Therefore, silk fibroin supports the incorporation of many functionalizing materials or bio-signaling molecules in order to improve the performance of the device.

5. Experimental Section

5.1. Preparation of Silk Fibroin Solution

A 10 wt% silk fibroin solution was obtained using a previously established protocol.[21] Briefly, silk cocoons from the *Bombyx mori* silkworm were cut into small pieces and boiled for 30 minutes in a 0.02 M Na_2CO_3 aqueous solution. The silk fibroin fibers were rinsed three times in DI water then allowed to dry at room temperature. The dry fibroin fibers were dissolved in a 9.3 M solution of LiBr for up to 4 hours at 60°C. The fibroin/LiBr solution was dialyzed against DI water using Slide-a-Lyzer dialysis cassettes (3,500 MWCO, Thermo Fisher Scientific) for 3 days to remove salts. The fibroin solution was centrifuged twice to remove solid contaminants. The final concentration was about 6 wt%. The solution was concentrated to 10 wt% by evaporation of the solvent. The final solution was stored at 4°C for up to 6 weeks.

5.2. Electrospinning

A 10 wt% SF solution was mixed at a ratio of 4:1 with a 5 wt% solution of poly(ethylene oxide) (PEO, average M_v ~900,000, Sigma-Aldrich) resulting in a 8 wt%/1 wt% SF/PEO spinning solution. The spinning solution was dispensed through a 19 G stainless steel spinneret (Ramé-Hart Instrument Co.) at a flow rate of 1 $mL \cdot hr^{-1}$ while a voltage between 10-15 kV was administered. An electrospinning rotating drum collector made in-house used to collect the silk fibers had a diameter of 12.8 cm and a width of 3 cm. The drum was positioned on the same axis as the spinneret at a

distance of 12.5 cm from the tip of the spinneret. The entire system was enclosed in a Plexiglas containment area with a controlled humidity range of 25-35%. To obtain an aligned fiber material, the spinning solution was dispensed continuously for 90 minutes while the collector rotated at 4,000 RPM resulting in a surface velocity of 26.8 $m \cdot s^{-1}$. To obtain a tri-layered material consisting of a first layer of aligned fibers, then a layer of randomly deposited fibers, followed by a final layer of aligned fibers, the spinning solution was dispensed for a total of 90 minutes: 30 minutes with a collector rotation speed of 4,000 RPM, followed immediately by 30 minutes at 400 RPM (surface velocity of 2.68 $m \cdot s^{-1}$), then followed by 30 minutes at 4,000 RPM. To obtain a randomly deposited fiber material, the spinning solution was dispensed continuously for 90 minutes with a collector rotation speed of 400 RPM. Aluminum foil was used to cover the collector surface before each process to allow for easy sample recovery.

5.3. Implant Fabrication - Jacketed, Multi-channel Design

The tri-layered electrospun material was carefully peeled from the collector and a 5 mm (parallel to aligned fibers) by 3 cm (perpendicular to aligned fibers) rectangle of the material was cut using a scalpel blade. The material was then rolled while adding a Teflon-coated stick (0.2 mm diameter) after every full rotation. Once completely rolled, the free edge of the material was tightly pressed to the outside of the rolled tube and the tube was immediately immersed in methanol for 5 min to induce β-sheet formation. The tube was allowed to air-dry for 1 hr and the Teflon-coated sticks were then removed resulting in a 5 mm long multi-channeled tube.

From the tri-layered electrospun material, a 7 mm (parallel to aligned fibers) by 3 cm (perpendicular to aligned fibers) rectangle was cut. The multi-channel tube was placed at the bottom-center on this rectangle (aligned fibers in the same direction). The larger material was then rolled around the tube for 3 rotations to create a “jacket”. The edge was tightly pressed to the tube and the entire device was water vapor annealed at room temperature for 4 hours to induce β-sheet formation. The implants were immersed in Milli-Q water overnight at 37°C then rinsed three

times in order to eliminate traces of PEO. The implants were then sterilized in 70% ethanol overnight. Finally, they were rinsed three times with sterile water and immersed in sterile PBS for storage.

5.4. Scanning Electron Microscope Imaging

Electrospun fiber materials were gold sputter coated and analyzed using a scanning electron microscope at the surface and the edge of the material. To observe the three layers of the tri-layered material samples, the material was frozen in liquid nitrogen before being sectioned for a clean, blunt edge for analyses.

5.5. Mechanical Strength Testing

For tensile strength tests, purely aligned, randomly deposited, and tri-layered electrospun material samples were rolled 4 rotations to produce a hollow tube. The tubes were water vapor annealed for 4 hours at room temperature then immersed in Milli-Q water overnight at 37°C to extract the PEO from the fibers. The tubes were subsequently rinsed then immersed in PBS prior to testing. Hydrated material samples were consecutively secured lengthwise between the upper and lower holding grips with a gauge length of 3 mm. Each trial was carried out at a cross-head speed of 0.06 $mm \cdot s^{-1}$ while recording load measurements every 100 ms until rupture. Assays for each material were done in triplicate. All values are represented by mean ± standard deviation.

In order to test the tear strength of the materials, aligned and tri-layered material samples wear punctured with a 9-0 round bodied suture needle with a polyamide 6/6 thread 1 mm from the materials' edge. The suture thread was trimmed on both sides of the puncture, but not knotted. The threaded material was secured in the lower holding grips at the opposite edge of the puncture while the two free suture threads were secured in the upper holding grips. The sutured material was adjusted automatically in order to assure equal tension between both sides of the suture thread. The tensile force of the system was then measured with a cross-head speed of 0.06 mm·s

[1] up to a maximum displacement of 4 mm. Essays were done in triplicate. All values are represented by mean ± standard deviation.

5.6. Surgery

12 six week old, male Sprague Dawley rats were each anesthetized with Vetflurane (Virbac) throughout the entirety of the operation. The rats' right hind limbs were each shaved and sterilized. For each rat, an incision parallel to the femur was made and the sciatic nerve was exposed, isolated, and fixed with two micro clips 10 mm apart. The nerve was severed at the distal end of the fixed section and the implant's outer layer was sutured (Ethicon Ethilon Polyamide 6/6 suture, 9-0 round bodied) twice to the distal segment's epineurium (at 0° and 180°) enveloping the epineurium and nerves fascicles. From the proximal nerve segment, a 3-4 mm portion of nerve was extracted and discarded. The exposed epineurium and fascicles of the proximal nerve segment were inserted into the small cavity of the implant, and the implant's outer layer was sutured twice to the epineurium (at 0° and 180°). The operated area was then cleaned and the wound was closed and sutured.

5.7. Fiber diameter and angle analysis

From SEM images at randomly chosen areas of the aligned material surface, 100 fiber diameters were measured and 50 fiber angles were measured using ImageJ image analysis software. Diameters of each fiber were measured at the center of the SEM image unless otherwise hidden from view at the image's center. Fiber angles were measured by drawing straight lines along the fiber and the y axis of the image. All angles are expressed relative to the primary alignment of the aligned fibers (0°) which was calculated by subtracting the average fiber angle from the measured fiber angle relative to the y axis of the image. All calculated fiber angles were from a single SEM image. All values are represented by mean ± standard deviation.

Acknowledgements

The authors would like to thank the Hauts-de-France Region and the European Regional Development Fund (ERDF) 2014/2020 for the funding of this work. We are also grateful to Ms. Nolwenn Lavagen for her high quality technical support during the surgical procedures.

References

[1] E. A. Heubner, S. M. Strittmatter, *Results Probl. Cell Differ.* **2009**, *48*, 339.

[2] U. Carraro, S. Boncompagni, V. Gobbo, K. Rossini, S. Zampieri, S. Ravara, A. Nori, R. Stramare, F. Ambrosio, F. Piccione, S. Masiero, V. Vindigni, P. Gargiulo, F. Protasi, H. Kern, A. Pond, A. Marcante, *Eur. J. Transl. Myol.* **2015**, *25(2)*, 4832.

[3] M. G. Burnett, E. L., Zager, *Neurosurg. Focus* **2004**, *16(5)*, E1.

[4] M. J. Geden, M. Deshmukh, *Curr. Opin. Neurobiol.* **2016**, *39*, 108.

[5] K. Belanger, T. M. Dinis, S. Taourirt, G. Vidal, D. L. Kaplan, C. Egles, *Macromol. Bioscience* **2016**, *16(4)*, 472.

[6] K. S. Houschyar, A. Momeni, M. N. Pyles, J. Y. Cha, Z. N. Maan, D. Duscher, O. S. Jew, F. Siemers, J. van Schoonhoven, *Plast. Surg. Int.* **2016**, *2016*, 4175293.

[7] A. N. Koppes, D. M. Thompson, *Regenerative Engineering of Musculoskeletal Tissues and Interfaces* **2015**, *2015*, 293.

[8] S. H. Payne Jr., *J. South Orthop. Assoc.* **2001**, *10(3)*, 173.

[9] S. K. Lee, S. W. Wolfe, *J. Am. Acad. Orthop. Srug.* **2000**, *8(4)*, 243.

[10] G. H. Altman, F. Diaz, C. Jakuba, T. Calabro, R. L. Horan, J. Chen, H. Lu, J. Richmond, D. L. Kaplan, *Biomaterials* **2003**, *24(3)*, 401.

[11] T. M. Dinis, G. Vidal, R. R. Jose, P. Vigneron, D. Bresson, V. Fitzpatrick, F. Marin, D. L. Kapln, C. Egles, *PloS One* **2014**, *9(10)*, e109770.

[12] D. Grinsell, C. P. Keating, *BioMed Res. Int.* **2014**, *2014*, 698256.

[13] R. Gaudin, C. Knipfer, A. Henningsen, R. Smeets, M.Heiland, T. Hadlock, *BioMed Res. Int.* **2016**, *2016*, 3856262.

[14] S. Kehoe, X.F. Zhang, D. Boyd, *Injury* **2011**, *43(5)*, 553.

[15] T. M. Dinis, R. Elia, G. Vidal, Q. Dermigny, C. Denoeud, D. L. Kaplan, C. Egles, P. Marin, *J. Mech. Behav. Biomed. Mater.* **2015**, *41*, 43.

[16] C. R. Wittmer, A. Hébraud, S. Nadjari, G. Schlatter, *Polymer* **2014**, *55(22)*, 5781.

[17] L. Yao, K. L. Billiar, A. J. Windebank, A. Pandit, *Tissue Eng. Part C* **2010**, *16(6)*, 1585.

[18] M. D. Bender, J. M. Bennett, R. L. Waddell, J. S. Doctor, K. G. Marra, *Biomaterials* **2004**, *25(7-8)*, 1269.

[19] J. Qu, D. Wang, H. Wang, Y. Dong, F. Zhang, B. Zuo, H. Zhang, *J. Biomed. Mater. Res. Part A* **2013**, *101(9)*, 2667.

[20] N. P. Biscola, L. P. Cartarozzi, S. Ulian-Benitez, R. Barbizan, M. V. Castro, A. B. Spejo, R. S. Ferreira Jr., B. Barraviera, A. L. R. Oliveira, *J. Venomous Anim. Toxins Incl. Trop. Dis.* **2017**, *23*, 13.

[21] H. J. Jin, S. V. Fridrikh, G. C. Rutledge, D. L. Kaplan, *Biomacromolecules* **2002**, *3(6)*, 1233.

Chapter 3

Results: Part 2

Material Functionalization

Introduction

Silk fibroin from the *Bombyx mori* is a natural biocompatible material produced, in conjunction with sericin proteins, by the silkworms to form their cocoons. The fibroin fibers can easily be extracted from the cocoons during a degumming process; eliminating the hydrophilic sericin proteins from the hydrophobic fibroin is essential since sericin in the presence of fibroin can elicit an immune response (Wang et al., 2014). Fibroin is an advantageous material for biomedical applications as it is a natural material with robust mechanical properties readily chemically modified and may be functionalized with numerous types of substances.

Silk fibroin is a promising biomaterial for the fabrication of nerve guidance conduits for peripheral nerve repair. A device comprised solely of fibroin however is not sufficient considering the complex mechanisms involved in successful nerve regeneration. In complexifying the fibroin material with additional elements, one may acquire a multifunctional composite material capable of improved results as a nerve support. The versatility of silk fibroin functionalization was therefore explored using a variety of substances, both chemical and biochemical structures, including conductive or magnetic nanoparticles and proteins. The functionalization of fibroin examined in this work corresponds specifically to potential approaches for applications in the area of peripheral nerve regeneration.

Silk and growth factors

Growth factors are signaling molecules produced endogenously by nervous tissue for the regulation of neuron health, growth, regeneration, or death (Belanger et al., 2016). Growth factors have been extensively studied for the incorporation in bioengineered NGCs in order to stimulate axonal regeneration. Growth factors can be used to stimulate faster regeneration of specific types of neurons, but have also been shown to guide axonal sprouting (Dinis et al., 2014a).

Growth factors chosen for this study include nerve growth factor (NGF), neurotrophin-3 (NT-3), and ciliary neurotrophic factor (CNTF). NGF is the most studied growth factor for peripheral nerve regeneration and was chosen as it has long been understood to be an important signaling molecule for peripheral nerve regeneration. As Schwann cells proliferate after a nerve injury, they synthesize new NGF receptors in order to present the molecule to the axonal sprouts

(Sofroniew et al., 2001). It has been discovered that NGF promotes the extension of axons during regeneration and is crucial to the survival of peripheral neurons (Sofroniew et al., 2001). In addition, it has been revealed that NGF also promotes the migration of proliferating Schwann cells (Madduri et al., 2010), which would encourage proliferating Schwann cells to fill a bioengineered NGC functionalized with NGF. NGF, however, has been found to have much less or no influence on the regeneration of motor neurons (Braun et al., 1996). NT-3 was chosen as it is known for promoting the regeneration of both sensory and motor neurons. In particular, NT-3 has been shown to help restore conduction speed of axons and increased myelination (Sterne et al., 1997; Tonda-Turo et al., 2017). Finally, CNTF is a less commonly used growth factor peripheral nerve regeneration, but was chosen for its support in regenerating motor neurons. CNTF has been found to help increase the diameter of axons, supporting improved nerve conduction and increased myelination (Zhang et al., 2004; Dinis et al., 2015).

Quantities of each growth factor molecule to incorporate into the SF fibers were chosen in respect to protocols found in the literature for cell culture promoting the growth of primary sensory neurons; concentrations of growth factor added to culture media were adapted for the functionalization of the SF fibers. Therefore, 100 ng/mL, 50 ng/mL and 10 ng/mL (mass of growth factor per volume of spinning solution) were chosen as working concentrations for NGF, NT-3, and CNTF respectively.

Characterization of SF fibers functionalized with growth factors such as nerve growth factor (NGF) has been established prior to the beginning of this study. First, Dinis et al. have demonstrated that the addition of growth factors does not alter the secondary structure of the SF, presenting 56% β-sheets in both functionalized and pure SF fibers using FTIR (Dinis et al., 2014a). Second, Dinis et al. have illustrated the efficiency of the SF fibers to hold onto growth factors after the electrospinning process: ELISA testing indicated that NGF and CNTF release was undetectable from the functionalized SF fibers after 5 days immersed in PBS, however, when the fibers were dissolved in LiBr, 27.5 pg/mL of NGF was identified in the solution (Dinis et al., 2014a, 2014b). The results of this work not only confirm that growth factors like NGF, if introduced to SF before the electrospinning process, will be trapped within the SF fibers, but also that the entrapped NGF was protected from degradation. In addition, the work done by Dinis et al.

determines that the GFs trapped within the SF fibers are still accessible to cells as demonstrated by the successful gradient bio-signaling results for unidirectional extensions of sensory neurons in culture (Dinis et al., 2014a).

Primary rat sensory neurons cultured on aligned SF, SF/NGF/CNTF, and SF/NGF/NT-3 fibers

SF fibers either non-functionalized, functionalized with NGF, functionalized with NGF and CNTF, and functionalized with NGF and NT-3 were electrospun onto glass coverslips for a short period of time (between 5 and 20 minutes) in order to avoid completely covering the surface of the coverslips. SF Fibers were either randomly deposited or aligned on the glass coverslips.

First, DRG and isolated primary sensory neurons from rat embryos were cultured on non-functionalized or functionalized, randomly deposited or aligned SF fiber samples for between 7 and 9 days in order to evaluate the alignment of the neurons in respect to the alignment or lack thereof of the SF fibers. As depicted in Figure 2.1A, when sensory neurons grow on a random fiber network, neurites advance in all directions with no apparent organization. Contrarily, neurons growing on a surface containing aligned SF fibers tend to extend their neurites along the length of the aligned fiber as seen in Figure 2.1B&C. In addition, as there was abundant space between fibers, it is clear that the neurons prefer to adhere to the SF fibers instead of the glass coverslip surface. Virtually no neuron was found growing solely between fibers.

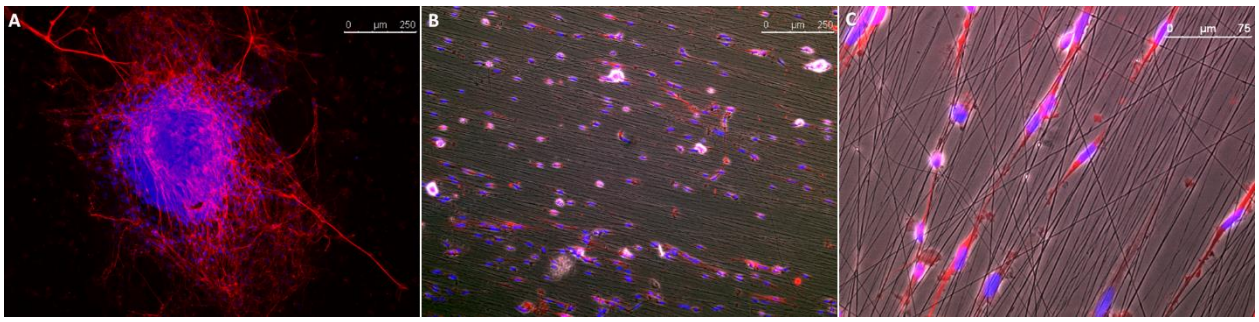

Figure 2.1. Primary sensory neurons from fetal rat dorsal root ganglia cultured for (A) 7 days on randomly deposited non-functionalized SF fibers on glass coverslips (A) 9 days on aligned SF fibers functionalized with NGF and CNTF on glass coverslips and (B) 9 days on aligned SF fibers functionalized with NGF and NT-3 on glass coverslips.

In order to evaluate the performance of the functionalized SF fibers for neurite growth, isolated primary sensory neurons from rat embryos were cultured on non-functionalized, NGF functionalized, NGF and CNTF functionalized, and NGF and NT-3 functionalized aligned SF fiber samples for 9 days (Figure 2.2). However, NGF was not included in the culture media as is standard protocol for neuronal cell culture. Neurons were isolated from other cells naturally residing in DRG before being culture on the materials in order to prevent all possible sources of neurotrophic factors.

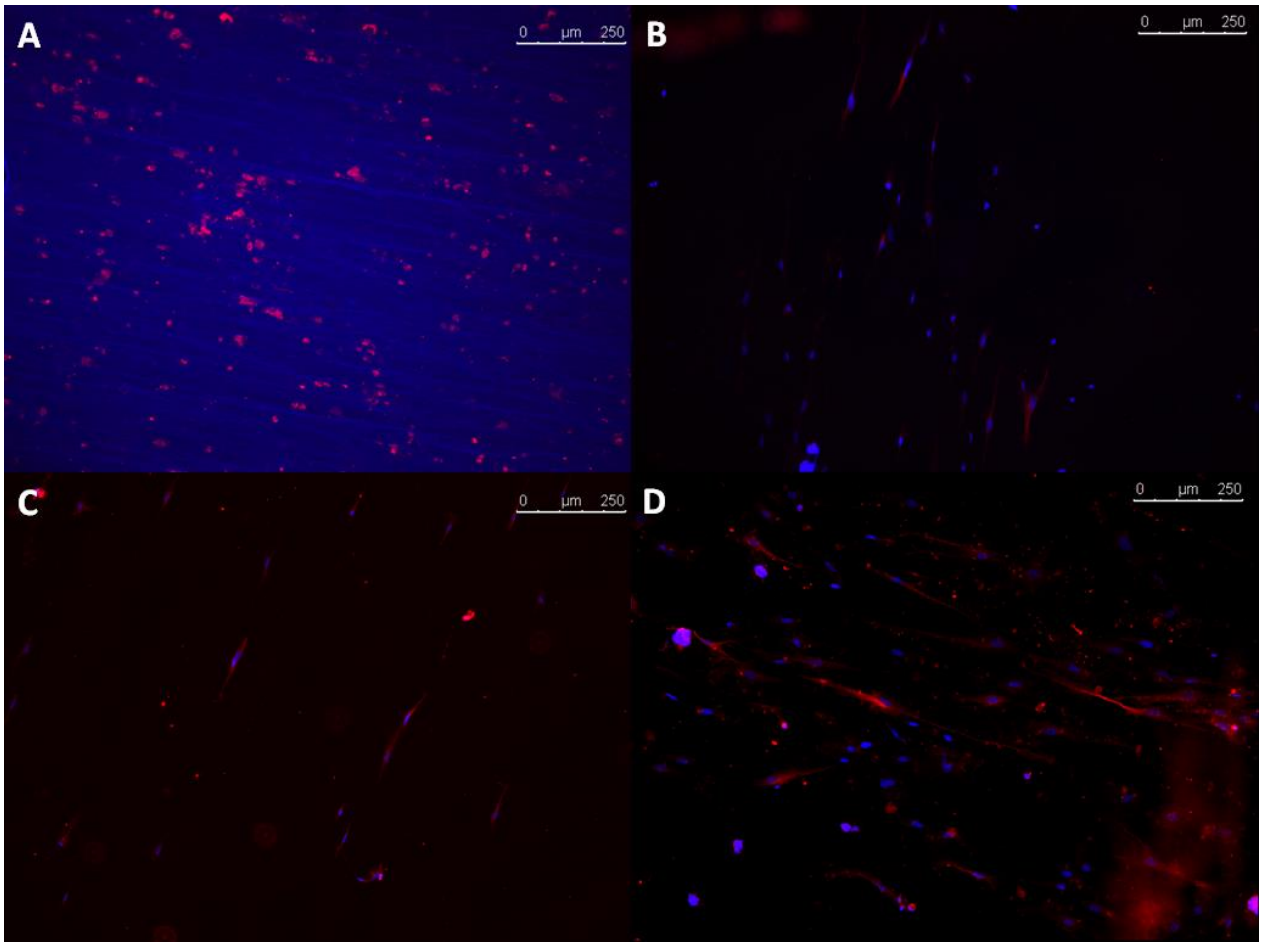

Figure 2.2. Primary sensory neurons from fetal rat dorsal root ganglia cultured for 9 days on (A) aligned non-functionalized SF fibers on glass coverslips, (B) aligned SF fibers functionalized with NGF on glass coverslips, (C) aligned SF fibers functionalized with NGF and CNTF on glass coverslips, and (D) aligned SF fibers functionalized with NGF and NT-3 on glass coverslips. Culture media contained no NGF.

As expected, only debris from neurons remained adhered to the non-functionalized SF fibers after 9 days in culture deprived of NGF. Samples containing functionalized SF fibers, however, still had many neurons with extensions growing on the material. The length of the largest neurite from at least 25 randomly chosen neurons was measured. The average largest neurite lengths for neurons cultured on NGF functionalized SF fibers, NGF and CNTF functionalized SF fibers, and NGF and NT-3 functionalized SF fibers were 89.7 µm, 53.8 µm, and 159.3 µm respectively (standard error of the mean for all samples were ± 12.7 µm, ± 35.3 µm, and 17.0 µm). Neurite lengths varied widely throughout each sample, ranging from 20.1 µm to 230.0 µm on the NGF functionalized SF fibers, from 11.2 µm to 145.4 µm on the NGF and CNTF functionalized SF fibers, and from 48.1 µm to 292.5 µm on the NGF and NT-3 functionalized SF fibers (Figure 2.3). As depicted in the second graph of Figure 2.3, neurite lengths from neurons on NGF and NT-3 functionalized SF fibers are consistently larger than those from neurons on NGF functionalized SF fibers which are consistently larger than those from neurons on NGF and CNTF functionalized SF fibers.

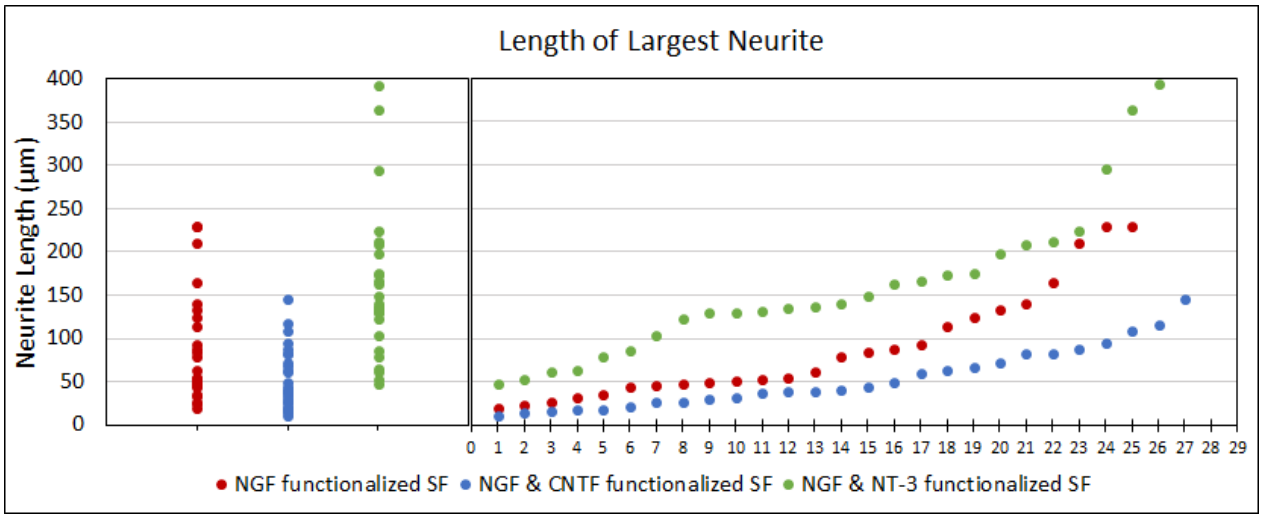

Figure 2.3. Distributions of the length of the largest neurite belonging to one neuron in each sample type (NGF functionalized SF fibers, NGF and CNTF functionalized SF fibers, and NGF and NT-3 functionalized SF fibers) after 9 days in primary rat sensory neuron cultures with NGF-deprived culture media.

The results from these cultures show the important role growth factors play in neurite extension. The results also show that it is possible to distinguish between the efficacies of different SF functionalization, which are evidence that the neurons are capable of accessing the growth factors that are impregnated in the SF fibers during the electrospinning process. Some information is missing from these cell cultures, however. Neuronal cultures extracted from DRG are a limited study as only sensory neurons are being cultured on the material. Therefore, as CNTF is a growth factor with specific interactions with motor neurons, the benefits from the incorporation of this growth factor is still not understood. In addition, NT-3 is known to affect the growth of both sensory and motor neurons, and therefore, the same constraint is met. NGF, however, interacts specifically with sensory neurons.

Schwann cell migration on aligned SF/NGF fibers

Rat Schwann cells were found to align themselves on the SF/NGF fibers after 48 hours in culture (Figure 2.4). Schwann cells exhibit an elongated morphology adhering to the fibers unlike the morphology seen on the control samples providing no physical guidance. Schwann cells on the aligned functionalized fibers. On the aligned SF/NGF fibers, Schwann cells tend to make connections with cells along the same fiber, while on the control sample Schwann cells make random interactions with many extensions in several directions.

The migration behavior of Schwann cells was observed using time-lapse microscopy (TLM). Three examples of migrating Schwann cells are shown in Figure 2.5 with their migration paths mapped out in the first and last still frames and the starting and ending point indicated with an arrow. From these three randomly chosen migration paths, an average cell migration velocity was found to be 11.9 ± 3.8 nm·s^{-1}.

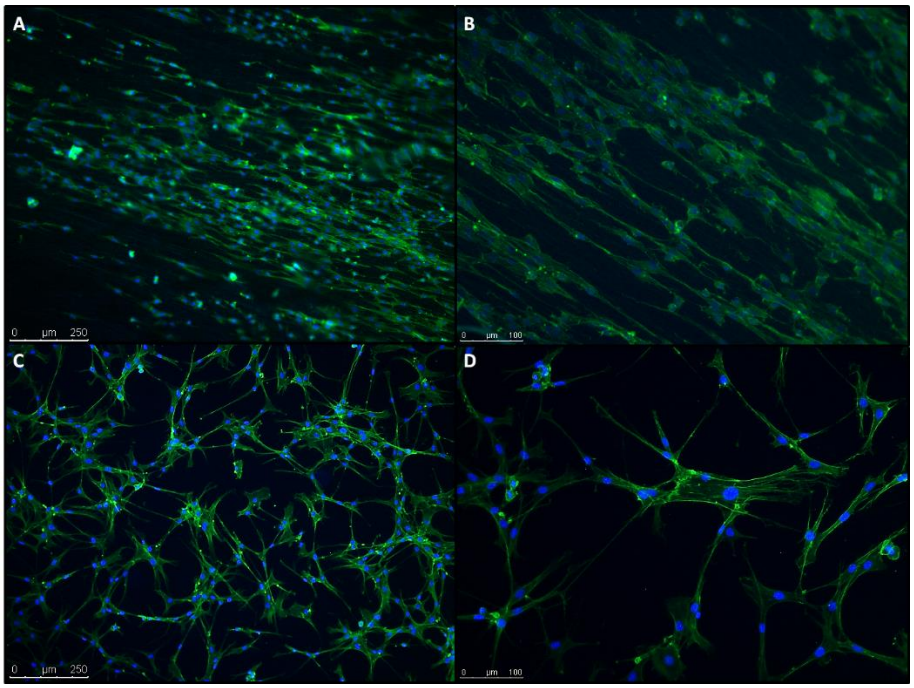

Figure 2.4. Fluorescence micrographs of a 48 hour cell culture of rat Schwann cells on (A&B) aligned SF/NGF fibers and (C&D) on glass coverslips.

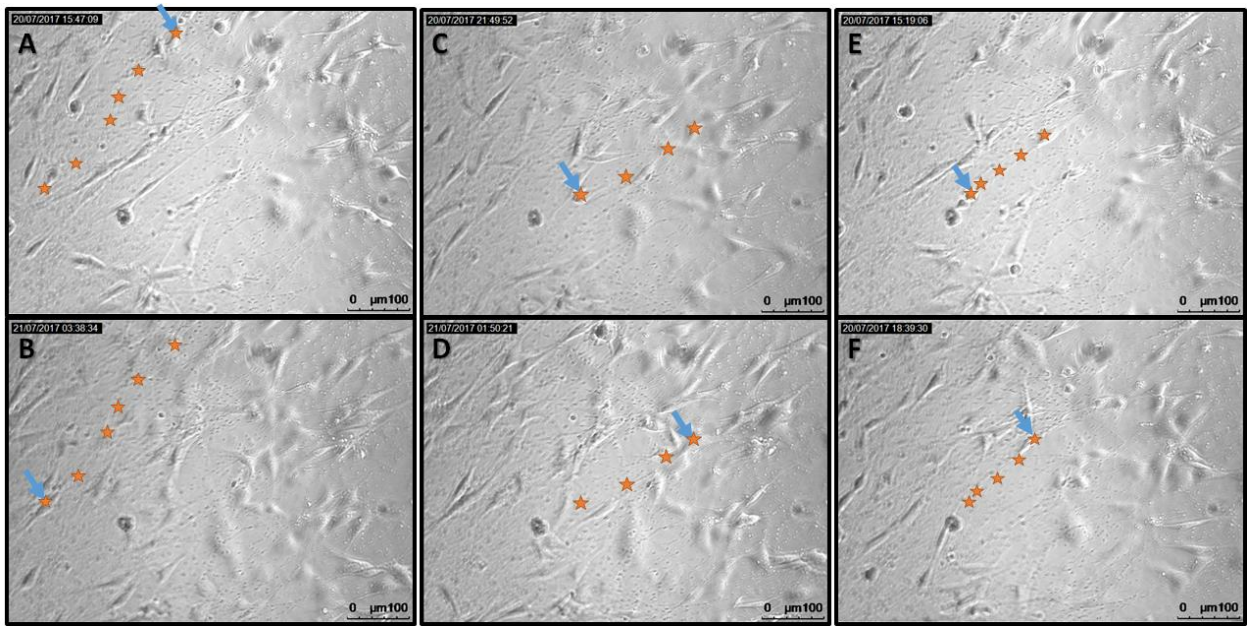

Figure 2.5. Migration paths (A&B, C&D, and E&F) of Schwann cells on aligned SF/NGF fibers over time taken by time-lapse microscopy. Migration path A-B was carried out over 11h51m55s, migration path C-D was carried out over 4h00m29s, and migration path E-F was carried out over 3h20m24s. Orange stars indicate the position at still frames captured throughout cell movement.

Silk and fibronectin

SF/PEO spinning solutions were successfully electrospun with fibronectin at a concentration of 0.01 ng/mL spinning solution. It was confirmed using fluorescence microscopy that fibronectin was successfully embedded in the silk fibers and remained present after water vapor annealing and rinsing treatment of the fibers. Fibronectin tagged with fluorochrome Alexa Fluor 488 or Alexa Fluor 568 was observed under both the epifluorescence microscope and the confocal microscope (Figure 2.6) and found homogeneously throughout the fibers of each sample. As SF produces an auto-fluorescence, FN-tagged/SF and pure SF fiber materials were visualized under the Alexa Fluor 488 or 568 filters at identical parameters at which the auto-fluorescence of the SF is undetectable (Figure 2.6B, C, E, & F).

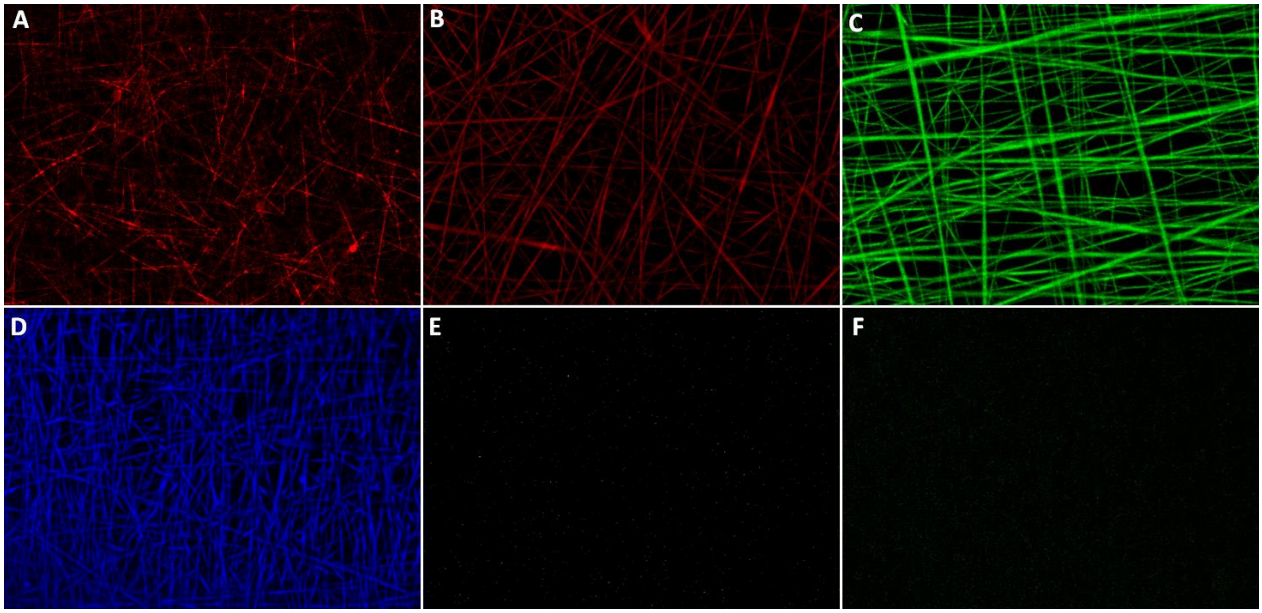

Figure 2.6. Alexa Fluor 568-tagged SF/FN fibers observed under (A) an epifluorescence microscope and (B) a confocal microscope, (C) Alexa Fluor 488-tagged SF/FN fibers observed under a confocal microscope, (D) auto-fluorescence of pure SF fibers observed under a confocal microscope, (E) pure SF fibers using identical parameters to those in image B with the Alexa Fluor 568 filter, and (F) pure SF fibers using identical parameters to those in image C with the Alexa Fluor 488 filter.

Primary rat sensory neurons were cultured on the SF/FN fibers for two days in order to visualize the initial sprouting of the neuronal extensions in respect to the organization of the functionalized fibers. All neuron cell bodies were observed to have adhered to a SF/FN fiber with any neuronal extensions following the length of the fibers very closely (Figure 2.7A-D). In addition, cells from the PC12 cell line were differentiated on the SF/FN fibers in a 7-day culture. The neuron-like cells produced large extensions that clearly followed the slightly randomized organization of the SF/FN fibers; the extensions displayed portions that are completely straight while also at some points, taking sharp turns switching direction in order to stay closely associated to the fibers (Figure 2.7E).

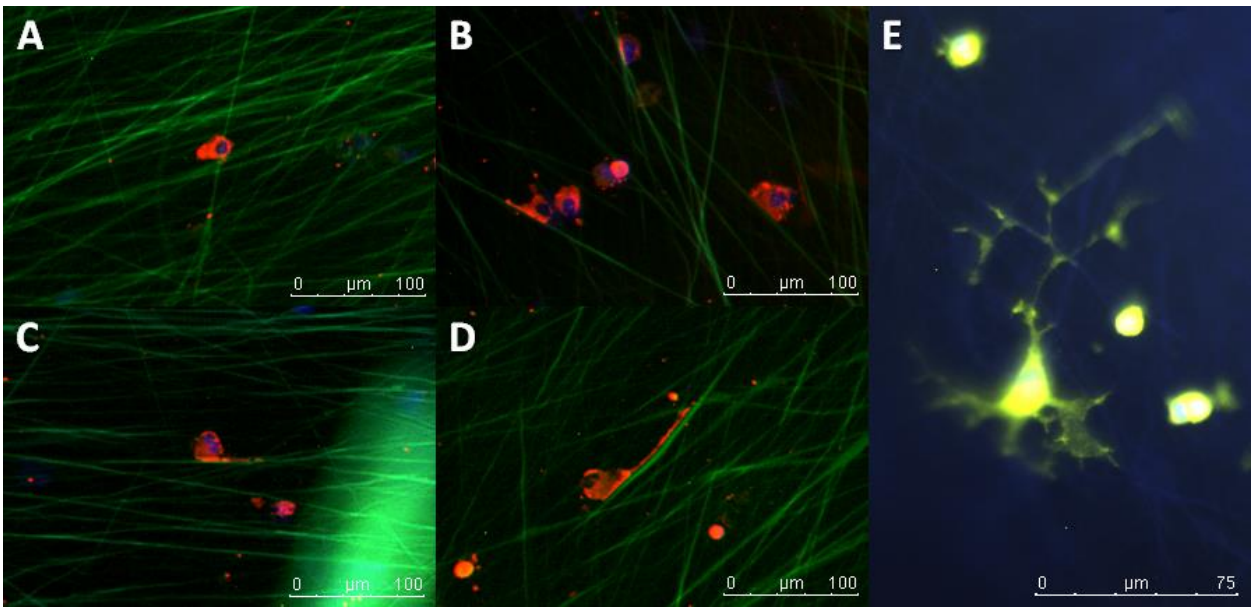

Figure 2.7. (A-D) Primary rat sensory neurons on SF/FN-488 fibers after 2 days in culture, and (E) PC12 cells differentiated on SF/FN fibers after 7 days in culture in the presence of NGF-containing media.

Silk and nanoparticles

Characterization of gold and iron oxide nanoparticles

Gold and iron oxide nanoparticle diameters were characterized using a transmission electron microscope (Figure 2.8). GNPs and IONPs had average diameters of 14.1 ± 1.1 nm and 10.2 ± 0.2 nm respectively.

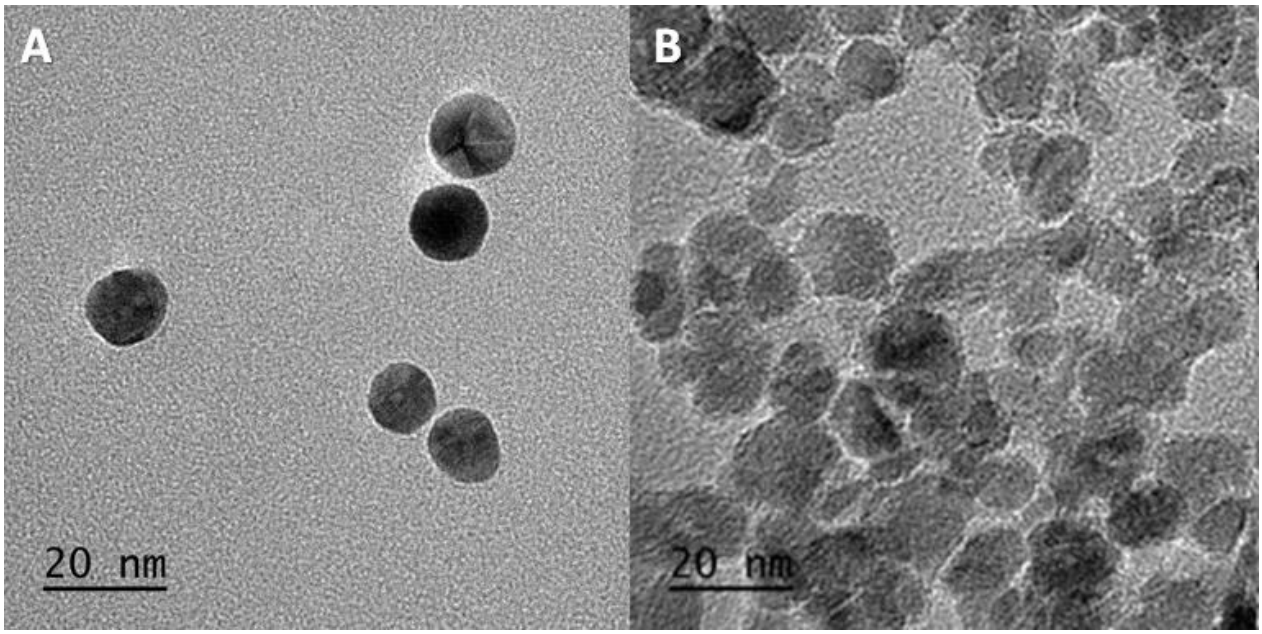

Figure 2.8. TEM images of (A) gold nanoparticles and (B) iron oxide nanoparticles.

Characterization of SF/GNP and SF/IONP electrospun fibers

SF/PEO spinning solutions containing two different concentration of GNPs (0.05 mM and 0.11 mM) and two different concentrations of IONPs (22.5 mM and 45 mM) were all successfully electrospun at similar parameters to the SF/PEO basic spinning solution. Electrospun material samples were analyzed using SEM, TEM, and STEM (Figures 2.9, 2.10, and 2.11) in order to qualitatively evaluate the impregnation of nanoparticles into the fibers. At both concentrations of GNPs and IONPs, nanoparticles were successfully identified and found to be homogeneously distributed throughout the fibers; the nanoparticles did not display a tendency to accumulate within the fibers.

The functionalization of the SF-based fibers did not result in a dramatic change in average fiber diameter (Figure 2.12), as all average fiber diameters remained below 550 nm and all fiber diameters measured were between 100 nm and 900 nm. Fibers functionalized with a lower concentration of GNPs resulted in a slightly higher average diameter than all other fibers, however, the fibers had a larger range of fiber diameters than the non-functionalized or the other functionalized fibers and contained fibers as small as 350 nm. Non-functionalized fibers were found to have the smallest fibers (measuring as small as 100 nm in diameter) but had a diameter

range similar in magnitude to the SF-based fibers functionalized with GNPs at 0.05 mM. Fibers functionalized with IONPs and fibers functionalized with GNPs at a concentration of 0.11 mM had very similar diameter measurement ranges while presenting insignificant differences in average fibers diameters with each other and with non-functionalized SF fibers. Therefore, the functionalization of SF fibers was not shown to compromise the nanoscale properties of the SF fibers and in almost all cases, not only maintained a similar average size, but also produced more uniform fibers with a more precise range of diameters.

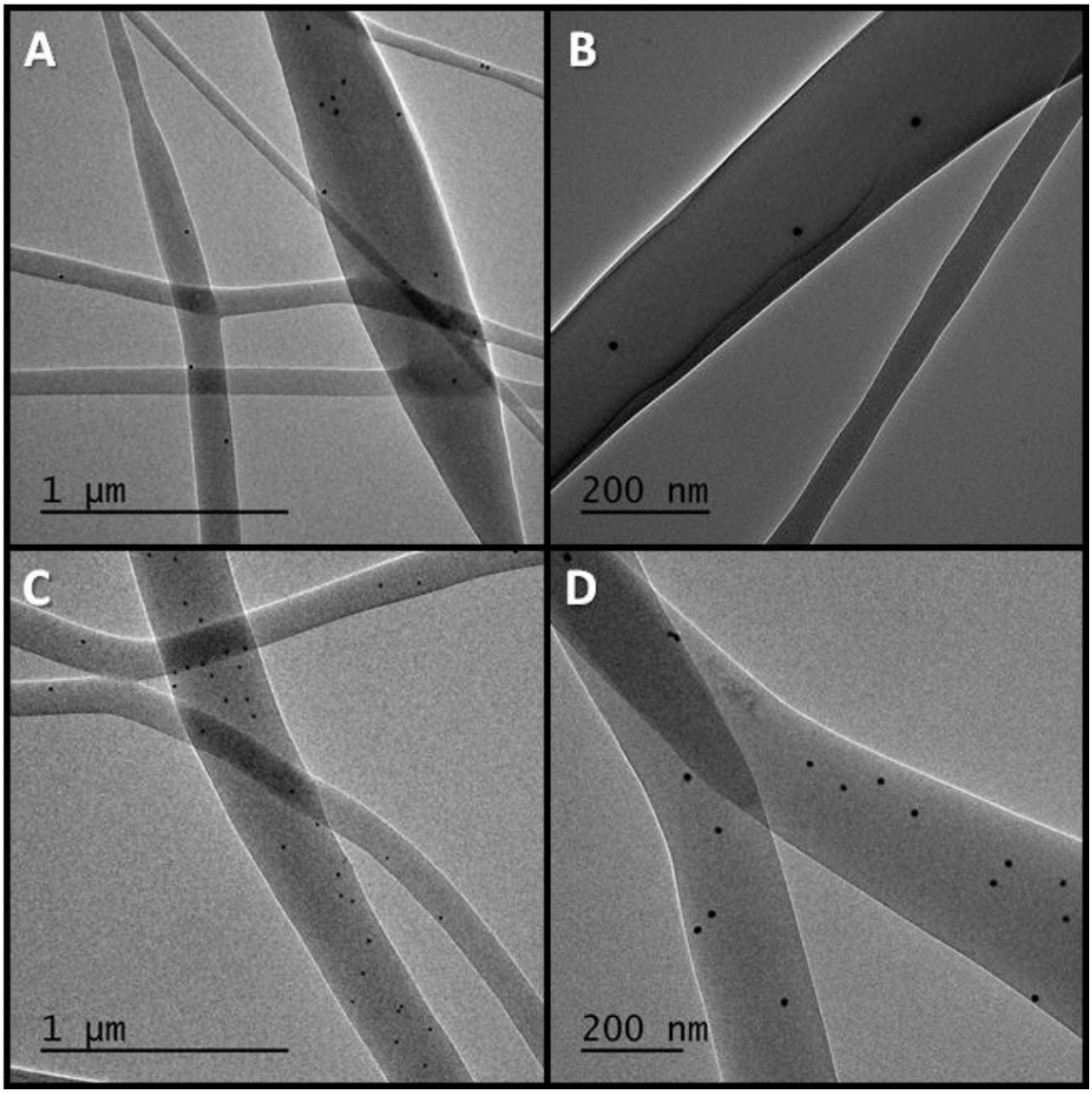

Figure 2.9. TEM images of (A&B) 0.05 mM GNP spinning solution fibers and (C&D) 0.11 mM GNP spinning solution fibers.

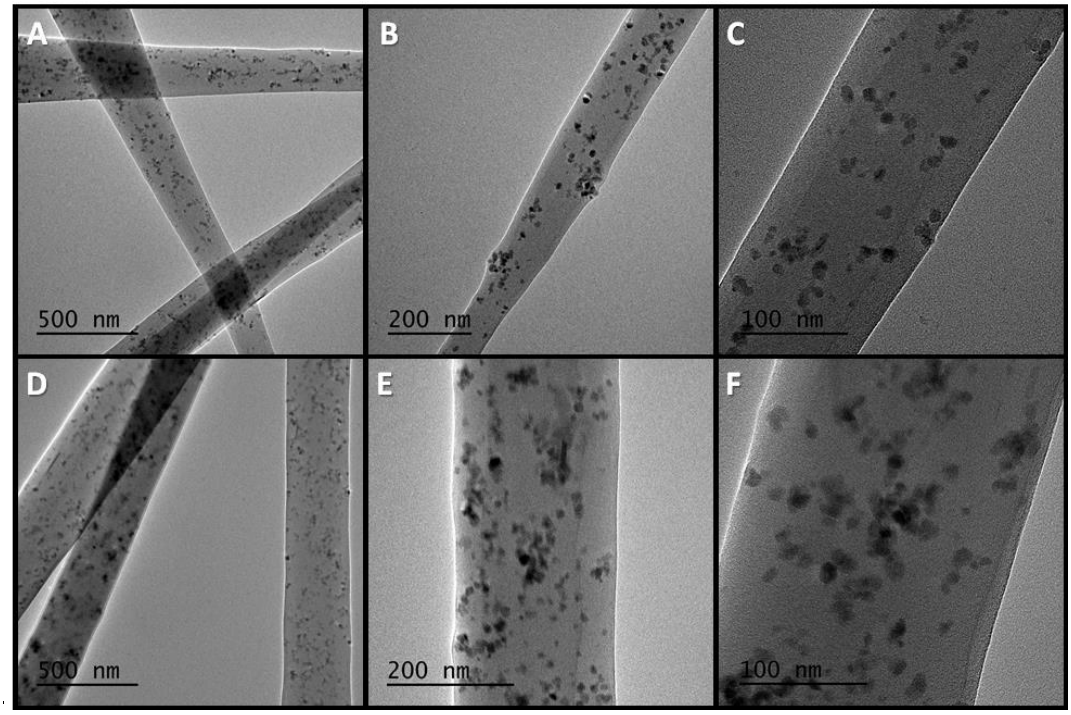

Figure 2.10. TEM images of (A-C) 22.5 mM IONP spinning solution fibers and (D,E,&F) 45 mM IONP spinning solution fibers.

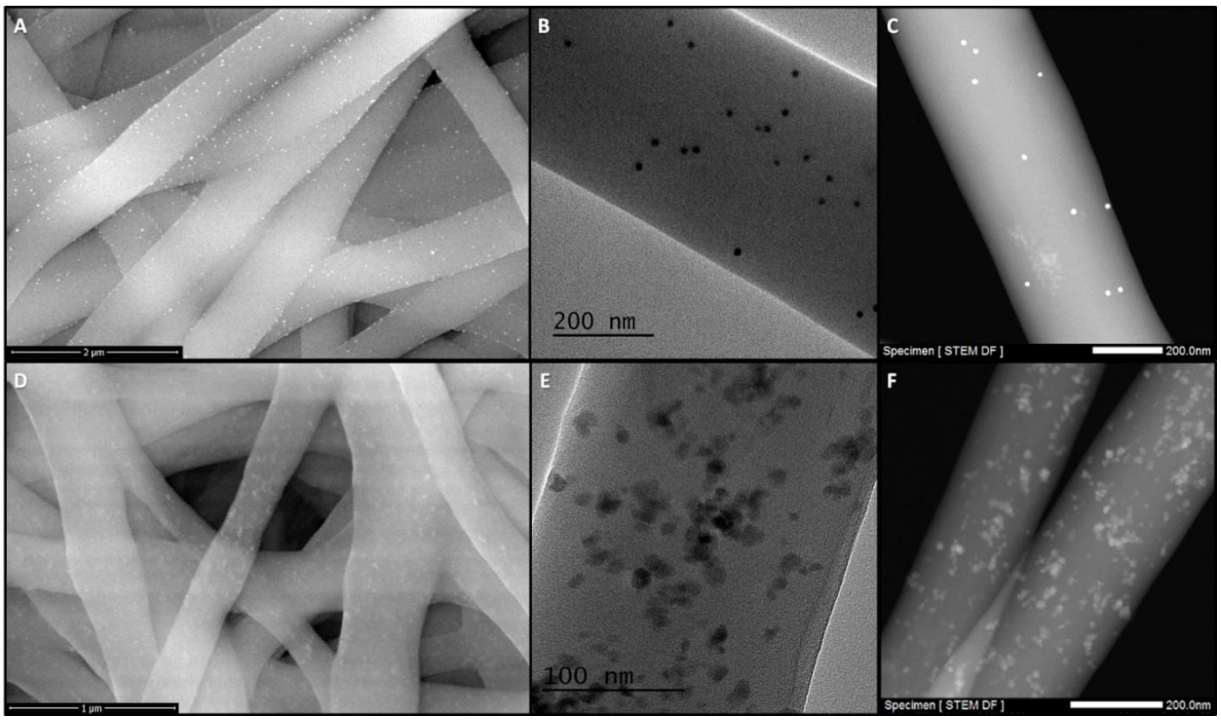

Figure 2.11. (A) SEM, (B) TEM, and (C) STEM images of SF/GNP fibers at a GNP concentration of 0.11 mM. (D) SEM, (E) TEM, and (F) STEM images of SF/IONP fibers at an IONP concentration of 45 mM.

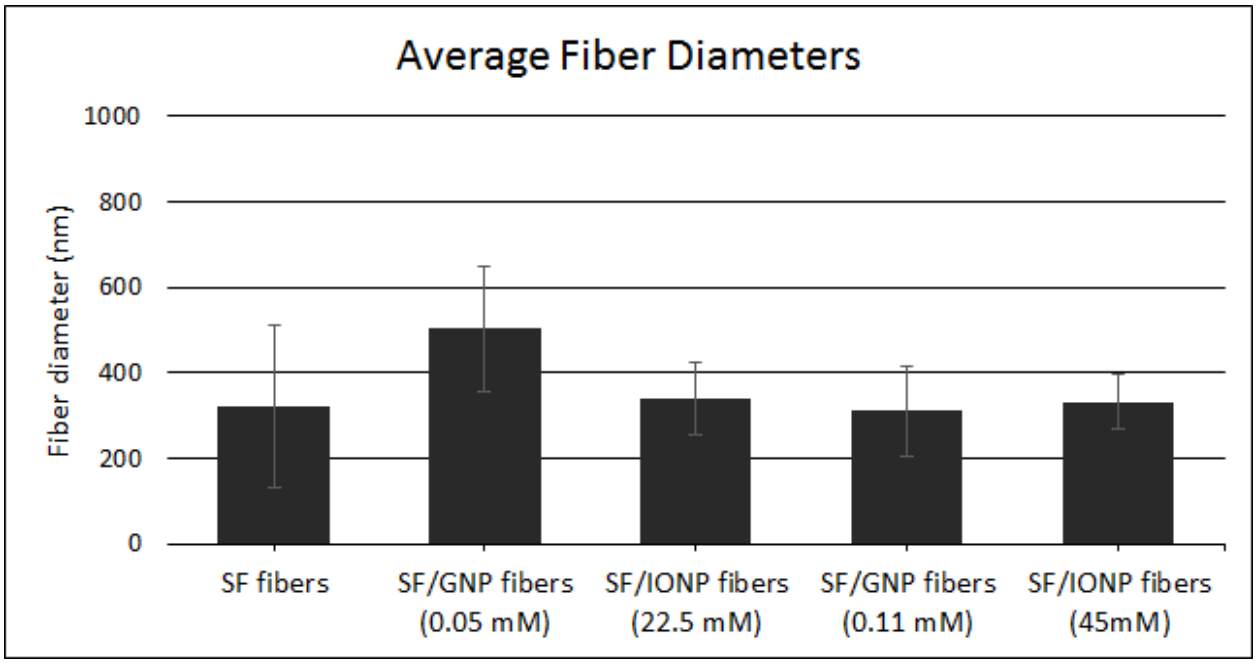

Figure 2.12. Average fiber diameters of electrospun SF-based fibers non-functionalized, functionalized with gold nanoparticles with a concentration of 0.05 mM or 0.11 mM, and functionalized with iron oxide nanoparticles with a concentration of 22.5 mM or 45 mM.

Biomaterial evaluations using L929 cell line

As higher concentrations of both GNPs and IONPs are desired for a functionalized material with conductive or magnetic properties, the fibers created at 0.11 mM and 45 mM respectively were used in cell culture. After 72 hours of a L929 culture, the cells showed a healthy morphology both the SF/GNP fibers and the SF/IONP (Figure 2.13) compared to the control (L929 cells cultured on a glass coverslip) and pure SF electrospun fibers.

The materials were tested for cytotoxicity using MTS assays (Figure 2.14). The results suggest that both nanoparticle-embedded materials may be good candidates for the use as biomaterials as there was no indication of cytotoxicity from either sample. The viability of the cells remained at virtually 100% for concentrations of 30, 60, and 100% of material-incubated media in contact with cells for both functionalized samples (Figure 2.14A&D). The metabolic activity of the cells also remained just under 100% for all concentrations of the test media for both materials (Figure 2.14C&F). Furthermore, the proliferation index for each media concentration was comparable to that of the negative control in both material tests. In addition,

using 100% of the pre-incubated test media, both material samples displayed a slightly higher index in than the negative control (Figure 2.14B&E).

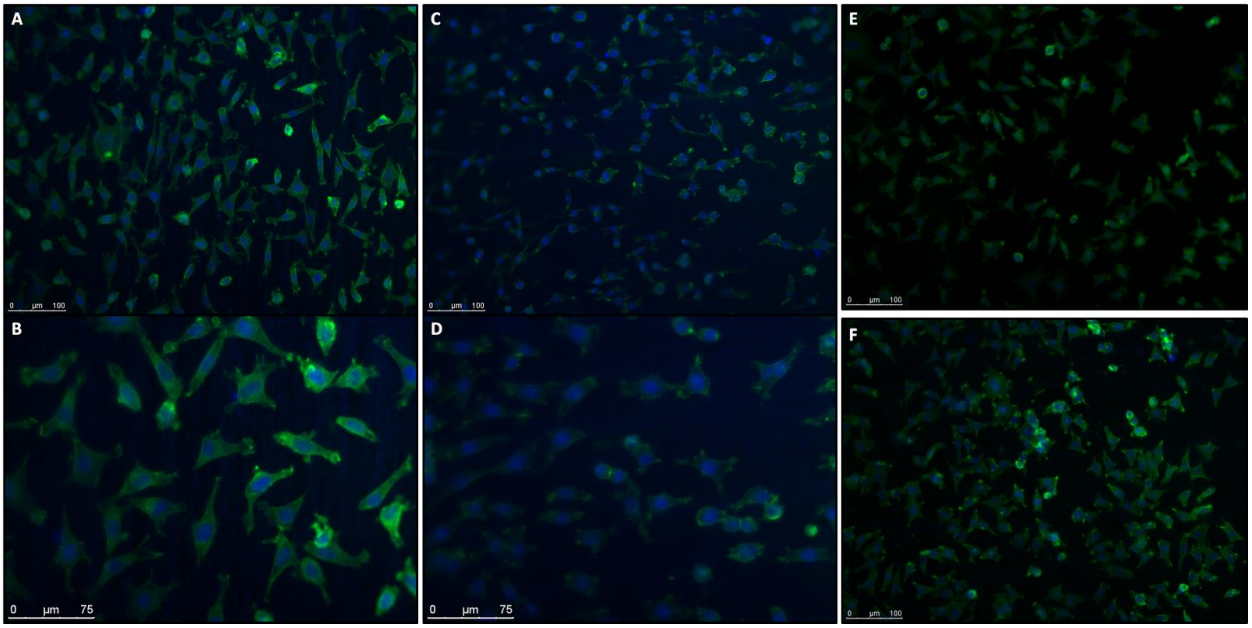

Figure 2.13. Fluorescence micrographs of a 72 hour L929 cell culture on (A&B) SF/IONP fibers, (C&D) SF/GNP fibers, (E) a glass coverslip control, and (F) pure SF fibers.

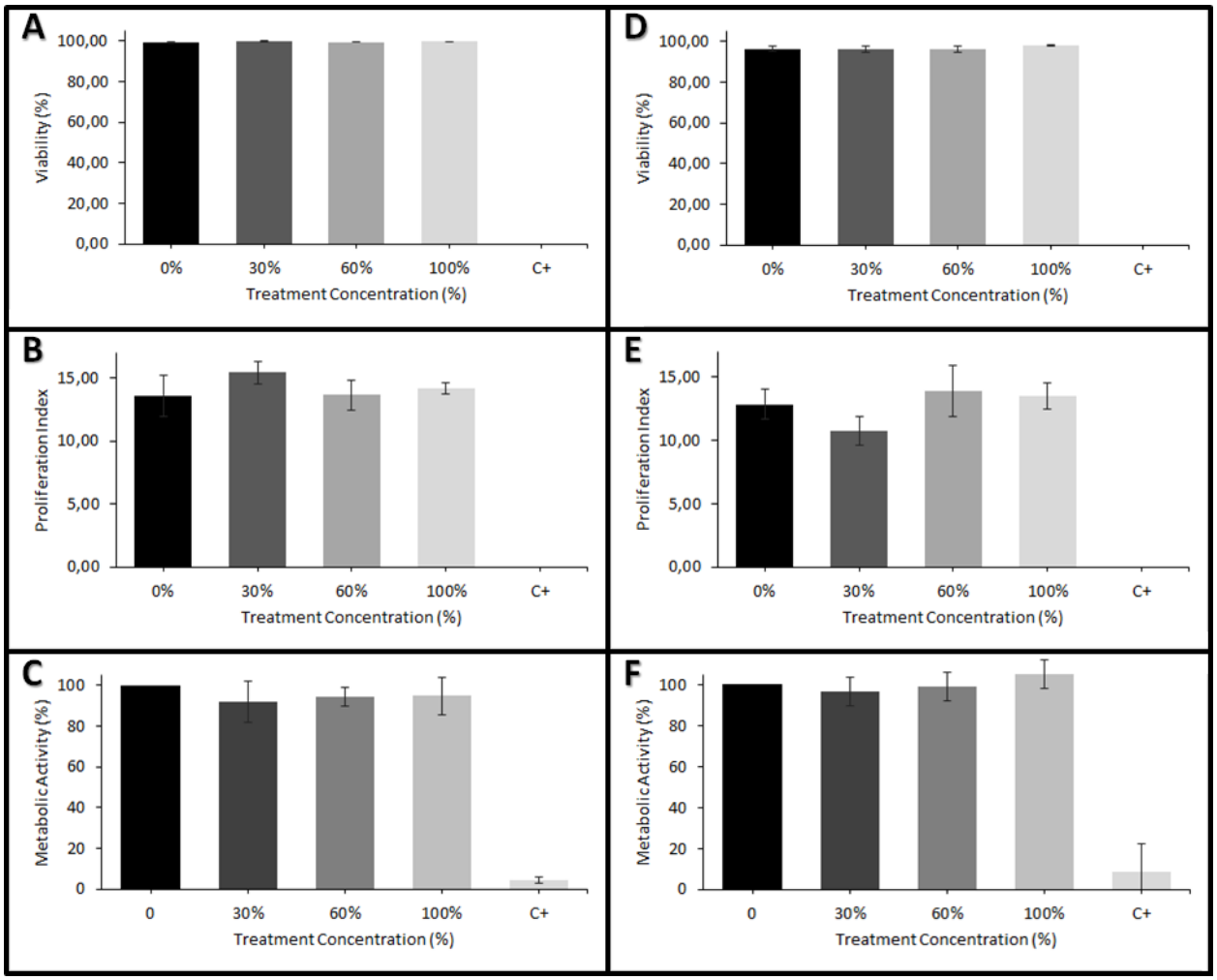

Figure 2.14. MTS assay results of (A&D) cell viability, (B&E) proliferation, and (C&F) metabolic activity after a 72-hour L929 cell culture in order to evaluate the cytotoxicity of the SF fibers functionalized with (A-C) GNPs and (D-F) IONPs. Tests were carried out on media containing 0%, 30%, 60%, or 100% of media pre-incubated with the SF/GNP or SF/IONP fiber material for 24 hours and a positive control.

Biomaterial evaluation using Schwann cells

Rat Schwann cell cultures were then carried out on aligned SF/GNP and aligned SF/IONP fibers in order to determine if the Schwann cells would adhere and aligned themselves onto the functionalized materials. After 48 hours of culture, Schwann cells indeed aligned themselves along both the SF/GNP and SF/IONP fibers as seen in Figure 2.15. Figure 2.15E&F show a stark contrast in morphological behavior of the Schwann cells on a glass coverslip compared to the

aligned functionalized fibers. On the fibers functionalized with GNPs and IONPs, the Schwann cells are elongated in the direction of the fiber alignment making close contact with neighboring cells along the fiber. Schwann cells displayed on the control sample take on a different shape, extending in random directions in order to make contact with any surrounding cells.

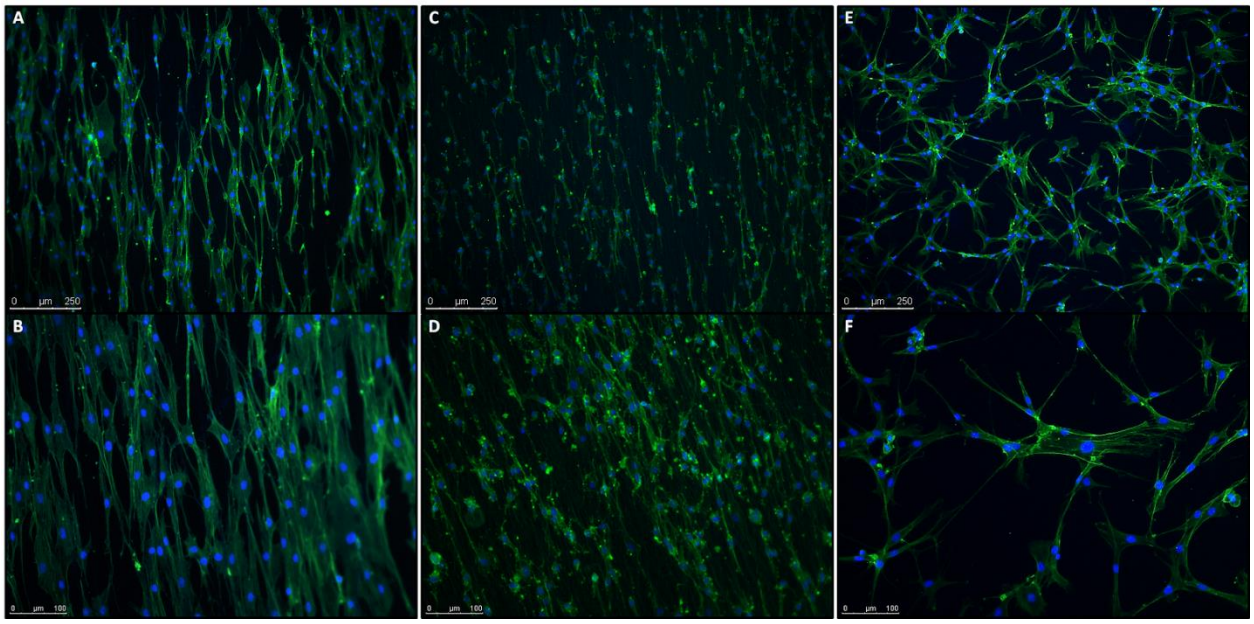

Figure 2.15. Fluorescence micrographs of a 48-hour cell culture of rat Schwann cells on (A&B) aligned SF fibers functionalized with GNPs, (C&D) aligned SF fibers functionalized with IONPs, and (E&F) a glass coverslip control.

Chapter 3

Results: Part 3

In Vivo Study

Introduction

The mechanisms involved with peripheral nerve regeneration are exceptionally complex. When a nerve injury is minor, the nerve is often able to regenerate without the assistance of a nerve graft; the predetermined pathways provided by the endoneurium allow Schwann cell migration which subsequently signal to regenerating neurons using biochemical cues that communicating with growth cones. When a nerve injury is more serious, spontaneous regeneration is much less likely to occur without surgical intervention. In this case, surgeons will implant a nerve guide bridging the gap between two nerve segments in order to support successful nerve regeneration.

The article "A Multi-layered Nerve Guidance Conduit Design Adapted to Facilitate Surgical Implantation" presented in Part 1 describes a novel nerve guidance conduit base design made from organized electrospun silk fibroin. This conduit provides mechanical support during the implantation process due to the robust mechanical properties of silk fibroin organized in a tri-layered structure containing two surfaces of aligned SF nanofibers and a center layer of randomly deposited SF nanofibers. In addition, the conduit provides physical support and guidance for the regenerating axons from the micro-channels presenting aligned nanofiber surfaces.

This SF-based NGC is a promising foundation design for peripheral nerve repair due to its satisfactory mechanical stability, its supportive micro-channel structure, and the nano-scale surface architecture. This basic design however lacks, a biofunctional component able to provide a more favorable environment for nerve regeneration. Axons are not only guided by a physical framework which is provided by the proposed NGC, but also the chemical cues from surrounding cells signaling regrowth, most importantly neurotrophic factors from proliferating Schwann cells.

Therefore, SF-based NGCs were functionalized by incorporating growth factors previously shown to improve the extension of regenerating axons and support the migration of Schwann cells (Chapter 2) directly into the electrospun fibers. Non-functionalized SF-based conduits, SF-based conduits functionalized with NGF and CNTF, and SF-based conduits functionalized with NGF and NT-3 were all produced for this study.

16 Sprague Dawley rats were divided into 4 experimental groups. The right sciatic nerve of each animal in three of the four groups was cut and a 5 mm NGC was sutured to the

epineurium, connecting the two severed segments of each nerve. The right sciatic nerve of each animal in the fourth group was cut, but no NGC was implanted; the nerve segments were sutured end-to-end. There was one control animal that was not operated on.

To encourage successful rehabilitation, all animals underwent swimming sessions, twice a week for 1 month, which aimed to encourage the animals to continue to move the injured leg throughout the early stages of recovery in order to resist muscle shortening.

At 3, 4, 6, and 8 months, the animals* in the study underwent locomotive analyses including motion capture analysis and swimming analysis. At 4 or 8 months, electrophysiological tests and histological analyses were performed on each animal in all experimental groups (electrophysiological and histological analyses of the control animal were carried out at 8 months). Locomotive, electrophysiological, and histological analyses were combined for each experimental group throughout the study in order to evaluate the results from each experimental group and determine the most successful bio-functionalization combination in vivo.

Histochemical Analyses

Hematoxylin and eosin staining

Transverse sections of each experimental and control sciatic nerve were stained using a hematoxylin and eosin staining procedure. All sections were taken within 10 mm distal to the site of injury in order to evaluate the success of cellular regrowth after passing through the NGC. Figure 3.1 shows stained sections from all experimental groups after 4 months in vivo compared with a control. Section from the cut & suture experimental group and the two functionalized SF experimental groups appear to resemble the control sample as many axons can be seen dispersed throughout the images indicated by black arrows in addition to several Schwann cell nuclei indicated by green arrows situated adjacent to several unstained halos around axons demonstrating the myelination of the axon. However, many less axons per surface area and proportionally more cell nuclei can be seen in these experimental sections compared with the control. The non-functionalized experimental group section resembles the control the least. Only several small axons can be found grouped together and not well dispersed as seen from the other sample sections. There are also proportionally more cell nuclei per surface area in the non-

*After 6 months, only 9 animals remained in the study. In addition, one animal in the non-functionalized SF group was euthanized at 7 months for ethical reasons and could not participate in any testing after the 7th month of the study.

functionalized section similar to the other experimental groups. The larger abundance of cell nuclei may be due to the presence of numerous macrophages and proliferated immature Schwann cells that have not yet come in contact with regenerating axons. There remains an excess of protein between myelinated axons, tubular in shape, which could indicate empty endoneurium channels containing undifferentiated immature Schwann cells as a result of Wallerian degeneration.

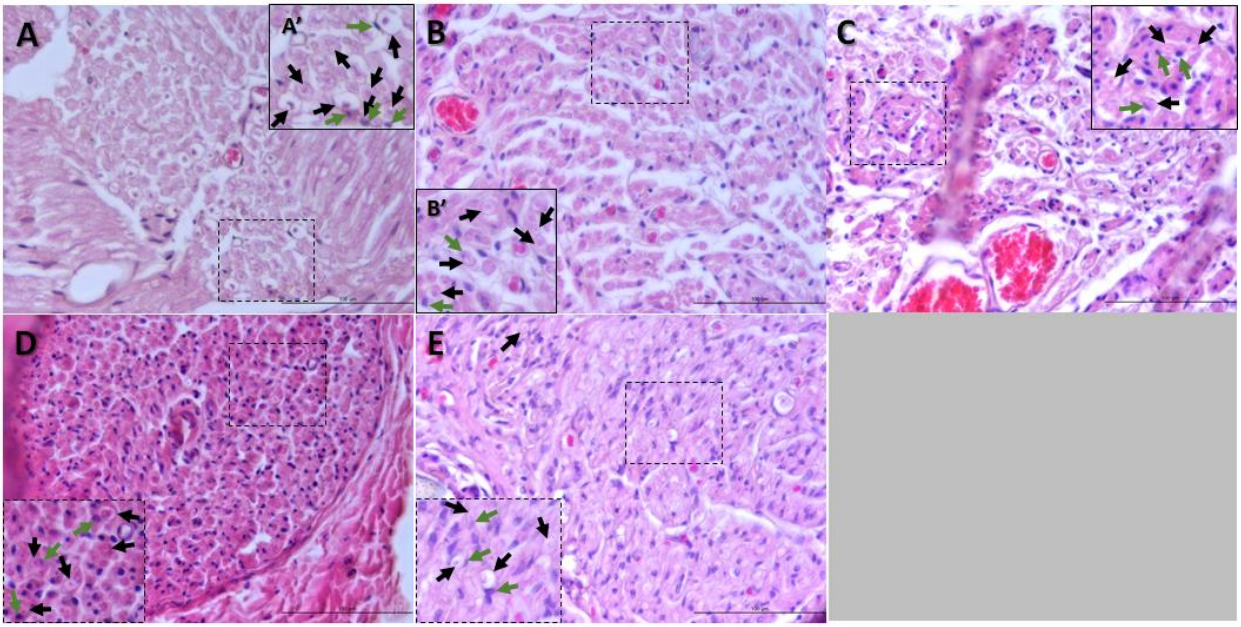

Figure 3.1. HE stain of transverse sections from a rat sciatic nerve (A) from a healthy rat, (B) distal to a cut & sutured procedure, (C) distal to a non-functionalized SF-based NGC, (D) distal to a NGC functionalized with NGF and CNTF, and (E) distal to a NGC functionalized with NGF and NT-3 after 4 months in vivo. Black arrows indicate axons and green arrows indicate Schwann cell nuclei.

Figure 3.2* shows stained sections from the cut and suture, NGF and CNTF functionalized SF, and NGF and NT-3 functionalized SF experimental groups after 8 months in vivo in addition to a control. All experimental samples at 8 months can be seen to resemble much more the control sample displaying many more myelinated axons than in the 4 month samples. The experimental samples continue to present a higher proportion of cell nuclei than the control sample, but the proportion has seemed to decrease in all samples after 4 more months in vivo. This may be

*Performing HE staining for the non-functionalized SF experimental group was impossible due to an error during the fixation of the extracted nerve.

directly related to the increase in myelinated axons found in the experimental samples in figure 3.2 compared to figure 3.1.

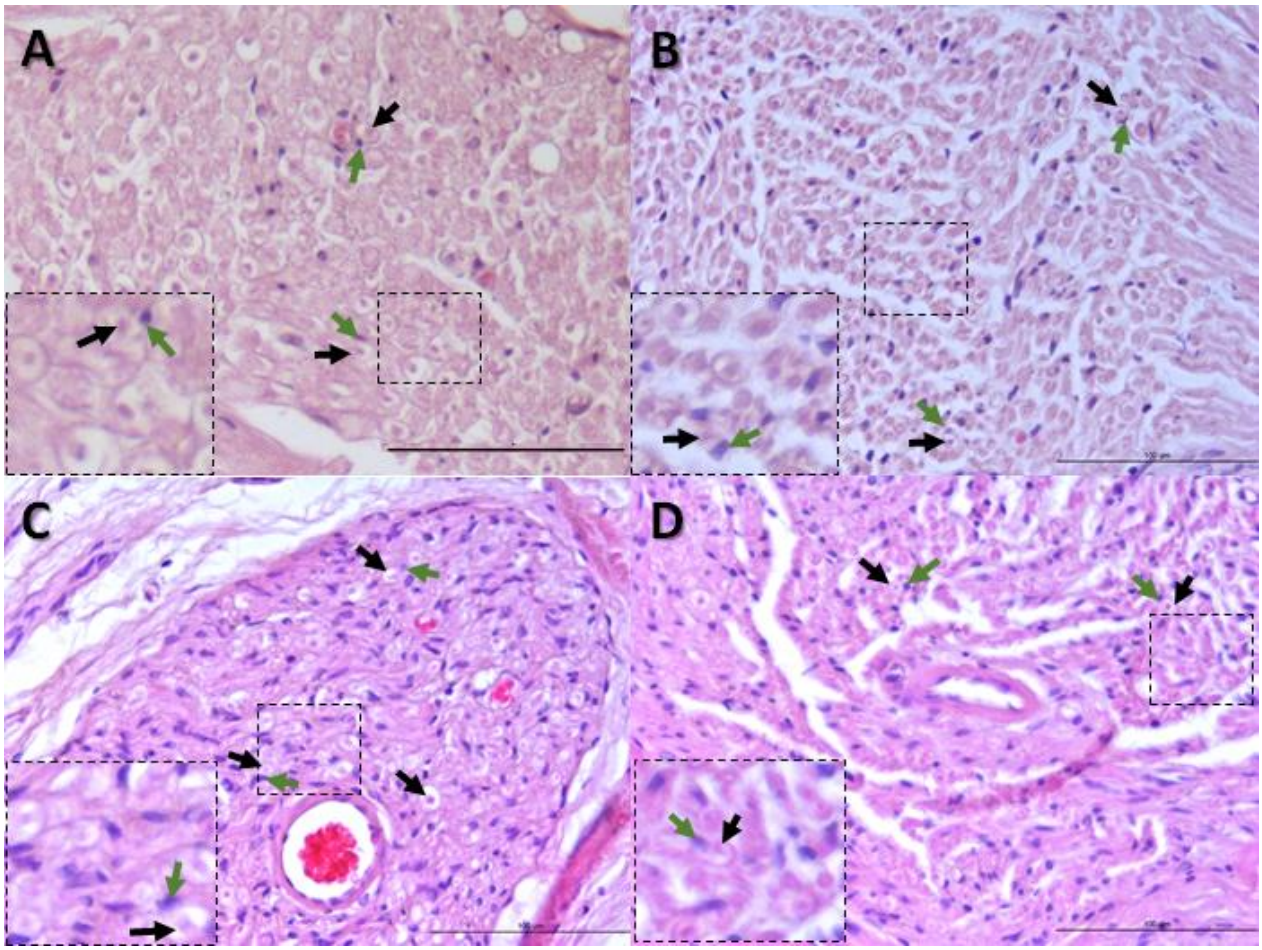

Figure 3.2. HE stain of transverse sections from a rat sciatic nerve (A) from a healthy rat, (B) distal to a cut & sutured procedure, (C) distal to a NGC functionalized with NGF and CNTF, and (D) distal to a NGC functionalized with NGF and NT-3 after 8 months in vivo. Black arrows indicate axons and green arrows indicate Schwann cell nuclei.

Cholinesterase activity stain analysis

Transverse sections of each experimental and control sciatic nerve were stained using a cholinesterase activity staining procedure. Sections were taken within 10 mm distal to the site of injury. Staining for cholinesterase activity allows the exclusive visualization of motor neurons within the section. In compliance with the HE stained sections, there was a significant difference

in the results from the 4 month samples and the 8 months samples. Figure 3.3 presents the stained samples from 4 months after nerve injury. Compared to the control sample, the experimental samples show very little cholinesterase activity indicated by a low presence of motor neuron axons 4 months after nerve injury. The cut and suture sample shows the most regenerated motor neuron axons compared to the other experimental samples. Samples from the non-functionalized SF group and the NGF and CNTF functionalized SF group both show few stained axons while the sample from the NGF and NT-3 functionalized SF group was taken from inside the NGC and shows virtually no CE activity.

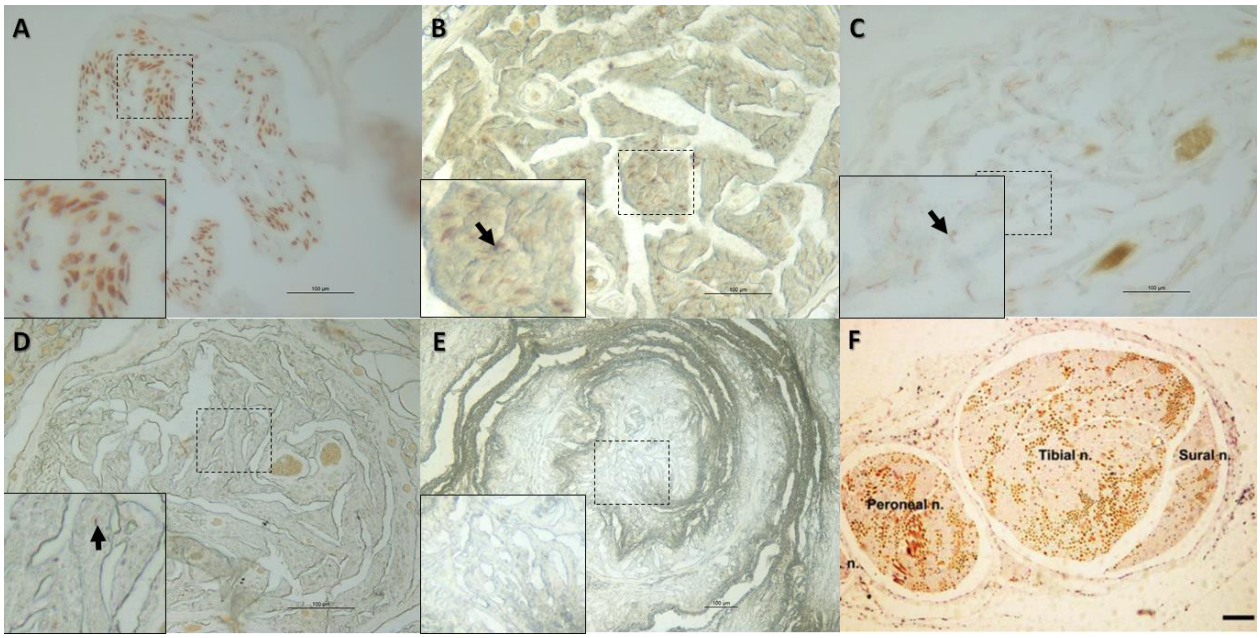

Figure 3.3. Cholinesterase activity stain of transverse sections from a rat sciatic nerve (A) from a healthy rat (peroneal nerve), (B) distal to a cut & sutured procedure after 4 months in vivo, (C) distal to a non-functionalized NGC after 4 months in vivo, (D) distal to a NGC functionalized with NGF and CNTF after 4 months in vivo, and (E) distal to a NGC functionalized with NGF and NT-3 after 4 months in vivo. Figure F presents a choline acetyltransferase stain of a healthy rat sciatic nerve distal section by Badia et al.; motor neuron axons are stained in brown (scale bar=100 µm) (Badia et al., 2010). Arrows indicate stained motor neuron axons.

Figure 3.4 presents stained sections from all experimental groups after 8 months in vivo compared with the control and a similar control stain specific for axons of motor neurons found in the literature. The peroneal nerve, a mixed nerve, was identified from each section. All samples display CE activity indicating the presence of motor nerve fibers. This striking contrast in stained samples from 4 months and 8 months therefore indicates the late regeneration tendency of axons from motor neurons after peripheral nerve injuries.

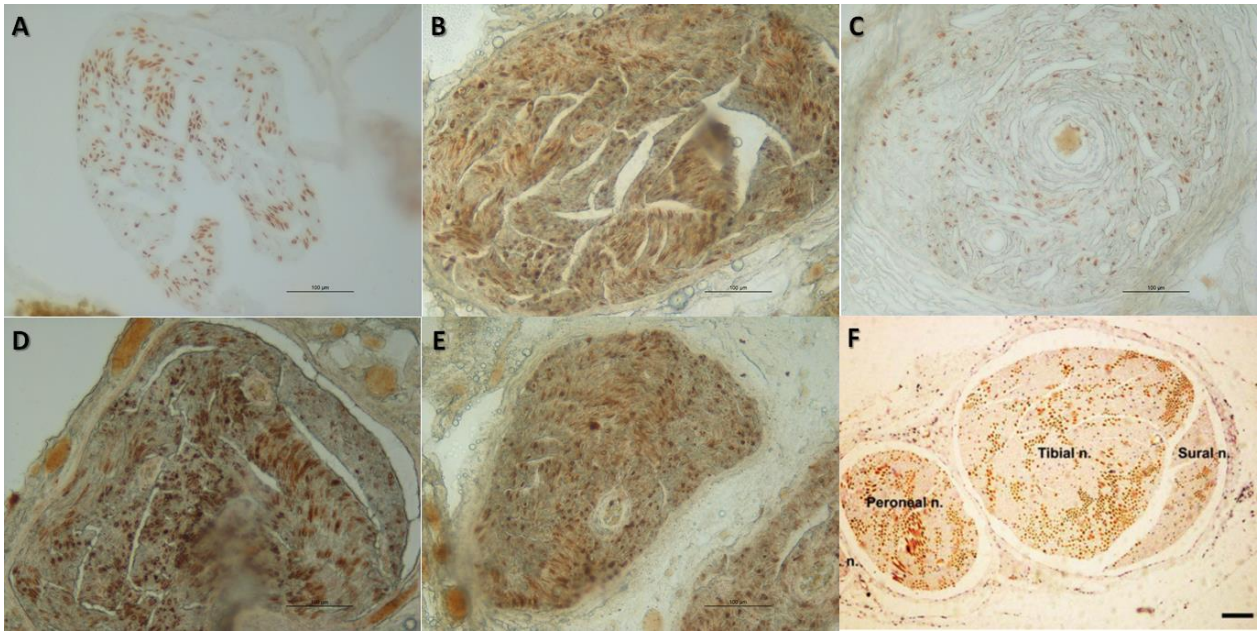

Figure 3.4. Cholinesterase activity stain of transverse sections from a rat sciatic nerve (A) from a healthy rat (peroneal nerve), (B) distal to a cut & sutured procedure (peroneal nerve) after 8 months in vivo, (C) distal to a non-functionalized NGC (peroneal nerve) after 8 months in vivo, (D) distal to a NGC functionalized with NGF and CNTF (peroneal nerve) after 8 months in vivo, and (E) distal to a NGC functionalized with NGF and NT-3 (peroneal nerve) after 8 months in vivo. Figure F presents a choline acetyltransferase stain of a healthy rat sciatic nerve distal section by Badia et al.; motor neuron axons are stained in brown (scale bar=100 µm) (Badia et al., 2010).

The section from the cut and suture experimental group, unlike the control sample, displayed CE activity that almost completely fills the nerve fascicle leaving very little surface unstained. This may be due to misdirected motor nerve fibers into the peroneal nerve fascicle

causing a greater concentration of motor nerve fibers than is found in a healthy, uninjured peroneal nerve fascicle. This may result in targeting errors, for example motor neurons that once innervated one muscle, reinnervating a different muscle.

On the contrary, the section from the non-functionalized SF-based NGC show very little CE activity. The motor nerve fibers identified in this sample also are dispersed homogeneously throughout the fascicle which is inconsistent with the organization found in the control sample. As the nerve continues to branch off into more specialized nerves in the periphery, bundles of motor or sensory nerve fibers must be grouped together properly. In this sample, there is no organization of motor nerve fibers throughout the fascicle. Both functionalized SF-based NGC group samples show CE activity in addition to an organized distribution. In both samples, clear groups of motor nerve fibers and unstained areas can be observed. Organization of motor nerve fibers in each fascicle may be impossible to evaluate correctly since the positioning of fibers continuously changes throughout the nerve. As some sections may have been taken more distal to others, no two sections will present the same fascicle organization. Observing the peroneal nerve sections from 3.2 and 3.3 A&F supports this claim as two healthy rat sciatic nerve sections do not exhibit the same motor nerve fiber organization in the same fascicle.

Immunohistochemical stain analysis

As consistent with all other staining procedure, transverse sections of each experimental and control sciatic nerve were taken within 10 mm distal to the site of injury. First sections were immunostained with DAPI, anti-β-tubulin III antibody (Sigma Aldrich), and Alexa Fluor™ 488 phalloidin (Thermo Fisher Scientific) in order to visualize cell nuclei, microtubules found in the axons of neurons, and actin from non-neuronal cells. Nerve fibers considered to be well-developed are depicted as hollow red circles from the anti-β-tubulin III stain; this organization represents the microtubule structure inside a healthy axon.

Figure 3.5 shows sample sections from all experimental groups at 4 months and 8 months after injury and a control. Figure 3.6 presents magnified portions of the samples found in figure 3.5. First, microtubules from regenerating or regenerated axons can be found in all samples throughout the entire nerve fascicles. However, at 4 months, many of these axons appear only as

round dots most likely signifying a very small diameter or a growth cone as the axons are still regenerating. At 4 months, the sample from the cut and suture group shows the most successful regeneration of both small-diameter and large-diameter axons compared to the three NGC groups. In figure 3.6 A, several well-developed axons are apparent, both large-diameter and small-diameter. This sample contains the most well-developed axons compared to the other samples at 4 months. The sample from the NGF & CNTF functionalized SF group also contains several well-developed axons while the non-functionalized SF group and the NGF and NT-3 functionalized SF group display virtually well-developed nerve fibers; the vast majority of nerve fiber representation is by small round dots. However, the well-developed axons in Figure 3.6E have a smaller diameter than the larger axons in figure 3.6A or the control (Figure 3.6I).

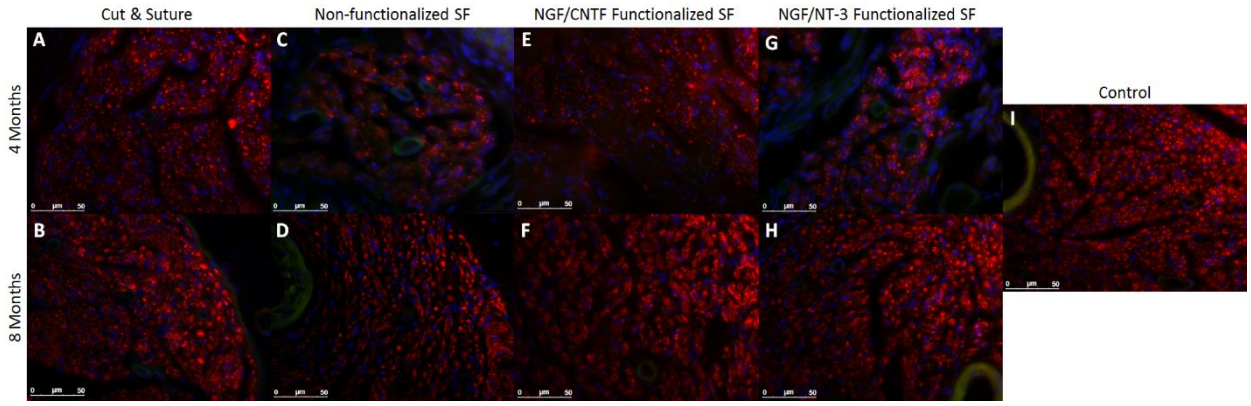

Figure 3.5. Immunostained sciatic nerve sections from all experimental groups 4 and 8 months after injury and a control viewed under an epifluorescence microscope (Scale = 50 µm). DAPI (blue), Anti-β-tubulin III (red), and phalloidin (green)

All samples at 8 months after injury show an improvement in axon regeneration in comparison to the 4 month samples. The cut and suture, NGF and CNTF functionalized SF, and NGF and NT-3 functionalized groups all contain well-developed axons both with larger diameters and smaller diameters. There are several small red dots still found in these three samples as seen in the 4 month samples, but there are also several similar red dots found in the control sample. The red dots may indicate small-diameter nerve fibers that are unmyelinated. Several unmyelinated axons can be supported by a single nonmyelinating Schwann cell which may explain

why these small-diameter nerve fibers appear to be grouped in bundles. The sample from the non-functionalized SF group (Figure 3.6D) however does not display a large proportion of well-developed axons. Most microtubule representation is in a form similar to the cut and suture sample at 4 months (Figure 3.6A).

In a small area randomly chosen from each sample of 8 months, 50 axon diameters were measured at random and the average axon diameter of each group plus the control was calculated. The average axon diameters of the control sample, cut and suture group sample, non-functionalized SF group sample, NGF and CNTF functionalized SF group sample, and NGF and NT-3 functionalized SF group sample were 2.55 ± 0.97 µm, 2.84 ± 1.01 µm, 2.39 ± 0.70 µm, 2.57 ± 0.77 µm, and 2.81 ± 0.89 µm respectively. In each 0.04 mm² area, the largest axon diameters were found to be 5.38 µm for the control sample, 5.56 µm for the cut and suture group sample, 3.66 µm for the non-functionalized SF group sample, 4.96 µm for the NGF and CNTF functionalized group sample, and 5.74 µm for the NGF and NT-3 functionalized group sample.

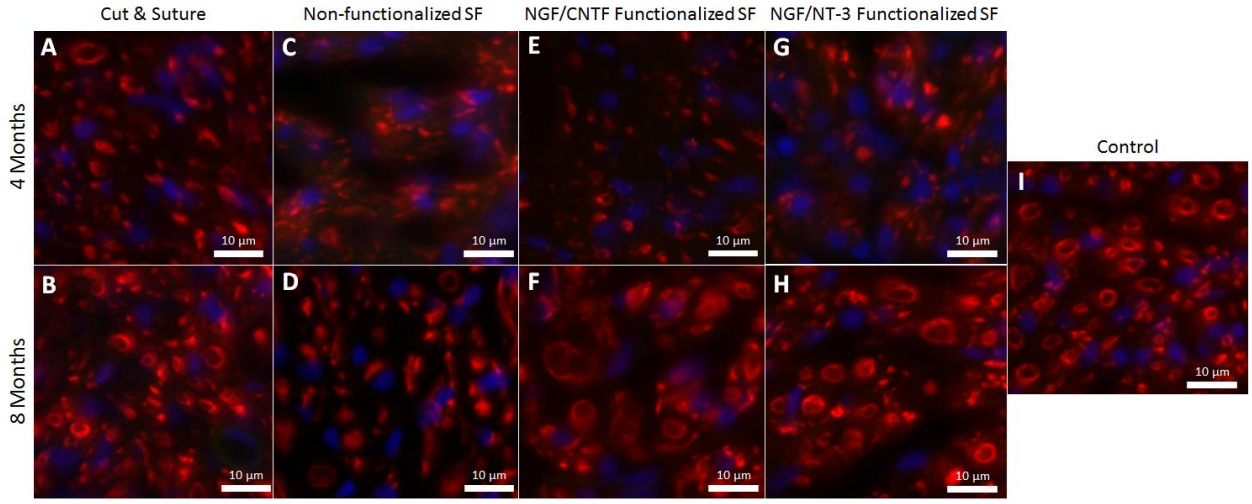

Figure 3.6. Immunostained sciatic nerve sections from all experimental groups 4 and 8 months after injury and a control viewed under an epifluorescence microscope. DAPI (blue), Anti-β-tubulin III (red), and phalloidin (green)

The average diameter of axons in a designated area of a nerve fascicle is not the only value to take into consideration however. Since there exists both small and large diameter axons within

nerves, and the organization of these axons is specific to the portion of the fascicle being evaluated, it is possible that the randomized area chosen from analysis contained more small-diameter axons or large-diameter axons compared to a different section of the fascicle. In addition, axon diameters smaller than 0.9 µm were unable to be measured as the microtubules' cylindrical structures cannot be visualized at the available image resolution. Therefore, a qualitative evaluation along with measured values should be considered in conjunction in order to evaluate the success of nerve repair.

Next, sections were immunostained with DAPI and anti-myelin protein zero antibody (Abcam) in order to visualize cell nuclei and protein zero found in the myelin sheaths formed by Schwann cells. Axons in the peripheral nervous system with a diameter larger than about 0.7 µm are enveloped by a myelin sheaths produced by Schwann cells located virtually the entire length of the axon (Verkhratsky & Butt, 2007). This is consistent with immunostained samples found in the control, depicted in Figure 3.7, as myelinated axons consistently had a measured diameter superior to the 0.7 µm threshold. In figure 3.7B, both unmyelinated, small-diameter axons (circled) and myelinated, large-diameter axons (yellow arrow) are found. In addition, unmyelinated axons are found in bundles which is expected as one non-myelinating Schwann cell envelopes multiple small-diameter axons. In addition, it can be observed that the thickness of the myelin sheath is directly proportional to the axon diameter as is supported in the literature.

In Figure 3.8, sections from all experimental groups after 4 and 8 months in vivo are portrayed. After 4 months, recognizable myelin sheaths can be found in all samples with the exception of the non-functionalized SF experimental group. This may be caused by the fact that the regenerating axons from this group have not reached their innervation targets 4 months after injury suggesting a slower regeneration rate compared with all other experimental groups as myelin production is accelerated from electrical activity of the neuron (Taveggia et al., 2010; Demerens et al., 1996; Tauber et al., 1980). The section from the cut and suture sample after 4 months in vivo appears to present the most developed myelin sheaths compared to the other experimental groups. Both sections from the functionalized SF groups present very similar results of axon myelination.

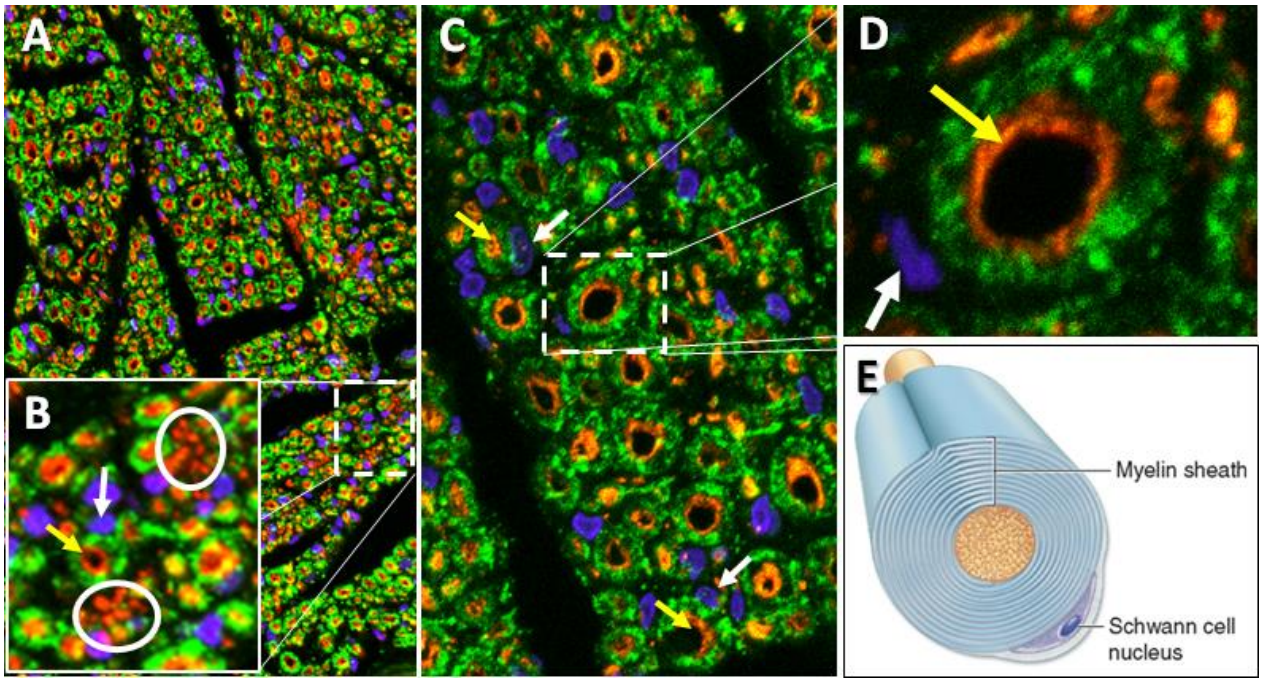

Figure 3.7. (A-D) Immunostained sciatic nerve sections from a control viewed with a confocal microscope. DAPI (blue) Anti-β-tubulin III (red), and anti-myelin protein zero (green). (E) Illustration of the morphology of the interaction of a Schwann myelinating a large-diameter axon.

Sections from samples taken 8 months after injury, appear very similar with no sample showing significantly better results of axon myelination. Myelination appears to have improved drastically from the nun-functionalized SF group between 4 and 8 months, showing comparable results to all other experimental group samples at 8 months in vivo. Figure 3. 9. Presents a more extensive evaluation of the myelination results after 8 months in vivo. In Figure 3.9A, C, E, G, & I, images taken at a lower power objective show comparable results between the cut and suture, NGF and CNTF functionalized SF, and NGF and NT-3 functionalized groups. Samples also appear very similar in myelinated axon concentration to the control sample. The non-functionalized SF sample however displays a visually lower concentration of myelinated axons compared with the other samples. Myelin thickness for randomly chosen myelinated axons were measured in each sample after 8 months in vivo. Average myelin thickness found in cut and suture, non-functionalized SF, NGF and CNTF functionalized SF, NGF and NT-3 functionalized, and control group samples was 1.18 ± 0.30 µm, 0.74 ± 0.33 µm, 0.77 ± 0.26 µm, 0.87 ± 0.44 µm, and 1.23 ± 0.17 µm respectively

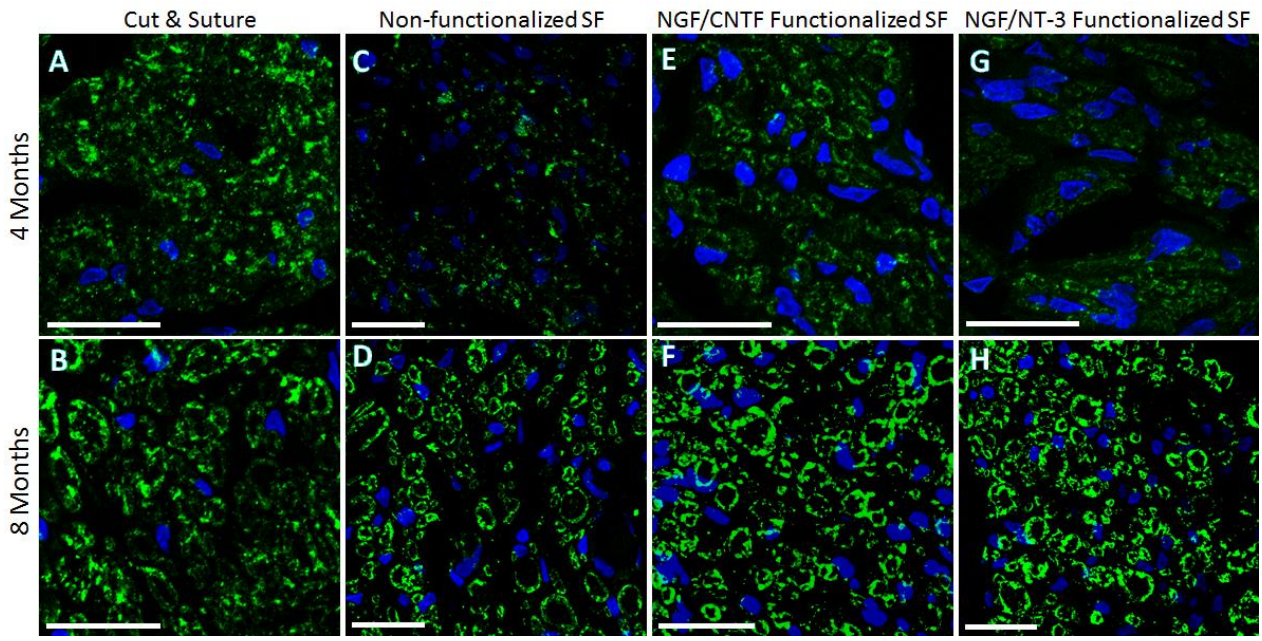

Figure 3.8. Immunostained sciatic nerve sections from all experimental groups 8 months after injury and a control viewed with a confocal microscope. DAPI (blue) and anti-myelin protein zero (green) (Scale = 20 µm).

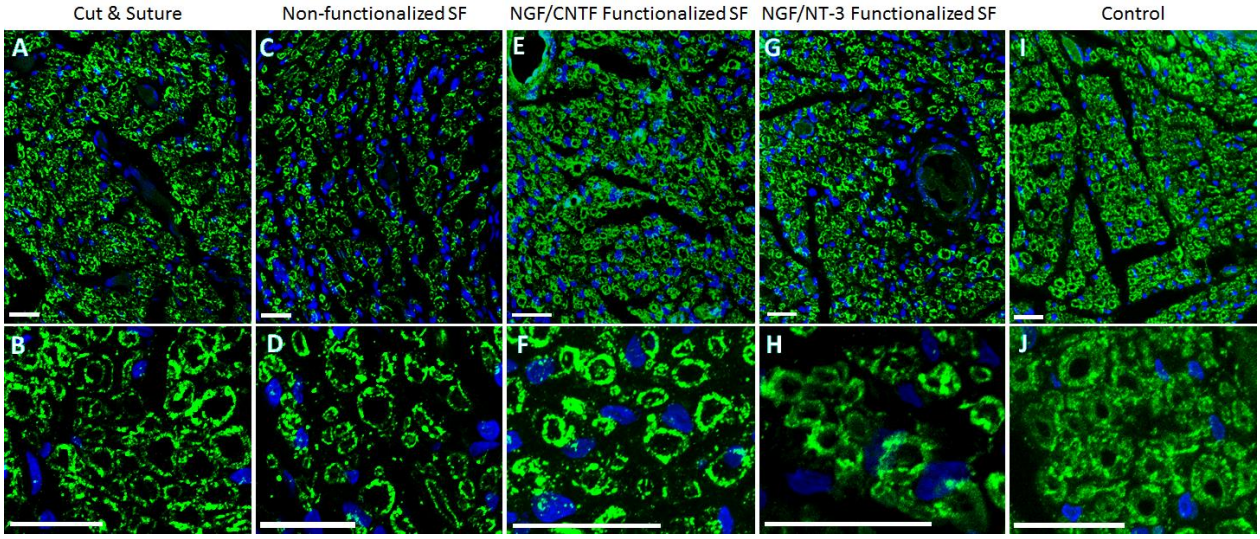

Figure 3.9. Immunostained sciatic nerve sections from all experimental groups 8 months after injury and a control visualized with a confocal microscope. DAPI (blue) and anti-myelin protein zero (green) (Scale = 20 µm).

Electromyography evaluations

Needle electromyography (Figure 3.10) results after 8 months of the in vivo study are shown in Figure 3.11. The gastrocnemius muscle was tested for all experimental groups including the control. The EMG results are presented in comparison to the muscle response of the control test with the response limit of the control representing 100% muscle response according to the EMG amplitude over varying intensities of nerve stimulation located at the proximal end of the sciatic nerve. As EMG testing is specific to the motor neurons innervating a skeletal muscle, the EMG gives additional information not acquired in the traditional histochemical analyses. For example, staining for CE activity allows a qualitative analysis of the population and organization of regenerated motor neurons in a nerve section, but does not give a quantitative analysis on the innervation of each muscle. In addition, not all motor neurons stained for CE activity necessary innervate the correct innervation target, rendering one or more muscle inefficiently innervated by the appropriate motor neurons. EMG testing gives a quantitative analysis of the electrical activity in a specific muscle which is directly related to the level of reinnervation from motor neurons.

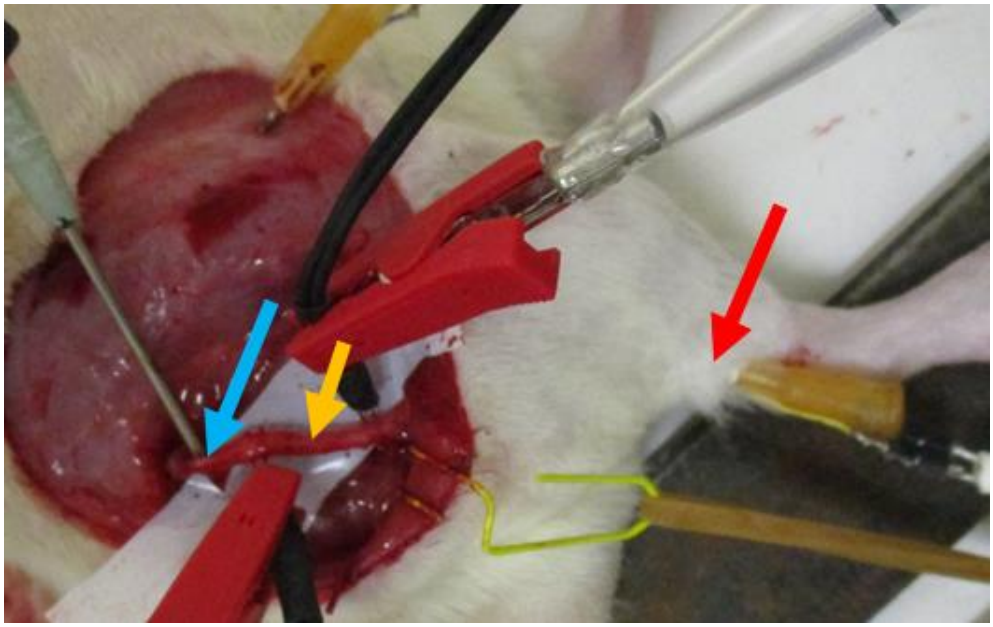

Figure 3.10. Setup for EMG testing with an electrical stimulation needle placed against the proximal potion of the sciatic nerve (blue arrow), and an electrode inside the gastrocnemius muscle (red arrow). The NGC 8 months post-injury is identified by the yellow arrow.

As seen in Figure 3.11, all animals reach at least 80% of the EMG amplitude detected from the control animal 8 months after injury. However, each experimental group shows a separate acceleration to reach 80% in respect to stimulation intensity. The animal tested from the cut and suture experimental group and SF functionalized with NGF and CNTF group reached 80% EMG amplitude at stimulation intensities of about 6 V and 10 V respectively while the animals tested from the non-functionalized SF group and SF functionalized with NGF and NT-3 group reached 80% EMG amplitude at stimulation intensities of about 28 V and 29 V respectively. These results are compared to the control EMG results which reached 80% of its average EMG amplitude limit at a stimulation intensity of about 1 V.

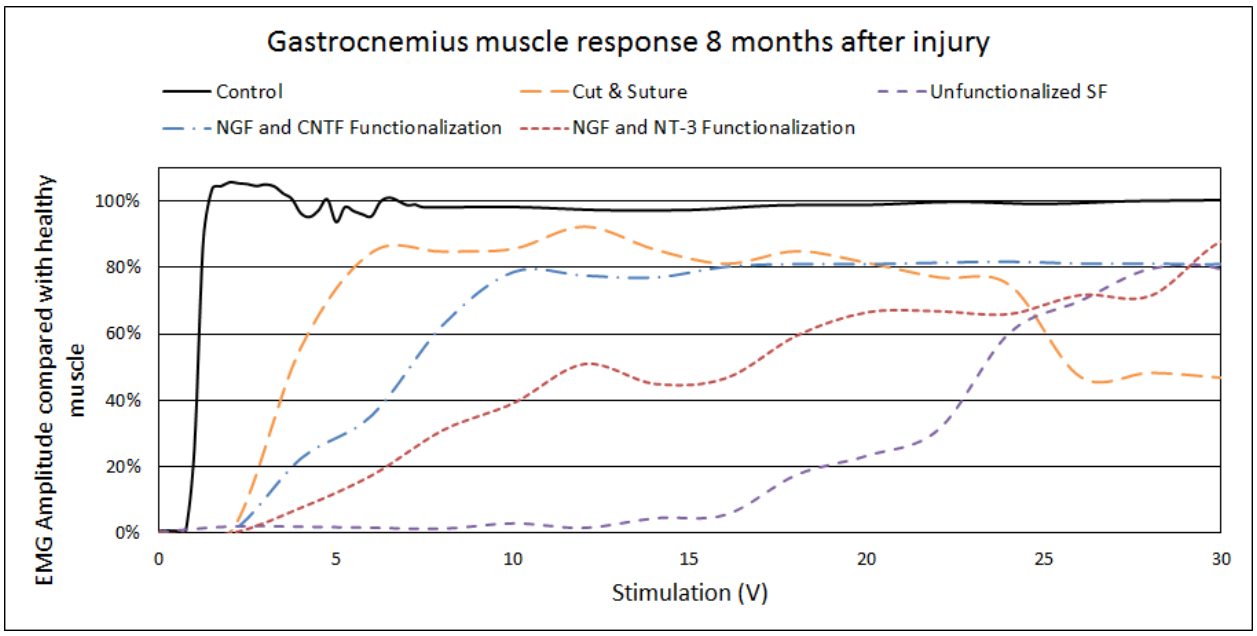

Figure 3.11. Needle electromyography results of the gastrocnemius muscle response of animals from all experimental groups (cut and suture, non-functionalized SF-based NGCs, NGF and CNTF functionalized SF-base NGCs, and NGF and NT-3 functionalized SF-based NGCs) and a control. Results are presented in comparison to the average maximum EMG amplitude of the control once equilibrium had been reached (100% muscle response) in respect to stimulation intensities in volts applied a proximal location on the sciatic nerve.

Furthermore, the control EMG analysis shows a steep peak of EMG amplitude before reaching equilibrium at 100% muscle response, while the EMG analyses from the experimental groups display a peak much later and with an inferior slope. While the control EMG amplitude reached 20% at a stimulation intensity of about 1 V, the experimental groups cut and suture, SF functionalized with NGF and CNTF, SF functionalized with NGF and NT-3, and non-functionalized SF reached 20% at stimulation intensities of about 3 V, 4 V, 6 V, and 19 V respectively. Therefore, animals in experimental groups cut and suture and SF functionalized with NGF and CNTF revealed the steepest slopes with more considerable muscle responses at the lowest stimulation intensities compared to the two other experimental groups. Finally, the animal in the cut and suture experimental group displayed the most similar muscle response to the control test.

Locomotive evaluations

Walking analysis

Motion capture evaluations were taken after 6 months in vivo of each animal as they walked across a straight plank. Reflective markers were placed on the sacrum, the 5th lumbar vertebrae, right and left greater trochanter (hip), right and left knee, right and left lateral malleolus (ankle), and right and left cuboid (base of 5th metatarsal, toe). As the animal walked in a straight path, reflective cameras continually captured the x, y, and z positions of each marker in order to evaluate the movement patterns from each animal. A walking cycle of at least 3 steps from each side was taken for evaluation.

In figure 3.12, the displacement of the ankle and the base of the 5th toe during a walking cycle for animals in each experimental group are observed. From these data, the average height achieved during a step (relative to the baseline foot position) by the ankle and the toe along with the average distance taken during one step was measured in each cycle (Table 3.1).

The height vs. distance foot displacement patterns from cut and suture experimental group were clearly distorted compared to the control animal's walking patterns. First of all, two peaks in height can be seen from the experimental right ankle during one step, the higher peak coming first. The control step pattern exhibits a much smaller peak just before the larger peak in height of the ankle. In addition, at the end of each step, the ankle has a tendency to move slightly

backward as touches the ground which is not seen with the control. However, the average distance traveled with each step is only 70% that of the control.

Table 3.1. Average measurements during walking analysis cycle.

		Total Step (mm) [Percent of control]	Total Step (s) [Percent of control]	Height (mm) [Percent of control]	Peak (s) [Percent of control]
Control	Ankle	143	0.48	35	0.12
	Toe		0.42	22.7	0.14
Cut & Suture	Ankle	100 [69.9%]	0.37 [77.1%]	28.5 [81.4%]	0.13 [108.3%]
	Toe		0.39 [92.9%]	21.5 [94.7%]	0.12 [85.7%]
Non-functionalized SF	Ankle	133 [93.0%]	0.22 [45.8%]	30 [85.7%]	0.16 [133.3%]
	Toe		0.16 [38.1%]	15.3 [67.4%]	0.09 [64.3%]
NGF & CNTF Functionalized SF	Ankle	153 [107.0%]	0.25 [52.1%]	23.3 [66.6%]	0.16 [133.3%]
	Toe		0.25 [59.5%]	19 [83.7%]	0.15 [107.1%]
NGF & NT-3 Functionalized SF	Ankle	147 [102.8%]	0.41 [85.4%]	28.3 [80.9%]	0.14 [116.7%]
	Toe		0.23 [54.8%]	18 [79.3%]	0.10 [71.4%]

The non-functionalized SF group height vs. distance foot displacement patterns appeared more natural than those of the cut and suture group illustrating one prominent peak in height from the ankle with a steep descent and one prominent peak in height from the toe with slightly more gradual decent which is similar to the control. The average distance traveled with each step was 93% that of the control.

The height vs. distance foot displacement patterns of the NGF and CNTF functionalized group display an initial peak in height of both the ankle and the toe followed by a very gradual descent. The average distance traveled with each step was found to be exaggerated at 107% of that of the control.

The height vs. distance foot displacement patterns of the NGF and NT-3 functionalized group appear to have the most similar curve morphologies compared to the ankle and toe

displacement patterns of the control. The average distance traveled with each step was also only 5 mm greater than that of the control (103%).

In figure 3.13, the vertical displacement of the ankle and the base of the 5th toe during the same walking cycle for animals in each experimental group are observed over time. These graphs present additional information on the vertical foot displacement patterns of the animals in each experimental group. Duration of gait is not considered significant due to the fact that the animals may have walked at different speeds during exercise. Nonetheless, the curves represented by positioning of height over time plus the relationships of step duration of the toe in respect to the ankle is important to evaluate.

While the cut and suture group walking patterns reveal a much shorter displacement achieved by each step of the injured leg compared to the control, the duration of each step was found to be very similar to the control lasting an average of 0.37 s and 0.39 s for the ankle and toe respectively (toe step duration was 105% that of the ankle). The control patterns were measured to have step durations of an average of 0.48 s and 0.42 s for the ankle and toe respectively (toe step duration was 87.5% that of the ankle). The morphology of the curves suggest a distorted walking pattern which corresponds to the patterns in Figure 3.12.

Walking patterns in respect to time from the non-functionalized SF group and the NGF and CNTF functionalized group exhibit very similar morphologies containing one prominent peak for both the ankles and the toes. Both of these patterns are lacking a gradual increase in height in respect to time before the maximum height is reached for both the ankle and the toe. Steps were also found to last a shorter period of time for these two experimental groups, averaging 0.22 s and 0.25 s for ankles of the non-functionalized SF group and the NGF and CNTF functionalized group respectively and averaging 0.16 s and 0.25 s for toes of the cut and suture group and the NGF and CNTF functionalized group respectively (toe step durations for the non-functionalized SF group and the NGF and CNTF functionalized group were 72.7% and 100% that of the durations of the ankles respectively).

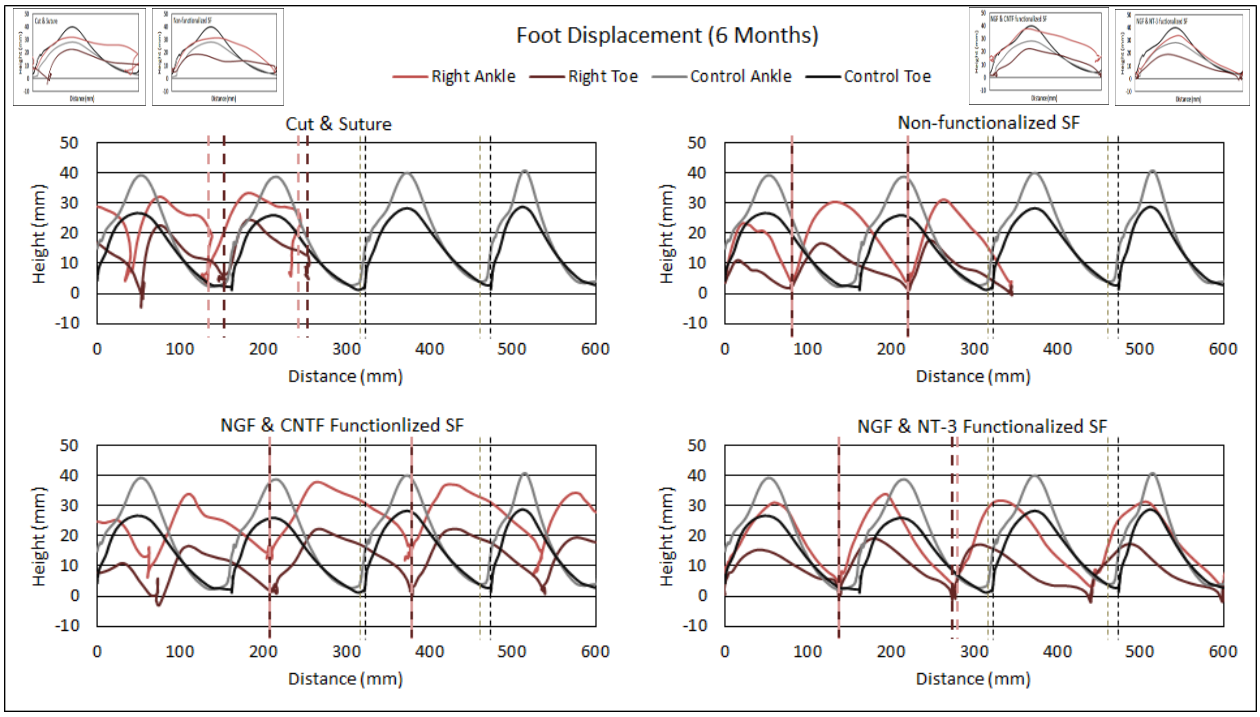

Figure 3.12. Walking analyses after motion capture tests after 6 months in vivo. Vertical and horizontal displacement for each experimental group during a step cycle is displayed.

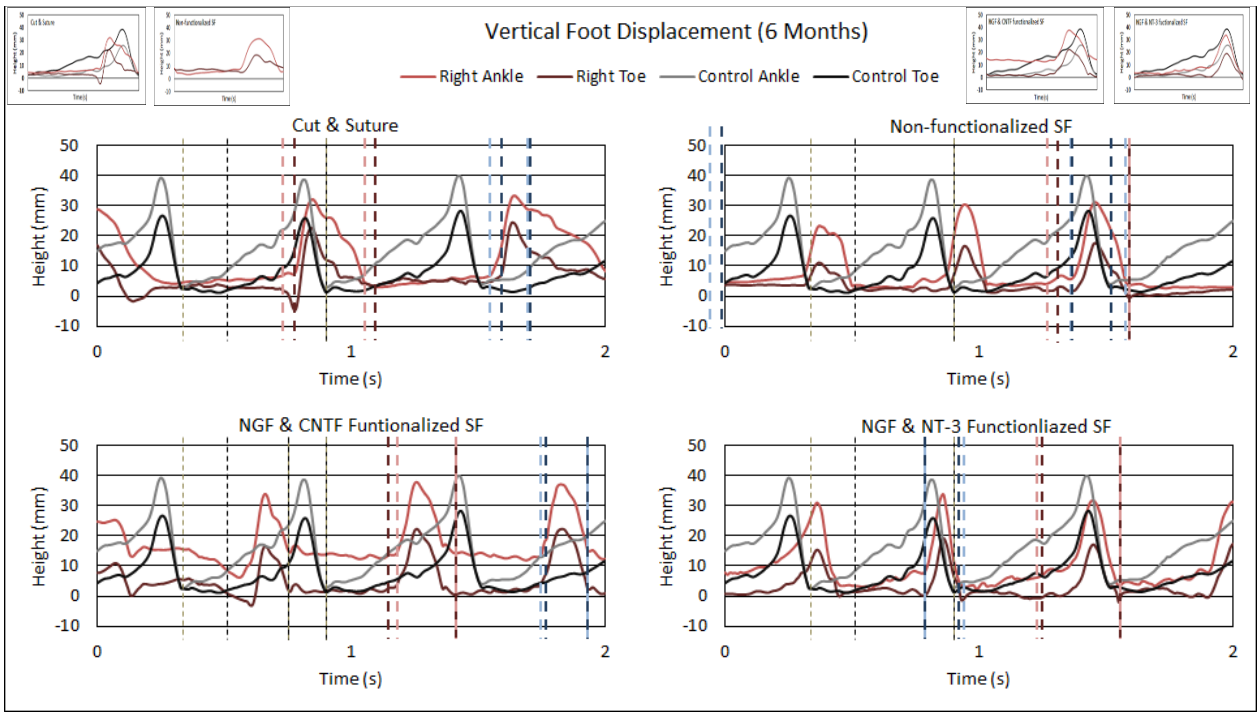

Figure 3.13. Walking analyses after motion capture tests after 6 months in vivo. Vertical displacement over time for each experimental group during a step cycle is displayed.

Finally, the morphology of the curves representing the walking patterns of for the NGF and NT-3 functionalized group, consistent with Figure 3.12, is very similar to those of the control. Average step duration was found to be 0.41 s and 0.23 s for the ankle and toe respectively (toe step duration was 56% that of the ankle) which is a larger difference in duration compared to the ankle and toe of the control suggesting that the toe of the animal in this experimental group was late to be lifted due to possible foot drop from muscle weakness after nerve injury.

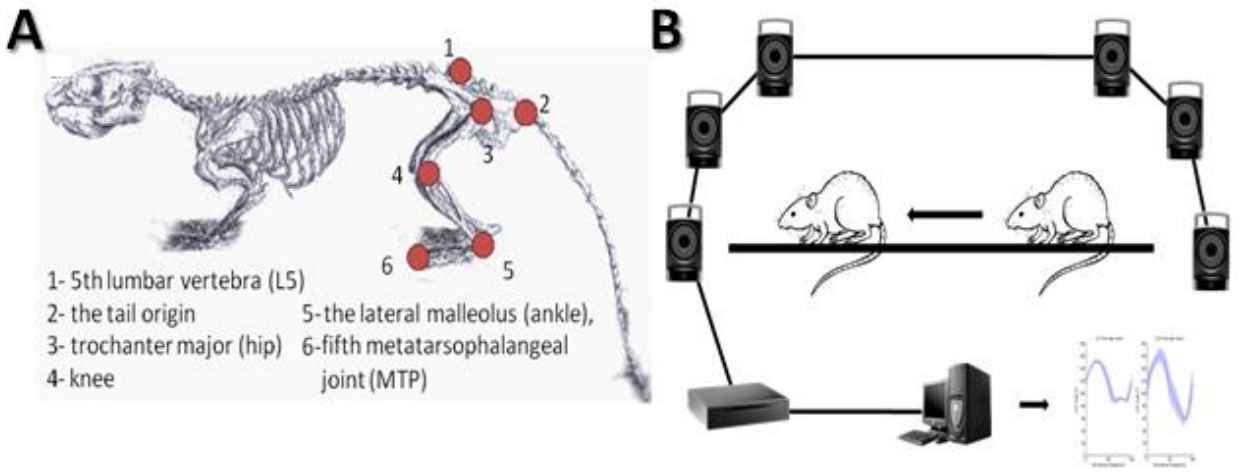

Figure 3.14. (A) placement of retroreflective markers for motion capture analysis and (B) general dipiction of the setup for motion capture assays; 18 cameras are positioned around a plank on which the animal walks in a a straight line.

As shown in Figure 3.14, angles of the hip, the knee, and the ankle were also measured throughout the walking cycle of each animal. In Figures 3.15, 3.16, and 3.17, the angle patterns from the hip, the knee, and the ankle respectively are demonstrated including patterns of each experimental group and a control. For each experimental group, a normalized step pattern taken randomly from the experimental right and experimental left of each walking cycle in respect to the control is presented to the right of each graph.

Table 3.2. Average measurements of hip angle patterns during a walking cycle.

Hip Angles

Group	Limb	Minimum Angle (deg)	Maximum Angle (deg)	Amplitude (deg)	Duration (s)
Control	Right	66.5 ± 4.1	93.3 ± 2.0	26.9 ± 4.7	0.61 ± 0.05
	Left	65.2 ± 2.0	89.6 ± 1.3	23.9 ± 1.9	0.61 ± 0.10
Cut & Suture	Right	50.9 ± 6.8	90.4	39.5	0.79
	Left	64.3 ± 1.3	92.8 ± 1.8	28.2 ± 1.3	0.86 ± 0.04
Non-functionalized SF	Right	52.1 ± 0.9	102.5 ± 1.0	50.6 ± 0.8	0.40 ± 0.04
	Left	52.6 ± 1.6	92.8 ± 1.0	40.1 ± 0.1	0.40 ± 0.03
NGF & CNTF Functionalized SF	Right	71.8 ± 1.5	94.3 ± 0.8	22.8 ± 1.0	0.62 ± 0.08
	Left	60.5 ± 2.0	99.7 ± 1.3	39.0 ± 2.6	0.59 ± 0.01
NGF & NT-3 Functionalized SF	Right	64.2 ± 1.5	94.7 ± 0.7	30.7 ± 0.8	0.60 ± 0.07
	Left	49.8 ± 2.7	89.2 ± 0.6	39.8 ± 1.5	0.61 ± 0.05

Considering the hip angle measurements of each experimental group (Table 3.2), the NGF and NT-3 functionalized SF group portrayed the most similar angle pattern to the control. The injured limb presents a hip angle pattern almost identical to the control. The left limb exhibits a very similar pattern as well, but is shifted down slightly which may have been due to a slight misplacement of the reflective marker. The NGF and CNTF functionalized SF group also presents a very similar hip angle pattern of the injured limb compared to the control, however the curve does not exhibit the prominent initial peak; there appears to by two peaks before the final downward slope. The left limb displays a more natural movement compared to the control, in parallel with the control hip angle pattern throughout the step. The non-functionalized SF group presents a similar curve morphology to the control, but shows a much more extreme range of motion as the step begins and ends at a tighter angle and peaks at a larger angle than the control. In addition, there appears to be a small second peak shortly after the initial peak that is not present in the control. The left limb hip angle pattern is almost identical to that of the left limb from the NGF and CNTF functionalized SF group. Finally, the cut and suture group's right hip pattern exhibits an initial peak similar to that of the control, but is then followed by a second smaller peak during the downward slope. The left limb presents a very similar hip angle pattern to the control, but with the initial peak slightly earlier than that of the control.

Table 3.3. Average measurements of knee angle patterns during a walking cycle.

Knee Angles

Group	Limb	Minimum Angle (deg)	1st Peak Maximum Angle (deg)	1st Peak Amplitude (deg)	2nd Peak Maximum Angle (deg)	2nd Peak Amplitude (deg)	Duration (s)
Control	Right	49.1 ± 1.9	100.6 ± 2.1	51.9 ± 2.7	115.0 ± 2.7	66.3 ± 2.3	0.61 ± 0.06
	Left	35.0 ± 1.4	109.2 ± 1.6	74.4 ± 1.8	120.6 ± 3.2	85.9 ± 4.1	0.62 ± 0.06
Cut & Suture	Right	69.2 ± 4.9	91.2 ± 3.3	24.3	111.5 ± 1.8	43.6	0.92
	Left	54.0 ± 5.5	100.3 ± 1.0	47.4	98.9 ± 2.0	43.4	0.84
Non-functionalized SF	Right	74.1 ± 6.9	129.0 ± 2.1	57.8 ± 3.6	102.2 ± 2.0	31.1 ± 2.5	0.40 ± 0.02
	Left	39.1 ± 1.9	99.1 ± 1.4	59.3 ± 0.12	98.4 ± 5.6	56.8 ± 4.0	0.60 ± 0.04
NGF & CNTF Functionalized SF	Right	27.2 ± 7.4	106.0 ± 3.5	81.3 ± 4.2	121.9 ± 1.7	96.4 ± 6.0	0.59 ± 0.02
	Left	49.9 ± 5.0	106.3 ± 1.1	56.9 ± 2.1	114.9 ± 1.1	65.1 ± 4.0	0.60 ± 0.04
NGF & NT-3 Functionalized SF	Right	48.7 ± 3.9	80.6 ± 3.5	30.0 ± 2.6	106.4 ± 4.4	59.2 ± 4.1	0.58 ± 0.08
	Left	23.8 ± 2.3	80.1 ± 2.5	56.5 ± 2.6	90.4 ± 3.0	66.8 ± 4.2	0.60 ± 0.05

In regards to the knee angle patterns (Table 3.3), the NGF and CNTF functionalized SF group exhibited a pattern almost identical to that of the control for both the right limb and the left limb. The right knee however, presents a slightly smaller angle at the beginning and the end of the step and a slightly larger angle at both peaks. The NGF and NT-3 functionalized SF group's right knee also follows a similar pattern to the control, however the first angle peak is not at large as presented by the control. The left knee angle pattern's morphology is almost identical to the control, but with proportionally lower angles which could be due to a slight misplacement of the reflective marker. The cut and suture group presents a similar overall morphology to the control, but exhibits a less prominent initial peak and a more exaggerated second peak in the knee angles of the right limb. The right knee does not display as large of a range of motion as the control as it does not reach as tight angles in the beginning or end of the step. The left knee angle pattern is very similar to the control, but exhibits a smaller second peak toward the end of the step. Finally, the non-functionalized SF group's right limb presents the least similar knee angle pattern morphology compared to the control. Two peak are demonstrated during the step, however the low and high peak are both elongated. The smallest angle attained during the step is also between

the two peaks instead of at the beginning and end of the step. The left knee angle pattern, however, is almost identical to the control.

Table 3.4. Average measurements of ankle angle patterns during a walking cycle.

Ankle Angles

Group	Limb	1st Min. Angle (deg)	1st Peak Max. Angle (deg)	1st Peak Amp. (deg)	2nd Peak Amp. (deg)	2nd Peak Max. Angle (deg)	2nd Peak Amp. (deg)	Duration (s)
Control	Right	86.6 ± 1.0	130.7 ± 1.6	44.0 ± 1.1	84.2 ± 2.3	135.7 ± 0.7	51.3 ± 1.2	0.64 ± 0.06
	Left	74.6 ± 1.6	139.3 ± 2.8	64.0 ± 1.4	91.9 ± 2.7	137.3 ± 1.1	46.0 ± 1.9	0.62 ± 0.06
Cut & Suture	Right	41.2 ± 9.1	156.3 ± 6.0	114.5 ± 0.3	76.7 ± 5.6	77.4 ± 1.1	0	0.83 ± 0.02
	Left	87.5 ± 6.6	147.7 ± 1.8	62.5 ± 1.5	89.7 ± 7.2	126.2 ± 0.4	34.8 ± 2.4	0.87 ± 0.04
Non-functionalized SF	Right	103.3 ± 2.6	173.9 ± 2.8	72.7 ± 2.5	-	-	-	0.40 ± 0.4
	Left	95.4 ± 1.2	164.7 ± 1.4	68.9 ± 1.3	114.8 ± 11.6	135.8 ± 6.7	21.1 ± 13.2	0.40 ± 0.2
NGF & CNTF Functionalized SF	Right	35.5 ± 5.2	135.4 ± 8.7	97.2 ± 2.9	99.9	109.3	-	0.59 ± 0.02
	Left	87.7 ± 5.7	146.2 ± 3.5	79.0 ± 7.3	64.5 ± 9.5	136.9 ± 1.3	69.3 ± 6.0	0.60 ± 0.03
NGF & NT-3 Functionalized SF	Right	84.- ± 6.4	136.7 ± 1.4	52.6 ± 5.6	84.9 ± 10.5	94.6 ± 6.9	11.5 ± 4.2	0.58 ± 0.08
	Left	82.2 ± 2.4	148.8 ± 3.8	68.1 ± 4.1	84.7 ± 15.9	133.4 ± 4.6	48.7 ± 13.2	0.60 ± 0.05

Finally, ankle angle patterns were measured and evaluated (Table 3.4). Both the NGF and CNTF functionalized SF and NGF and NT-3 functionalized SF groups' right limbs presented a similar curve morphology to the control exhibiting a large rounded peak followed by a quick second peak. The NGF and NT-3 functionalized SF group's ankle angle pattern follows that of the control very closely until reaching the second peak, which is much weak than that of the control. The left ankle presents a similar pattern to the control but taking more time during the first peak in proportion to the second peak. The NGF and CNTF functionalized SF group's right ankle angle pattern, while presenting a similar curve morphology, is slightly distorted compared to the control. The ankle exhibits tighter angles at the beginning and end and only a small second peak. In addition, the first peak is much less gradual and rounded than the control, exhibiting a sharper inclines and declines with a plateau at the maximum angle in the place of a smoothly rounded peak. The left ankle, however, presents an ankle angle pattern almost identical to that of the control. The cut and suture group's right ankle presents an initial gradual peak similar to the control, but displays

only a very minor second peak thereafter. The first peak is also more exaggerated than that of the control beginning with a tighter angle around 50 degrees and obtaining a maximum angle at about 155 degrees whereas the first peak of the control curve remains between 80 degrees and 130 degrees. The second peak of the experimental right ankle angle pattern is very slight and appears to be more representative of a plateau than a second peak. The left ankle presents a similar pattern to the control but taking more time during the first peak in proportion to the second peak similar to the left ankle angle pattern of the NGF and NT-3 functionalized SF group. Finally, the non-functionalized SF group's right ankle angle pattern is very dissimilar to that of the control. Only one peak can be observed in this angle pattern with no trace of a second minor peak thereafter. This suggests that the animal does not have any or enough strength in the foot in order to independently perform dorsiflexion. This is supported by the extent to which the ankle is dropped during the step, as represented by the larger angles reached during the motion. The right ankle reaches a maximum angle of about 175 degrees while the initial and second control peaks reach a maximum angles of about 130 degrees and 135 degrees respectively. The left ankle presents a similar pattern morphology to the control, exhibiting two distinguishable peaks, but with larger angles reached during the first peak. This distortion of the uninjured ankle angle pattern may be due to the adapted movement developed by the animal in order to compensate for the lack of strength in the injured leg.

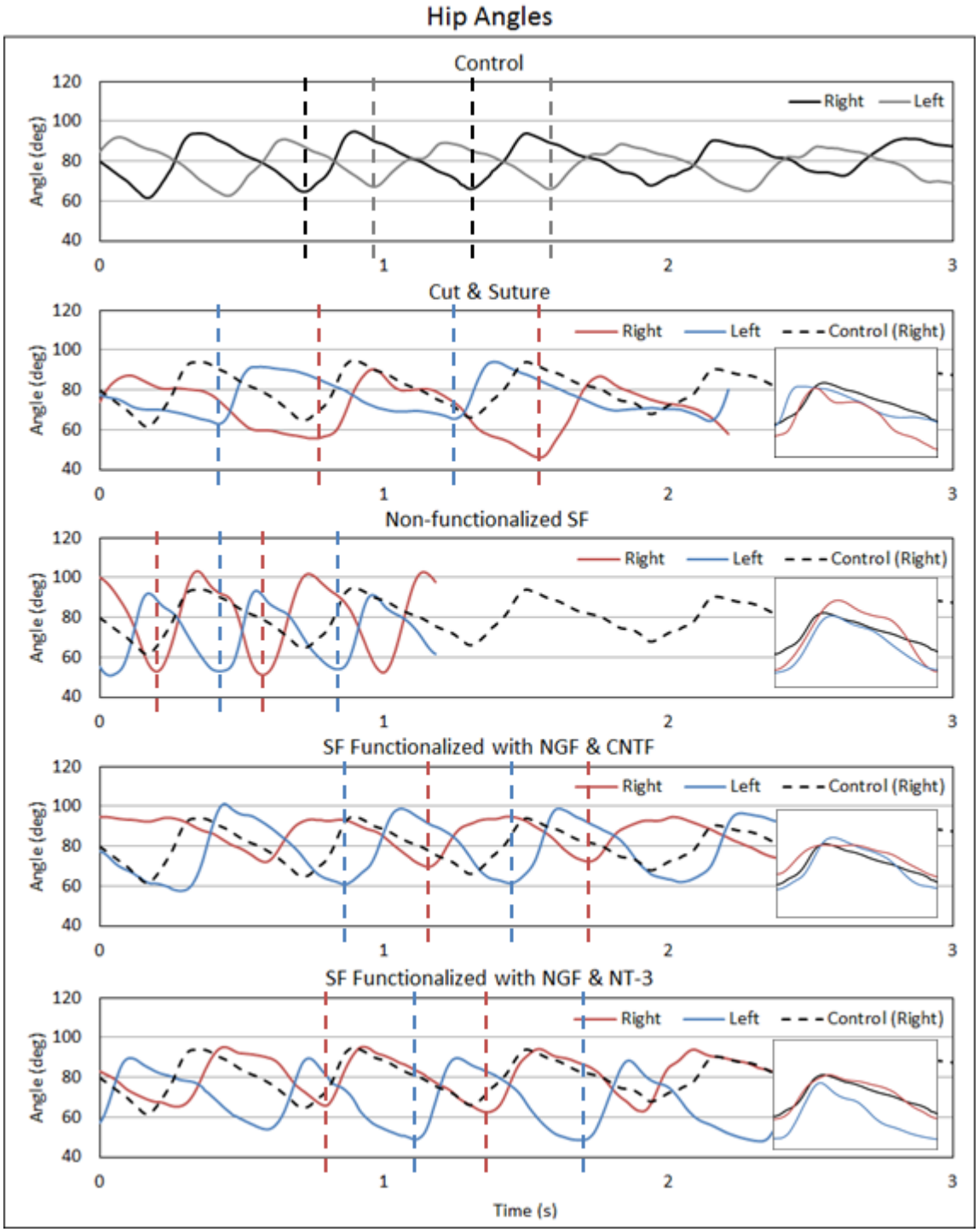

Figure 3.15. Hip angle patterns during a walking cycle of left and right limbs for animals in each experimental group after 6 months in vivo in comparison with the control. Normalized step patterns are depicted in the box to the right of each graph.

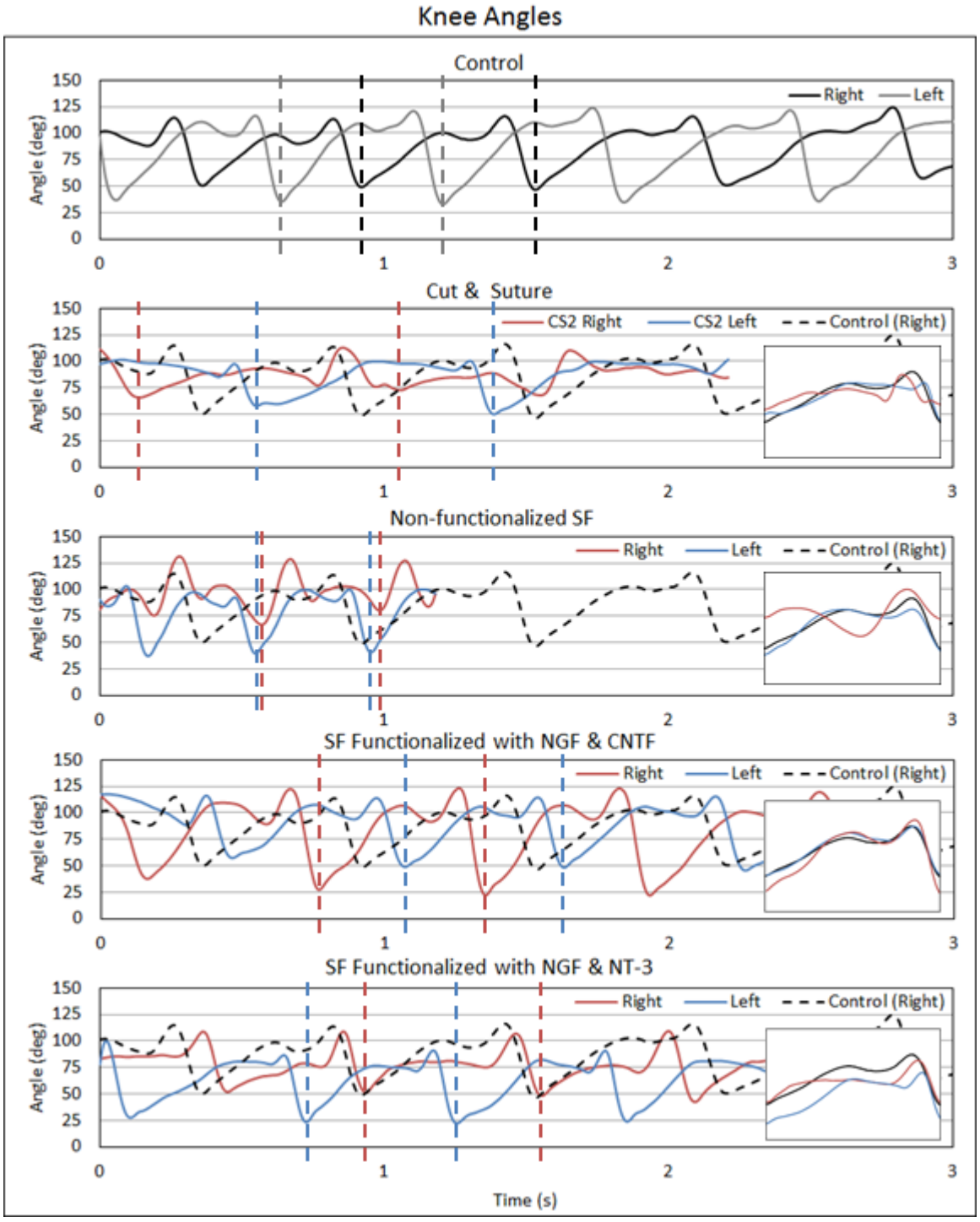

Figure 3.16. Knee angle patterns during a walking cycle of left and right limbs for animals in each experimental group after 6 months in vivo in comparison with the control. Normalized step patterns are depicted in the box to the right of each graph.

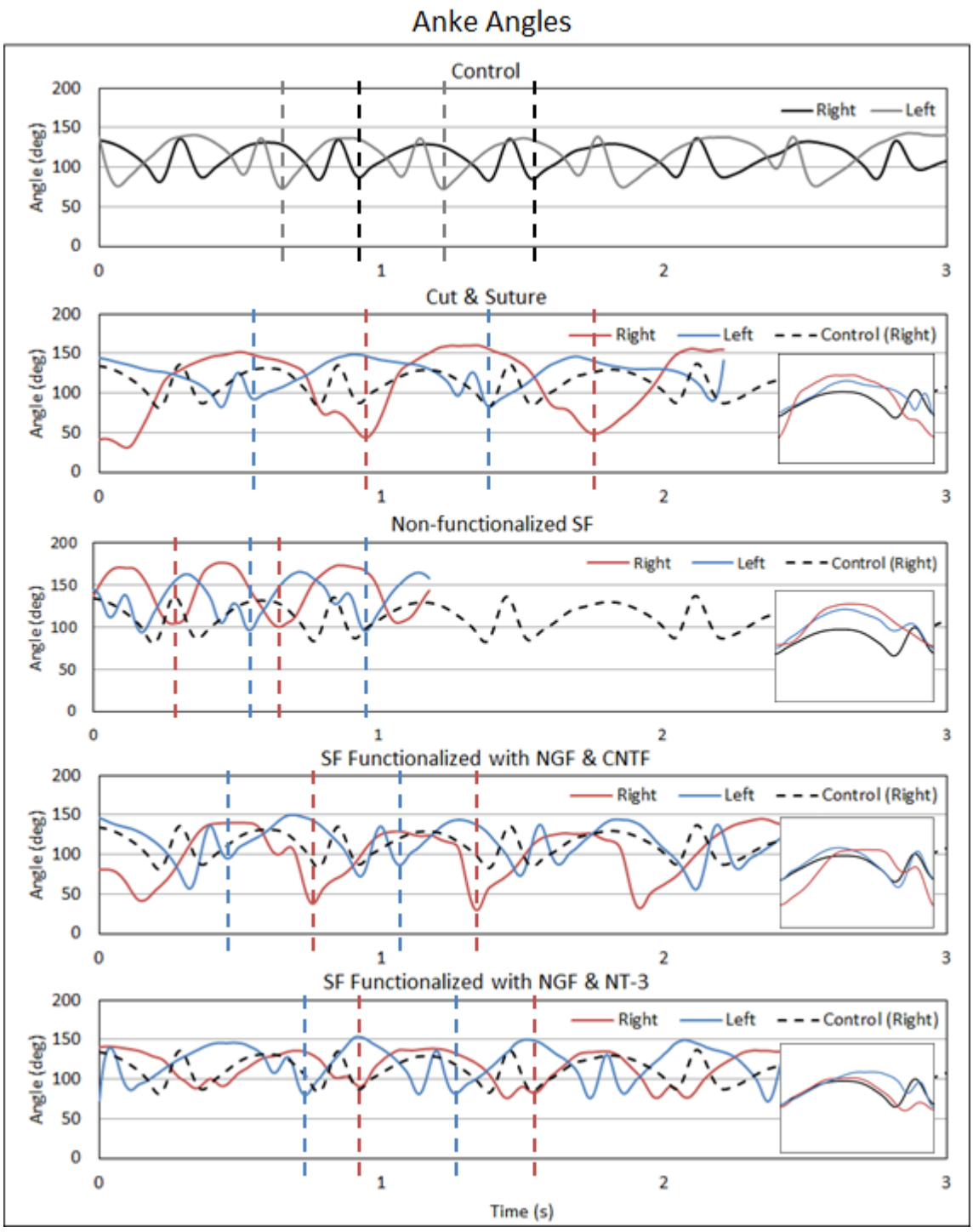

Figure 3.17. Ankle angle patterns during a walking cycle of left and right limbs for animals in each experimental group after 6 months in vivo in comparison with the control. Normalized step patterns are depicted in the box to the right of each graph.

Chapter 4

Discussion

Part 1

Currently, the only nerve guides from biomaterials found on the market are hollow tubular NGCs such as Neuroflex or NEuraGen. Creating a NGC that mimics the morphology of an organic nerve was the first priority of this newly developed device. The nerve autograft has been considered the gold standard for nerve repair for over 30 years and continues to be the preferred method for large nerve gaps despite the 50% successful functional recover rate (Lee and Wolf, 2000). There are therefore numerous advantages to the nerve autograft that have not yet been reproduced in a bioengineered NGC. One of these advantages includes the multi-channeled architecture naturally constructed by the endoneurium. Regenerating nerve fibers are easily guided through these individualized channels and not lose their path toward their innovation targets. With hollow NGCs, nerve fibers may be much more likely to change their initial paths and reinnervation success may be much lower. Therefore, a multi-channeled conduit may be a more advantageous structure for nerve regeneration than a hollow tube.

Emphasis is given on the guidance properties of a NGC as misdirected nerve fibers will not yield satisfactory functional recovery. Axonal projections of peripheral neurons may, in the best case of misguided regeneration, reinnervate incorrect tissue similar to its original post synaptic target causing the need for re-education therapy in order for the brain to recognize and process new input from incorrectly reinnervated tissue (Payne, 2001). In less fortuitous cases, axonal projections are misguided to inappropriate organs which are unable to support synaptic connection, and programmed cell death will occur (Oppenheim and Milligan, 2009). Therefore, in addition to the multi-channeled architecture of this developed device for axonal guidance, the material was based on aligned nanofibers. Aligned nanofibers at the size produced in this study have been shown in the literature to promote the good cell adhesion and alignment of neuronal extensions (Dinis et al., 2014a; Qu et al., 2013).

Purely aligned fibers however lack certain mechanical properties found in randomly deposited nanofibers such as plasticity and resistance to tearing. Purely aligned fiber-base materials were shown to be more brittle under tensile strength than randomly deposited fiber-based materials. In application, purely aligned fiber-based materials could not easily withstand the punctures from a suture needle. If the material is unsuturable, then it is useless for

implantation. To overcome this obstacle, a tri-layered material containing aligned fibers on each surface and randomly deposited fibers in the center layer was developed. This complex material design provided improved resistance to tearing along with increasing the plasticity without compromising greatly the ultimate tensile strength of the material. In this way, the device becomes easily suturable without compromising the guidance component from the alignment of the nanofibers.

A concern brought to light during the application of this new multi-channeled conduit based on a tri-layered fiber material was the difficulty to delicately position the edge of the material to the edge of each severed nerve segment. In fact, as the outer layer of the conduit was sutured to the epineurium, the surgeon was unable to avoid the blunt edge of the NGC to crush the protruding nerve fascicles on each end. This must be avoided as the deformation of the proximal and distal nerve fascicles may cause severe axonal misdirection. This particular drawback of a multi-channeled conduit, as the microchannel walls create a blunt edge on either side of the conduit, is constantly overlooked in the literature (e.g. Yoa et al., 2010, Bender et al., 2004, and Dinis et al., 2015) but was addressed in this work with the addition of an outer layer, or a jacket layer, of the nanofiber material. This jacket layer continued 1 mm longer on each end of the conduit which allowed sufficient working space for epineurial suture without putting pressure on the nerve fascicles. The jacket layer also improved the ease of the suturing process as each nerve segment could be gently placed inside the pocket created by the jacket layer on the ends of the NGC and readily positioned in order to assure the alignment of the corresponding proximal and distal nerve fascicles.

The material chosen for this device was the natural polymer silk fibroin. Silk fibroin (SF) is biocompatible polymer naturally produced in the cocoons of the *Bombyx mori* silkworm and is known for its robust mechanical properties. SF is easily extracted from the cocoons and solubilized into a solution readily electrospun into nano-scale fibers. SF is also an advantageous biomaterial because it slowly degrades in vivo allowing nerve repair through the conduit before the deterioration of the NGC structure can occur (Yang et al., 2009). Finally, SF is easily functionalizable by large or small molecules in order to improve the performance of the material to further promote successful axonal regeneration.

Part 2

As previously discussed in this work, silk fibroin was chosen for this study because of its many advantageous properties for a biomaterial; it is easily cultivated from the cocoons naturally produced by the *Bombys mori* silk worm, it is has robust mechanical properties for a natural polymer, it can be readily chemically modified in order to fabricate many types of materials (gels, films, fibers, sponges, microspheres, etc.), it has already been approved by the FDA in the form of surgical sutures, and it is easily functionalized by numerous types of substances. In Part 2 of this work, the functionalization of the SF fibers utilized in Part 1 was explored in anticipation of further development of a complex nerve guidance conduit as presented in Part 1.

The environment surrounding a lacerated nerve constitutes many complex mechanisms essential for successful nerve regeneration. Therefore, complexifying the material used in NGCs is necessary in order to obtain functional recovery comparable to that achieved by nerve autografts. Nerve autografts have the advantage that the tissue is autologous nervous tissue, prepared to host regenerating axons in a more organic environment. In order to reach or exceed the efficacy of the naturally favorable environment found in autografts, the NGC material must provide similar support to regenerating neurons, stimulating guided and rapid axonal extension and eventual reinnervation of target organs. Functionalizing the SF material may allow us to reach this goal as several types of molecules or particles together can create a complex and more favorable environment provided by the NGC that stimulates efficient nerve regeneration in either an artificial or organic manner.

Silk and Growth Factors

Materials functionalized with growth factors for peripheral nerve regeneration have long been studied as the significance of these neurotrophic molecules has continues to be established by ongoing research. Several growth factors including nerve growth factor have been extensively studied and understood to play a crucial role in the regeneration of nervous tissue. Therefore, the functionalization by a combination of growth factors believed to promote improved nerve regeneration in the developed SF fiber material was first explored.

Nerve growth factor (NGF), neurotrophin-3 (NT-3), and ciliary neurotrophic factor (CNTF) were chosen for this study for their diverse functions in nerve regeneration. NGF is a signaling molecule that promotes axonal extension of sensory neurons and signals the migration of proliferating Schwann cells (Sofroniew et al., 2001; Madduri et al, 2010; Braun et al., 1996). The presence of NT-3 has been shown to improve the restoration of conduction speed of axons and increase myelination by Schwann cells. NT-3 has been demonstrated to stimulate axonal regeneration in both motor and sensory neurons (Sterne et al., 1997; Tonda-Turo et al., 2017). CNTF is a growth factor known to support conduction restoration and increased myelination specifically for motor neurons (Zhang et al., 2004; Dinis et al., 5015).

First and foremost, the guidance properties of aligned SF fibers were tested using DRG and isolated primary sensory neuron cultures. Indeed, the neurons were found to favor the SF fibers as they readily adhered to the fibers and extended neurites along the length of the SF fibers. Neurons cultured on randomly deposited SF fibers consequently revealed a randomized network of neurites.

Next, SF fibers were functionalized with growth factors mentioned previously. A previous study by Dinis et al. (2014a), revealed that growth factors incorporated into the SF fibers were not released, but secured within the stable nanofibers. While the growth factors are within the fibers, it was shown that they are still accessible to the neurons; functionalized SF fiber samples continued to promote neuron viability and the extension of neurites in a growth factor-deprived culture environment while non-functionalized SF fibers could not continue to sustain neuron viability in the same environment. This suggests that the impregnated growth factors are still able to stimulate neuron survival and growth. It has also been suggested in the literature that growth factors released into the environment are less efficiently exploited by regenerating neurons which supports the argument for functionalization thusly (Esaki et al., 2011).

The three functionalized SF fiber group samples therefore exhibited promising results in an unfavorable environment for neuron survival and growth. Sensory neurons are unipolar neurons and therefore extend two cell processes. Uniquely the longest processes of the sensory neurons in culture were measured in length. SF fibers bi-functionalized with NGF and CNTF presented samples with the overall smallest principle neurite lengths. SF fibers functionalized

with NGF presented samples with an average principle neurite length 67% longer than that of the NGF and CNTF functionalized SF fibers. Finally, SF fibers bi-functionalized with NGF and NT-3 promoted on average the longest principle neurite outgrowth; the average neurite length from neurons cultured on NGF and NT-3 functionalized SF fibers was 178% larger than that of the NGF functionalized SF fiber samples and 296% larger than that of the NGF and CNTF SF fiber samples.

The difference seen in growth tendencies of the cultured sensory neurons in identical environments suggests that the different fiber functionalization indeed affected the material-cell interaction. Fibers functionalized with both NGF and CNTF may have shown the least optimal neuron growth due to the fact that CNTF is specific to motor neurons and does not promote sensory neuronal growth. As NGF and CNTF are positioned within the fibers, it is possible that less NGF was available to the neurons than in the material functionalized solely with NGF. However, CNTF is not likely inhibiting the interaction between NGF and the TrkA receptor, as CNTF has affinity specifically to its corresponding receptor, CNTFα. NGF and NT-3 functionalized SF yielded the most favorable results compared to the two other functionalized materials which is unsurprising as both NGF and NT-3 are known to promote improved growth in sensory neurons. In addition, both NGF and NT-3, despite both proteins being classifying in the same neurotrophin family, have affinity for different receptors, and complement each other by stimulating different mechanisms for improved neuronal regeneration. These results are demonstrative of the different responses by regenerating sensory neurons to different growth factorsembedded in SF, but does not tell the whole story and are not completely dependable to predict the more effective material for clinical application. A very obvious constraint to this study is the lack of cultured motor neurons in parallel to cultured sensory neurons. As CNTF is a growth factor specific to signaling improved regeneration of motor neurons, the relative efficacy of a bi-functionalized material containing both a sensory neuron-specific growth factor (NGF) and a motor neuron-specific growth factor (CNTF) cannot be deduced from a neuron cell culture exclusive to sensory neurons.

Neurite-fiber interaction is important particularly at the early stages of axonal sprouting after implantation of an NGC as there is not yet the presence of glial cells to help guide the regenerating axons toward a post synaptic target. The alignment of the fibers in addition to the

functionalization of the material is crucial in particular at this early timeframe. However, the material should also aim to attract the migration of proliferating Schwann cells as quickly as possible in order to fill the NGC with naturally signaling glial cells that will create clear paths for the regenerating axons.

In order to evaluate the behavior of Schwann cells on this developed material, SF fibers functionalized with NGF were utilized. NGF was chosen for this study since it the growth factor chosen for this studied that has been shown to encourage the migration of Schwann cells. First of all, Schwann cells were cultured on the aligned NGF functionalized SF fibers for two days and the morphology of the Schwann cells on these samples were compared with the morphology of Schwann cells cultured on randomly deposited NGF functionalized SF fibers. The difference in Schwann cell positioning and morphology was clear, as cells on aligned fibers oriented themselves along the fiber alignment and the cell bodies were strength along the length of the fiber making connections with neighboring cells on the same fiber. Next, an evaluation of the Schwann cells' migration tendencies on the functionalized aligned SF fibers showed that Schwann cells traveled along the length of the fiber at an average speed of 11.9 nm/s. Extrapolating these results, this suggests that Schwann cells may achieve migration through a 5 mm NGC after about 5 days.

Silk and Fibronectin

In addition to the functionalization of the SF material with growth factors, it is also possible to incorporate other polymers. The integration of a second polymer into the SF fibers would allow an advantageous combination of the favorable properties of SF plus the favorable properties of the new polymer which may compliment any shortcomings of the SF alone ultimately improving support for nerve regeneration.

In this study, fibronectin (FN) was chosen as a candidate for SF fiber functionalization. FN is naturally produced in neural tissue, being a component of the peripheral nerve extracellular matrix and would therefore help mimic a natural environment for nerve regeneration. FN plays an integral role during early nerve development in which it aids in the migration and differentiation of neural crest cells for successful neural development (de Luca et al., 2014). In mature nervous systems, FN is understood to be involved in healthy neuronal support and nerve

regeneration (Mukhatyar et al., 2011; de Almeida et al., 2016). Specifically, fibronectin has been found to encourage Schwann cell migration after nerve injury and to improve neurite extension during axonal regeneration (Gonzalez-Perez et al., 2013; Tonge at el., 2012).

The development of a protocol for electrospinning SF/FN successfully was developed in this study. After adding a FN concentration of 0.01 ng/mL to the spinning standard SF spinning solution, the correct parameters were established for nanofiber production. Two main uncertainties for the incorporation of FN into the SF fibers included (1) the possibility of the FN to not be homogeneously dispersed throughout the SF fibers due to the low concentration of the FN added to the SF solution and (2) the possibility that the FN would not be secured within the SF fibers permitting any FN to be washed away after water annealing and rinsing of the material.

The success of the resulting SF/FN fiber-based material was therefore evaluated by the use of fluorescence microscopy. FN was tagged by either Alexa Fluor 488 or 568 fluorochromes before the inclusion of FN into the SF spinning solution. After electrospinning a sample layer of SF/FN488 or SF/FN568 fiber on a piece of aluminum foil, the material was water vapor annealed in order to induce β-sheet formation of the SF rendering the polymer insoluble. The material was thoroughly rinsed and subsequently visualized for the presence of FN. The results show that the FN was indeed incorporating into the SF fibers, and found to be homogeneously integrated throughout the fibers as desired. Therefore, the low concentration of FN did not restrict the even distribution of the polymer, and the FN was found to be secured in the SF fibers even after thorough rinsing of the material.

The material was tested in vitro with primary rat sensory neurons in a 2 day culture and a 7-day PC12 cell culture in order to confirm good cell adhesion and guidance of the neurites. Both sensory neurons and differentiated PC12 cells were found to have neurites following very closely to the SF/FN fibers. Even on a randomly deposited fiber material sample, neurites from the differentiated cell are found to extend sprouts that take sharp turns in order to continue along the paths of crisscrossing fibers. Therefore, a SF/FN composite material nanofiber was successfully developed for potential use as a base material in nerve regeneration; further functionalization by growth factors or other substances may be explored for further enhancement of material properties.

Silk and Nanoparticles

Nanoparticles are becoming more and more researched in the field of bioengineering because of the many different unique functions they provide such as the delivery of medicine in the body, diagnostic potential for the detection of cell abnormalities, the creation of an efficiently enhanced catalytic environment, and much more. In addition, at the nanoscale, materials have been found to possess different physical and chemical properties compared to the same material at a larger scale because of the drastic increase of the surface area to volume ratio; differences in particle size at the nanoscale may also lead to the modification of certain properties exhibited by specific materials.

With the following goals in mind, functionalization with gold nanoparticles and iron oxide nanoparticles were explored. Gold nanoparticles were chosen because of the electrically conductive properties they possess as SF is an insulating material possessing virtually no electrical conductive capabilities and recent research on the addition of electrical stimulation during nerve regeneration has demonstrated an improvement to the efficacy of nerve regeneration (Haastert-Talini and Grothe, 2013; Zhang et al., 2013; Elzinga et al., 2015; Willand et al., 2015; Gordon, 2016). Studies that show promising results for improved nerve repair include an application of brief low-frequency electrical stimulation of the nerve at a point proximal to the injury (Willand et al., 2016, Haastert-Talini and Grothe, 2013; Elzinqa et al., 2015). Results from such methods include an acceleration of tissue regeneration (Haastert-Talini and Grothe, 2013), improved nerve conduction (Zhang et al., 2013), increased thickness of myelin sheaths (Zhand et al., 2013), an increase in the proliferation and expression of growth factors from Schwann cells distal to the injury site (Haastert-Talini and Grothe, 2013; Willand et al., 2016; Gordon, 2016), accelerated sensory and motor axon outgrowth (Elzinga et al., 2015; Willand et al., 2016), and an improvement of motor functional recovery (Haastert-Talini and Grothe, 2013; Willand et al., 2016). Although improved motor recovery after the application of electrical stimulation has been demonstrated, there has not been evidence of an improvement to the number of misguided axons of motor neurons innervating the wrong muscles (Haastert-Talini and Grothe, 2013; Willand et al., 2016).

The use of gold nanoparticles for electrical stimulation in nerve regeneration applications has not been extensively developed. Park et al. showed however that a gold nanoparticle-coated surface promotes neurite outgrowth in vitro when electrical stimulation is carried out in similar patterns to those used in successful clinical studies (Park et al., 2009). Gold nanoparticles were successfully incorporated into the SF nanofibers developed in this study and shown to be homogenously distributed throughout the fibers without drastically changing the size of the produced fibers. First of all, as expected, this composite material's biocompatibility was supported by L929 cell morphology and MTS assay results showing virtually 100% cell viability and metabolic activity while presenting a proliferation index similar to the control. In addition, there were no apparent changes in the morphology of Schwann cells compared to non-functionalized SF fibers or SF fibers functionalized with growth factors.

As future prospects for this study, the concentration of gold nanoparticles should be adjusted in order to find the optimal distribution of gold nanoparticles in order to create a continuous electric current throughout the length of the SF fiber. In vitro tested using brief low-frequency electrical stimulation will be the next step of this study in order to verify the effectiveness of an electrically stimulated, gold nanoparticle/SF composite aligned nanofiber material. Other functionalization methods may also be incorporated into the material as previously described for a more complex and multi-functional system. In addition, gold nanoparticles may themselves be functionalized with growth factors or relevant molecules by coating the nanoparticles. The gold nanoparticles used in this study were fabricated with the capability of incorporating a biomolecule coating (Aufaure et al., 2014)

In parallel, iron oxide nanoparticles were chosen because of the magnetic properties that they possess. In addition to electrical stimulation, magnetic stimulation has also been demonstrated as a successful technique to improve nerve regeneration (Pal et al., 2013; Gunay and Mert, 2010). Therefore, functionalized SF fibers with superparamagnetic iron oxide nanoparticles were explored in order to create a biomaterial capable of stimulating nerve regeneration utilizing magnetic stimulation.

SF fibers were successfully impregnated by iron oxide nanoparticles and the nanoparticles were homogeneously dispersed throughout the SF fibers as visualized with SEM, TEM, and STEM.

Electrospinning of IONP functionalized SF yielded fibers very similar in diameter to non-functionalized SF fibers. Similar preliminary in vitro results for IONP functionalized SF fiber samples compared with GNP functionalized SF fiber sample were obtained; the SF/IONP material's biocompatibility was indeed supported by L929 cell morphology and MTS assay results showing virtually 100% cell viability and metabolic activity while presenting a proliferation index similar to the control. No apparent changes in the morphology of Schwann cells compared to non-functionalized SF fibers were observed.

Future prospects for this study are testing this material in vitro for neurite outgrowth with the stimulation using an applied magnetic field. An application of a pulsed magnetic field would be the preferred method as it has been previously found to promote nerve regeneration in the central and peripheral nervous systems (Gunay and Mert, 2012; Zhivolupov et al., 2012). In addition to the application of magnetic field stimulation, and as explained for gold nanoparticles, SF fibers or the IONPs themselves may be functionalized also with growth factors or relevant molecules by methods previously described in this study or by coating the nanoparticles. The IONPs used in this study were fabricated with the capability of incorporating a biomolecule coating (Demey-Drouhard et al., 2013).

Part 3

The NGCs used in this in vivo study based on the developed device design from part 1 were functionalized with either a combination of NGF and CNTF or a combination of NGF and NT-3. Non-functionalized NGCs were also fabricated for this study and a cut and suture procedure was carried out in order to mimic the results from an autograft procedure. Three analyses techniques were utilized in this study in order to evaluate the success of nerve regeneration from each experimental group. Many studies focus on histological analysis to determine the effectiveness of nerve regeneration, but functional recovery cannot be well understood without considering the many other factors of nerve repair. Therefore, electromyography and motion capture was used in this study in order to paint a clearer picture of the efficacy of nerve repair for each experimental group.

Three separate staining methods (hematoxylin and eosin stain (HE), cholinesterase (CE) activity stain, and immunostaining for nuclei, axons, and myelin sheaths) were carried out on sections of a distal portion of the regenerated nerve. Using the three staining methods together, we observed that all samples after 8 months in vivo presented many regenerated axons that passed through the distal portion of the nerve.

HE stained sections did not reveal significant differences from the experimental groups compared to the control, however the cut and suture sample appeared the most similar to the control section. A clear increase in the quantity of regenerated axons and myelination after 8 months compared to 4 months for all samples (sample for the non-functionalized SF not available) was observed.

The CE activity stains after 4 and 8 months in vivo was very telling, and there was a drastic change in the results obtained from after 4 months compared with after 8 months in vivo. Few motor neurons are observed in the 4 month samples of the cut and suture group, the non-functionalized group, and the NGF and CNTF functionalized SF group, while no stained motor neurons were observed from the NGF and NT-3 functionalized SF group sample. However, after 8 months in vivo, all experimental groups, except for the non-functionalized SF group, presented a good presence of motor neurons regenerated through the distal portion of the nerve. The non-functionalized SF group demonstrated a small regenerated population of motor neurons

compared to the other experimentation groups. In addition, the motor neurons were very well dispersed presenting no apparent organization or bundling of motor neurons which is naturally found in healthy nerves since the sciatic nerve will branch off into other smaller nerves eventually containing only sensory or only motor axons. This result suggests a low efficiency of regenerated motor neurons in the non-functionalized SF group with a high level of misdirected axons. However, as the CE activity stain only demonstrates motor neuron regeneration, it is difficult to understand the sensory regeneration success. We can use the non-differentiating immunostain as a reference as we can observe that there are regenerated axons filling the nerve fascicles which suggests that most unstained area found in the CE activity stain represents area occupied by sensory neurons.

From the results obtained from the immunostained sample sections, we can observe a dense population of axons in each sample after 8 months in vivo. Comparing the results after 4 months and after 8 months in vivo, an increase in the diameter of most axons can be observed for all samples. Unsurprisingly, the non-functionalized SF group sample presents the least advanced regeneration both after 4 months and after 8 months. Diameters of the axons found in the 8 month sample are, on average, much lower than those found in all other samples suggesting that the functionalization of the material made an important difference in axon regeneration. Cut and suture presented better results than all other samples after 4 months in vivo. This could be due to the fact that the axons from the cut and sutured nerve had much less distance to travel since a 5 mm NGC wan not put in place in between the two severed nerve segment. This may also be due to the axons benefiting from the direct suture to the distal nerve segment which presents an organic, regeneration-encouraging environment with all neurotrophic factors naturally found in spontaneous regeneration.

Results from the myelin sheath immunostain were consistent with those found from other histochemical stains. A drastic improvement of myelination was observed from samples after 8 months compared to samples after 4 months. Again, the cut and suture group sample presented better results after 4 months than all other group samples and the non-functionalized SF group sample produced the weakest myelination after 4 months compared to the functionalized SF group samples. Myelination thickness results were consistent with results obtained for the

average diameters of the nerve fibers after 8 months in vivo, which is expected since myelination is normally proportional to axon diameter. Non-functionalized SF group samples were found to have the lowest average myelin sheath thickness, followed by the NGF and CNTF functionalized SF group sample. The NGF and NT-3 functionalized SF group sample presented myelin sheaths that were, on average, thicker than those found in both other NGC experimental samples.

Combining the results from all three staining methods, the cut and suture group appeared to have the best nerve regeneration success, approaching the results taken from the control samples. In addition, the cut and suture group showed accelerated neurite outgrowth and myelination compared to the other experimental groups. The non-functionalized SF group appeared to have the weakest nerve regeneration both in the short term (after 4 months in vivo) and in the long term (after 8 months in vivo) compared to all experimental groups. The functionalized SF groups both had good nerve regeneration, but differed in certain aspects. For example, results from immunostained samples show that the NGF and NT-3 functionalized SF group produced larger axon diameters and thicker myelin sheaths after 8 months in vivo compared to those of the NGF and CNTF functionalized SF group. CE activity stained samples show that both functionalized SF group samples had, qualitatively, a good regeneration of motor neurons with an apparent organization of stained axons similar to the control and the control from the literature. Also, HE stained samples show similar nerve regeneration. If only histochemical analyses were considered, the conclusion from this study may be that the cut and suture group had the most successful nerve regeneration, followed by the NGF and NT-3 functionalized SF group, following closely by the NGF and CNTF functionalized SF group, followed by the non-functionalized SF group displayed weak nerve regeneration.

EMG tests of the gastrocnemius muscle of the animals after 8 months in vivo was carried out. The results obtained by these tests demonstrated that the cut and suture group had the most muscle response regeneration compared to the other experimental groups. This group appeared to regain about 85% of the muscle response of an uninjured gastrocnemius muscle. This group also reached a reference of 20% of full muscle response (from control) at a lower stimulation intensity than that of the other experimental groups. The group with the second best muscle response recovery was not the NGF and NT-3 functionalized SF group however, but the NGF and

CNTF functionalized SF group. The NGF and CNTF functionalized SF group exhibited a muscle response recovery of about 80% and reached 20% at a slightly higher stimulation intensity that of the cut and suture group. Therefore, muscle recovery of these two experimental groups presented very similar levels of motor neuron regeneration/reinnervation. The NGF and NT-3 functionalized SF group reached about 85% muscle response, but at about 430% the stimulation intensity of that needed for the cut and suture group. Similarly, the non-functionalized SF group was able to reach about 80% muscle response recovery, but at a similar stimulation intensity to that of the NGF and NT-3 functionalized SF group. These two groups show drastically different results for muscle response sensitivity however; the NGF and NT-3 functionalized SF group reached a reference muscle response of 20% at less than half the stimulation intensity needed for the non-functionalized SF group to reach the 20% reference.

Referencing solely these EMG results, it appears that the cut and suture group produced the most successful nerve regeneration, followed by the NGF and CNTF functionalized SF group, followed by the NGF and NT-3 functionalized SF group, followed by the non-functionalized SF group that demonstrated low regeneration success. These results are slightly different than what was observed with histochemical analyses proving that histochemical analysis cannot be the only analysis technique used when evaluating nerve regeneration. The difference in results could be from a misdirection of motor neurons that cannot be predicted with histochemical analysis alone. Therefore, as many motor neurons had regenerated in the NGF and NT-3 functionalized SF samples, and thicker axons/myelin was observed, it is possible that they did not all reinnervate the correct post synaptic target.

Finally, motion capture analysis was done in order to qualitatively and quantitatively evaluate the walking patterns of the injured animals compared to a control. As not all animals walked at the same speed during the analysis, a normalized walking pattern for one step in the cycle was taken in comparison to the control. Observing the normalized foot displacement and vertical foot displacement normalized step patterns, the NGF and NT-3 functionalized SF group appears to have the most similar pattern to the control compared with the other experimental groups. And contrary to both the histochemical and EMG analysis, the cut and suture group presents the most altered walking pattern compared to all other experimental groups. The NGF

and CNTF functionalized SF group presented the next most similar walking pattern to the control followed by the non-functionalized group.

These results therefore demonstrate that despite the fact that the cut and suture group's histochemical analyses were superior to those of the NGF and NT-3 functionalized SF group, it was the latter group that regained the most efficient functional recovery (walking). Similarly, despite the cut and suture group and the NGF and CNTF functionalized SF group exhibiting superior EMG results, they did not perform better in the motion capture evaluations. Further results on the angle patterns of the hip, knee, and ankle continue to support that the NGF and NT-3 functionalized group regained the most successful functional recovery, and that the NGF and CNTF functionalized SF group also performed better than the non-functionalized SF group and the cut and suture group.

In all three analysis methods the evaluation of the most successful regeneration yielded different conclusions when taken alone. It is for this reason that a more extensive evaluation process is needed when studying the effectiveness of nerve repair. Considering all three analysis methods together, the superior NGC was found to be the NGF and NT-3 functionalized SF-based conduit, as we observed larger diameter axons, thicker myelination, and despite the less sensitive muscle response of the gastrocnemius muscle, the walking patterns of this group were observed to be superior to all other walking patterns including the cut and suture group. Even though the cut and suture group showed superior histochemical and EMG results, the walking patterns were much more distorted than the two functionalized SF group which signals a problem in nerve regeneration. The most important result of a nerve intervention would be to regain proper function, and the cut and suture group failed to show adequate movement suggesting proper functional recovery. Therefore, the NGF and NT-3 functionalized SF-based NGC would be the favorable choice to continue research for improved nerve repair.

This study used three analysis methods in order to evaluate the effectiveness of non-functionalized SF and functionalized SF-based conduits because it gives a more comprehensive assessment of nerve regeneration and functional recovery. However, there are still several variables that could give additional details aiding in making a more informed conclusion on the study. First of all, conduction speed through the conduit was a variable hoped to be studied in

this work. Unfortunately, these electrophysiological assays were met with an excess of unfavorable setbacks preventing the acquisition of these results. Results from this analysis technique would have allowed the evaluation of the speed and intensity of electrical activity through the NGC.

In addition, histochemical stains specifically for sensory neurons were attempted in order to, in conjunction with a motor neuron-specific stain, directly analyze the distribution between motor and sensory nerve fibers.

Furthermore, an analysis of sensory functional recovery is missing from this study that is very important in understanding regeneration success. Working with animals, however, makes this evaluation very complicated given the inability for the animals to communicate how they may experience sensory stimuli. Indirect methods for the functional analysis of sensory pathways like dull shock and heat application are possible, but may not allow a thorough explanation of the extent of functional recovery.

In addition to analysis techniques, there are also procedures to overcome obstacles during the study that are constantly overlooked in the literature. First of all, during the first weeks after the initial injury, the animals need to adapt to the injured foot. The animals have lost function in their right limb and the result is that they start to bite the injured leg without sensing pain. Therefore, if the animals are not closely examined, they will continue to bite their intensive limb. This problem was overcome in this study by the placement and constant replacement of a plastic cast around their injured limb. Cones were not used around the animals' necks as they were known to cause the animal stress. This method was used for the first few weeks after the injury until the animals no longer tried to chew their limbs.

The second important obstacle that needs to be overcome during a nerve regeneration study is the lack of physical therapy for the animals. In order to evaluate the functional regeneration in indirect ways (since the animals are unable to communicate or readily follow instructions), physical therapy is very important in order to assure the best possible results from motion analysis. This is because the muscles in the limb, in addition to undergoing muscular atrophy after denervation, shorten and natural movement becomes more restricted. Therefore, consistent periodic stretching is needed during the time that motor nerve fibers are extending

toward the denervated skeletal muscle. However, the animals are not cooperative for stretching sessions and so in order to overcome this obstacle, animals were subjected to swimming sessions in order to oblige the attempted movement of the injured limb. Animals were subject to swimming sessions twice per week for one month immediately after casts were removed (after about 3 weeks after injury; each swimming session lasted 5-10 minutes and all animals were able to continue swimming for the entire session from the first session. Therefore results of motion capture are hoped to be more accurate due to this additional intervention during the first weeks of injury.

Chapter 5

Conclusions

During this thesis, a nerve guidance conduit design based on the biomaterial silk fibroin was explored for possible functionalization techniques, and tested in vivo for nerve regeneration efficiency. The device itself, which was submitted for patenting on July 12, 2017 and as an article currently being reviewed for publication, consists of a tri-layered electrospun material: two aligned nanofiber surfaces and one randomly deposited fiber interior layer. This device was rolled into a multi-channeled tube and covered with a jacket layer of the same material. This device gives guidance factors to regenerating neurons, mimics the natural morphology of a nerve, and provides a jacket layer for assistance during the implantation process. This is a base design for an eventual complexified device for peripheral nerve regeneration.

Several techniques for the enhancement of the silk fibroin material in order to promote improved nerve regeneration were explored by the incorporation of growth factors (nerve growth factor, ciliary neurotrophic factor, and neurotrophin-3), a second polymer (fibronectin), and conductive or magnetic nanoparticles (gold nanoparticles and iron oxide nanoparticles. All functionalization techniques were achieved and prove to be promising for future testing for the efficiency of nerve regeneration. Once the functionalization of the silk fibroin material is optimized, potentially with a combination of the proposed techniques of this work, additional in vivo studies may be carried out.

An in vivo study using the developed device functionalized with either a combination of nerve growth factor and ciliary neurotrophic factor or nerve growth factor and neurotrophin-3 was also carried out. A device with non-functionalized silk fibroin was used as a reference for the effect of functionalization as well as a cut and sutured method to represent results obtained from an autograft. Three separate analysis techniques were used in order to obtain a comprehensive evaluation of the success of each experimental group including histochemical analyses, EMG tests on the gastrocnemius muscle, and motion capture analyses on walking patterns. Taking all the results together, the most successful recovery was observed from the device functionalized with nerve growth factor and neurotrophin-3.

The next step in this study would be to incorporate fibronectin and continue with electrical stimulation and magnetic stimulation studies with the use of nanoparticles in order to develop a more complex and functional material for future in vivo studies.

Publications and Communications

Review article (April, 2016)

"Recent strategies in tissue engineering for guided peripheral nerve regeneration"

Kayla Belanger, Tony M. Dinis, Sami Taourirt, Guillaume Vidal, David L. Kaplan, & Christophe Egles

Macromolecular Bioscience, 16, 472-481. DOI: 10.1002/mabi.201500367

Manuscript under review

"A multi-layered nerve guidance conduit design adapted to facilitate surgical implantation"

Kayla Belanger, Guy Schlatter, Anne Hébraud, Frédéric Marin, Sylvie Testelin, Stéphanie Dakpé, Bernard Devauchelle, & Christophe Egles

Submitted to Health Science Reports

European patent (2017)

"Fibrous Polymer Material Comprising Fibroin and Polymer Scaffolds Comprising Thereof"

Inventors: Kayla Belanger, Christophe Egles, Guy Schlatter, Anne Hébraud, & Bernard Devauchelle

Submission number: 1000413489

Date of receipt: July 12, 2017

Poster presentation at international conference (June, 2016)

Nano in Bio – Advances for Life & Materials Sciences (Le Gosier, Guadeloupe)

"Functionalized Silk Fibroin-Based Nanofiber Guidance Conduits for Peripheral Nerve Regeneration"

Kayla Belanger, Tony Dinis, Bernard Devauchelle, & Christophe Egles

Oral presentation & poster at international conference (June, 2017)

6th International Conference on Tissue Engineering in conjunction with the 3rd International Conference on Regenerative Biomedical Materials (Crete, Greece)

"Biofunctionalized Silk Nanofiber Nerve Guidance Conduit for Peripheral Nerve Regeneration"

Kayla Belanger, Pascale Vigneron, Guy Schlatter, Anne Hébraud, Bernard Devauchelle, & Christophe Egles

Recipient of the *Aegean Conference Travel Award* for oral presentation

Oral presentation at international conference (June, 2017)

19th International Conference of Tissue Engineering and Regenerative Medicine (London, England)

"Biofunctionalized Silk Nanofibers for Peripheral Nerve Regeneration"

Kayla Belanger, Pascale Vigneron, Guy Schlatter, Bernard Devauchelle, & Christophe Egles

References

Agarwal, S., Wendorff, J.H., Greiner, A. (2008). Use of electrospinning technique for biomedical applications. *Polymer, 49,* 5603-5621. doi: 10.1016/j.polymer.2008.09.014

Allen, N. J. and Barres, B. A. (2009). Glia - more than just brain glue. *Nature, 457,* 5. doi: 10.1038/457675a

Allodi, I., Udina, E., Navarro, X. (2012). Specificity of peripheral nerve regeneration: Interactions at the axon level. *Progress in Neurobiology, 98,* 16–37. doi: 10.1016/j.pneurobio.2012.05.005

Arai, T., Freddi, G., Innocenti, R., Tsukada, M., (2004). Biodegradation of Bombyx mori silk fibroin fibers and films. *J. Appl. Polym. Sci., 91*, 2383–2390. doi:10.1002/app.13393

Aufaure, R., Lalatonne, Y., Lièvre, N., Heintz, O., Motte, L., Guénin, E. (2014). One pot microwave assisted synthesis of bisphosphonate alkene cappened gold nanoparticles. *RCS Advances, 4,* 59315. doi: 10.1039/c4ra11847b

Azevedo, F. A. C., Carvalho, L. R. B., Grinberg, L. T., Farfel, J. M., Ferretti, R. E. L., Leite, R. E. P., Filho, W. J., Lent, R., Hervulano-Houzel, S. (2009). Equal Numbers of Neuronal and Nonneuronal Cells Make the Human Brain an Isometrically Scaled-Up Primate Brain. *The Journal of Comparative Neurology, 513,* 532-541. doi: 10.1002/cne.21974

Aznar-Cervantes, S., Roca, M., Martinez, J., Meseguer-Olmo, L., Cenis, J., Moraleda, J., Otero, F. (2012). Fabrication of conductive electrospun silk fibroin scaffolds by coating with polypyrrole for biomedical applications. *Bioelectrochemistry, 85,* 36-43. doi: 10.1016/j.bioelechem.2011.11.008

Bear, M. F., Connors, B. W., Paradiso, M. A. (Eds.). (2007). *Neuroscience* (Vol. 2). Lippincott Williams & Wilkins.

Belanger, K., Dinis, T.M., Taourirt, S., Vidal G., Kaplan, D.L., Egles, C. (2016). Recent strategies in tissue engineering for guided peripheral nerve regeneration. *Macromolecular Bioscience, 16,* 472-481. doi: 10.1002/mabi.201500367

Bhat, N.V., Ahirrao, S.M., (1983). Investigation of the structure of silk film regenerated with lithium thiocyanate solution. *J. Polym. Sci. Polym. Chem. Ed., 21*, 1273–1280. doi:10.1002/pol.1983.170210504

Bhatheja, K. and Field, J. (2006). Schwann cells: Origins and role in axonal maintenance and regeneration. *The International Journal of Biochemistry & Cell Biology, 38,* 1995-1999. doi: 10.1016/j.biocel.2006.05.007

Birch, R. (2013). *Peripheral Nerve Injuries: A Clinical Guide*. London: Springer-Verlag.

Birch, R., (2011). Surgical Disorders of the Peripheral Nerves. Springer Science & Business Media.

Blessing, B. and Gibbins, I. (2008). Autonomic nervous system. *Scholarpedia, 3*(7), 2787. doi: doi:10.4249/scholarpedia.2787

Braun, S., Croizat, B., Lagrange, M.C., Warter, J.M., Poindron, P. (1996). Neurotrophins increase motorneurons' ability to innervate skeletal muscle fibers in rat spinal cord-human muscle cocultures. *J Neurol Sci, 136*(1-2), 17-23.

Burnett M. G. and Zager E. L. (2004). Pathophysiology of peripheral nerve injury: a brief review. *Neurosurg Focus, 16*(5), E1.

Cao, Y. and Wang, B. (2009). Biodegradation of silk biomaterials. *Int J Mol Sci, 10*(4), 1514-24. doi: 10.3390/ijms10041514

Campbell WW., (2008). Evaluation and management of peripheral nerve injury. *Clin. Neurophysiol., 119*(9):1951-65. doi: 10.1016/j.clinph.2008.03.018. Epub 2008 May 14.

Ciaramitaro, P., Mondelli, M., Logullo, F., Grimaldi, S., Battiston B., Sard, A., Scarinzi, C., Migliaretti, G., Faccani, G., Cocito, D. (2010). *J Peripher Nerv Syst., 15*(2):120-7. doi: 10.1111/j.1529-8027.2010.00260.x.

Chhabra, A., Ahlawat, S., Belzberg, A., Andreseik, G. (2014). Peripheral nerve injury grading simplified on MR neurography: As referenced to Seddon and Sunderland classifications. *Indian Journal of Radiology and Imaging, 24*(3), 217-24. doi: 10.4103/0971-3026.137025

Chiono, V., & Tonda-Turo, C. (2015). Trends in the design of nerve guidance channels in peripheral nerve tissue engineering. *Progress in Neurobiology, 131,* 87–104. doi: 10.1016/j.pneurobio.2015.06.001

Claudepierre, T., Koncina, E., Pfrieger, F. w., Bagnard, D., Aunis, D., Reber, M., 2008. Implication of neuropilin 2/semaphorin 3F in retinocollicular map formation. *Dev. Dyn. 237*, 3394–3403. doi:10.1002/dvdy.21759

Cunha, C., Panseri, S., Antonini, S. (2011). Emerging nanotechnology approaches in tissue engineering for peripheral nerve regeneration. *Nanomedicine: Nanotechnology, Biology, and Medicine, 7,* 50-59. doi:10.1016/j.nano.2010.07.004

Das, S., Sharma, M., Saharia, D., Sarma, K. K., Sarma, M. G., Borthakur, B. B., Bora, U. (2015). In vivo studies of silk based gold nano-composite conduits for functional peripheral nerve regeneration. *Biomaterials, 62,* 66-75. doi: 10.1016/j.biomaterials.2015.04.047

de Almeida, P. G., Pinheiro, G. G., Nunes, A. M., Gonçalves, A. B., Thorsteinsdóttir, S. (2016). Fibronectin assembly during early embryo development: A versatile communication system between cells and tissues. *Developmental Dynamics, 245,* 520-535. doi: 10.1002/dvdy.24391

de Luca, A., Lacour, S. P., Raffoul, W., di Summa, P. G. (2014). Extracellular matrix components in peripheral nerve repair: how to affect neural cellular response and nerve regeneration? *Neural Regeneration Research, 9*(22), 1943-1948. doi: 10.4103/1673-5374.145366

Demay-Drouhard, P., Nehlig, E., Hardouin, J., Motte, L., Guénin, E. (2013). Nanoparticles under the Light: Click Functionalization by Photochemical Thiol-yne Reaction, Towards Double Click Functionalization. *Chemistry*, 19(26), 8388-92. doi: 10.1002/chem.201300903

Demerens, C., Stankoff, B., Logak, M., Anglade, P., Allinquant, B., Couraud, F., Zalc, B., Lubetztki., C. (1996). Induction of myelination in the central nervous system by electrical activity. *Proc Natl Acad Sci USA, 93,* 9887-92.

Dellon,E. S., & Dellon, A. L. (1993). The first nerve graft, Vulpian, and the nineteenth century neural regeneration controversy. *J Hand Surg Am., 18*(2), 369-72. doi: 10.1016/0363-5023(93)90378-G

Dinis, T. M., Elia, R., Vidal, G., Auffret, A., Kaplan, D. L., Egles, C. (2014a). Method to form a fiber/growth factor dual-gradient along electrospun silk for nerve regeneration. *ACS Applied Materials & Interfaces, 6*(19), 16817-26. doi: 10.1021/am504159j

Dinis, T. M., Vidal, G., Jose, R. R., Vigneron, P., Bresson, D., Fitzpatrick, V., Marin, F., Kaplan, D. L., Egles, D. (2014b). Complimentary Effects of Two Growth Factors in Multifunctionalized Silk Nanofibers for Nerve Reconstruction. *PLoS One, 9*(10), e109770. doi: 10.1371/journal.pone.0109770

Dinis, T.M., Elia, R. Vidal, G., Dermigny, Q., Denoeud, C., Kaplan, D.L., Egles, C., Marin, F. (2015). 3D multi-channel bi-functionalized silk electrospun conduits for peripheral nerve regeneration. *Journal of the Mechanical Behavior of Biomedical Materials, 41,* 43-55. doi: 10.1016/j.jmbbm.2014.09.029

Doshi, J. and Reneker, D.H. (1995). Electrospinning Process and Applications of Electrospun Fibers. *Journal of Electrostatics, 35,* 151-160.

Elzinga, K., Tyreman, N., Ladak, A., Savaryn, B., Olson, J., Gordon, T. (2015). Brief electrical stimulation improves nerve regeneration after delayed repair in Sprague Dawley rats. *Exp Neurol, 269,* 142-53. doi: 10.1016/j.expneurol.2015.03.022

Esaki, S., Kitoh, J., Katsumi, S., Goshima, F., Kimura, H., Safwat, M., Yamano, K., Watanabe, N., Nonoquchi, N., Nakamura, T., Coffin, R. S., Miyatake, S. I., Nishiyama, Y., Murakami, S. (2011). Hepatocyte growth factor incorporated into herpes simplex virus vector accelerates facial nerve regeneration after crush injury. *Gene Ther, 18*(11), 1063-9. doi: 10.1038/gt.2011.57

Farley, A., McLafferty, E., Johnstone, C., Hendry, C. (2014). Nervous system: Part 3. *Nursing Standard, 28*(33), 46-50. doi: 10.7748/ns2014.04.28.33.46.e8187

Faroni, A., AtefehMobasseri, S., Kinghamc, P. J., Reid, A. J. (2015). Peripheral nerve regeneration: Experimental strategies and future perspectives. *Advanced Drug Delivery Reviews, 82-83,* 160-167. doi: 10.1016/j.addr.2014.11.010

Fuhs, T., Reuter, L., Vonderhaid, I., Claudepierre, T., Kas, J.A., (2013). Inherently slow and weak forward forces of neural growth cones measured by a drift-stabilized atomic force microscope. *Cytoskelet. Hoboken NJ 70*, 44-53. doi:10.1002/cm 21080

Gaudin, R., Knipfer, C., Henningsen, A., Smeets, R., Heiland, M., Hadlock, T. (2016). Approaches to Peripheral Nerve Repair: Generations of Biomaterial Conduits Yielding to Replacing Autologous Nerve Grafts in Craniomaxillofacial Surgery. *BioMed Research International, 2016,* 3856262. doi: 10.1155/2016/3856262

Gonzalez-Perez, F., Udina, E., Navarro, X. (2013). Extracellular matrix componentrs in peripheral nerve regeneration. *Int Rev Neurobiol, 108,* 257-75. doi: 10.1016/B978-0-12-410499-0.00010-1

Goodman, C. S. (1996). Mechanisms and molecules that control growth cone guidance. *Annu Rev Neurosci, 19,* 341-77. doi: 10.1146/annurev.ne.19.030196.002013

Gordon, T. (2016). Electrical stimulation to enhance axon regeneration after peripheral nerve injuries in animal models and humans. *Neurotherapeutics, 13*(2), 295-310. doi: 10.1007/s13311-015-0415-1

Griffin, J. W., Hogan, M. V., Chhabra, A. B., Deal, D. N. (2013). Peripheral Nerve Repair and Reconstruction. *J Bone Joint Surg Am., 95,* 2144-51. doi: 10.2106/JBJS.L.00704

Griffin, M. F., Malahias, M., Hindocha, S., Khan, W. S. (2014). Peripheral Nerve Injury: Principles for Repair and Regeneration. *The open orthopaedics journal, 8*(Suppl 1: M10), 199-203. doi: Retrieved from https://benthamopen.com/FULLTEXT/TOORTHJ-8-199

Grinsell, D., & Keating, C. P. (2014). Peripheral Nerve Reconstruction after Injury: A Review of Clinical and Experimental Therapies. *BioMed Research International, 2014,* 698256. doi: 10.1155/2014/698256

Gu, X., Ding, F., Yang, Y., Liu, J. (2011). Construction of tissue engineered nerve grafts and their application in peripheral nerve regeneration. *Progress in Neurobiology, 93,* 204–230. doi: 10.1016/j.pneurobio.2010.11.002

Gunay, I., Mert, T. (2010). Pulsed magnetic fields enhance the rate of recovery of damaged nerve excitability. Bio Electro Magnetics, 32(3), 200-208. doi: 10.1002/bem.20629

Haastert-Talini, K., Grothe, C. (2013). Electrical stimulation for promoting peripheral nerve regeneration. *Int Rev Neurobiol, 109,* 111-24. doi: 10.1016/B978-0-12-420045-6.00005-5

Hendry, C., Farley, A., McLafferty, A., Johnstone, C. (2014). Nervous system: Part 2. *Nursing Standard, 28*(32) 45-49. doi: 10.7748/ns2014.04.28.32.45.e7931

Huang, J., Zhang, Y., Lu, L., Hu, X., Luo, Z. (Electrical stimulation accelerates nerve regeneration and functional recovery in delayed peripheral nerve injury in rats. *Eur J Neurosci, 38*(12), 3691-701. doi: 10.1111/ejn.12370

Huang, Z.-M., Zhang, Y.-Z., Kotaki, M., Ramakrishna, S. (2003). A review on polymer nanofibers by electrospinning and their applications in nanocomposites. *Composites Science and Technology, 63,* 2223-2253. doi: 10.1016/S0266-3538(03)00178-7

Huebner, E. A., & Strittmatter, S. M. (2009). Axon Regeneration in the Peripheral and Central Nervous Systems. *Results Probl Cell Differ., 48,* 339–351. doi:10.1007/400_2009_19

Jessen, K. A. (2004) Glial Cells. *The International Journal of Biochemistry & Cell Biology, 36,* 1861–1867. doi: 10.1016/j.biocel.2004.02.023

Jessen, K. R. and Mirsky, R. (2005). The origin and development of glial cells in peripheral nerves. *Nature Reviews Neuroscience, 6*(9), 671-82. doi: 10.1038/nrn1746

Jiang, X., Lim, S. H., Mao, H-Q., Chew, S. Y. (2010). Current applications and future perspectives of artificial nerve conduits. *Experimental Neurology, 223,* 86–101. doi: 10.1016/j.expneurol.2009.09.009

Kaiser R. (2016). [Surgical treatment of lower extremity peripheral nerve injuries]. *Cas Lek Cesk.,155*(3), 16-20. Retrieved from http://www.prolekare.cz/

Kehoe, S., Zhang, X. F., Boyd, D. (2012). FDA approved guidance conduits and wraps for peripheral nerve injury: A review of materials and efficacy. *Injury, Int. J. Care Injured, 43,* 553-572. doi: 10.1016/j.injury.2010.12.030

Kandel,E., Schwartz, J., (2013) *Principles of neural science, Fifth Edition.* McGraw Hill Professional

Kettenmann, H., Hanisch, U-K., Noda, M., Verkhratsky, A. (2011). Physiology of Microglia. *Physiological Reviews, 91,* 461-553. doi: 10.1152/physrev.00011.2010

Kakade, M.V., Givens, S., Gardner, K., Lee, K.H., Chase, D.B., Rabolt, J.F., (2007). Electric Field Induced Orientation of Polymer Chains in Macroscopically Aligned Electrospun Polymer *Nanofibers. J. Am. Chem. Soc., 129*, 2777–2782. doi:10.1021/ja065043f

Kim, U.-J., Park, J., Joo Kim, H., Wada, M., Kaplan, D.L.,(2005). Three-dimensional aqueous-derived biomaterial scaffolds from silk fibroin. *Biomaterials, 26*, 2775–2785. doi:10.1016/j.biomaterials.2004.07.044

Kim, J. A., Lee, N., Kim, W. J., Yoon, S., Hyeon, T., Park, T. H. (2011). Enhancement of neurite outgrowth in PC12 cells by iron oxide nanoparticles. *Biomaterials, 32,* 2871-2877. doi: 10.1016/j.biomaterials.2011.01.019

Konofaos, P., & Ver Halen, J. P. (2013). Nerve Repair by Means of Tubulization: Past, Present, Future. *J Reconstr Microsurg, 29,* 149-164. doi: 10.1055/s-0032-1333316

Koppes, A. N., & Thompson, D. M. (2015). Neural innervation of engineered musculoskeletal tissues. *Regenerative Engineering of Musculoskeletal Tissues and Interfaces* (pp. 293-321). doi: 10.1016/B978-1-78242-301-0.00012-4

Lalatonne, Y., Paris, C., Serfaty, J.M., Weinmann, P., Lecouvey, M., Motte, L. (2008). Bis-phosphonated-ultra small superparamagnetic iron oxide nanoparticles : a platform towards diagnosis and therapy. *Chem Commun, 14,* 2553-5. doi: 10.1039/b801911h

Li, D. and Xia, Y. (2004). Electrospinning of Nanofibers: Reinventing the Wheel? *Advanced Materials, 16*(14), 1151-1170. doi: 10.1002/adma.200400719

Li, M., Lu, S., Wu, Z., Yan, H., Mo, J., Wang, L., (2001). Study on porous silk fibroin materials. I. Fine structure of freeze dried silk fibroin. *J. Appl. Polym. Sci*., 79, 2185–2191. doi: 10.1002/1097-4628(20010321)79:12<2185::AID-APP1026>3.0.CO;2-3

Little,K. M., Zomorodi, A. R., Selznick, L. A., Friedman, A. H. (2004). An eclectic history of peripheral nerve surgery. *Neurosurg Clin N Am, 15,* 109–123. doi: 10.1016/j.nec.2003.12.002

Liu, G-Y., Jin, Y., Zhang, Q., Li, R. (2015). Peripheral nerve repair: a hot spot analysis on treatment methods from 2010 to 2014. *Neural regeneration research, 10*(6), 996-1002. doi: 10.4103/1673-5374.158368

Madduri, S., di Summa, P., Papaloïzos, M., Kalbermatten, D., Gander, B. (2010). Effect of controlled co-delivery of synergistic neurotrophic factors on early regeneration in rats. *Biomaterials, 31*(32), 8402-9. doi: 10.1016/j.biomaterials.2010.07.052

Marieb, E.N., (2006). *Human Anatomy & Physiology. Benjamin Cummings* ; Pearson.

Martini, R., (1994). Expression and functional roles of neural cell surface molecules and extracellular matrix components during development and regeneration of peripheral nerves. *J. Neurocytol., 23*, 1–28.

Mita, K., Ichimura, S., James, T.C., (1994). Highly repetitive structure and its organization of the silk fibroin gene., *J. Mol. Evol. 38*, 583–592. doi:10.1007/BF00175878

Mitsingou, J.., Goma, P., (1993). Le crush-syndrome au cours de l'écrasement du membre supérieur (A propos d'un cas observé à la clinique chirurgicale des Armées de Pointe-Noire - CONGO). *Médecine Afr. Noire 12*

Mukhatyar, V., Salmerón-Sánchez, M., Rudra, S., Mukhopadaya, S., Barker, T. H., Garcia, A. J., Bellamkonda, R. V. (2011). Role of fibronectin in topographical guidance of neurite extension on electrospun fibers. *Biomaterials, 32*(16), 3958-3968. doi: 10.1016/j.biomaterials.2011.02.015

Nazarov, R., Jin, H.-J., Kaplan, D.L., (2004). Porous 3-D Scaffolds from Regenerated Silk Fibroin. *Biomacromolecules, 5*, 718–726. doi:10.1021/bm034327e

Ndubaku, U., de Bellard, M. E. (2008). Glial cells: Old cells with new twists. *Acta histochemica, 110,* 182-195. doi: 10.1016/j.acthis.2007.10.003

Nedjari, S., Eap, S., Hébraud, A., Wittmer, C.R., Benkirane-Jessel, N., Schlatter, G. (2014). Electrospun Honeycomb as Nests for Controlled Osteoblast Spatial Organization. *Macromolecular Bioscience, 2014*. doi: 10.1002/mabi.201400226

Oppenheim, R., & Milligan, C. (2009). Programmed Cell Death. P. Hof & C. Mobbs (Eds.), *Handbook of the Neuroscience of aging* (pp. 131-138). Academic Press.

Pal, A., Singh, A., Nag, T. C., Chattopadhyay, P., Mathur, R., Jain, S. (2013). Iron oxide nanoparticles and magnetic field exposure promote functional recovery by attenuating free radical-induced damage in rats with spinal cord transection. *International Journal of Nanomedicine, 8*(1), 2259-2272. doi: 10.2147/IJN.S44238

Palispis, W. A., & Gupta, R. (2017). Surgical repair in humans after traumatic nerve injury provides limited functional neural regeneration in adults. *Experimental Neurology, 290,* 106–114. doi: 10.1016/j.expneurol.2017.01.009

Park, J. S., Park, K., Moon, H. T., Woo, D. G., Yang, H. N., Park, K-H. (2009). Electrical pulsed stimulation of surfaces homogeneously coated with gold nanoparticles to induce neurite outgrowth of PC12 cells. *Langmuir, 25,* 451-457. doi: 10.1021/la8025683

Pereda, A.E., (2014). Electrical synapses and their functional interactions with chemical synapses. *Nat. Rev. Neurosci.* 15, 250–263. doi:10.1038/nrn3708

Pisanic, T. R., II., Blackwell, D. J., Shubayev, V. I., Fiñones, R. R., Jin, S. (2007). Nanotoxicity of iron oxide nanoparticle internalization in growing neurons. *Biomaterials, 28,* 2572-2581. doi: 10.1016/j.biomaterials.2007.01.043

Purves D., 2001. *Neuroscience, 2nd edition*

Purves, D., 2005. *Neurosciences: De Boeck Supérieur*.

Purves, D., Augustine, G. J., Fitzpatrick, D., et al., editors. Neuroscience. 2nd edition. Sunderland (MA): Sinauer Associates; 2001. Electrical Synapses. Available from: https://www.ncbi.nlm.nih.gov/books/NBK11164/

Rockwood, D. N., Preda, R. C., Yücel, T., Wang, X., Lovett, M. L., Kaplan, D. L. (2011). Materials fabrication from *Bombyx mori* silk fibroin. *Nature Protocols, 6*(10), 1612-1631. doi: 10.1038/nprot.2011.379

Rodrigues, M. C. O., Rodrigues, A. A., Jr., Glover, L. E., Voltarelli, J., Borlongan, C. V. (2012). Peripheral Nerve Repair with Cultured Schwann Cells: Getting Closer to the Clinics. *The Scientific World Journal, 2012,* 1-10. doi: 10.1100/2012/413091

Rossi, F., Gianola, S., Corvetti, L. (2007). Regulation of intrinsic neuronal properties for axon growth and regeneration. *Progress in Neurobiology, 81,* 1–28. doi: 10.1016/j.pneurobio.2006.12.001

Safa, B., & Buncke, G. (2016). Autograft Substitutes Conduits and Processed Nerve Allografts. *Hand Clin, 32*(2), 127–140. doi: 10.1016/j.hcl.2015.12.012

Saika, T., Senba, E., Noquchi, K., Sato, M., Yoshida, S., Kubo, T., Matsunaga, T., Tohyama, M. (1991). Effects of nerve crush and transection on mRNA levels for nerve growth factor receptor in the rat facial motorneurons. *Brain Res Mol Brain Res, 9*(1-2), 157-60.

Sashina, E.S., Bochek, A.M., Novoselov, N.P., Kirichenko, D.A., (2006). Structure and solubility of natural silk fibroin*. Russ. J. Appl. Chem*., *79*, 869–876. doi:10.1134/S1070427206060012

Schmidt CE., Leach JB., (2003). Neural tissue engineering: strategies for repair and regeneration. *Annu. Rev. Biomed. Eng., 5*, 293-347. doi: 10.1146/annurev.bioeng.5.011303.120731

Sherrington, C., (1906). *The Integrative Action of the Nervous System*. Cambridge University Press.

Silver, J. and Miller, J. H. (2004). Regeneration beyond the glial scar. *Nature Reviews Neuroscience, 5*(2), 146-56. doi: 10.1038/nrn1326

Sofroniew, M.V., Howe, C.L., Mobley, W.C. (2001). Nerve growth factor signaling, neuroprotection, and neural repair. *Annu Rev Neurosci, 24,* 1217-81. doi: 10.1146/annurev.neuro.24.1.1217

Spassky, N., Merkle, F. T., Flames, N., Tramontin, A. D., García-Verdugo, J. M., Alvarez-Buylla, A. (2005). Adult Ependymal Cells Are Postmitotic and Are Derived from Radial Cells during Embryogenesis. *The Journal of Neuroscience, 25*(1), 10-18. doi: 10.1523/JNEUROSCI.1108-04.2005

Sterne, G.D., Brown, R.A., Green, C.J. Terenghi, G. (1997). Neurotrophin-3 delivered localy vio fibronectin mats enhances peripheral nerve regeneration. *Eur J Neurosci, 9*(7), 1388-96.

Stoll, G., Müller, H.W., (1999). Nerve Injury, Axonal Degeneration and Neural Regeneration: *Basic Insights. Brain Pathol., 9*, 313–325. doi:10.1111/j.1750-3639.1999.tb00229.x

Stölting, M. N. L., Arnold, A. S., Haralampieva, D., Handschin, C., Sulser, T., Eberli, D. (2016). Magnetic stimulation supports muscle and nerve regeneration after trauma in mice. *Muscle Nerve, 53*(4), 598-607. doi:10.1002/mus.24780

Tansey, E.M., (2006). Henry Dale and the discovery of acetylcholine. *C. R. Biol. 329*, 419–425. doi:10.1016/j.crvi.2006.03.012

Tauber, H., Waehneldt, T.V., Neuhoff, V. (1980). Myelination in rabbit optic nerves in accelerated by artificial eye opening. *Neurosci Lett, 16*(3), 235-8.

Taveggia, C., Feltri, M.L., Wrabetz, L. (2010). Signals to promote myelin formation and repair. *Nat Rev Neurol, 6*(5), 276-287. doi: 10.1038/nrneurol.2010.37

Tonda-Turo, C., Gnavi, S., Ruini, F., Gambarotta, G., Gioffredi, E., Chiono, V., Perroteau, I., Ciardelli, G. (2017). Development and characterization of novel agar and gelatin injectable hydrogel as filler for peripheral nerve guidance channels. *J Tissue Eng Regen Med, 11*(1), 197-208. doi: 10.1002/term.1902

Tonge, D. A., de Burgh, H. T., Docherty, R., Humphries, M. J., Craig, S. E., Pizzey, J. (2012). Fibronectin supports neurite outgrowth and axonal regeneration of adult brain neurons in vitro. *Brain Res, 1453*(100), 8-16. doi: 10.1016/j.brainres.2012.03.024

Vepari, C., Kaplan, D.L., (2007). Silk as a biomaterial. *Prog. Polym. Sci., Polymers in Biomedical Applications, 32*, 991–1007. doi:10.1016/j.progpolymsci.2007.05.013

Verkhratsky, A. and Butt, A. (2007). *Glial Neurobiology*. Retrieved from http://www.books.google.com/

Volterra, A. and Meldolesi, J. (2005). Astrocytes, from brain glue to communication elements: the revolution continues. *Nature Reviews Neuroscience, 6*(8), 626-40. doi: 10.1038/nrn1722

Waller, A., (1850). Experiments on the Section of the Glossopharyngeal and Hypoglossal Nerves of the Frog, and Observations of the Alterations Produced Thereby in the Structure of Their Primitive Fibres. *Philos. Trans. R. Soc. Lond*., 140, 423–429. doi:10.1098/rstl.1850.0021

Wang, Z., Zhang, Y., Zhang, J., Huang, L., Liu, J., Li, Y., Zhang, G., Kundu, S. C., Wang, Lin. (2014). Exploring natural silk protein sericin for regenerative medicine: an injectiable, photoluminescent, cell-adhesive 3D hydrogel. *Scientific Reports, 4,* 7064. doi: 10.1038/srep07064

Willand, M. P., Nguyen, M. A., Borschel, G. H., Gordon, T. (2016). Electrical stimulation to promote peripheral nerve regeneration. *Neurorehabil, 30*(5), 490-6. doi: 10.1177/1545968315604399

Yang, Y., Ding, F., Wu, J., Hu, W., Liu, J., Gu, X. (2007). Development and evaluation of silk fibroin-based nerve grafts used for peripheral nerve regeneration. Biomaterials, 28, 5526-5535. doi: 10.1016/j.biomaterials.2007.09.001

Yang, Y., Zhao, Y., Gu, Y., Yan, X., Liu, J., Ding, F., Gu, X. (2009). Degradation behaviors of nerve guidance conduits made up of silk fibroin in vitro and in vivo. *Polymer Degradation and Stability, 94,* 2213-2220. doi: 0.1016/j.polymdegradstab.2009.09.002

Zhang, J., Lineaweaver, W.C. Oswald, T., Chen, Z., Chen, Z., Zhang, F. (2004). Ciliary neurotrophic factor for acceleration of peripheral nerve regeneration: an experimental study. *J Reconstr Microsurg, 20,* 323-327. doi: 10.1055/s-2004-824891

Zhang, X., Xin, N., Tong, L., Tong, X. J. (2013). Electrical stimulation enhances peripheral nerve regeneration after crush injury in rats. *Mol Med Rep, 7*(5), 1523-7. doi: 10.3892/mmr.2013.1395

Zhivolupov, S. A., Odinak, M. M., Rashidov, N. A., Onischenko, L. S., Samartsev, I. N., Jurin, A. A. (2012). Impulse magnetic stimulation facilitates synaptic regeneration in rats following sciatic nerve injury. *Neural Regen Res, 7*(17), 1299-1303. doi: 10.3969/j.issn.1673-5374.2012.17.003